NOTICE

The quality of this microform is heavily dependent upon the quality of the original thesis submitted for microfilming. Every effort has been made to ensure the highest quality of reproduction possible.

If pages are missing, contact the university which granted the degree.

Some pages may have indistinct print especially if the original pages were typed with a poor typewriter ribbon or if the university sent us an inferior photocopy.

Reproduction in full or in part of this microform is governed by the Canadian Copyright Act, R.S.C. 1970, c. C-30, and subsequent amendments.

AVIS

La qualité de cette microforme dépend grandement de la qualité de la thèse soumise au microfilmage. Nous avons tout fait pour assurer une qualité supérieure de reproduction.

S'il manque des pages, veuillez communiquer avec l'université qui a conféré le grade.

La qualité d'impression de certaines pages peut laisser à désirer, surtout si les pages originales ont été dactylographiées à l'aide d'un ruban usé ou si l'université nous a fait parvenir une photocopie de qualité inférieure.

La reproduction, même partielle, de cette microforme est soumise à la Loi canadienne sur le droit d'auteur, SRC 1970, c. C-30, et ses amendements subséquents.

Canada

The Static and Dynamic Spectroscopic Studies of 7-Aminocoumarins,
Their Cyclodextrin Complexes; and of Nitrobenzene Derivatives

YouXian WEN

A Thesis

in

The Department

of

Chemistry & Biochemistry

Presented in Partial Fulfillment of the Requirement
for the Degree of Doctor of Philosophy at
Concordia University
Montreal, Quebec, Canada

April, 1993

© YouXian WEN, 1993

Canada

To my wife, son, mother, parents-in-law

and memory of my father

ABSTRACT

The Static and Dynamic Spectroscopic Studies of 7-Aminocoumarins,

Their Cyclodextrin Complexes; and of Nitrobenzene Derivatives

YouXian WEN,   Ph. D.
Concordia University, 1993

On the basis of a thorough study of 7-aminocoumarin dyes in different

solvents, the methodology of amplified spontaneous emission (ASE) gain

spectroscopy at pumping threshold is established and has been applied to study

the complexation of 7-diethylamino-4-methylcoumarin (C1) in different co-solvent

systems. The advantage of ASE gain spectroscopy over conventional

spectrofluorimetry is the ease of separating heavily overlapping emission spectra

of 'free' and complex species, which is important for the study of complexation in

biological system.

The photophysical behaviour of conformationally sensitive 7-

aminocoumarin dyes in different solvents and their cyclodextrin (CD) complexes

in water is studied using picosecond time-resolved transient absorption and

emission techniques. These studies offer some important information about the

possible twisted intramolecular charge transfer (TICT) state of C1 (not the rigid

C102) in protic solvents. The structures of C1/CD complexes in water are

deduced from both static and dynamic studies and are supported by the study of

these dyes in pure or binary solvents. The time-resolved emission spectral study of C1 and C102 in protic solvents, shows that the solvation dynamics can be explained by a multi-state model in kinetics rather than a single excited state undergoing a continuous solvent relaxation process. This has been confirmed by (i) the simulation results, and (ii) the shape of the decay associated spectrum which is the normal preexponential distribution of the exponential time-dependent fluorescence (TDF). One of the wavelength-independent decay times of TDFD is closer to the longitudinal relaxation time of solvent than that of the single state model.

Time-resolved pump-probe technique has been also used to investigate the poorly understood excited state photophysical behaviour of nonfluorescent nitrobenzene derivatives in solution. A remarkable solvation effect is found in the ESA study of dimethoxynitrobenzenes. The lowest excited state observed on ESA spectra is attributed to an intramolecular charge transfer state. The rate constant of the time-dependent *blue-shift* ESA spectra is comparable to the rate constant of the longitudinal relaxation of solvent. This observation implies an alternative method to study the solvation dynamics. A relationship between excited state absorption (ESA) spectra of some alkylnitrobenzenes and the structure of substituted nitrobenzene is found. Finally, in order to understand and to control the photochemical process, the biradical intermediate of *o*-nitrobenzyl *p*-cyanophenyl ether in acetonitrile has been identified from ESA spectra which provides information about the partitioning singlet/triplet pathway of the photochemical reaction.

ACKNOWLEDGEMENT

CONTENTS

ABBREVIATION

4NB15CW5	4'-nitrobenzene-15-crown-5
15CW5	15-Crown-5
α	Fraction of the Incident Photon Absorbed by Complex
$\alpha_i(\lambda)$	Preexponential Distribution to the ith Decay Component
$\alpha_j(\lambda)$	Species (j) Associated Spectrum (SAS)
AE	Amplified Emission
AMMNBA	α-Methyl-m-nitrobenzyl alcohol
AN	Acetonitrile
ASE	Amplified Spontaneous Emission
BR	Biradical
C1	Coumarin-1(Coumarin-460)
C2	Coumarin-2 (Coumarin-450)
C102	Coumarin-102 (Coumarin-480)
C1F	Coumarin-1F (Coumarin-152, Coumarin-481)
C102F	Coumarin-102F (Coumarin-153)
CD	Cyclodextrin
CHD	5-Methyl-5-(hydroxymethyl)-1,3-cyclohexadiene
CP	Cyclization Product
CT	Charge Transfer
D	Dye
DAS	Decay Associated Spectrum
$DAS_i(\lambda)$	The Fractional Contribution to the Steady State Fluorescence from the ith Exponential Decay (i=1..n)
D-CD	Dye-Cyclodextrin

DMABN	4-Dimethylaminobenzonitrile
DMONB	1,2-Dimethoxy-4-nitrobenzene
ε	Dielectric Constant
ESA	Excited State Absorption
Φ	Quantum Yield
FWHM	Full Width at Half Maximum
$G(\lambda)$	Gain Coefficient
I	Emission Intensity
ICT	Intramolecular Charge Transfer
K	Ground State Equlibrium Constant
K_{ASE}	ASE Constant
K_Q	Quenching Constant
k_q	Excited State Forward Transition Rate
k_{-q}	Excited State Backward Transition Rate
K_{SV}	Stern-Volmer Constant
KDP	Potassium dihydrogen phosphate (KH_2PO_4)
λ	Wavelength (nm)
L	Slit Width
n	Optical Refractive Index
NLO	Nonlinear Optics
NM	Nitromesitylene
NT	Nitrotoluene
N(t)	Population
OD	Optical Density
OMA	Optical Multichannel Analyzer
ONB	o-Nitrobenzyl
ONBAA	o-Nitrobenzaldehyde acetal

ONBBPE	*o*-Nitrobenzyl-*p*-phenyl
ONBCPE	*o*-Nitrobenzyl-*p*-cyanophenyl ether
ONPEG	*o*-Nitrophenylethylene glycol
o-Q	*o*-Quinonoid
PEG	Poly(ethylene glycol)
Q	Quencher
RMSR	Root Mean Sum of Weighted Squares of Residuals
SAS	Species Associated Spectr~*um* or ~*a*
$SAS_j(\lambda)$	The Fractional Contribution to the Steady State Fluorescence from the Species j (j=A..Z)
SR	Spectral Reconstruction
SVR	Serial Variance Ratio
τ	Decay Time *or* Lifetime
τ_L	Longitudinal Relaxation Time of Solvent
τ_D	Debye Dieletric Relaxation Time
T	Transmission
TDF	Time-Dependent Fluorescence
THF	Tetrahydrofuran
TICT	Twisted Intramolecular Charge Transfer
TRES	Time-Resolved Emission Spectrum
υ	Wavenumber (cm^{-1})
W	Power of the Incident Light

FIGURE CAPTIONS

TABLE CAPTIONS

LIST OF SCHEMES

Chapter 1: INTRODUCTION

1.1 Photophysics

Photophysics is the study of physical processes (without chemical change) initiated by electronic excitation of a molecule or system of molecules by non-ionizing electromagnetic radiation (photons). Transitions between different electronic states can be separated into (i) absorption; (ii) radiation (emission); and (iii) nonradiative processes. Transitions between excited states of different spin such as singlet and triplet states is termed intersystem crossing. These various intramolecular transitions are usually summarized schematically as a Jablonski Diagram[1] in which the energy levels of a given spin state are displayed vertically, and the spin states, horizontally. Intramolecular interactions, or interactions between the electronic states of different molecules can also occur. These include full or partial nonradiative transfer of an electron to form a Donor-Acceptor complex,[2] or of energy (electronic energy transfer and sensitization).[3] Experimentally, some of these photophysical processes can be detected using *static* and/or *dynamic* spectroscopic techniques.

1.1.1 Steady state spectroscopic methods

UV/VIS absorption is the detectable photophysical process of transition from the ground state up into excited singlet states excited by incident light in the ultra-violet and visible region. In contrast to absorption, **fluorescence** is the observable deactivation by radiation of the excited single state back to the ground state. By considering the fast relaxation of vibronic *Franck-Condon states*, mirror image absorption and fluorescence spectra can be observed

experimentally. The energy of the frequency spacing between these two peaks is called *Stokes' shift*. For charge transfer (CT) species, the *Stokes' shift* is related linearly to the polarity of the solvent,[4] and satisfies the Lippert-Mataga equation.[5] Such solvent-dependent or *solvatochromic shifts* are typical of CT states.[5,6] The technique used to monitor these photophysical processes with constant photon flux is defined as *Steady State Spectroscopy* such as: uv/vis absorption spectrophotometry and spectrofluorimetry.[7,8] These techniques have been conventionally applied in chemistry, biology, and medicine for study of the photoactive species in different environments.[7-10]

To study complexation of a radiative solute molecule (e.g., organic dye[11,12]) with an additional species, Q (e.g., impurity, quencher), it is very important to identify the contributions to the fluorescence spectrum of the excited state complex originating from absorption of both (1) the
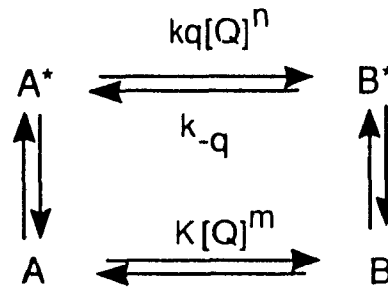
$$A^* \underset{k_{-q}}{\overset{k_q[Q]^n}{\rightleftharpoons}} B^*$$
$$A \underset{}{\overset{K[Q]^m}{\rightleftharpoons}} B$$

Scheme 1-1

ground state solute which dynamically forms the excited state complex (excited state $A^* \rightarrow B^*$ "*dynamic complexation*") and (2) the ground state complex (ground state $B \rightarrow B^*$ "*static complexation*").[13-16] In this thesis, we have formulated the kinetic relation among these components. On basis of this study, the fraction of each contribution to the fluorescence spectrum of the excited state complex can be identified experimentally.

Spectrofluorimetry has been used to study excited state molecular complexation in different areas for more than three decades.[9,10] These include biologically important systems in polar solvents,[17-21] guest-host complexation,[22-25] dyes in different solvents,[16,26] dimerization or isomerization,[27] etc. Although highly sensitive, conventional spectrofluorimetric

measurements on solution molecular complexes often be difficultly identified in components and thus, in order to resolve the overlapping fluorescence bands into their components, extremely precise measurements and assumptions regarding the shapes of the component bands are necessary. By contrast, the bands from amplified spontaneous emission gain spectroscopy introduced by Silfvast et al.,[28-30] are intrinsically narrower than those of the corresponding fluorescence emission due to laser characteristics of the probe molecule (e.g., laser dye).

Amplified spontaneous emission (ASE) is the amplification of spontaneously radiated photon flux from the excited singlet state to the ground state. In contrast to the absorption coefficient $\varepsilon(\lambda)$ in Beer-Lambert law, the *gain coefficient* $G(\lambda)$ of the emission is defined by

$$G(\lambda) = \left(\sigma_e(\lambda) - \sigma_s(\lambda)\right) \int_0^\infty N_s(t)\,dt - \sigma_T(\lambda) \int_0^\infty N_T(t)\,dt \tag{1}$$

where $\sigma_e(\lambda)$, $\sigma_s(\lambda)$, and $\sigma_T(\lambda)$ are the *cross sections* in cm^2 of the *stimulated emission, excited singlet state absorption* and *intersystem* (singlet to triplet state) *crossing*, respectively. The *population* density at the first excited singlet state S_1 and triplet state T_1 is represented by $N_S(t)$ and $N_T(t)$ in cm^{-3}, respectively. For relatively weak excited state absorption ($\sigma_s(\lambda)$) and intersystem crossing ($\sigma_T(\lambda)$), *ASE gain spectra* correlate in a simple fashion to the *conventional fluorescence spectra*. The direct relation between the *gain* coefficient $G(\lambda)$ (cm^2) or *emission cross section* $\sigma_e(\lambda)$ (cm^2) and the *fluorescence spectrum* $E(\lambda)$ can be simply expressed by the following relationship:[30,31]

$$G(\lambda) = \sigma_e(\lambda) \int_0^\infty N_s(t)dt = \frac{\lambda^4 E(\lambda)}{8\pi\tau cn^2} \int_0^\infty N_s(t)dt \qquad (2)$$

Here τ is the fluorescence lifetime in seconds, n is the dimensionless refractive index of the solvent, and c is the velocity of light in *vacuo* in cm/s. Since the 1970's, ASE gain spectroscopy has been used almost exclusively to study the fundamental characteristics of lasers.[32-35] *Recently*, distinctly resolved bands were observed in the study of the dual ASE of 7-aminocoumarin dyes in different solvents.[36] In this thesis, results on the origin of the dual ASE bands are presented. We find that dual emission is due to uncomplexed and hydrogen-bonded complexes rather than the formation of an exciplex with twisted amino group at the 7 position.[36] We have established a kinetic correlation between ASE and conventional fluorescence both experimentally and theoretically. Our results show that ASE spectroscopy is a useful technique to resolve normally heavily overlapping bands due to 'free' and complexed dyes or dyes in heterogeneous environment.

1.1.2   Time-resolved spectroscopic methods

With the rapid development of laser technologies, the flash photolysis technique of Norrish and Porter,[37] has proved to be a powerful tool to probe the dynamics of molecular orientation, excited state relaxation, molecular rearrangement, and other fast processes.[38,39] Flash photolysis is a time-resolved technique to study the photoactive species initiated by *a short-duration photon flux* . This technique is of benefit not only to chemistry and physics, but also in biology.[40,41] In this thesis, two types of time-resolved spectroscopy are applied. These are (i) *transient absorption* spectroscopy;[39] and (ii) *emission spectroscopy*.[40-42]

Time-resolved transient absorption spectroscopy can be divided into two categories: (1) those in which the detector itself possesses adequate time resolution for the task at hand; (2) those in which the response of the system is sampled by means of a second ("probe ") pulse delayed in time from the initial ("pump ") pulse. By varying the delay times, a set of time-resolved spectra can be obtained. In the latter case, referred to as *pump-probe spectroscopy*, the time resolution of the detection is unimportant and experimental time resolution is limited by the pump- and probe-pulse duration. Reflecting the high activity in the application of this technique to study photochemical and photophysical processes, a number of reviews on various specialized topics have appeared in the last two decades. These include vibrational dynamics in liquids and solids;[43] photoinduced charge and energy transfer process;[44] photodissociation;[38] isomerization;[45] photoreactions;[46] biradicals;[47] cage effect, orientational relaxation, internal convention and intersystem crossing;[48,49] localized electrons;[50] and the photophysics of pyrene in solution,[51] etc.

In this study, time-resolved transient absorption measurements were carried out at the Canadian Center for Picosecond Laser Spectroscopy at Concordia University. The spectra were recorded using the pump-probe technique with variable delays of up to 10 ns between the probe and excitation pulses, in which a Nd:YAG laser system was used consisting of a passively mode-locked (Kodak 9740 dye in chlorobenzene) at 355 nm with a pulse duration of 35 ps (full width at half-maximum (FWHM)).[45,52] Details are given in section 3.2.

Time-resolved emission spectroscopy is a technique to obtain fluorescence emission spectra at discrete times during the fluorescence decay, or a

fluorescence decay at a single wavelength position. Time-resolved emission spectroscopy (TRES) can yield both qualitative and quantitative information about many photophysical processes that can not be gleaned from conventional fluorescence spectra of even extremely high optical resolution. It is helpful, and even necessary, to characterize kinetically complex excited state phenomena.[42] Since the 1970's,[53] this technique has attracted tremendous attention for studies of molecular reorientation,[54-56] solvation dynamics,[57,58] cage effect,[59,60] especially, the effect of the local environment in biological molecules on the spectral characteristics of fluorescent probes.[41,61,62]

In this project, the time-resolved emission measurements were carried out in the laboratory of Dr. A. G. Szabo at the Biology Division, National Research Council of Canada, Ottawa. The emission was generated from a Spectra Physics mode-locked synchronously pumped and cavity dumped dye laser system with a pulse width of 20 ps at a repetition rate of 825 kHz. The decay curves were measured with single photon-counting instrumentation.[63] Details are given in section 5.2.

1.1.3   Solvation dynamics

Solvation dynamics is the study of time-dependent molecular relaxation process of a solvent due to the molecular dipole-dipole interaction induced by the sudden change of the dipole moment of an excited solute molecule. The effect of macroscopic solvent parameters (i.e., viscosity, polarity) on chemical dynamics has been extensively studied for many decades.[6] These studies show that to some extent, the nature of solvent effects on chemical reactions can be accounted for in terms of the changes of the potential energy barrier and relative free energies of the reactants and products.[64,65] In order to understand

dynamic solvent effects on chemical reactions, it is necessary to determine the time scale for solvent dielectric relaxation as well as to evaluate the time dependent forces, or dielectric friction, that the polar solvent exerts on the reacting molecule.

Time-resolved fluorescence spectroscopy of polar fluorescent "probes" has been used extensively to study microscopic solvation dynamics for a broad range of solvents.[57,58,66-70] One of the basic methods extracts the polarization function C(t) which is the fractional change of the instantaneous fluorescence maximum as a function of time[71] defined by

$$C(t) = \frac{v_m(t) - v_m(\infty)}{v_m(0) - v_m(\infty)}$$

(3)

where $v_m(0)$, $v_m(t)$, and $v_m(\infty)$ is the zero-, instantaneous, and infinite time frequency at emission maximum. In this method, the solvation process has been assumed to be a dynamic shift of a single excited state undergoing continuous solvent relaxation from the initial excited state to the solvated excited state.[65,72] Therefore, the decay of the time-dependent fluorescence i(λ,t) can be expressed by:

$$i(\lambda, t) = f(\lambda, t)e^{-t/\tau(t)}$$

(4)

In eq. (4), τ(t) is the lifetime of the solvating state and should vary with time; and f(λ,t) is the fluorescence profile with time-dependent spectral shape. For the excited solvating state undergoing continuous solvent relaxation, there should be no kinetic correlation between initial and final excited states. However, in our recent time-dependent fluorescence decay TDFD measurements of 7-diethylamino-4-methylcoumarin in 1-butanol, we found one negative

preexponential distribution $\alpha_i(\lambda)$ from the exponential fittings of the fluorescence decay spectra

$$i(\lambda,t) = \sum_{i=1}^{n} \alpha_i(\lambda)e^{-t/\tau_i} . \qquad (5)$$

Here, the decay of the fluorescence at each wavelength, has been considered as the sum of all contributions from incremental individual decay components with wavelength-independent decay time τ_i (i=1..n). About ten years ago, the study of these preexponential distributions indicated that for an irreversible
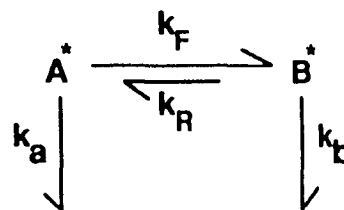
Scheme 1-2

two-state system (k_a+k_F » k_b+k_R and k_R « k_F in Scheme 1-2), one of the two preexponential distributions appears to be negative in part of the spectral region, which the other one remains positive overall.[73,74] This has been accepted as a signature for studying the kinetics of the irreversible two-state system.[73-78] Apparently, a similar observation (a negative preexponential distribution) in our experiment indicates a kinetic relationship between the unsolvated (initial) and the solvated (final) excited states. One of the wavelength-independent decay times from the exponentially fitted fluorescence decay spectra appears to depend on the solvent rather than the probes. The value is comparable to the longitudinal relaxation time of the solvent.

The longitudinal relaxation time τ_L of solvent is conventionally used to study solvent dynamics. In highly polar solvents, τ_L is much smaller than the single Debye relaxation time τ_D, and can be approximated by the ratio $\varepsilon_\infty/\varepsilon_0$ of high- and zero-frequency dielectric constants as below:

$$\tau_L \approx \left(\frac{\varepsilon_\infty}{\varepsilon_0}\right)\tau_D \qquad (6)$$

This approximation is often applied in experimental studies for correlating time-resolved emission spectra (TRES) shift time to the Debye relaxation time τ_D.[57,58,63-72]

In this thesis, the kinetic relationship between the initial and the final excited states has been discussed. In order to verify the multistate kinetic model, we have made the following comparisons in: (1) the decay times from the exponential fit of C(t); (2) the spectral shape parameters of TRES between the spectral reconstructed (SR) TRES and the simulated TRES. The agreement among these results provides clear evidence of the multistate kinetics. However, for the short-lived component (e.g., in 1-octanol), the *decay time* from the exponential fit of C(t) of both SR and simulated TRES, is different from *that* of the exponential fit of the time-dependent fluorescence decay TDFD. Such difference raises a question about the functional time-dependency of C(t). Therefore, the TRES $i(\upsilon_m,t)$ dependent $C(\upsilon_m,t)$ has been formulated according to the multistate model. In order to obtain the best-fit decay time of C(t), this TRES dependent $C(\upsilon_m,t)$ has been used to simulate the C(t) data of SR TRES, instead of using a multiexponential function, while the peak positions υ_m of SR TRES and the SR TRES at peak $i(\upsilon_m,t)$ are applied in the optimization. The values of the decay times from this optimization are closer to those of the exponential fitting of TDFD than those of the exponential fit of C(t).

1.2   **Photophysical Characteristics of Selected Organic Species**

For nearly three decades, there have been increasing interests in the determination of the microscopic polarity in both biological and non-biological systems using fluorescent probes.[79-85] In general, the probe molecule contains an electron donor (e.g., dialkylamino group) and an electron acceptor (e.g., nitro

group) attached on the same or linked aromatic ring. Presently, the factors affecting the Intramolecular charge transfer (ICT) of both emissive and non-emissive species are the subject of intense investigations.[57,58,71,72,79-102]

C460(C1)   C450(C2)   C480(C102)

C481(C1F)   C152(C311F)   C153(C102F)
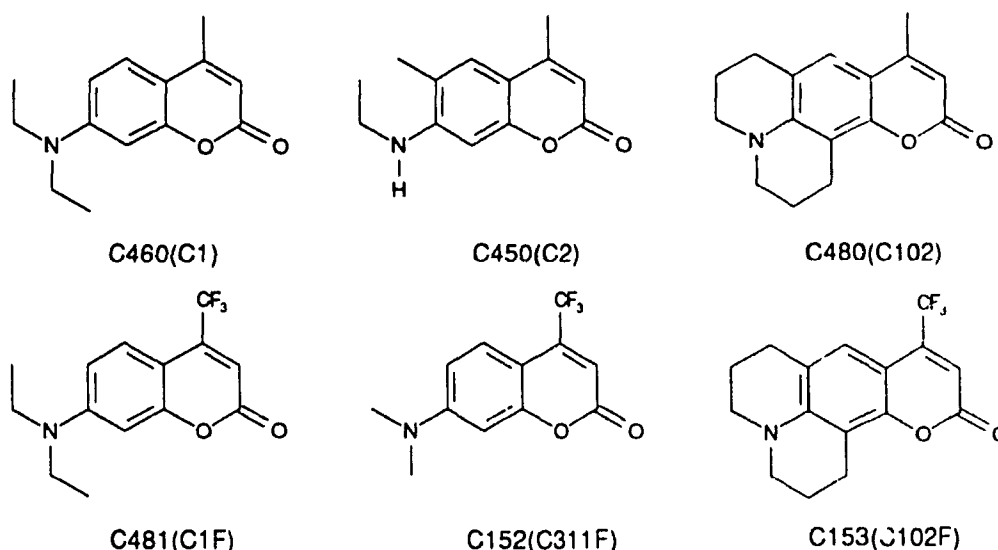
Fig. 1-1 Molecular Structures of 7-Aminocoumarins

Organic dyes (i.e., Rhodamines, oxazines, coumarins, etc.) used as probes are known as the members of the donor-acceptor family.[89] Among the vast number of dyes, the coumarin derivatives, especially, the alkylaminocoumarins with alkylamino (donor) and carbonyl (acceptor) groups on the two sides of the coumarin skeleton (Fig. 1-1), posses conformationally sensitive ICT state. Their photophysical properties (e.g., quantum yield) are very sensitive to the environment.[15,16,23-26,87-90,92-95,100] This photophysical behaviour affected as by structural and the environmental factors, has still not been satisfactorily interpreted. Especially, the effect of possible formation of the excited *twisted intramolecular charge transfer* (TICT) state,** is not directly

---

** The stable ICT state by twisting of the amino group due to full or partial charge separation between donor and acceptor. (details were given in Ref. 101-103)

observable in normal fluorescence spectra of 7-aminocoumarin dyes. Their fluoerscence spectra only show a single fluorescence band rather than dual fluorescence bands of the typical TICT compound (e.g., 4-Dimethylaminobenzonitrile, etc.).[101-103] The objective is to study the fundamental photophysical behaviour of selected coumarin dyes, with flexible or constrained amino group at the 7 position of the coumarin skeleton, in different environments using both static and dynamic spectroscopic techniques.

To understand the photobehavior of the real and complex system and its potential applications, it is necessary to investigate the structural, substituent, excited state conformationally and environmental electronic factors on the photophysical and primary photochemical processes of the model systems. The interpretation of these effects on chromophores (including probes) similar to the real system in complex environments, is surely helpful to get insight on the more complex system. For nitrobenzene derivatives (Fig. 1-2), interest in the photochemistry has grown considerably over more than three decades.[104] Nitrobenzene and substituted nitrobenzenes display a remarkably wide variety of photochemical reactions.[105] The photophysical
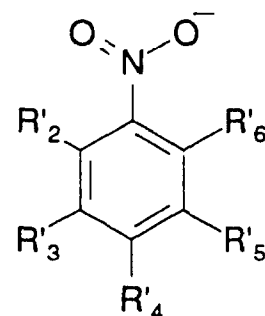
Fig. 1-2

properties of the nitro compounds have also been studied extensively[106] not only for photochemical reactivity and fundamental understanding of photophysics,[14] but also owing to the recently fast growing attention to the nonlinear optical (NLO) properties[107] for potential roles in optical storage and information processing.[108] In these applications, the excited state photobehaviour plays an extremely important role. In the second part of this thesis, photochemically rich but poorly understood excited state properties of

nonluminescent nitrobenzene derivatives (nitroaromatic systems) have been chosen to study the substituent, environmental factors on their excited states.

1.2.1 Aminocoumarin dyes

The importance of **aminocoumarins** as laser dyes and fluorescent probes for a wide spectral region has been recognized for more than two decades.[89] Recently, many investigators have focused on the role of the solvent in controlling the intramolecular charge transfer (ICT) process of these dyes;[87,88,90,92-94] the interaction of solvent-solute molecules, or the solute-impurity complexation;[16,26] and dipole-dipole interaction induced molecular relaxation of solvent (**solvation dynamics**[64-74]) as fluorescent probes.[57,58,74] With respect to characteristics of the conformationally sensitive 7-aminocoumarin dyes (see Fig. 1-1),[90,94] twisting of the flexible amino group at the 7 position on the coumarin ring could reduce the fluorescence quantum yield in more polar solvents due to formation of a nonradiative twisted intramolecular charge transfer (TICT)[90,92-95,100] state. The twisting angle of amino group at the 7 position depends on the charge transfer probability between amino group and carbonyl group on the coumarin skeleton.[94] Such characteristics have been applied to study the guest-host complexation of biologically important species such as cyclodextrins.[23-25,92,109]

1.2.2 Cyclodextrins and crown ethers

The growing significance of supramolecular chemistry has already been documented in a number of reviews[110-114] with early emphasis on the complexation of metal ions,[112,113] and on the noncovalent interaction between host and guest molecules.[110,114] The interaction between guest and host molecules can be classified into two categories: (i) ion-dipole interactions which

are the principle forces offered by crown ethers;[115] and (ii) hydrophobic interactions of cyclodextrins[116] and cyclophanes.[117] There are considerable number of studies on ground state host-guest interaction,[110-117] for applications in pharmacy, medicine, chemical analysis,[110] and chromatography,[118] as well as catalysis[119] and material science.[120] Recently, there is growing interest in the potential role of molecular recognition *in the excited state* in (i) biological systems,[121-123] (ii) optical storage and computing,[124] and (iii) optical sensors.[125,126]

Cyclodextrins (CDs) are cyclic oligosaccharides of 6-8 α(1-4) linked D-glucose units called α-, β- and γ-CD (Fig. 1-3), respectively. The most remarkable property of CD is its ability to form inclusion complexes with a great variety of guest molecules due to the hydrophobic character of CDs' cavity.[127] From the microscopic point of view, this can lead to
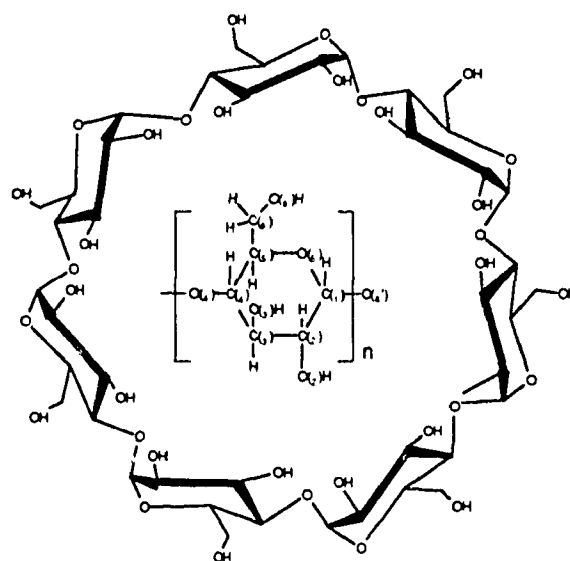
Fig. 1-3 Cyclodextrins

advantageous changes in chemical and physical properties on micro-encapsulation by CDs for: (i) fundamental studies in chemistry, biology and medicine;[22-25,109,110,128,129] (ii) industries like pharmacy, foodstuffs, plant protective agents and toilet articles.[130,131] The photophysical and photochemical behaviour of the complexes of CDs with guest molecules, has received considerable attention using both static and dynamic spectrophotometry[22-25,59,60,109,129-133] owing to their potential roles in

13

various areas. The time-resolved spectroscopies offer more detailed information about the complexation either qualitatively or quantitatively.[59,60,134]

Crown ethers (cyclic ether) are potentially exolipophilic compounds which can selectively complex with alkali and alkaline earth metal cations in their endopolarophilic cavities.[135] Efforts to modify the widely useful properties[136] of such crown ethers (Fig. 1-4) by variation of all possible structural parameters have continued in order to make accessible new ligand systems, and to study the relationship between structure and cation selectivity as well as their complex chemistry.[137] The selectivity of binding to different cationic species is thus determined by both the nature of the electronic interactions and the ability of the crown ether to adopt specific conformations that maximize these energetic interactions between the macrocyclic polyether oxygen ligands and the substrate.[136] Recently, the complexation by crown ether binding of organic ammonium cations has been reported both experimentally and computationally.[138-140] Such crown molecules could serve as separating agents for biologically active amino hormones that have very similar structures as suggested by Lehn.[141]
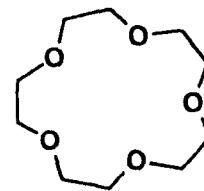
Fig. 1-4 15-CW-5

1.2.3   Nitrobenzene derivatives

Almost 35 years ago, Nagakura's group ascribed the solvent polarity dependent electronic absorption band of nitrobenzene to the excited intramolecular charger transfer (ICT) state.[142] This ICT is formed by an electron transfer from the benzene ring (Donor) to the nitro group (Acceptor).[142c] The nitrobenzene derivatives are well known to be nonluminescent due to the fast singlet-triplet intersystem crossing.[143] The

influences of structural, substituent, and environmental electronic factors on the photobehaviour of nitrobenzene derivatives have been studied for more than three decades.[142-151] For nitrobenzene derivatives,[144] the effect of the substituent is to change the ionization potential (IP) of the ring (donor) and therefore the energy of the CT state.[14] Apparently, the CT state is very sensitive to the polarity of solvent. Additional to the observable *effect of the solvent polarity* on the ground state absorption of alkylnitrobenzenes,[142] the lower excited triplet solvated state of 4-nitro-4'-methoxystilbenes in different solvents was found to be a charge transfer state by ESA spectroscopy.[145] Experimentally, (i) we observe the *static* blue-shift of the triplet ESA spectra of two dimethoxynitrobenzenes in different solvents; (ii) in alcohols, we find a remarkably *dynamic* blue-shift of the ESA 'red' band in picosecond time region. The rate constant of the *dynamic* blue-shift of the triplet ESA band depends on the solvent but not on the probe molecues. It is comparable to $1/\tau_L$ in which τ_L is the longitudinal relaxation time of the solvent as mentioned before.

In the infrared absorption study, the oscillator strength, and the position of the absorption band of the symmetric and asymmetric stretching modes[106] (Scheme 1-3) of the nitro group showed a dependence on the other substituents, the position of the substituent on the nitrobenzene ring, and the dipole moment of the molecule.[146] Within the framework of the Herzberg-Teller model, the ground state vibrational frequency can be applied to identify the excited vibronic interaction under certain approximations. The validity of this application was verified in the study of the phosphorescence spectrum of benzene which is particular rich in vibronic
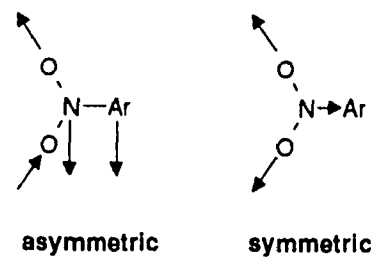
asymmetric   symmetric

Scheme 1-3

structure.[147] Indeed, the resonance interaction of nitro group in the excited triplet state was observed in ESA study of p-nitroaniline.[148] In comparison to the triplet ESA spectrum of aniline which only shows a '*blue*' ESA band[149] characteristic of locally excited benzene ring, the '*red*' ESA band of p-nitroaniline is more like the locally excited nitro group. Therefore, the assignment of the structure on ESA '*blue*' band of p-nitroaniline to the symmetric stretching of NO_2 is arguable.

In this thesis, similar to p-nitroaniline, structured ESA spectra are observed for the most of alkylnitrobenzenes. The spectral shapes of these ESA spectra appear to be affected by the numbers and position of the substituent on the nitrobenzene ring, and/or the polarity of solvent. The fine structure on the ESA bands appears to reflect excited state vibronic interaction. The frequency spacing of these coupled fine structures is similar to the frequency of the ground state vibronic modes of NO_2 or benzene.

In contrast with the above-mention nitrobenzenes, the o-nitrobenzenes are photochemically active owing to the benzylic hydrogens. The general photoreactivity of o-nitrobenzyl systems with intramolecular hydrogen abstraction has attracted considerable attention for development of photochromic compounds and photolabile protecting groups,[152] in which a biradical species has been implicated as intermediate in the photochemical process.[153] Therefore, the detection of the biradical appears to be a key step to obtaining insight into the photochemical process in order to control the photochemical reaction.[45] In this project, the biradical intermediate is identified during the picosecond laser absorption investigation of o-nitrobenzyl p-cyanophenyl ether (ONBCPE) in acetonitrile. We have obtained some valuable information about

the partitioning between the singlet and triplet pathways during the photochemical reaction.[154]

1.3   Organization of this thesis

Following the review of the present studies related to this project, Chapter 2 focuses mainly on the kinetic correlation between the ASE gain spectra and the fluorescence spectra from the 7-aminocoumarin C1. In Chapter 3, the photophysical behaviour (ESA and AE) of 7-aminocoumarin dyes and their guest-host complexes with β-CD in different solvents has been investigated. In Chapter 4, the study of *static solvation* using these dyes, especially in binary solvents is presented. From dynamic shifts of TRES of the 7-aminocoumarins in 1-butanol and 1-octanol, in Chapter 5, a multi-state kinetics in the dynamic solvation process is discussed, and gives a more reasonable interpretation of the experimental results than that of the single state model of continuous solvent relaxation.[58,59,65-72] In Chapter 6, the following topics are discussed: (i) the solvation related *static* and *dynamic* ESA shift of dimethoxynitrobenzenes in different solvents, and the preliminary test of the salt effect[135,136] on ESA of 4'-nitrobenzene-15-CW-5; (ii) the substituent and solvent effects on photophysical properties of nitrobenzene derivatives; (iii) the identification of the biradical of *o*-nitrobenzyl derivatives in acetonitrile.

Chapter 2: NOVEL AMPLIFIED SPONTANEOUS EMISSION (ASE) GAIN SPECTROSCOPIC STUDiES of EXCITED STATE COMPLEXATION in COMPARISON with CONVENTIONAL SPECTROFLUORIMETRY

2.1 Introduction

Since the 1960's, spectrofluorimetry has been widely applied to study excited state molecular complexation in both biological and chemical systems.[8-10,17-27] Although highly sensitive, conventional spectrofluorimetric measurements on molecular complexes in solution often lack spectral resolution on the intrinsic emission spectra and thus, in order to resolve the overlapping fluorescence bands into their components, extremely precise measurements and assumptions regarding the shapes of the component bands are necessary. By contrast, the bands from amplified spontaneous emission (ASE) gain spectroscopy introduced by Silfvast et al.,[28,29] are intrinsically narrower than those of the corresponding fluorescence emission. This is because of the laser characteristics of the probe molecule (i.e., laser dye). Since the 1970's, ASE spectroscopy has been used almost exclusively to study the fundamental characteristics of lasers.[29-36] In this chapter, the possibility of applying the ASE spectroscopic technique to resolve normally heavily overlapping bands in conventional fluorescence spectra due to 'free' and complexed dyes or dyes in heterogeneous environment, will be considered.

Towards this end, we have set up the ASE gain spectroscopic system to (i) establish a relationship between a constant derived from ASE gain

measurements and the Stern-Volmer constant[14] for fluorescence quenching or ground state complexation constant from uv/vis absorption study, and (ii) carry out ASE gain measurements on weakly bound complexes comprising excited state 7-diethylamino-4-methylcoumarin (C1) in solvent systems containing either dichloromethane or n-butyl acetate as co-solvents. In these solvent systems, steady state fluorescence spectra show no or extremely small frequency shifts with added concentrations of the co-solvents. The clearly resolved bands observed in the ASE gain in the same systems demonstrate the superior frequency resolution of the method.

2.2   Experimental Section

Three different spectrometers were used: (i) a system to measure the ASE gain; (ii) a uv/vis absorption spectrophotometry; and (iii) a spectrofluorimetry. All the experimental measurements were carried out at Département de Chimie, Université du Québec à Montréal.

2.2.1   ASE gain spectroscopic system

The ASE was generated using a 337 nm laser beam from a PRA LN100 N$_2$ laser ($E_p \approx 60$ μJ, pulse width ≈ 0.3 ns, $W_p \approx 200$ kW) which was focused through a 2" focal length quartz cylindrical lens to transversely excite dye solution contained in an upright 1 cm rectangular 4-window quartz fluorescence cell. The ASE through a 0.8 mm pin-hole was detected using a JY HR 320 monochromator and a silicon diode array/optical multichannel analyzer OMA (EG&G 1412F/1461) system. A sharp cut-off filter (Schott, KV-375) was placed in front of monochromator to protect the detector from uv light including the excitation beam, as illustrated in Fig. 2-1. The size of the excitation beam focused on the cell without an excitation slit, is ~10.0mm (length) x 1.0 mm
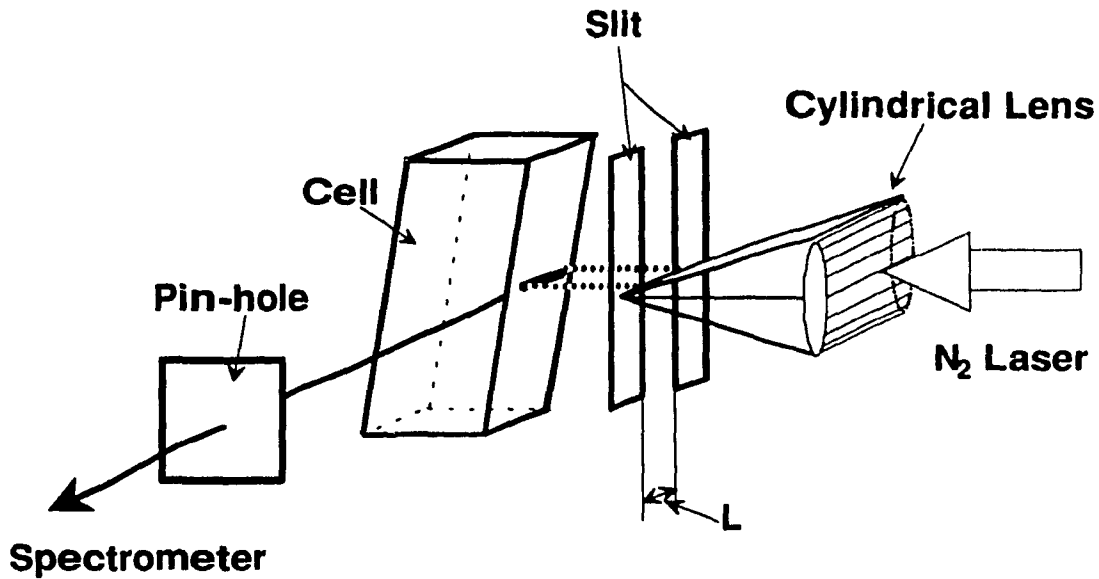
Fig. 2-1 ASE gain spectroscopic system

(width). The upright angle of the cell is set ~ 3 ° to reduce the interference of reflection beams. The entrance slit width of the monochromator is set at 50 μm. The high voltage supply of the PRA LN 100 N_2 laser is set at 16.0 kV under pressure of the pure N_2 of 30 psi. Digital data from the EG&G 1461 detector interface was collected and analyzed using an IBM AT connected to the 1461 interface unit via the first serial port (COM1). To avoide damage from moisture
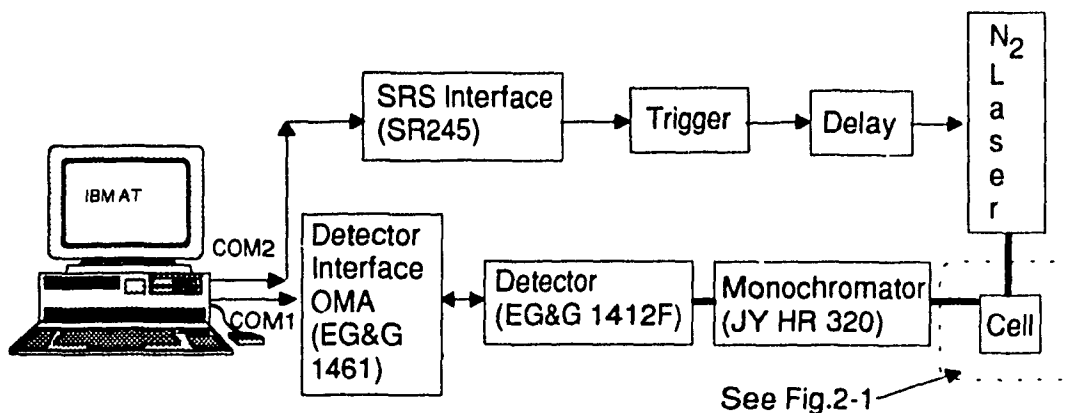
Fig. 2-2 Control diagram of the ASE gain spectroscopic system

on the detector at low temperature, the vacuum of the detector unit (EG&G
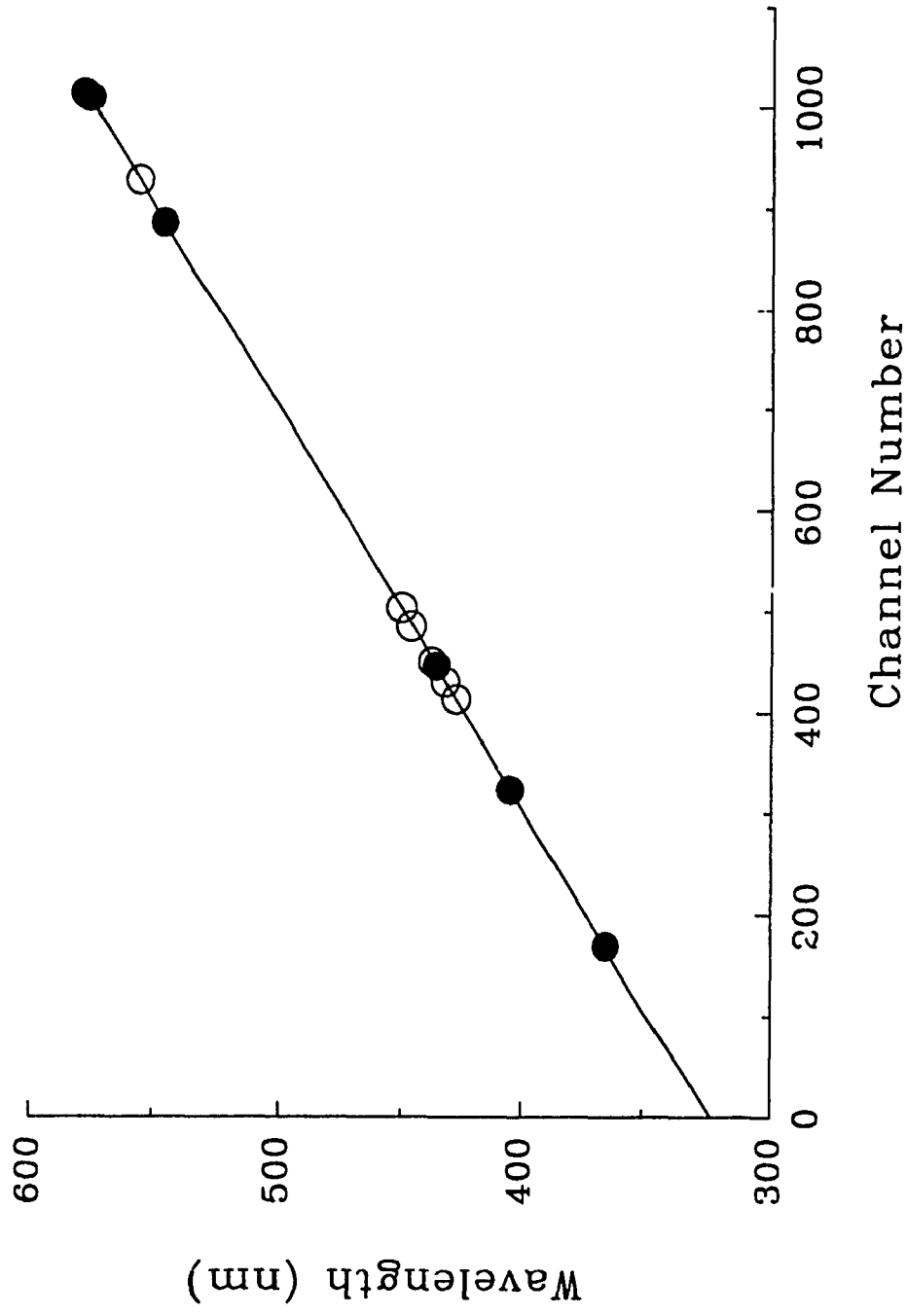
Fig. 2-3   Channel Numbers vs. Wavelengths of Hg (●) and Kr (O) lines used for calibrating OMA

22

In order to obtain the ASE gain spectra, the following equation can be applied to calculate the ratio ($R = I_L(\lambda)/I_{2/3L}(\lambda)$, or $R = I_L(\lambda)/I_{1/2L}(\lambda)$) of the average ASE spectra $I_L(\lambda)$ and $I_{2/3L}(\lambda)$ or $I_{1/2L}(\lambda)$ with full (L=3.6 mm) and partial (2/3L=2.4 mm or 1/2L=1.8 mm) excitation slit width (refer to Appendix A):

$$I_L(\lambda) = \frac{\Pi}{G(\lambda)}\left(e^{G(\lambda)L} - 1\right)$$

$$G(\lambda) = \begin{cases} \dfrac{2}{L}\ln(R-1) & \left(R = I_L/I_{(1/2)L}\right) \\[2mm] \dfrac{3}{L}\ln\left\{\dfrac{1}{2}\left[(R-1) + \sqrt{(R-1)^2 + 4(R-1)}\right]\right\} & \left(R = I_L/I_{(2/3)L}\right) \end{cases} \tag{1}$$

where Π is a wavelength dependent parameter including the instrumental response function which is independent of the excitation slit width and can be cancelled from the ratio of the ASE spectra with different excitation slit width.

In order to protect the detector, the counts of the ASE have to be kept less than 15,000 using different neutral density filters (ON series of Polaroid) in the visible region. The uv/vis absorption spectra of these filters measured on Cary 2200 spectrophotometer, are shown in Fig. 2-4. The fit functions of these absorption spectra were used in the program SDAGF for calculating the corrected ASE spectra.

2.2.2   UV/Vis absorption spectrophotometry and spectrofluorimetry

Most uv/vis absorption spectra were measured on the double-beam Cary 2200 spectrophotometer (Varian). The baselines of the spectra were obtained from the absorption difference between the two quartz cells (1 cm) filled with solvent which were allowed to thermally equilibriate for at least a half hour before the measurement. Then, the sample measurements can be obtained using program PCCONT on an interfaced IBM pc/2 computer, in which the baseline
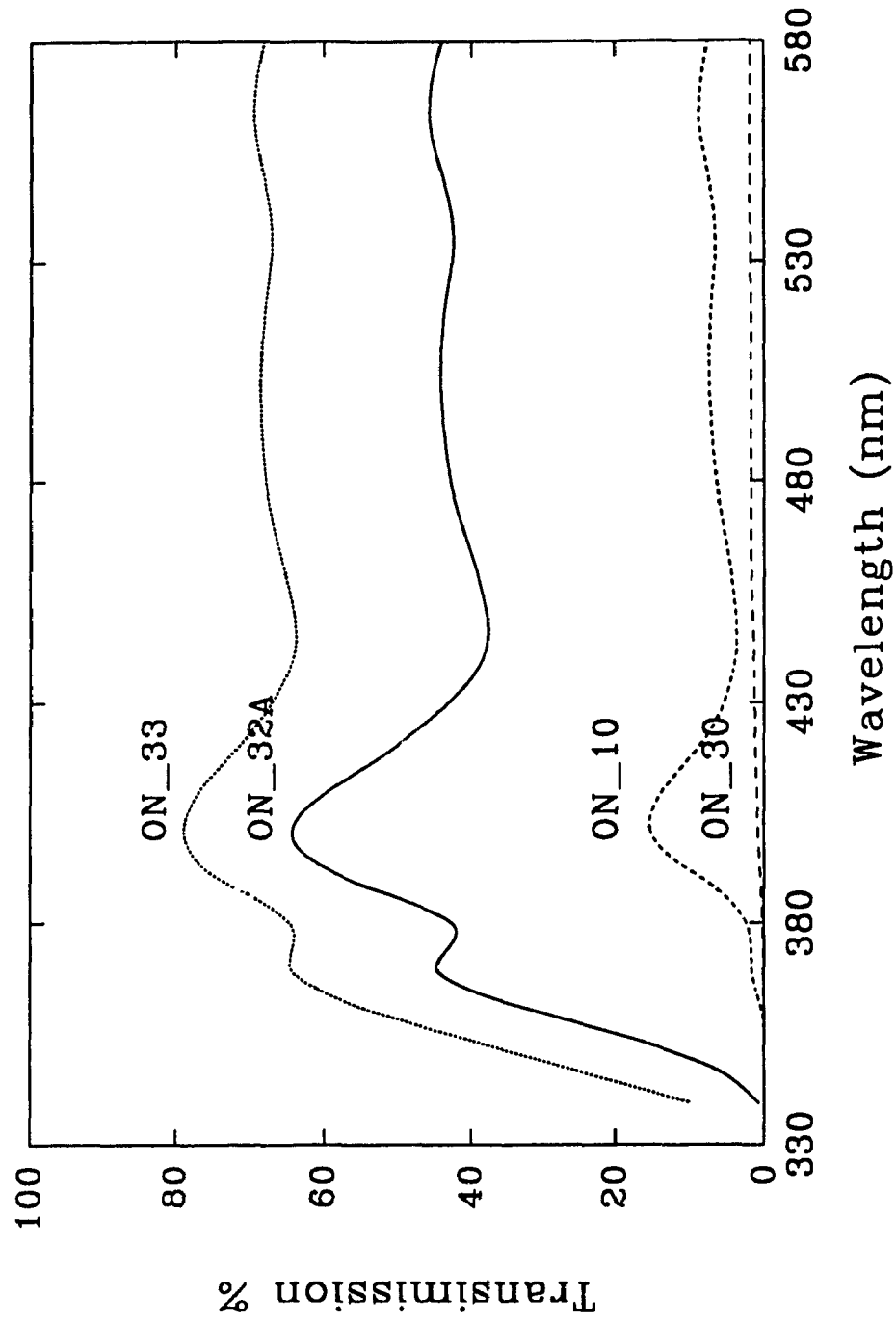
Fig. 2-4　Transmission spectra of Neutral Density Filters (ON series)

can be automatically subtracted from the spectrum (details see Operation

Manual of Cary 2200). In order to avoid the nonlinear effect due to saturation,

the maximum optical density (OD) of the solution in the 1 cm quartz cell, is kept

in the range 0.8~1.2 for quantitative analysis. Additionally, while the Cary 2200

was occupied, some uv/vis absorption measurements were done on a Pye

Unicam PU8800 (Phillips, double beam), PU8600 (Phillips, single beam), and

Beckman DU-8 (Beckman, single beam) uv/vis spectrophotometers.

The fluorescence spectra were measured using an MPF-44 (Perkin-

Elmer) fluorescence spectrophotometer with a xenon lamp. The typical

experimental conditions are listed in Table 2-2:

Table 2-2   Experimental condition of MPF-44 spectrophotometer

	Mode	Excitation		Emission	
Measurement	Energy	Slit (nm)	Scan (nm/min)	Slit (nm)	Scan (nm/min)
Wavelength Drive	Single	2.5	60	2.5	60
Photometric	AC	Dynode Voltage (V)		Dynode Voltage (V)	
Manual Dynode Voltage	Int	950		750	

The spectra were recorded using a Perkin-Elmer 56 recorder. The recording

rate is varied with the spectral scanning rate of excitation or emission. Details

can be found in the MPF-44 spectrophotometer operation manual. The stability

(~1%) of this spectrophotometer is sensitive to the instrumental sensitivity and

time. For the quantitative analysis, the reference spectrum (pure solution

without any additional species) was measured before measuring the spectrum of the solution with additional species. The concentrations of the solute in the reference and samples are the same. The emission spectra have not been calibrated with standard solution with similar spectral coverage (300 ~ 400 nm for excitation and 400 ~ 600 nm for emission) (e.g., quinine sulphate in H_2SO_4),[8] because the study of the complexation involves changes in magnitude of the spectra only at a specific wavelength.

2.2.3 Absorption and fluorescence titration

To study the complexation of either ground or excited state, systematic changes in the concentration of the added species were done using titration technique. This involves adding a certain amount of the species Q_A into one container with known volume of the stock solution B to prepare solution A ($[Q_A^0]$). The concentrations of the solute Q_B in both solutions are the same ($[Q_B]$). Then, a series of spectra can be obtained by measuring samples with different concentrations of the species A, but the same concentration ($[Q_B]$) of the solute B by adding different volumes (v_i, i=1..n) of solution A into the cell with initial volume (V_B). Thus, the concentration $[Q_A^n]$ of the species A after the nth (n≥1) dose satisfies:

$$[Q_A^n] = \frac{\sum_{i=0}^{n} v_i}{V_B + \sum_{i=0}^{n} v_i}[Q_A^0]$$

while the solute concentration is kept the same ($[Q_B]$).

2.2.4 Chemicals

n-Butyl acetate (nBuOAc) (Fisher reagent), and acetonitrile (Caledon

distilled in glass) were refluxed over CaH_2 for 1 h and distilled under high purity nitrogen flow. 1-Butanol (Fisher Certified A.C.S.), chloroform ($CHCl_3$) (Accusolv distilled in glass), dichloromethane (CH_2Cl_2) (Anachemia spectro), chlorobenzene (C_6H_5Cl) (Aldrich 99%), and 2,2,4-trimethylpentane (iso-octane) (Matheson Coleman & Bell spectro), cyclohexane (C_6H_{14}) (OmniSolv distilled in glass), methanol (Accusolv distilled in glass) have been used without further treatment. Preliminary studies of the ASE of coumarin-1 in untreated and CaH_2-treated dichloromethane gave, in contrast with nBuOAc, identical results.

Among the coumarin dyes illustrated in the previous section, the 7-diethylamino- 4-methylcoumarin (C1, C460) (Exciton) was recrystallized from methanol-water and sublimed; 2,3,5,6-1H,4H-tetrahydro-8-methylquinolazino [9,9a,1-gh] coumarin (C102, C480) (Exciton), and 7-diethylamino-4-trifluoromethylcoumarin (C1F, C481) (Eastman Kodak), were recrystallized from methanol; the 7-ethylamino-4,6-dimethylcoumarin (C2, C450) (Exciton) was used as received.

The glassware used for distillation were heated at 140 °C for at least 12 hours in the oven. Only the intermediate fraction of the distilled solvent was used to prepare the sample. The recrystallization was done by dissolving the dye into warm ($\sim$ 60 °C < the melting point of dye) alcohol or alcohol/water mixture to make a saturated solution. The clear saturated solution was transferred into another container through a filter paper at the same temperature. Then the crystallization occurred gradually as the temperature decreased. In order to gain more product, the temperature was dropped to $\sim$ 10 °C lower than the room temperature using a thermoelectric cold plate (TCP-2 of Thermoelectric Unlimited Inc.). The crystals were washed several times using pure alcohol at the same temperature, and were air dried on filter paper. The

residual moisture on the crystals was removed under vacuum. To avoid contamination from the pump oil, the pumping tube was passed through a cold trap using solid CO_2 before connecting to the container with the crystals. A microsublimation apparatus (Fisher) was used to sublime small amounts of dyes. Since the vapor pressures of these dyes are very low under 1 atm. pressure, the sublimation was done under vacuum (~0.1 torr).

2.3 Steady state fluorescence and ASE gain kinetics

2.3.1 Fluorescence quenching

For a normal two-component system, the ratio of fluorescence intensity at wavelength λ with and without quencher ($I(\lambda)$ and $I^\circ(\lambda)$ respectively), can be considered as the sum of two contributions from the free (A^*, B^*) and complexed species (refer to Scheme 2-1):

Scheme 2-1

$$I(\lambda)/I^\circ(\lambda) = \Phi_a/\Phi^\circ_a + \beta(\lambda)\,(\Phi_b/\Phi^\circ_b) \qquad (2)$$
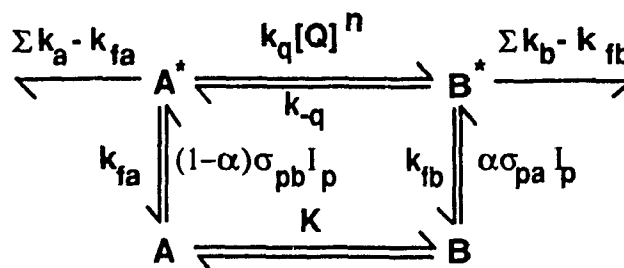
where Φ_i and Φ°_i (i= a or b), are the quantum yields with and without quencher (of free or complexed species respectively), and $\beta(\lambda)$ is the ratio of the intensity when the solvent has been completely replaced by quencher to that in neat solvent. In the far blue region shown in Fig. 2-5, the contribution of the complex can be eliminated ($\beta(\lambda) \rightarrow 0$). Thus, the intensity ratio in eq. (2) can be simply replaced by the quantum yield ratio of the free species, which should satisfy eq. (3):[13-16]

$$I(\lambda)/I^{\circ}(\lambda)=\Phi_a/\Phi^{\circ}_a = (1-\alpha)/(1+K_{SV}[Q]^n) \qquad (3)$$

where α is the fraction of the incident light absorbed by ground state complex **B** and satisfies:[13-16]

$$\alpha = K[Q]^m/(\sigma_{pa}/\sigma_{pb}+K[Q]^m) \qquad (4)$$

In eq. (4), $\sigma_{pi}(\lambda_p)$ (i=a,b) are the absorption cross sections of species **A** and **B**, and λ_p is the pumping (excitation) wavelength, and K_{SV} is the Stern-Volmer constant[14] defined by:

$$K_{SV} = k_q\tau_a/(1 + k_{-q}\tau_b) \qquad (5)$$

where τ_a, τ_b are the lifetimes of excited 'free' and complexed species defined as the reciprocal of Σk_a and Σk_b, respectively, and K, k_q and k_{-q} are the equilibrium and kinetic constants illustrated in Scheme 2-1; m and n are the stoichiometries of ground and excited state complexes, respectively.

2.3.2   Gain coefficient

The small-signal ASE gain is proportional to the population of the excited state as described in eq. (6):[29,35]

$$g(\lambda,t) = \sigma_e(\lambda)N(t) - g_{ai}(\lambda,t) \qquad (6)$$

where $\sigma_e(\lambda)$ is the stimulated emission cross section, N is the population of the fluorescing state, and g_{ai} is the sum of possible losses due to the internal transitions between excited singlet-singlet and triplet-triplet states. In view of the location of the singlet-singlet absorption band[100] and the near-unity quantum yields of coumarin-1 in aprotic and moderately polar protic solvents,[87,88,90,94] the gain of coumarin-1 in aprotic (iso-octane, nBuOAc, and CH_2Cl_2) or
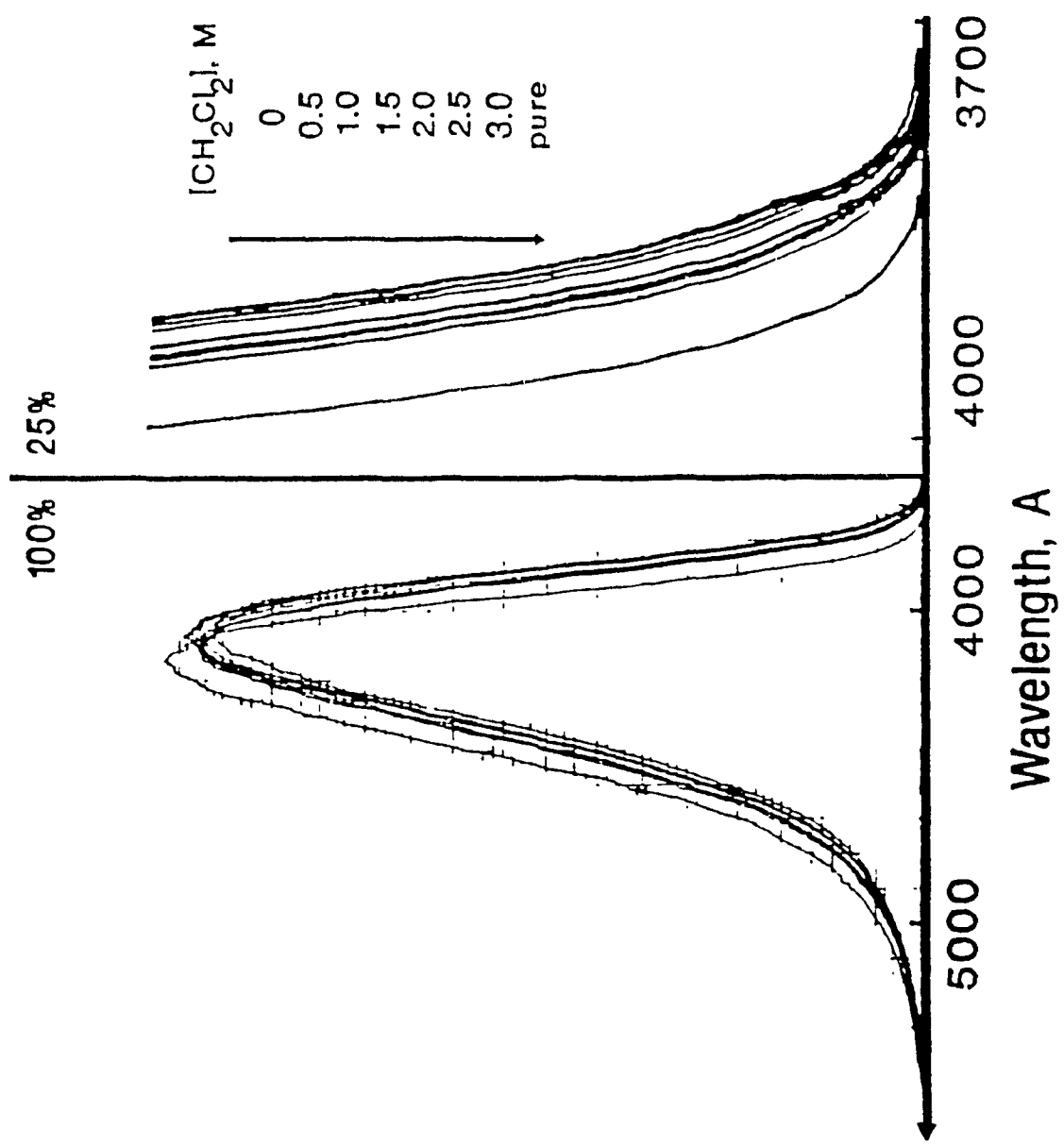
Fig. 2-5 Fluorescence spectra (excited at 361.2 nm) of C1 (0.035 mM) in nBuOAc containing different amounts of CH_2Cl_2 (0 to 3.0 M), and in pure CH_2Cl_2 at room temperature; right part is the expanded spectra from 3700 Å to 4000 Å.

moderately polar protic (nBuOH) solvents can be approximated by eq. (7):

$$g(\lambda,t) = \sigma_e(\lambda)N(t) \tag{7}$$

The experimentally observable ASE gain in eq. (1) is the integral of eq. (7) with respect to the exposure time of the detector as expressed below:

$$G(\lambda) = \int_0^\infty g(\lambda,t)dt = \sigma_e(\lambda)\int_0^\infty N(t)dt \tag{8}$$

The ASE gain ratio of excited state species B^* and A^* can be simply represented by:

$$R_g = G_b(\lambda_b)/G_a(\lambda_a) \tag{9}$$

$$= [\sigma_{eb}(\lambda)/\sigma_{ea}(\lambda)]\int_0^\infty [B^*(t)]dt/\int_0^\infty [A^*(t)]dt = [\sigma_{eb}(\lambda)/\sigma_{ea}(\lambda)] R_p$$

where σ_{ei}, (i=a,b) are the stimulated emission cross sections of species A^* and B^*, respectively, R_p is the ratio of the maximum population of species B^* and A^*.

2.3.3   Relationship between R_g and K_{SV} or K

The gain ratio (R_g) determined from ASE gain experiments is proportional to the ratio (R_p) of the integral populations as described in eq.(9). On the basis of the kinetics illustrated in Scheme 2-1, the differential populations of A^* and B^* with respect to time can be expressed by the following equations:

$$\begin{cases} \dfrac{d[A^*]}{dt} = (1-\alpha)I_p + k_{-q}[B^*] - \left(\sum k_a + k_q[Q]^n + \sigma_{ea}I_{ea}\right)[A^*] \\[3mm] \dfrac{d[B^*]}{dt} = \alpha I_p + k_q[Q]^n[A^*] - \left(\sum k_b + k_{-q} + \sigma_{eb}I_{eb}\right)[B^*] \end{cases} \tag{10}$$

where $[A^*]$, $[B^*]$ are the population of excited states; σ_{ei} (i=a,b) are the stimulated cross sections of species A and B; I_p and I_{ei} (I_p dependent) are the

pumping photon rate per area, and stimulated emission photon rate per area of species A^* and B^*; and the rest of the terms are defined in Scheme 2-1.

2.3.3.1 Excited state equilibrium pumping at threshold ($I_{ei} \rightarrow 0$, i=a,b)

Under transient conditions corresponding to excitation at t = 0 by a δ-function laser pumping of negligible duration,[155] which is valid for the short duration N_2 laser ($\tau_p \approx 300$ ps) in comparison to the lifetimes of fluorescence species ($\tau_i \approx 3$ ns), a zero pumping rate per area ($I_p = 0$) in the equation set (10) can be assigned for t > 0. Therefore, the equation set (10) can be simplified by eliminating the first terms and the stimulated emission (I_{ei}, i=a,b) as follows:

$$\begin{cases} \dfrac{d[A^*]}{dt} = k_{-q}[B^*] - k_1[A^*] \\ \dfrac{d[B^*]}{dt} = k_q[Q]^n[A^*] - k_2[B^*] \end{cases} \qquad (11)$$

where the coefficients: $k_1 = \Sigma k_a + k_q[Q]^n$; $k_2 = \Sigma k_b + k_{-q}$.

From eq. (11), the population of species B^* can be represented by the population of species A^* as follows:

$$[B^*] = (d[A^*]/dt + k_1[A^*])/k_{-q} \qquad (12)$$

Introducing the first-order derivative of eq. (12) with respect to time into eq. (11), and replacing $[B^*]$ in eq. (11) by eq. (12), the simple second-order differential equation of $[A^*]$ with respect to time is given by the following equation:

$$d^2[A^*]/dt^2 + B\, d[A^*]/dt + C\,[A^*] = 0 \qquad (13)$$

where $B = k_1 + k_2$, $C = k_1 k_2 - k_{-q} k_q[Q]^n$.

Since $B^2-4C = (k_1 - k_2)^2 + 4k_{-q}k_q[Q]^n > 0$, the population of species A^* can be solved from eq. (13) as:[156]

$$[A^*] = C_1 \exp(-s_1 t) + C_2 \exp(-s_2 t) \tag{14a}$$

where C_1, C_2 are the constants that can be found by considering the initial conditions (will be discussed later), the parameters $s_{1,2}$ are:

$$\begin{aligned} s_1 &= 0.5\left[B - \sqrt{B^2 - 4C}\right] \\ s_2 &= 0.5\left[B + \sqrt{B^2 - 4C}\right] \end{aligned} \tag{14b}$$

and the B, C are defined in eq. (13).

With eq. (12) and eq. (14), the population of species B^* can be expressed in the form of

$$[B^*] = [(k_1 - s_1)C_1 \exp(-s_1 t) + (k_1 - s_2)C_2 \exp(-s_2 t)]/k_{-q}. \tag{15}$$

Under the transient conditions, the initial populations of both species ($[A^*(0)]$, $[B^*(0)]$) excited by a δ - function laser pulse at $t = 0$, can be presented by:

$$[A^*(0)] = (1 - \alpha)I_0 \tag{16a}$$
$$[B^*(0)] = \alpha I_0 \tag{16b}$$

By introducing the initial conditions (eq. (16)) into eqs. (14) and (15), we get

$$[A^*(0)] = C_1 + C_2 = (1 - \alpha)I_0 \tag{17a}$$
$$[B^*(0)] = [(k_1 - s_1)C_1 + (k_2 - s_2)C_2]/k_{-q} = (1 - \alpha)I_0 \tag{17b}$$

Replacing C_2 in eq. (17b) by eq. (17a), and dividing the non-zero common factors of C_1 in both sides, the constants $C_{1,2}$ can be obtained:

$$C_1 = [k_{-q}\alpha - (k_1 - s_2)/(1 - \alpha)]I_0/(s_2 - s_1), \qquad (18a)$$

$$C_2 = [(k_1 - s_1)(1 - \alpha) - k_{-q}\alpha]I_0/(s_2 - s_1). \qquad (18b)$$

Since the experimental observable ASE gain ratio R_g is proportional to the ratio of the integral populations of species $\mathbf{B}^*$ and $\mathbf{A}^*$ as described in eq. (9), the integral populations of both species, which can be solved from eqs. (14), (15), and (18), are as follows:

$$
\begin{cases}
\int_0^\infty |A^*|dt = \int_0^\infty \left(C_1 e^{-s_1 t} + C_2 e^{-s_2 t} \right)dt = \dfrac{I_o}{P}\left[ak_{-q} + (1-a)k_2 \right] \\[3mm]
\int_0^\infty |B^*|dt = \int_0^\infty \left((k_1 - s_1)C_1 e^{-s_1 t} + (k_1 - s_2)C_2 e^{-s_2 t} \right)/k_{-q}\,dt \\[3mm]
\qquad\quad = \dfrac{I_o}{P}\left[(1-a)k_q[Q]^r + ak_1 \right]
\end{cases}
\qquad (19)
$$

Therefore, the gain ratio can be derived from eqs. (9) and (19) as:

$$R_g = (\sigma_{eb}/\sigma_{ea})\{\alpha k_1 + (1-\alpha)k_q[Q]^n\}/[(1-\alpha)k_2 + \alpha k_{-q}], \qquad (20)$$

where $k_{1,2}$ are defined in eq. (11).

(i)   Excited state complexation at $\alpha \to 0$ (or $K \to 0$).

For the dynamic quenching process, the ASE gain ratio R_g in eq. (20) can be simply expressed by:

$$R_g = (\sigma_{eb}/\sigma_{ea})k_q[Q]^n/k_2 = (\sigma_{eb}/\sigma_{ea})k_q[Q]^n/[\Sigma k_b + k_{-q}] \qquad (21a)$$

$$\quad = (\sigma_{eb}/\sigma_{ea})(\tau_b/\tau_a)K_{SV}[Q]^n = K_{ASE}[Q]^n$$

where $k_{1,2}$ have been replaced by the terms $\Sigma k_a + k_q[Q]^n$, and $\Sigma k_b + k_{-q}$,

respectively. Hence the K_{ASE} obtained from ASE gain measurement is related to the Stern-Volmer constant K_{SV} (defined in eq. (5)) by:

$$K_{ASE} = (\sigma_{eb}/\sigma_{ea})(\tau_b/\tau_a)K_{SV} \qquad (21a)$$

where $\tau_i = 1/\Sigma k_i$, $(i = a, b)$ are the lifetimes of species $\mathbf{A}^*$, and $\mathbf{B}^*$.

(ii)   Ground state complexation only

By ignoring the excited state complexation (dynamic quenching process) ($k_q[Q]^n \ll \alpha\Sigma k_a$, $k_{-q} \ll (1-\alpha)\Sigma k_b$), the ASE gain ratio can be obtained from eq. (20) by eliminating the terms with $k_q[Q]^n$ and k_{-q}, as expressed by the following equation:

$$R_g = (\sigma_{eb}/\sigma_{ea})\alpha k_1/[(1-\alpha)k_2] = (\sigma_{eb}/\sigma_{ea})(\Sigma k_a/\Sigma k_b)\,\alpha/(1-\alpha)$$

$$= (\sigma_{eb}/\sigma_{ea})(\sigma_{pb}/\sigma_{pa})(\tau_b/\tau_a)K[Q]^m = K_{ASE}[Q]^m \qquad (22a)$$

where $\alpha/(1-\alpha)$ has been replaced by the terms of $(\sigma_{pb}/\sigma_{pa})K[Q]^m$ from eq. (4). Therefore, the K_{ASE} constant obtained from ASE gain measurement can provide information about the ground state complexation by:

$$K_{ASE} = (\sigma_{eb}/\sigma_{ea})(\sigma_{pb}/\sigma_{pa})(\tau_b/\tau_a)K \qquad (22b)$$

where K is the ground state complexation constant with stoichiometry m.

2.3.3.2   Effect of pumping intensity

In the above discussion, the pumping intensity effect[17-21] represented by the stimulated emission rates (I_{ea}, and I_{eb}) in equation set (10) was not considered. Since the stimulated emission rate (I_{ea} or I_{eb}) is a function of the excited state population as well, the solution of the equation set (10), which could only be solved numerically, is very complicated. However, for moderate

pumping intensity with a small perturbation on the excited state population, the excited state population can be assumed constant. Therefore, the solution to the moderate pumping case can be found by derivations similar to those used for the threshold pumping case, except that the coefficients $k_{1,2}$ in eqs. (11)-(20) are now given by:

$$k_1 = \Sigma k_a + k_q[Q]^n + \sigma_{ea}I_{ea} \tag{23a}$$

$$k_2 = \Sigma k_b + k_{-q} + \sigma_{eb}I_{eb} \tag{23b}$$

instead of those in eq. (11).

As the pumping intensity is increased above the threshold value (W_{th}), the stimulated emission will compete with spontaneous emission and radiationless deactivation of species A^* and B^*, which leads not only to a shortening of the decay time but also to strengthen the non-exponential decay.[18] For the purpose of extrapolation to the K_{ASE} at the pumping intensity threshold value, $K_{ASE}(W_{th})$, eq. (20) can be simplified for the dynamic quenching process ($\alpha \rightarrow 0$):

$$R_g = (\sigma_{eb}/\sigma_{ea})k_q/k_2 \, [Q]^n = K_{ASE}[Q]^n \tag{24a}$$

Here the K_{ASE} constant obtained from ASE gain measurement can be described by:

$$
\begin{aligned}
K_{ASE} &= (\sigma_{eb}/\sigma_{ea})(k_q/k_2) \\
&= (\sigma_{eb}/\sigma_{ea})k_q/(\Sigma k_b + k_{-q} + \sigma_{eb}I_{eb}) \\
&= (\sigma_{eb}/\sigma_{ea})(1 + k_{-q}\tau_b)/(1 + k_{-q}\tau_b + \sigma_{eb}I_{eb})K_{SV}
\end{aligned} \tag{24b}
$$

Since the stimulated emission $\sigma_{eb}I_{eb}$ is pumping intensity dependent, eq. (24b) can be expressed in the simple form of:

$$K_{ASE} = K_{ASE}(W_{th})/\{1 + \Gamma_{eb}(W)\} \qquad (25)$$

where Γ is a constant and $K_{ASE}(W_{th})$ is defined in eq. (21b).

2.4   Application

2.4.1   Origin of the dual amplified spontaneous emissions (ASE) of 7-aminocoumarin derivatives

2.4.1.1   Dual ASE of 7-aminocoumarin in unpurified n-BuOAc

The ASE spectrum of C1 or C2 but not the rigidified C102 in unpurified nBuOAc showed two bands at 420 nm and 455 nm, consistent with previous observations.[36] However, further investigations of C1 in dried nBuOAc (or THF) revealed a single ASE band at 420 nm, with only a trace of the 455 nm band, and conversely in water-saturated nBuOAc solution.[15,16] These results (Fig.2-6 show conclusively that the ASE band at 455 nm from coumarin-1 in nBuOAc originates from traces of water probably H- bonded to the excited C1 dye and not from a Twisted Intermolecular Charge Transfer (TICT)[101-103-] solvent exciplex.[36]

The role of hydrogen bonding in the dual ASE of coumarin-1 in nBuOAc was investigated by adding submolar concentrations of methanol or n-butyl alcohol (nBuOH). Fig. 2-7b shows that the *proportion* of the long to short wavelength bands was altered by the addition of methanol. In contrast, the ASE spectra from C102 showed the normally observed continuous shift in the wavelength *position* of the single peak with increasing alcohol concentration. Though less dramatic, dual ASE was also observed for coumarin-1 in nBuOAc + dried acetonitrile (AN) as co-solvent (Fig. 2-7a). This unanticipated result
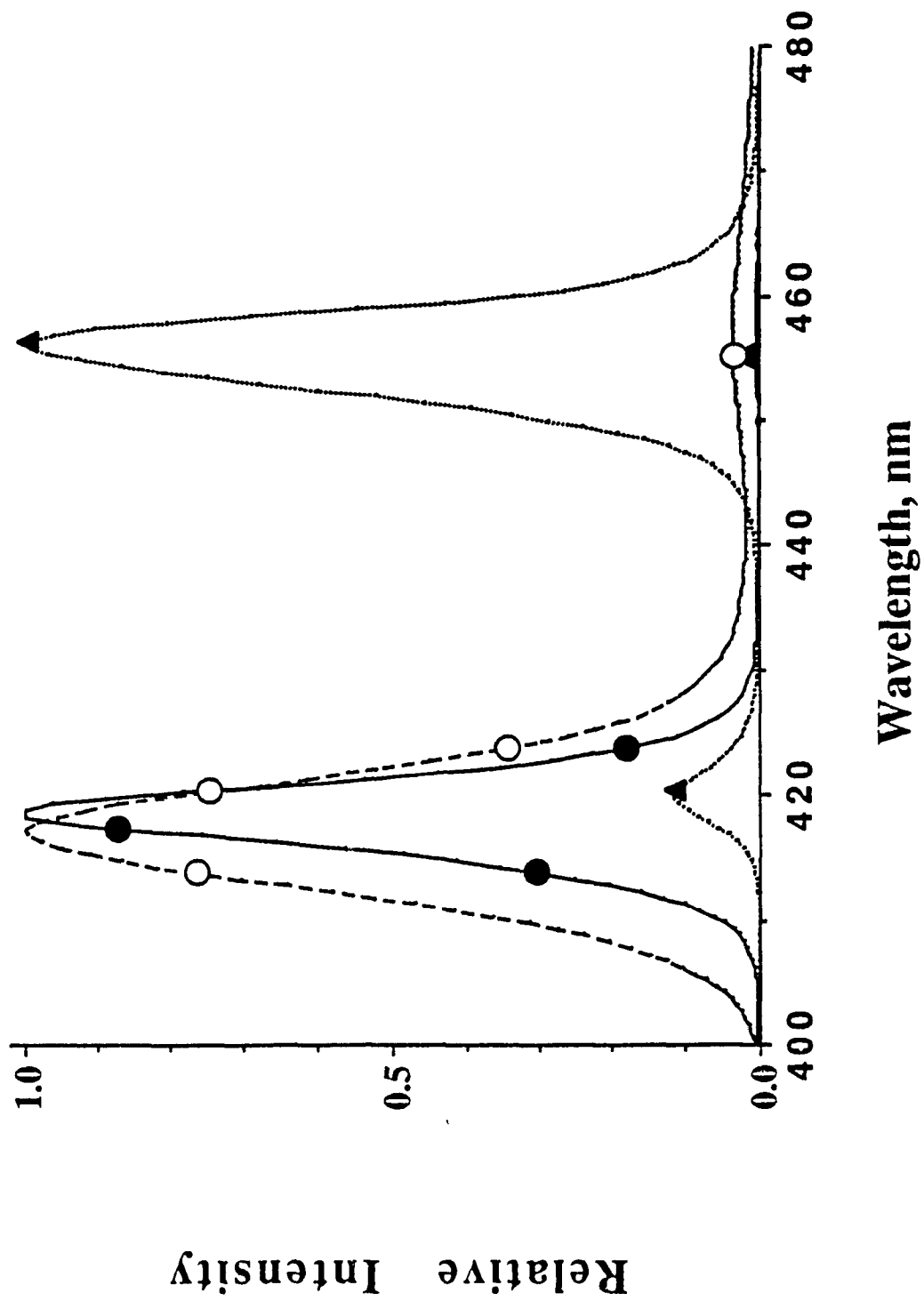
Fig. 2-6   ASE spectra of C1in: unpurified (O); dried (●); water-saturated nBuOAc (▲).
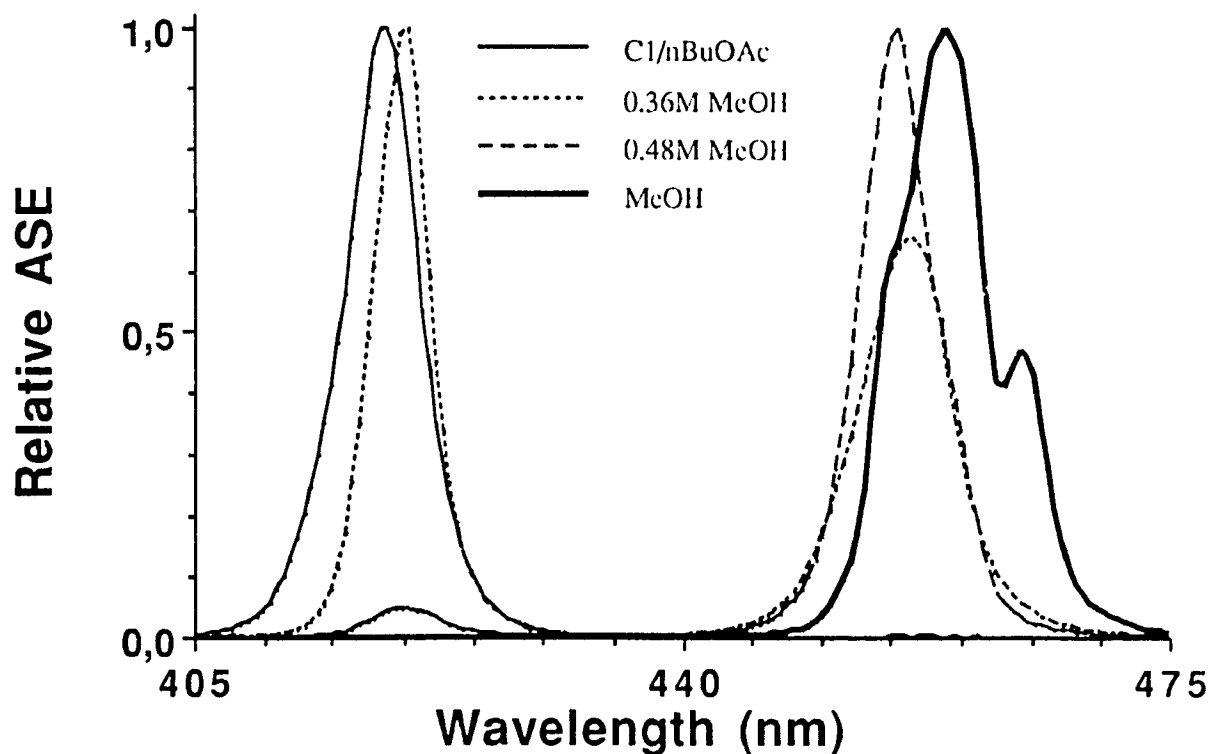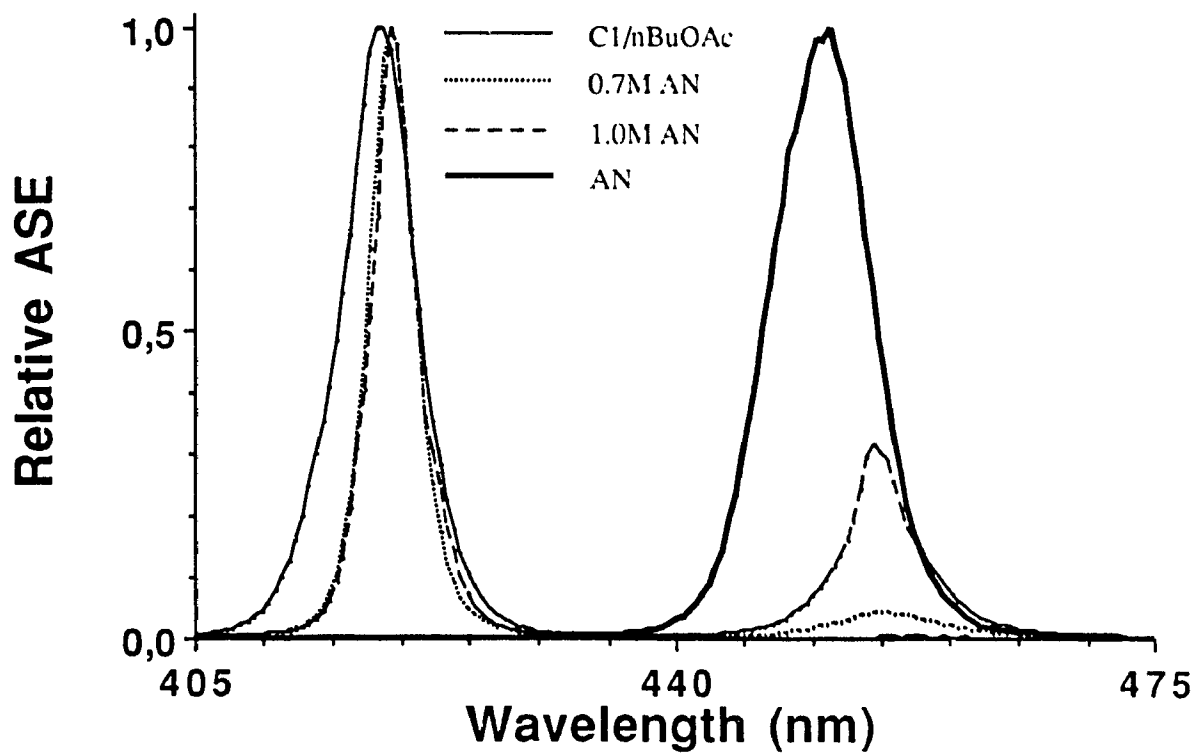
Fig. 2-7   ASE spectra of C1 in nBuOAc containing (a) acetonitrle; (b) methanol.

seems to suggest that high dielectric constant solvents such as AN can also participate in complexing with the highly polar excited state of C1. In this case, H-bonding is not important.

At high concentrated or neat methanol (or nBuOH), structure, due possibly to specific alcohol self-associated complexes with C1, can be observed reproducibly in the long-wavelength C1 ASE band. In Fig. 2-7b, there are three ASE bands at 455 nm (shoulder), 458 nm and 465 nm for C1 in methanol, respectively. The intensity ratios of these ASE bands (455nm, 458 nm, and 465 nm) varies shot by shot at room temperature. By diluting the concentration of C1 into half (~4 mM) at room temperature, there is only a structureless long-wavelength ASE band being observed. Under low temperature (~0 °C), the ASE 'red' band appears to be unresolvable. These observations indicate a temperature and concentration dependence of the ASE. Should these observations be substantiated by future experiments, ASE would then be a powerful technique to study alcohol self-association[157-160] in solution, since, as far as we are aware, there is no method of direct measurement in solution at ambient temperature of specific signals due to particular associated species of alcohol, although important indirect information can be gained from thermodynamic[157,158] and other methods.[159,160]

The uv absorption of C1 (and coumarin-102) in nBuOAc + nBuOH was studied to determine whether, as was in the case of 1-methylindole and nBuOH,[21] the ground state complexation was solely responsible for the fluorescence properties. The uv absorption spectra of coumarin-1 and C102 in nBuOAc with different concentrations of nBuOH showed isobestic wavelengths λ_{iso}^{ab} at 369 nm and 378 nm, respectively, which shows that the dyes form complexes with alcohol. For the equilibrium:

$$D + mQ = D \cdots mQ,$$
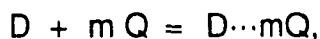
the corresponding absorbance A_{obs}, from both the free and complexed dye is given by:

$$[D]_0/(A_0-A_{obs}) = [(\varepsilon - \varepsilon_{cx})L]^{-1}(1 + K^{-1}[Q]^{-m}) \qquad (26)$$

which is similar to the Bensi-Hildebrand ralation.[161] In eq. (26), ε and ε_{cx} are the extinction coefficients of the "free" (species A^*) and complexed dye (B^*), and A_0 is the absorbance and $[D]_0$ is the dye concentration at $[Q]=0$. This equation follows from the definition of the equilibrium for formation of a dye-alcohol complex, in which the free dye concentration is expressed as a difference in concentration between the initial dye concentration and the concentration of complexed dye, i.e., $[D]_0-[D_{cx}]$; and replacing the free and complexed dye concentrations by their optical absorbances. Fig. 2-8 show the fitting of the experimental data to eq. (26) with different stoichiometry m for C1 and C102, respectively. The data clearly show a best fit using eq. (26) for $m = 2$ (D..2(nBuOH), D = C1 or C102) for both coumarin dyes. From the above plot, we obtained K = 0.19±0.03 (C1) and 0.016±0.003 M^{-2} (C102), which shows that C102 is only weakly complexed to alcohol in the ground state. The extent of complexation of C1 with alcohol in the ground state is non-negligible .

The fluorescence spectra of C1 and C102 in nBuOAc with different amounts of added nBuOH (Fig. 2-9) showed an isobestic wavelength for C1 ($\lambda''_{i,v}$ ~ 425 nm) but not clearly for C102. To assess the relative contribution of ground and excited state dye interaction in the alcohol to the fluorescence quenching by alcohol, the Stern-Volmer constant for fluorescence quenching of the "free" excited state dye by alcohol was determined by calculating the fraction of the total *absorbed light* and *fluorescence intensity* due to the free dye. The analysis

41
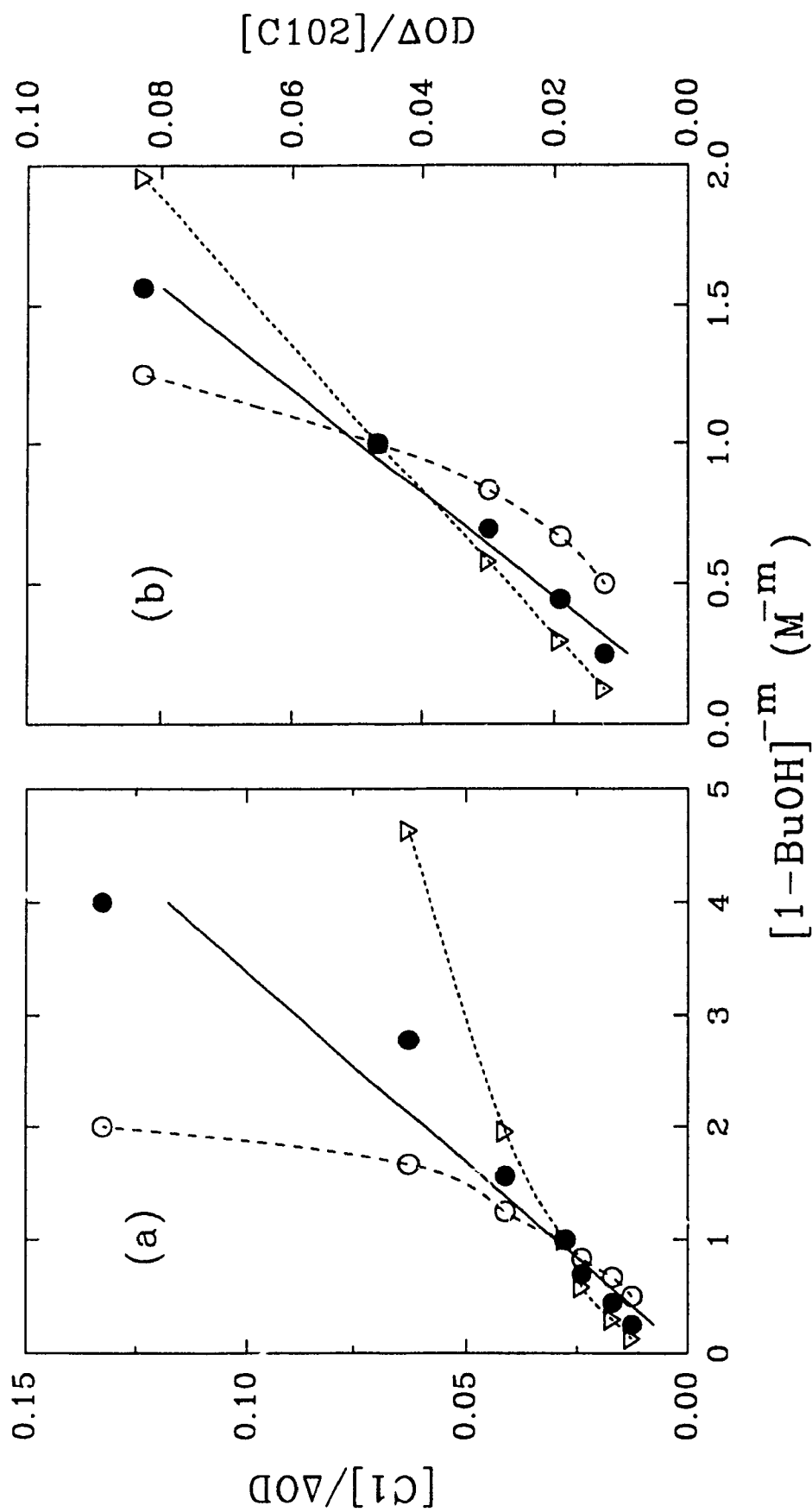
Fig. 2-8 Plot of [dye]/ΔOD vs. [1-BuOH]⁻ᵐ of eq. (26) for (a) C1 and (b) C102. The experimental data are represented by (O): for m=1; (●): for m=2; and (∇): for m=3, respectively. [dye]=0.04 mM; [1-BuOH]: 0→2 M.
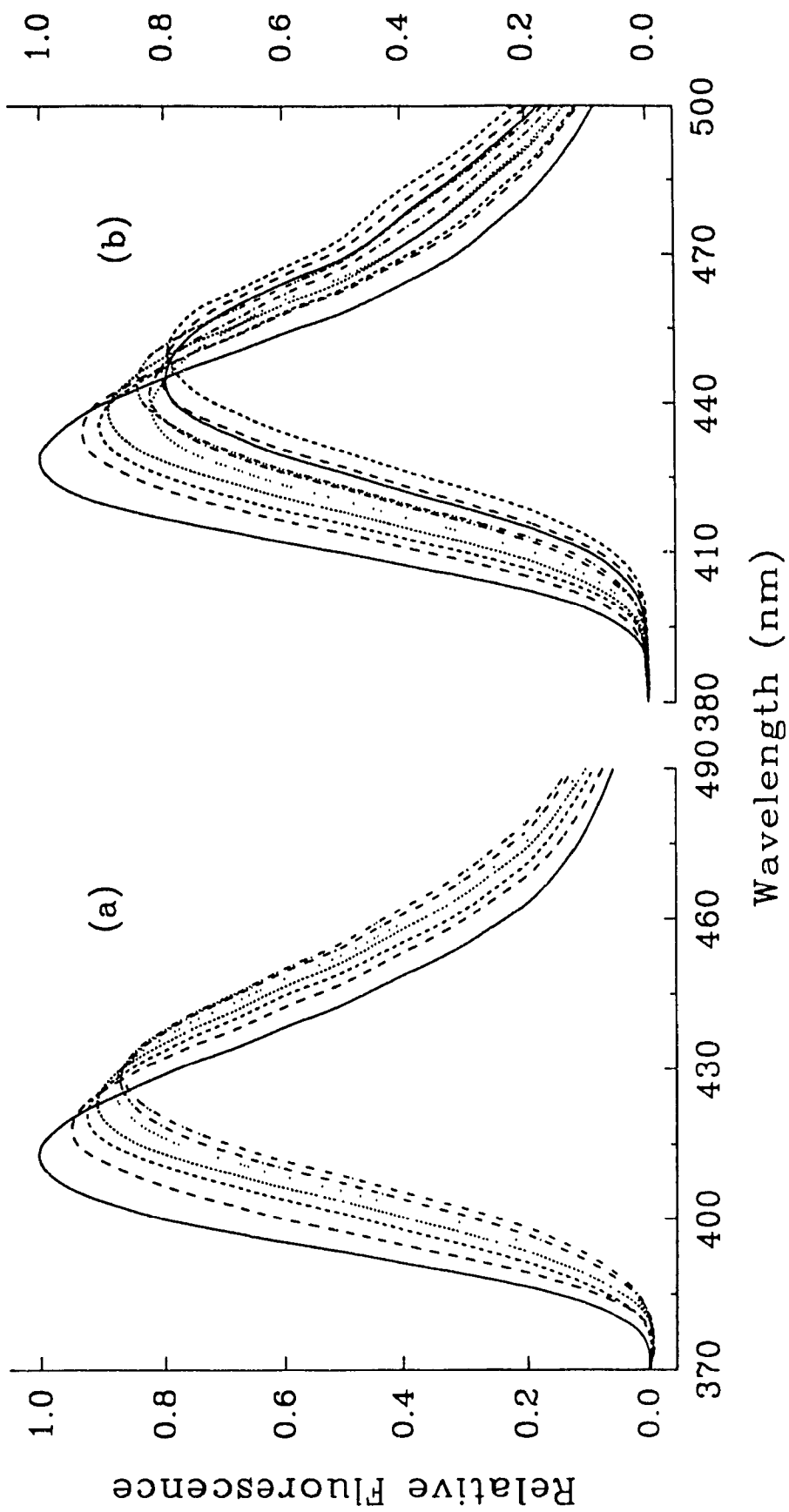
Fig. 2-9   Fluorescence spectra of (a) C1 (0.04 mM, excited at 369 nm); (b) C102 ((0.04 mM, excited at 378 nm), in nBuOAc containing different amounts of 1-BuOH (0→2 M), and pure 1-BuOH at room temperature.

was facilitated by exciting the dyes at their *absorption* λ_{iso}^{ab} (369 nm for C1, and 378 nm for C102, respectively) and keeping the dye concentration constant. Under these conditions, the intensity of light absorbed by the system is independent of the alcohol concentration and remains constant. Knowing the ground state equilibrium constant, the fraction of the total incident light absorbed by the ground state complexes can be calculated from the eq. (4) as:

$$\alpha = (K[Q]^m)/(1 + K[Q]^m) \tag{27}$$

where $\sigma_{pa} = \sigma_{pb}$ or $\varepsilon = \varepsilon_{cx}$, and the ground state stoichiometry m=2 for both C1 and C102 (refer to Fig. 2-8) has been applied. The fluorescence quantum yield ratio for the *uncomplexed* excited state dye, Φ_a/Φ_a^0 , can be obtained from the measured total fluorescence intensity ratios I/I^0, where I and I^0 are the intensities in the presence and absence of [ROH] (refer to eq. (2)). From the relationship between Φ_a/Φ_a^0 and the concentration of nBuOH [Q], the Stern-Volmer constant K_{SV} can be obtained from eq. (3). The data from both C1 and C102 in n-butyl acetate containing different amounts of nBuOH (Fig. 2-10) displayed a good fit to eq. (3) with n = 1 and K_{SV} = 5.3±0.8 M^{-1} for C1; and n=2 and K_{SV} = 2.5±0.8 M^{-2}. For C102, the stoichiometry of the complex does not appear to change under excitation. But, the ablity to form the complex seems to be stronger in the excited state. The fluorescence results taken together with those from absorption show that *the principal quenching process by alcohol is dynamic quenching of the excited state* and not that ground state complexation.

The result for C1 implies (i) detachment of one alcohol molecules upon excitation of the complex, consistent with a large dipole change (i.e., a highly dipolar C1*) and rupture of a H..N bond in C1*; or (ii) fluorescence inactive ground state H-bonded C1.
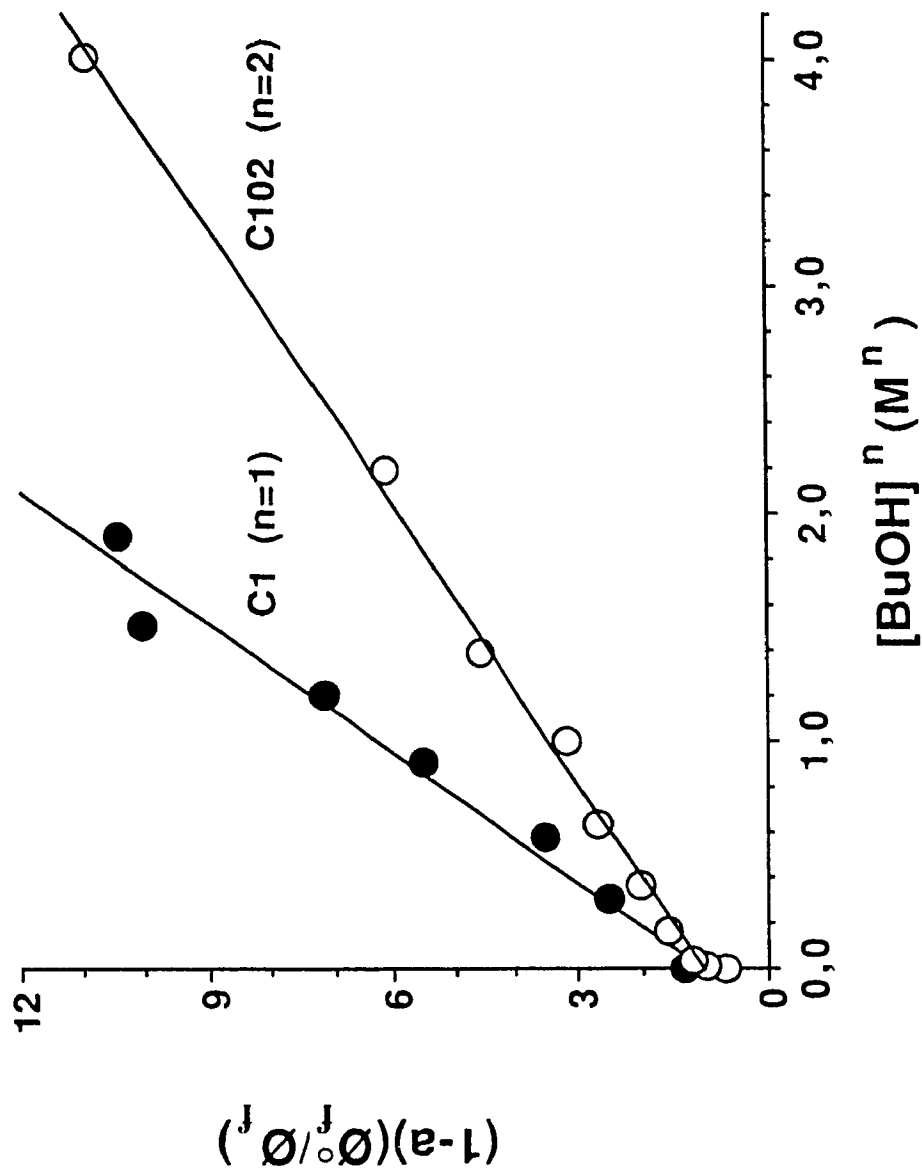
Fig. 2-10   Plot of $(1-\alpha)/(\Phi^0_f/\Phi_f)$ vs. $[BuOH]^n$. (●): for C1 with n=1 and (O) for C102 with n=2. [Dye]=0.04 mM; [BuOH]: 0→2 M)

The detachment of one alcohol from the complex for C1 but not for C102, could explain the presence of dual ASE bands for C1 and only one ASE band for C102, if H-bonded C-102 is fluorescence inactive. The data presented thus far suggest that in the presence of a hydroxylic component such as alcohol, excited C1 and its hydrogen-bonded complexes are in equilibrium:

$$C1^* + HOR = [C1..HOR]^* ,$$
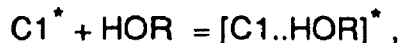
and that the two ASE bands (at 420 and 455 nm) are due to free and complexed dye molecules. If this is correct, then the ratio of the gain factors for the two ASE bands, $G(455nm)/G(420nm)$ should be linearly dependent on the alcohol concentration as derived in eqs. (20) - (22). The application of ASE gain measurement will be discussed in next section.

2.4.1.2   Dual ASE of C1 in chlorohydrocarbon solvents

In chlorohydrocarbon solvents, the solvent dependency of ASE was observed (Fig. 2-11), in which, the intensity ratio of two ASE bands ($R_{ASE} = I_{ASE}^{Long}$ / I_{ASE}^{Short}) follows the order of:

$$R_{ASE}(C_6H_5Cl) < R_{ASE}(CHCl_3) < R_{ASE}(CH_2Cl_2).$$

The empirical polarity (E_T^N [6]) of these chlorohydrocarbon solvents (Table 2-3), it is parallel to the order of R_{ASE} observed in experiment. Such behavior indicates the existence of the hydrogen bonding effect in the chlorohydrocarbon solvent. The activity of the chlorohydrocarbon solvent to form the H-bond with polar solute molecule can be represented by the empirical polarity (E_T^N) as listed in Table 2-3.
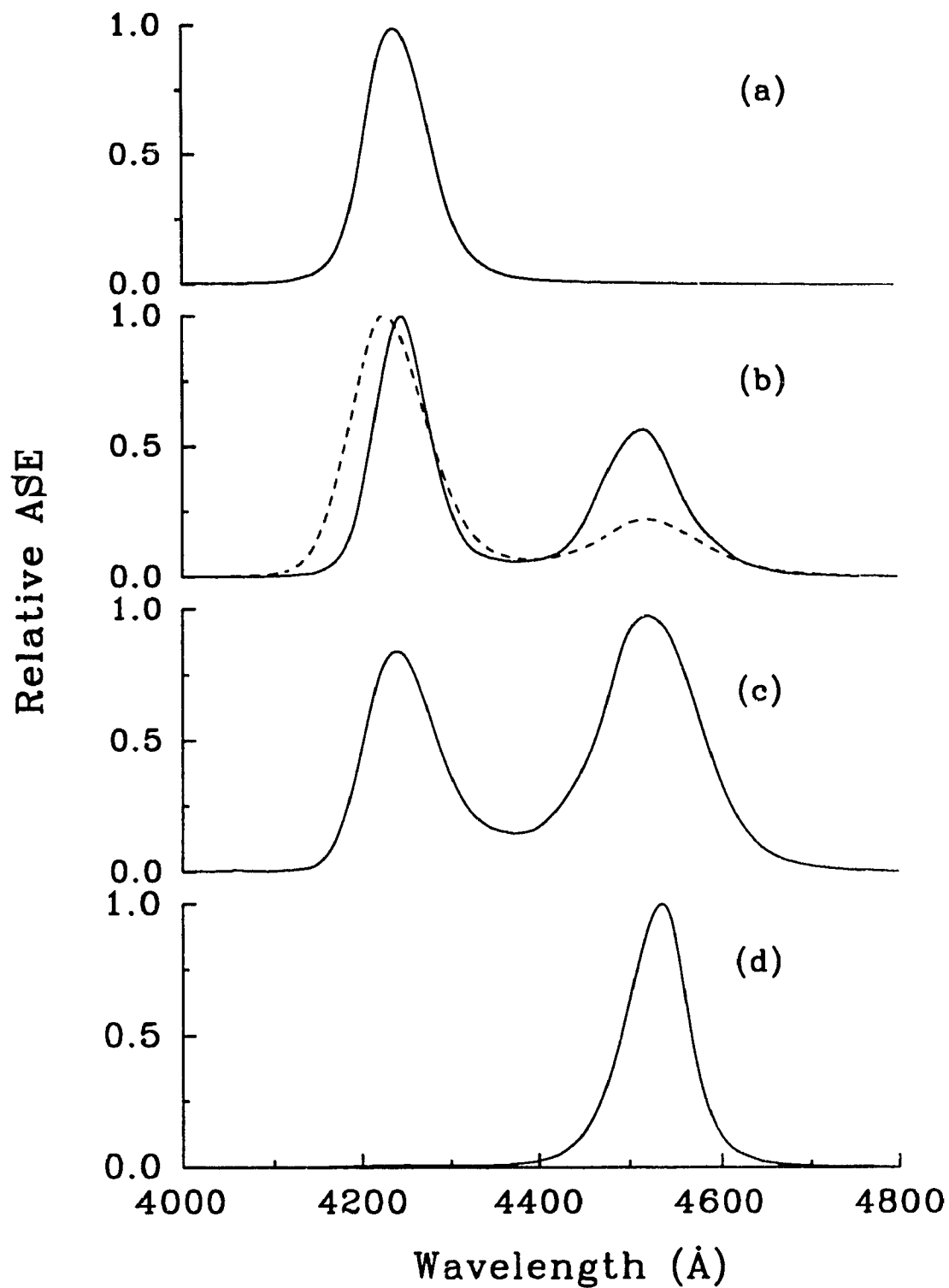
Fig. 2-11   ASE spectra of C1 in (a) C_6H_5Cl; (b) dried $CHCl_3$ (solid line) and $CDCl_3$ (broken line); (c) wet $CHCl_3$; and (d) CH_2Cl_2.

Table 2-3: **Comparision of R_{ASE} of C1 in Chlorohydrocarbon Solvents**

Solvent	E_T^N [6] (kcal/mole)	R_{ASE}
Chlorobenzene	37.5	0
Chloroform	39.1	0.5
Dichloromethane	41.1	100

The difference of R_{ASE} in the dry and wet chloroform (Fig. 2-11b,c) provides additional evidence of the H-bond effect as discussed above. Meanwhile, the isotope effect on the dual ASE has been preliminarily tested. The relatively weak 'red' ASE band in $CDCl_3$ in comparison to that in $CHCl_3$ (Fig.2-11b), may be due to its weak ability for forming the hydrogen bonded complex in chlorodeuterocarbon.

2.4.2 Amplified spontaneous emission gain spectra of 7- aminocoumarin derivatives in different solvents

2.4.2.1 Studies of excited state complexation of 7-aminocoumarin derivatives in different solvents by conventional spectrofluorimetry.

(i) The fluorescence spectra of coumarin-1 in nBuOAc containing different amounts of CH_2Cl_2 (refer to Fig. 2-5), show slight shifts in the peak position with concentration of CH_2Cl_2. This is mainly due to the excited state complexation between dye and quencher (CH_2Cl_2). The Stern-Volmer constant K_{SV}

determined from eq. (3) is much larger than that of the ground state constant K from uv/vis absorption study (as listed in Table 2-4) which implies a higher capability for complexation in the excited than the ground state. The polarity $(E_T^N$ [6]) of the chlorocarbons which have been investigated, are between aprotic solvents and alcoholic solvents. In a system containing nBuOH, significant changes in the fluorescence spectra have been observed due to strong H-bonding between alcohol and dye in the excited state as indicated earlier.

Table 2-4: Kinetic Constants of C1 in different solvent-mixtures:

| Solvent | Quencher | E_T^N of quencher[a] | Quenching constants (M^{-1}) | | K^d (M^{-1}) |
			K_{SV}[b]	K_{ASE}[c]	
n-BuOAc	nBuOH	0.602	5.3	4.9	0.2[e]
nBuOAc	CH_2Cl_2	0.309	0.40	0.33	0.09
iso-Octane	nBuOAc	0.241	0	0.4	0.33(0.26)[f]

[a] Reference 6; [b] From conventional spectrofluorimetric study (eq. (3)); [c] Under 100 kW pumping intensity, if not specified; [d] From uv/vis absorption study; [e] In unit of M^{-2}; [f] No dynamic contribution; K=0.26 M^{-1} was obtained from fluorescence spectra using eq (27b).

(ii)   In the iso-octane/nBuOAc system, where there is no H-bonding in the excited state, there is only a slight shift in the fluorescence spectra of coumarin-1 with increasing concentration of nBuOAc. The value of the Stern-Volmer constant for dynamic quenching in the excited state determined from eq. (3) was found to be zero. With $K_{SV} = 0$, eq. (3) for the fluorescence quenching

becomes:

$$\Phi_a/\Phi^\circ_a = 1 - \alpha \qquad (28a)$$

Since the sample is excited at the isobestic wavelength ($\lambda_p = \lambda^{ab}_{iso}$), the ratio of $\sigma_{pa}/\sigma_{pb} = 1$ in eq. (4) defining α, and eq. (28a) for the ground state equilibrium becomes:

$$\Phi_a/\Phi^\circ_a = 1/(1 + K[Q]^m) \qquad (28b)$$

The value of $K = 0.26$ M^{-1} obtained from the fluorescence quenching using equation (28b) (Table 2-4) is similar to that obtained from the absorption measurements.

Table 2-4 also shows that the Stern-Volmer constants increase in the order:

$$K_{SV} \text{(nBuOAc)} < K_{SV} \text{(CH}_2\text{Cl}_2) < K_{SV} \text{(nBuOH)} \qquad (29)$$

which parallels with the trend of the quencher polarity (E^N_T [6]). The most significant factor, however, appears to be H-bonding between dye and quencher, consistent with our earlier conclusion.

2.4.2.2   Studies of excited state complexation of 7-aminocoumarin derivatives in different solvents using ASE gain measurement

As discussed in the previous section, the gain ratio of complexed and free species should satisfy eq. (21a). A linear relation between Rg and concentration of CH_2Cl_2 has been observed in Fig. 2-12 as expected. The ASE quenching constants K_{ASE} obtained experimentally in nBuOAc with CH_2Cl_2 and nBuOH (Table 2-4) are comparable to their K_{SV} from conventional spectrofluorimetry as

mentioned in the above section. Since the increases of gain ratio Rg with CH_2Cl_2 or nBuOH are mainly due to excited state complexation between dye and CH_2Cl_2 or nBuOH (dynamic quenching), K_{ASE} should satisfy eq. (21b) with unit stoichiometric constant (n = 1) as observed experimentally. Similarly, the K_{ASE} constant of C1 in the co-solvents, iso-octane and nBuOAc should be directly related to its ground state constant K (refer to eq. (22b)).

2.4.3   Agreement between conventional spectrofluorimetry and ASE gain measurements

When the dominant process is dynamic quenching as in the case of C1 in nBuOAc mixed with nBuOH, the value of the K_{ASE} at threshold, 5.2 ± 0.3 M^{-1} should be consistent with that determined from the Stern-Volmer quenching. By estimating the ratios of $\sigma_{eb}(455nm)/\sigma_{ea}(420nm)$, τ_b/τ_a of coumarin-1 in pure nBuOH and nBuOAc as listed in Table 2-5, an ideal value of the K_{ASE} constant ($K_{ASE}=5.8\pm1.7$ M^{-1}) can be estimated from the K_{SV} determined from conventional spectrofluorimetry by means of eq. (21b). This value is similar to the K_{ASE} constant determined by extrapolation to the threshold intensity (W_{th}) using eq. (30) ($K_{ASE}(W_{th})=5.2\pm0.3$ M^{-1}). The agreement between these two estimations of K_{ASE} also confirms the anticipated equivalence of these two techniques for studying the excited state complexation.

Similarly, the weak binding of C1 in iso-octane mixed with nBuOAc, is also observed from their ASE gain spectra. To increase the signal, 200 kW pumping intensity was applied to get a gain ratio that satisfies the eq. (22a) (m=1). A value of the K_{ASE} constant obtained by using eq. (22a) in Table 2-4 is comparable to the ground state complexation constant K from uv/vis absorption studies as presented by eq. (22b).
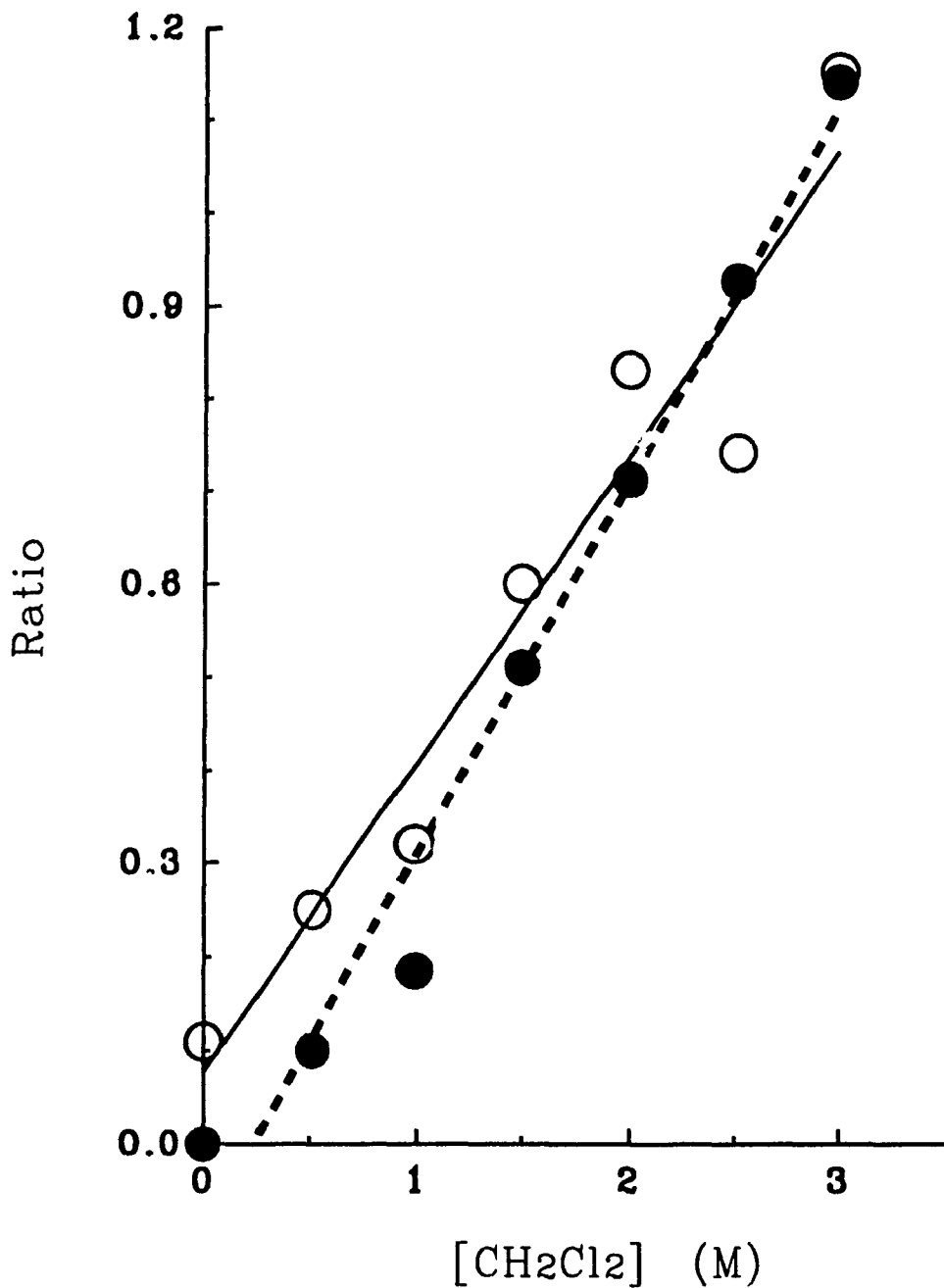
Fig. 2-12   Plot of $\Phi_a^0 / \Phi_a - 1$ and Rg vs. [CH$_2$Cl$_2$]. (●): $\Phi_a^0 / \Phi_a - 1$ ([C1]=0.035 mM) from conventional spectrofluorimetry fitted by dark dots (K$_{SV}$=0.40 1/M); (O): Rg ([C1]=8.0 mM) from ASE gain spectroscopy fitted by solid line (K$_{ASE}$=0.33 1/M)

Table 2-5: Comparison of K_{ASE} of C1 in nBuOAc containing different amounts of nBuOH from ASE gain spectroscopy to that from conventional spectrofluorimetry

σ_{eb}/σ_{ea} [a]	τ_b/τ_a [b]	K_{SV} M^{-1}	K_{ASE} [c] M^{-1}
1.4	0.85	5.3±0.8	5.2±0.3 (5.8±1.7) [d]

[a] The stimulated emission cross section $\sigma_{ei}(\lambda_i)$ (i=a,b) is given by the relationship.[31]

$$\sigma_{ei} = \lambda_i^4 E_i(\lambda_i)/(8\pi\tau_i c n_i^2),$$

where $E_i(\lambda_i)$ is the fluorescence line shape function, n_i the refractive index of the solution at wavelength λ_i, τ_i is the lifetime of fluorescing state without stimulated emission and c the velocity of light *in vacuo*. Therefore, the ratio of the stimulated emission cross section of coumarin-1 in nBuOH and that in nBuOAc can be estimated by

$$\sigma_{eb}/\sigma_{ea} = (\lambda_b/\lambda_a)^4(\tau_a/\tau_b)(n_a/n_b)^2(E_b(\lambda_b)/E_a(\lambda_a))$$

$$\approx (\lambda_b/\lambda_a)^4(\tau_a/\tau_b)(n_a/n_b)^2(\tau_b/\tau_a) = (\lambda_b/\lambda_a)^4(n_a/n_b)^2$$

$$= (455/420)^4 \cdot 1 = 1.4,$$

where the fluorescence line shape ratio at peaks (λ_b=455 nm, and λ_a=420 nm) is approximated by its quantum yield ratio under assumption of equal band width, and the index ratio can be assumed to be unity; [b] Equal to its quantum yield ratio in reference 94; [c] Obtained from the best fit (eq. (30)); [d] Estimated from the Stern-Volmer constant using eq. (21b)

2.4.4 Effect of the pumping intensity

At pumping intensity above the pumping threshold ($W \geq W_{th}$), we expect and observe an exponential dependence with respect to the pumping intensity for relatively small ASE signals.[30] The dependence of the total ASE (I_{ASE}) of C1 in pure nBuOH at peak position (λ_b = 455 nm) on the pumping intensity (W) is shown in Fig. 2-13. The circles are the experimental points and the solid line is the best fit computed from the equation:

$$I_{ASE} = 4103 \{ \exp(0.00909(W - W_{th})) - 1 \} \tag{30}$$

with $W_{th} = 80\pm5$ kW.

Since the spontaneous emission (I_{sb}) contribution is negligible ($I_{sb} \ll I_{eb}$) for pumping intensities $W > W_{th}$, the stimulated emission (I_{eb}) can be considered as the total ASE ($I_{eb} = I_{ASE}$). Applying eq. (25) to simulate the experimental values of K_{ASE} by considering eq. (30) as the pumping intensity dependence of the stimulated emission (I_{eb}) in eq. (25) for pumping intensities $W \geq W_{th}$, we obtain:

$$K_{ASE} = K_{ASE}(W_{th})/\{1+0.341[\exp(0.00909(W - W_{th}) - 1]\} \qquad (31)$$

where $K_{ASE}(W_{th}) = 5.2 \pm 0.3$ M^{-1}. The results are shown in Fig. 2-14 where the filled circles are the experimental values from the slopes of gain ratio (R_g) vs. concentration of nBuOH using eq. (21a), and the solid curve is calculated from eq. (31).

2.4.5   Advantage of ASE gain spectroscopy in comparison with conventional spectrofluorimetry

In Fig. 2-15, the separated two-component ASE gain spectra of C1 in nBuOAc with different amounts of CH_2Cl_2, were obtained directly from eq. (1). By comparison with their fluorescence spectra in Fig. 2-5, significantly higher resolution is observed for the gain spectra, which are very powerful for identifying multiple components with closely emissive peak positions.

During sample preparation, the gain ratio (R_g) was found to be relatively insensitive to the variation of the C1 concentration ($\pm 1 \times 10^{-4}$ M). By comparison the quantum yield ratio measurements from conventional spectrofluorimetry were carried out with C1 concentrations of 0.035 mM and the difference between each sample and reference had to be less than 0.5% or $\approx \pm 10^{-7}$ M.
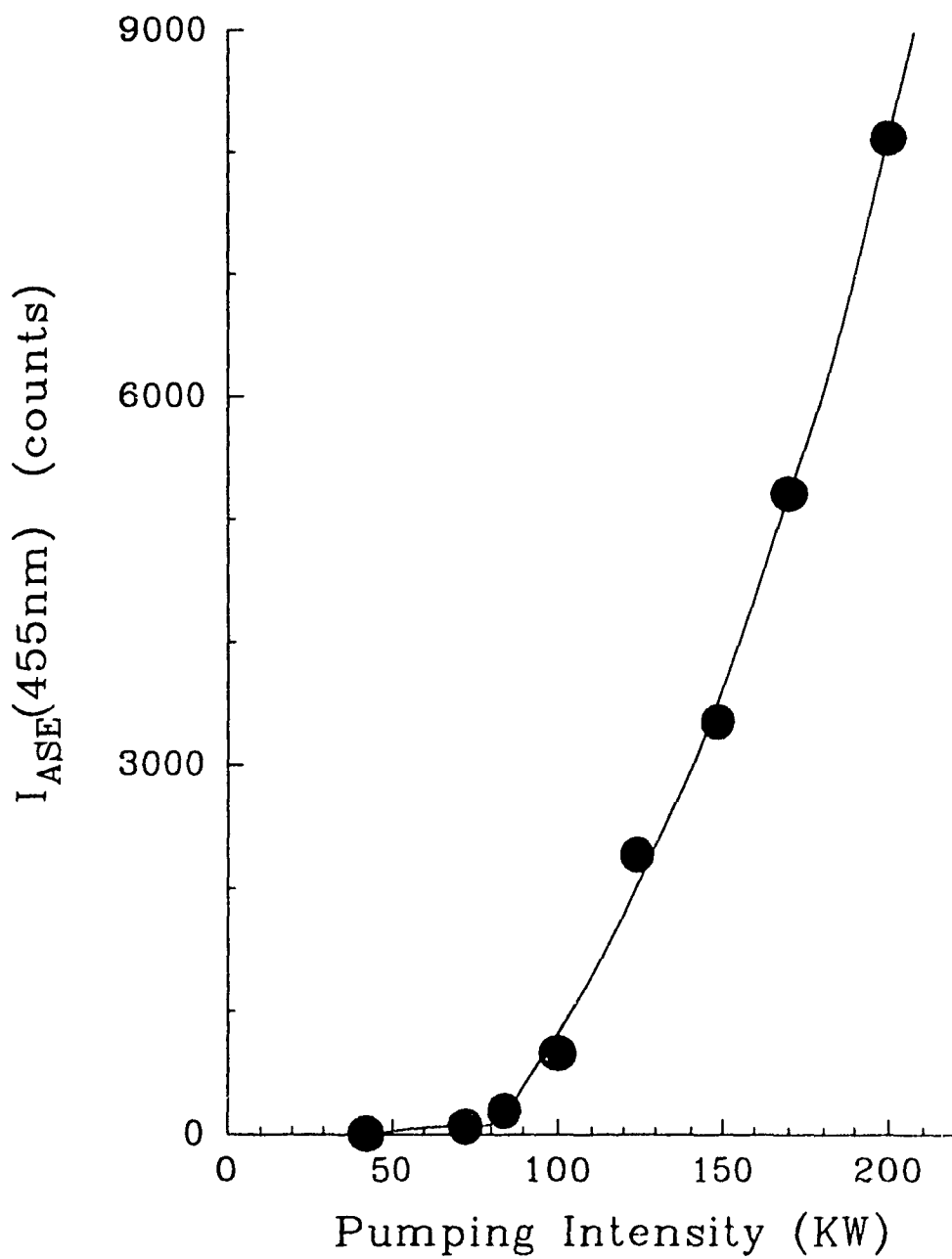
Fig. 2-13　　ASE intensity (I_{ASE}) of C1 (8.0 mM) in pure 1-BuOH, vs. pumping intensity (W) (●) fitted by solid line as expressed by eq. (22)
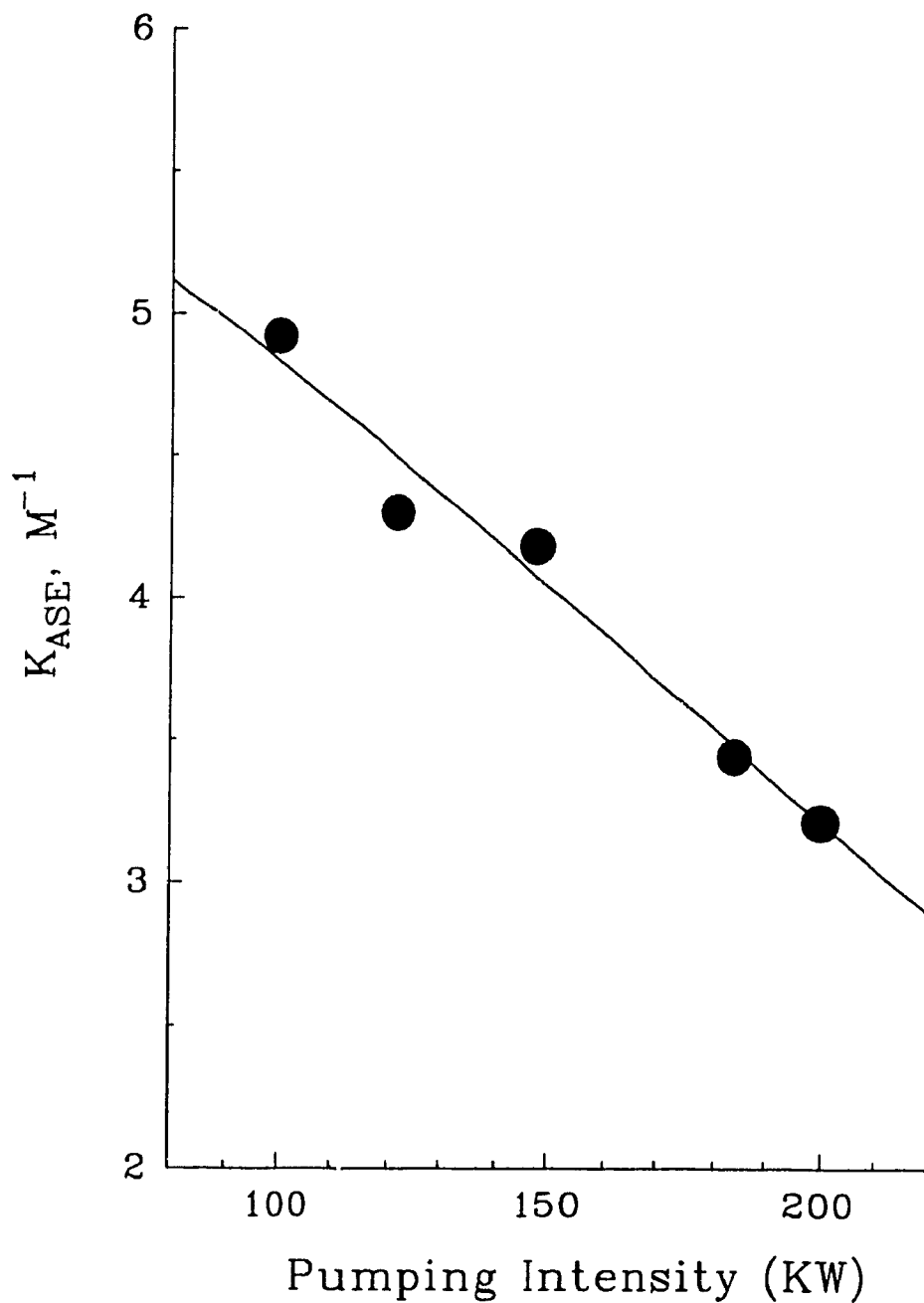
Fig. 2-14   Pumping intensity affects on K_{ASE} of C1 (8.0 mM) in nBuOAc
con*aining different amounts of 1-BuOH (●) fitted by solid line expressed
by eq. (21b)
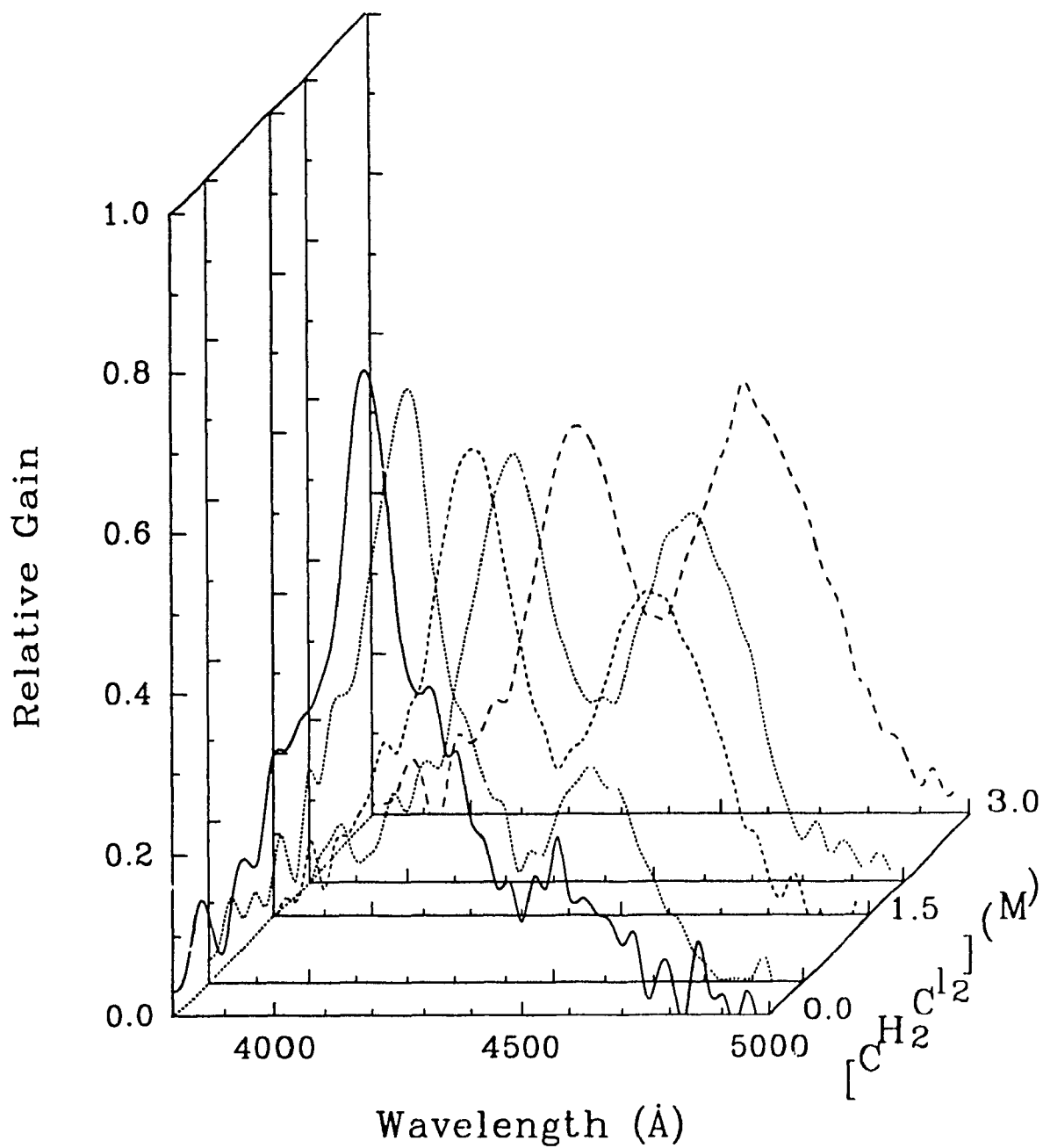
Fig. 2-15 Relative ASE gain spectra of C1 (8.0 mM) in nBuOAc
containing different amounts of CH$_2$Cl$_2$ (0→3 M) using eq. (1)

2.5   Conclusions

2.5.1   Further studies

In the above studies, the application of ASE gain measurement has been successfully applied to study dynamic and static complexation. But, it still has not been widely applied in other areas. However, the preliminary test of the isotope effect (Fig. 2-11b) does imply a potential role in this area, which could provide an alternative method for studying the formation of H-bonded complex in chlorohydrocarbons or chlorodeutrocarbons.

For a hydroxylic environment, e.g., methanol, the ASE of 7-aminocoumarins have been probed to observe temperature and concentration dependent fine structure. The origin of this fine structure is not clear. It could be the aggregation of the alcohol,[157-160] the depopulation of the temperature sensitive vibrational states, etc..

The 7-amino-4-trifluoromethylcoumarin does not absorb strongly enough at the 337 nm line of the N_2 laser to permit ASE gain measurements significant for study of its complexation with β-cyclodextrin in water. However, such studies should be possible by applying a higher output N_2 laser or other laser sources.

The principle of this dual ASE and its nonlinear pumping intensity dependence possess high potential for its application in Optical Computing as a Bichannel Optical Logic Device, details have been proposed elsewhere.[163]

2.5.2   Conclusion

Dual ASE from C1 in a polar environment originates from an excited state quasi-equilibrium concentration of H-bonded or acetonitrile-solvated complex.

The results are inconsistent with a planar ICT and an evanescent laser-excited population of TICT-nBuOAc exciplex as an explanation for the previously reported dual ASE from C1 in nBuOAc. The present results and those from parallel ESA studies[32-34] of C1 in nBuOAc indicate a single non-90° conformational (with respect to the ring C-N bond) excited state species that is significantly more polar than that of C102. Of significance to the use of coumarin dyes in laser applications is the sensitive dependence of the ASE profile from C1 in dried nBuOAc on the concentration of hydroxylic co-solvent. This suggests that the lasing profile can be tuned by adding a small quantity of alcohol. In addition, this sensitive ASE dependence on hydroxylic co-solvents can be used to selectively probe for H-bonded excited-state dye molecules whose normal fluorescence is usually obscured by that from the free C1 dye. The results for the coumarin C1 dye illustrate that the strongly overlapping normal fluorescence bands can be experimentally "deconvoluted" into two characteristic ASE bands due to distinct species of fluorophore. The origin of the fine structure observed in the ASE of C1 in nBuOAc at high or pure alcohol concentrations are not known but may be due to solvent structure.

The excited and ground state complexation of coumarin-1 in different solvents with or without quenchers has been investigated and a correlation between ASE gain spectroscopy and conventional spectrofluorimetry has been established which has been confirmed in both experiment and theory. Although obviously limited to fluorophores capable of undergoing stimulated emission, the advantages of ASE gain spectroscopy in comparison to that of conventional spectrofluorimetry, have been found to be:

a)   higher frequency resolution to permit identification of multicomponents with close band positions;

b)   easier sample preparation (no precise requirement of dye concentration);

c)   fast data treatment.

By comparing the excited state quenching constants with empirical parameters of proper quencher polarity E_T^N,[6] the reduction of the ASE gain of free species or enhancement of the ASE gain of complex with respect to the quencher polarity E_T^N, can be explained by the formation of H-bonding between dye and quencher.

Chapter 3: PICOSECOND EXCITED STATE ABSORPTION (ESA) & AMPLIFIED EMISSION (AE) of 7-AMINOCOUMARIN DERIVATIVES and CYCLODEXTRIN COMPLEXES

3.1 Introduction

3.1.1 ESA and AE of 7-aminocoumarin Dyes in Different Solvents

The important 7-aminocoumarin laser dye have been the subject of recent fluorescence studies concerning the role of the conformation of the amino group in the excited singlet internal charge transfer (ICT) state of the aminocoumarins.[87,88,90,94] The perpendicularly twisted conformation of the internal charge transfer (TICT) state has been unequivocally established for the excited 4-dimethylaminobenzonitrile (DMABN) archetypal model system as one which has a maximal dipole moment from full electron transfer, a low quantum yield energy dissipative state, and fluoresces uniquely at a lower frequency than does the planar form of the ICT excited state.[101-103]

Although the necessary condition of an amino group that is already in, or able to rotate to, the perpendicular configuration is met in the aminocoumarins, the experimental evidence on the sufficiency of this condition for formation of the TICT state in these molecules is less clear-cut: **dual emission** due to the planar and perpendicularly twisted conformations of the dialkylamino group, **has not been observed** even in the most polar solvents, nor has the excited stc e absorption (ESA) of the TICT state been observed. However, a difference in the fluorescence quantum yield of the flexible and constrained 7-aminocoumarins is observed. The quantum yield (Φ) of the flexible 7-aminocoumarins (e.g., C1, C2,

and C1F, etc.) shows a strong solvent dependence. The trend of the quantum yield is parallel to that of the fluorescence lifetime and drops dramatically by a factor of 10 or more from aprotic to protic solvent, especially in water (Φ~0.05 for C1 and ~0.01 for C1F).[90] By contrast, for the constrained 7-aminocoumarin (e.g., C102, C102F), the change in quantum yield with solvent is less dramatic than that of flexible 7-aminocoumarins (e.g., C1, C2 and C1F, etc.) as listed in Table 3-1. On the basis of fluorescence quantum yields and solvatochromic red shifts in alcohol, Rettig and Klock[94] have concluded that, for C1, the TICT state is only partially developed in the hydroxylic and polar solvent, such as methanol. However, the recent observation of dual amplified spontaneous emission from C1 in moderately polar solvents such as dichloroethane and n-butyl acetate suggested that population of a distinct TICT state of C1 is sufficient for stimulated emission to occur.[36] But, the origin of this dual amplified spontaneous emission (ASE) has been fully explained by the H-bonding effect instead of the solvent exciplex of the TICT state in n-butyl acetate and chlorohydrocarbon solvent itself[15,16] as discussed in the previous chapter.

3.1.2 Complexation of 7-aminocoumarin Dyes/Cyclodextrin

Cyclodextrins (CD's) are naturally occurring cyclic oligomers of glucose that have a cylindrical shape and are noted for their ability to complex small molecules within their interior due to their size and hydrophobic nature.[128,130] As a result, CD's have been used extensively to model protein-ligand and enzyme-substrate interactions.[127] They have found widespread application in separation sciences,[164] selective synthetic strategies,[165] in molecular recognition,[166] and have been used as color-change indicators,[126] probes of molecular photophysics,[22] or as chemical sensors.[125] There are a number of observations of fluorescence enhancement when CD's have been included in

Table 3-1: Quantum yield (Φ) of 7-aminocoumarins in different solvents[87,88,90]

Solvent	C1			C1F		
	Φ	Ratio$_\Phi$	τ	Φ	Ratio$_\Phi$	τ
ethyl acetate	0.99	1	3.1	1.09	1	4.6
acetonitrile	1.03	1	3.4	0.091	0.09	0.60
ethanol	0.73	0.7	3.1	0.09	0.09	0.85
water	0.055	0.06	0.4	0.011	0.01	

Solvent	C102			C102F		
cyclohexane	1.05	1	2.6	0.9	1	4.3
acetonitrile	0.91	0.9	3.3	0.56	0.43	5.6
ethanol	0.95	0.9	4.5	0.38	0.26	3.4
water	0.66	0.6	5.9	0.12	0.1	

the aqueous medium containing fluorescent species (i.e., dye), in which the conventional spectrofluorometric technique[23-25,92,109,133] or time-resolved

emission spectroscopic methods[59,60,134,167] have been used to study the formation of D-CD complexes.

3.1.3 Objectives

In this chapter, there are two objectives presented. (i) The picosecond time-resolved excited state absorption (ESA) and Amplified Emission (AE) of C1 in different solvents are examined in comparison to the rigid aminocoumarin C102's. In the absorption measurements, we attempt to detect the ESA spectrum of C1 in polar solvents and to determine whether a unique TICT ESA spectrum is observed and whether such TICT ESA spectrum follows the pattern of the simple systems. Information on the ESA of the TICT state is sparse.[102] Results on the simple model DMABN[168] and more recently on carbonyl derivatives of dimethylaniline[169] show that the absorption spectra of these compounds are very similar to a superposition of the nearly non-interacting radical ions resulting from the charge transfer. However, the ESA spectrum of the 10-anthryl-*p*-dimethylaniline system appears to be complex.[169] Probe pulse stimulated time-dependent amplified emission (AE) to monitor the population of the excited singlet state, although not normally used in pump-probe ESA experiments, should nevertheless be possible and should provide useful information in the present system where there are potentially one or more short-lived weakly emitting states.[100,172a]

(ii) The time-resolved pump-probe excited state absorption (ESA) and amplified emission (AE), and time-resolved fluorescence measurements are applied to investigate the photophysical behaviour of 7-aminocoumarin-βCD complex in aqueous medium, to obtain more adequate information about the

structure of the complexes. On the basis of specific information, the possible structures of D-CD complexes have been deduced and are discussed.

3.2 Experimental Section

3.2.1 Picosecond time-resolved absorption laser system

A Nd:YAG laser system was used consisting of a passively mode-locked (Kodak 9740 dye in chlorobenzene) 7.0 mm x 90 mm oscillator (ends at Brewster angle), a 7.0 mm x 115 mm preamplifier and a 9.35 mm x 115 mm amplifier, a KDP frequency doubler and tripler (type II) which produced frequency-tripled single pulses (up to approximately 4 mJ) at 355 nm with a pulse duration of 35 ps (full width at half-maximum (FWHM)). Time-resolved spectra were recorded using the pump-probe technique (Fig. 3-1).[45,52,100] The 355 nm uv excitation beam was split off from the collinear second harmonic and fundamental beams using a 355 nm reflecting/1.06 μm transmitting beam splitter. The transmitted 1.06 μm pulse was optically delayed by approximately 10 ns and then focused, using a 1 m focal length lens, into a 5 cm cell containing a solution of 30% H_3PO_4 in H_2O to generate the continuum probe pulse which provided useful coverage from approximately 390 nm to 750 nm. The coverage of each spectrum depends upon the calibration function of the OMA (250 channels) at the specific grating wavelength of the monochromator. Using a Hamamatsu C979 streak camera equipped with a C1000 type18 head, the FWHM of the polychromatic continuum pulse was found to be approximately 35 ps. Variable delays of up to 10 ns between the probe and excitation pulses were obtained by inserting a variable optical delay line (L_0=24.75 cm) in the path of the exciting uv pulse. To measure the spectrum and intensity of the probe beam. a portion was split off (using a prism beam splitter) for use as a
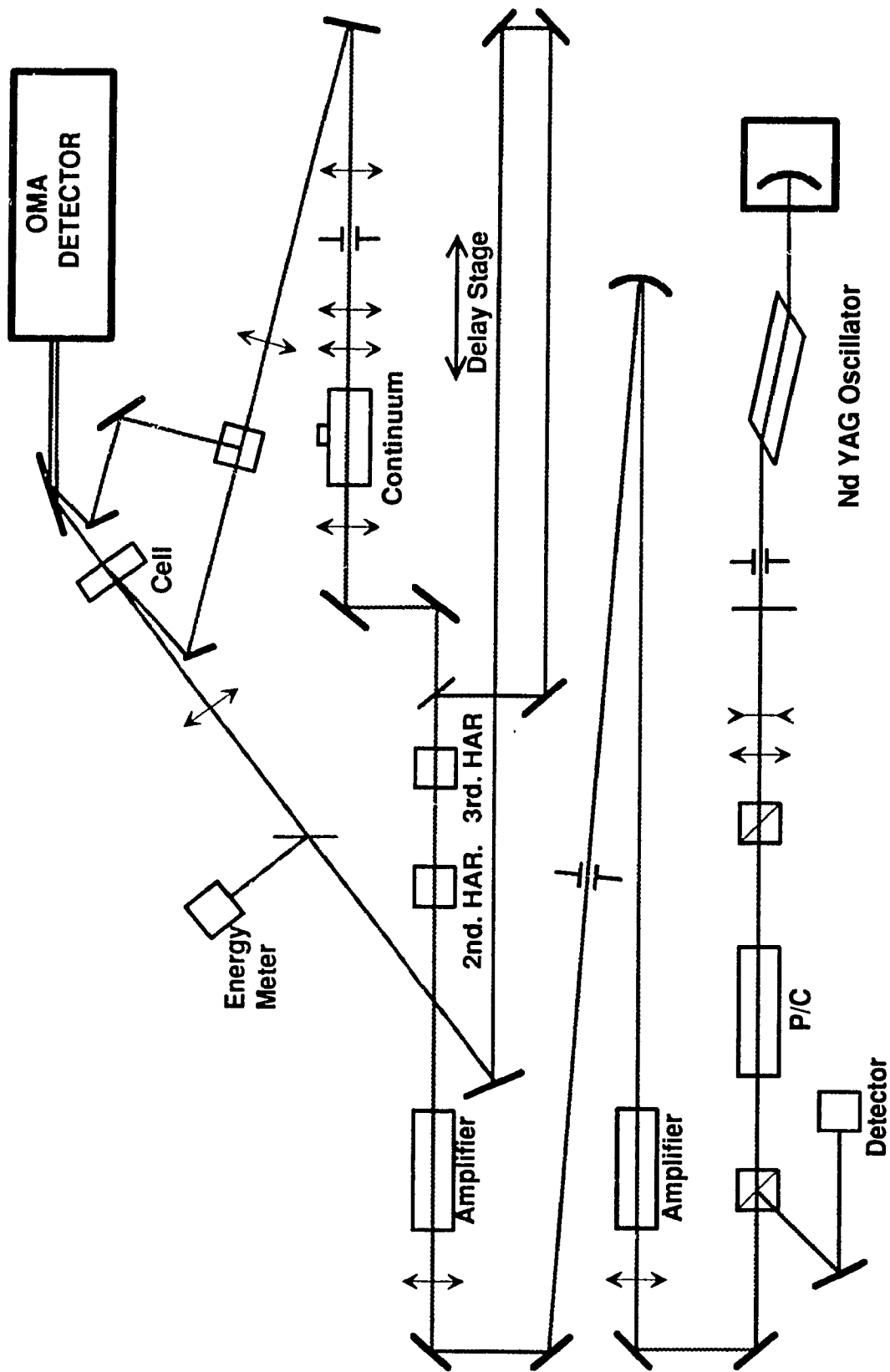
Fig. 3-1 Picosecond time-resolved transient absorption sepectroscopic system

"reference" beam. The spectrum of the "reference" beam (which bypassed the 2 mm path length sample cell) was recorded simultaneously with that of the main "sample" probe beam (which examined the excited portion of the sample cell) by focusing both beams at different heights along the slits of a monochromator-spectrograph (instrument SA (JY) model HR-320) fitted with a silicon intensified target (SIT) vidicon detector (EG&G PAR model 1254) with two-dimensional light sensing capabilities. The probe beam impinged on the sample cell at an angle of 2.5 ° with respect to the excitation beam. The main parameters of the system are listed in Table 3-2.

Table 3-2:   Main Parameters of the System

FWHM (ps)	Spectral Region	Delay Time	Pumping Energy
~ 35	395 ~ 645 nm (600 nm[a])	0 ~10 ns	< 4 mJ
	425 ~ 675 nm (610nm[a])		
	475 ~ 730 nm (640nm[a])		

[a] The grating wavelength of the monochromator

3.2.2   Chemicals

Dichloromethane (CH_2Cl_2) (CP), poly(ethylene-glycol) (Aldrich, MW.600), methanol (Accusolv spectro), and water (distilled) have been used without further treatment. The 7-diethylamino- 4-methylcoumarin (C1, C460) (Exciton) was recrystallized from methanol-water and sublimed; C102 or C480 (2,3,5,6-1H,4H-tetrahydro-8-methylquinolazino [9,9a,1-gh] coumarin) (Exciton), and 7-diethylamino-4-trifluoromethylcoumarin (C1F, C481) (Eastman Kodak), were recrystallized from methanol. The β-cyclodextrin (Aldrich) was recrystallized

from HPLC water and has no detectable fluorescence. The purification procedures have been described in section 2.2.4.

The **D-CD** aqueous solutions were prepared as described in reference[170] and used for absorption or fluorescence titration as described in section 2.2.3. The ground state absorption and excited state fluorescence spectra were done on a Cary 2200 (Varian) uv/vis spectrophotometer and an MPF-44 (Perkin-Elmer) spectrofluorimeter (see section 2.2.2) at Dépt. de Chimie, UQAM, respectively. The optical densities (OD) in 2 mm quartz cell at 355 nm of all samples were kept in the range of 0.3 ~ 1.0 for ESA studies, and ~0.1 for time-dependent fluorescence decay (TDFD) measurements. The time-dependent fluorescence decay (TDFD) measurements were carried out at the Biology Division, NRC, Ottawa. The system (Ar+, Rhodamine 6G dye laser, 310 nm)[63] is described in Chapter 5.

3.3 Excited State Absorption Data Analysis

The transmission of the probe beam $T(\lambda,t)$ at time t, and wavelength λ is given by the following expression:[171]

$$T(\lambda,t) = \exp\{G(\lambda,t)L\} \tag{1}$$

where L is the excited sample length and G is the gain coefficient.

For the wavelength region in which there is no significant ground state absorption (i.e., wavelengths are longer than 410 nm in methanol), the gain $G(\lambda,t)$ is given by:

$$G(\lambda,t) = \{\sigma_e(\lambda) - \sigma_S(\lambda)\}n_S(t) - \sigma_T(\lambda)n_T(t). \tag{2}$$

The first term in eq. (2) is the positive gain due to the stimulated emission, the second is loss due to singlet ESA and the third is loss due to triplet ESA, where $\sigma_e(\lambda)$, $\sigma_S(\lambda)$ and $\sigma_T(\lambda)$ are the stimulated emission, the $S_1 \rightarrow S_n$ absorption and the $T_1 \rightarrow T_n$ absorption cross-section, respectively. $n_S(t)$ and $n_T(t)$ are the populations of the singlet excited state S_1 and the triplet excited state T_1, respectively.

Since the triplet decay term $\tau_T^{-1} n_T(t) \ll \tau_S^{-1} n_S(t)$, $\tau_T^{-1} n_T(t)$ can be neglected due to relatively long lifetime of the excited triplet state, increased population of the triplet excited state T_1 at instance t, can be given by:

$$n_T(t) = Q_T\{n_S(0) - n_S(t)\} \qquad (3)$$

where the quantum yield of the triplet formation $Q_T = k_{ISC}\tau_S$, k_{ISC} is the rate constant for intersystem crossing from $S_1 \rightarrow T_1$ and τ_S is the lifetime of S_1. Substituting for $n_T(t)$ from eq. (3) into eq. (2), we get:

$$G(\lambda,t) = \{\sigma_e(\lambda) + \sigma_T(\lambda)Q_T - \sigma_S(\lambda)\}n_S(t) - \sigma_T(\lambda)Q_T n_S(0). \qquad (4)$$

Since the absorbance $A(\lambda,t) = -\log T$, we have:

$$A(\lambda,t) = -0.434 \{ [\sigma_e(\lambda) + \sigma_T(\lambda)Q_T - \sigma_S(\lambda)]n_S(t) - \sigma_T(\lambda)Q_T n_S(0) \}L. \qquad (5)$$

For the limited conditions:

(i)   At short wavelengths, where $\{\sigma_e(\lambda) \gg \sigma_T(\lambda)Q_T , \sigma_S(\lambda)\}$, the negative absorption (due to AE of the probe pulse) decays according to the population function $n_S(t)$ as:

$$A(\lambda,t) = -0.434 \, \sigma_e(\lambda)n_S(t)L. \qquad (6)$$

(ii)   At isobestic point $(\lambda = \lambda_{iso})$, $\sigma_e(\lambda) + \sigma_T(\lambda)Q_T - \sigma_S(\lambda) = 0$, A should be independent of $n_S(t)$, therefore, we expect no changes in the absorbance of the probe pulse with respect to time at this specific wavelength (λ_{iso}):

$$G(\lambda_{iso}) = - Q_T\sigma_T n_S(0) \tag{7a}$$

$$A(\lambda_{iso}) = 0.434 \, [Q_T\sigma_T n_S(0)]L. \tag{7b}$$

(iii)   At long wavelengths, the contribution of the stimulated emission can be ignored $(\sigma_e = 0)$. Thus, the change of the absorbance with time, depending on the magnitude of the triplet absorption term $Q_T\sigma_T$ relative to the singlet absorption cross-section σ_S is:

$$A(\lambda,t) = - 0.434 \, \{ \, [\sigma_T(\lambda)Q_T - \sigma_S(\lambda)]n_S(t) - \sigma_T(\lambda)Q_T n_S(0) \, \}L. \tag{8}$$

From the above model and assumptions, we expect the following absorbance changes: at short wavelengths, a decay of the negative absorption due to AE of the probe pulse; a wavelength where the AE is balanced by the singlet and the triplet ESA, resulting in no time-dependent absorbance changes; and at long wavelengths, the changes of absorbance depending on the relative magnitudes of $Q_T\sigma_T(\lambda)$ and $\sigma_S(\lambda)$ associated with the triplet and singlet excited states. Since decay of the AE and ESA depends on the same population function of the S_1 state, $n_S(t)$, we expect these two signals to have the same decay constant.

3.4   **Time-Resolved Excited State Absorption (ESA) and Amplified Emission (AE) Spectra of**

3.4.1   7-aminocoumarins in different solvents
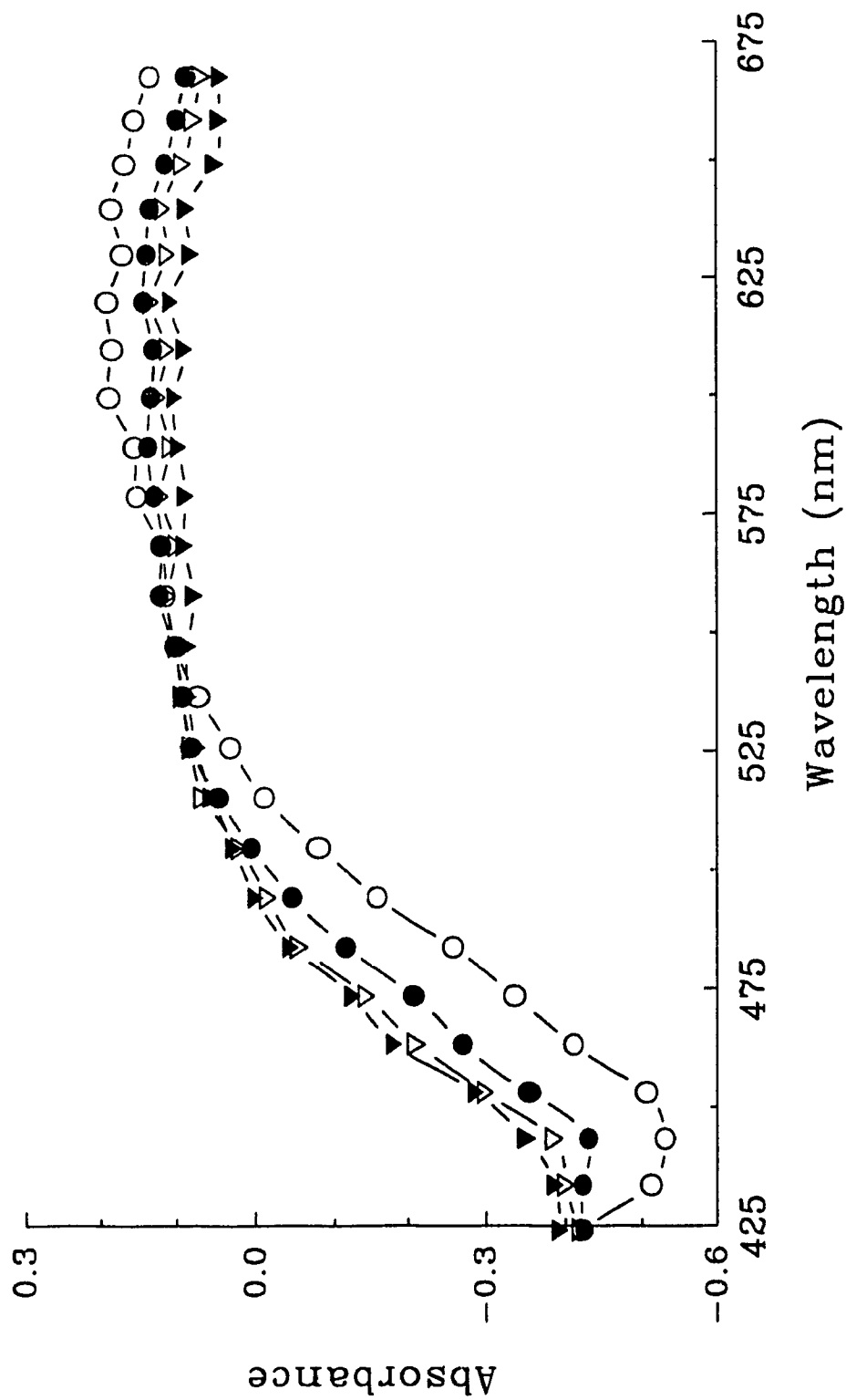
Fig. 3-2   Time-resolved amplified stimulated emission of 3.2x10⁻⁴ M C1 in methanol at (O): 100 ps, (●): 2 ns, (▽): 4 ns, and (▼): 5 ns.

71
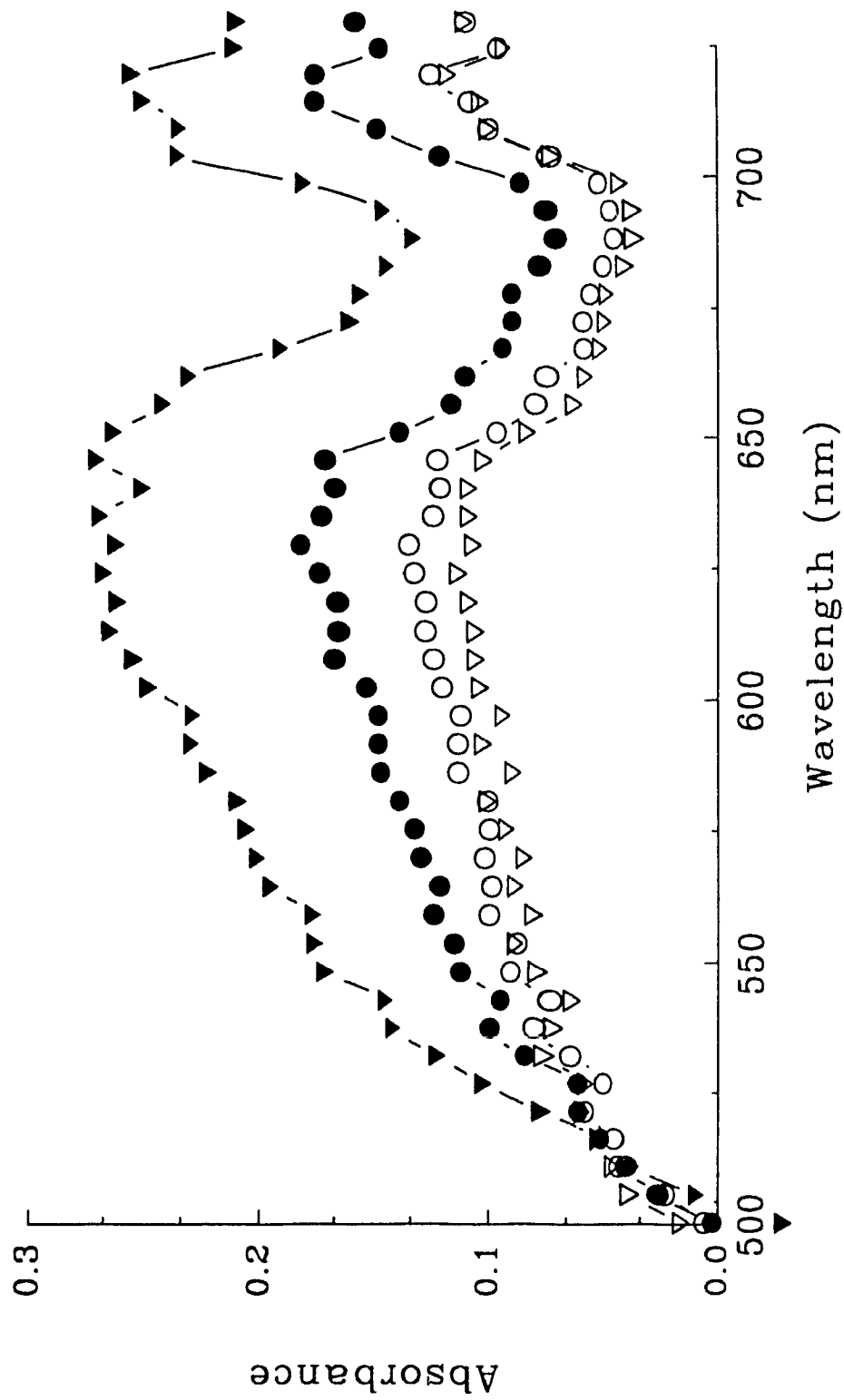
Fig. 3-3 Time-resolved excited state absorption of 3.2×10^{-4} M C1 in methanol at (▼): 1 ns, (●): 2 ns, (O): 5 ns, and (▽): 10 ns.

Time-resolved AE spectra of C1 in methanol which appears as the "negative absorption", and the short wavelength portion of the transient absorption are shown in Fig. 3-2. The transient absorption spectra (maxima at approximately 630 - 640 nm) between 1 ns and 10 ns are shown in Fig. 3-3. The emission at 400 - 550 nm consists of the AE of the probe pulse, which examines the population of the emitting state, and the non-time resolved amplified spontaneous emission. The amplified spontaneous emission appears as a residual background emission at long probe delay times. Clearly, if the AE and ESA originate from the same species, we expect from eq. (5): (i) decay of the AE signal, (ii) decay (if the singlet absorption dominates the triplet absorption) of the ESA signal at the same rate as the AE, and (iii) the appearance of an "isobestic" wavelength in which the absorption does not change with time during the decay of the singlet excited state (eq. (7)). The appearance of an "isobestic" wavelength in the time-resolved spectra (Fig. 3-2) is clearly in evidence as are the decays of both the AE and ESA (Fig. 3-3). The decay kinetics of the ESA (τ_{ESA} = 2.6±0.1 ns) are identical with those of the AE (τ_{AE} = 2.3±0.3 ns) (Fig. 3-4). These results show that both signals originate from the same excited state. The conclusion is further supported by the expected decrease in the lifetimes (τ_{ESA} = 1.4 ±0.3 ns and τ_{AE} = 1.5±0.5 ns) of both signals from C1 in a water-methanol solution containing 9.3 M water, and leaded in a decrease in fluorescence quantum yield with increased polarity of the solvent.[90,94] The excited state observed by the ESA and AE can be assigned to the singlet excited state on the basis of the short lifetime. The lifetime of the triplet excited state of C1 in ethanol is known to be of the order of microseconds.[172b] This assignment is in agreement with the independently determined single-photon fluorescence decay value (2.1 ns) of C1 in methanol (details are discussed in chapter 5).
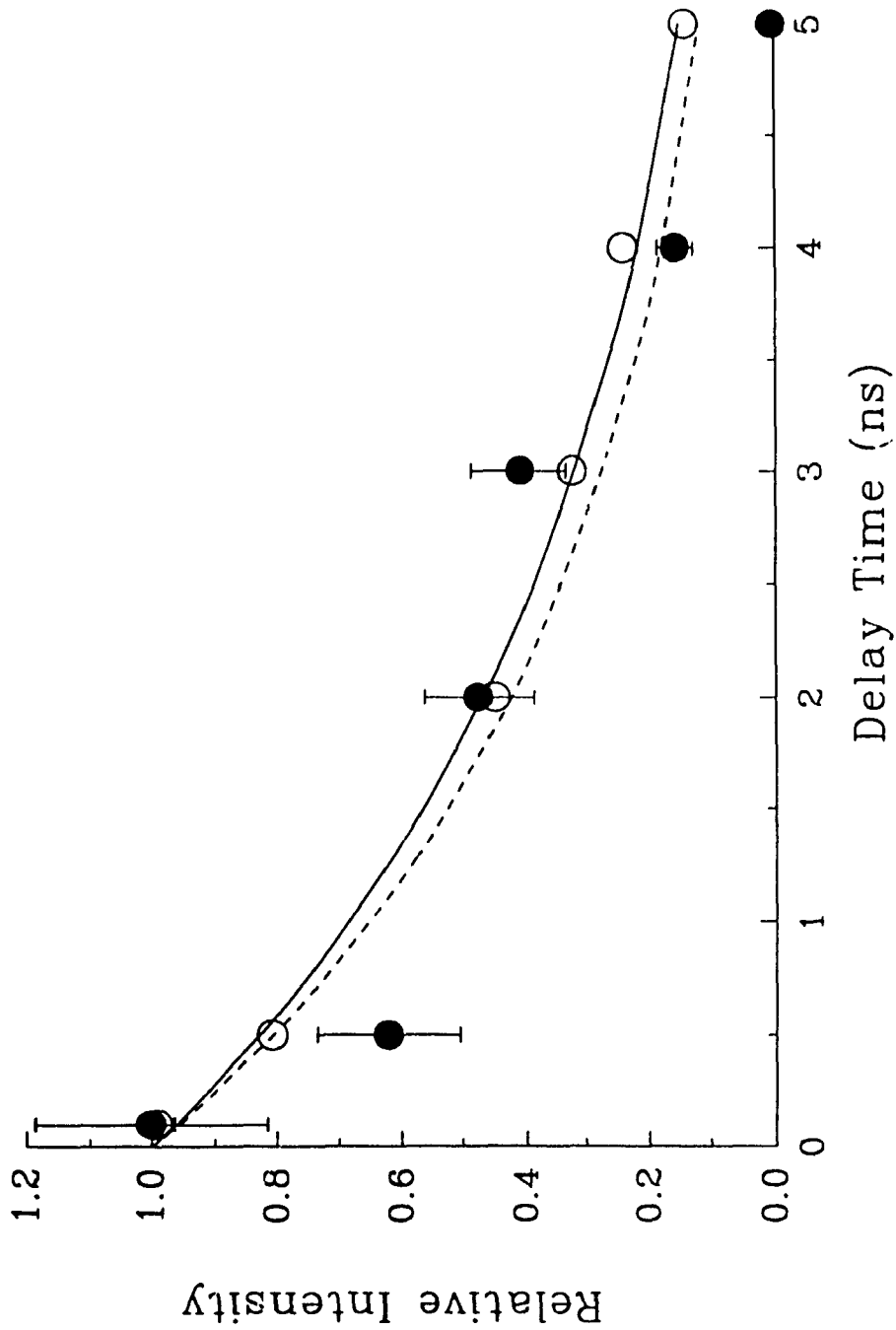
Fig. 3-4   Kinetic decay of ESA and AE signals from C1 in methanol, The solid and broken lines are the exponential fit to the decay of ESA (●) $\tau=2.3\pm0.3$ ns and AE (O) $\tau=2.6\pm0.1$ ns, respectively.

The remaining broad absorption at 10 ns (maximum at approximately 630 nm, Fig. 3-3), which is rather similar to the absorption at early times, can be assigned to the triplet excited state for the following reasons: (i) this is not the initially formed species; (ii) the same transient is observed in less polar solvents and from C102, C314, C334[172a] (where the possibility of formation of radical ions is less likely); (iii) the internal crossing time is obtained from the slow rise time of fluorescence intensity of C102, C314 and C334;[172a] (iv) the spectrum of this transient is virtually identical with the triplet excited state observed from flash photolysis of C1 in ethanol on a microsecond time scale.[172b]

The picosecond transient spectra of C1 in the other solvents (dichloromethane, water and PEG) Fig. 3-5 are similar to that observed in methanol and to that of C102 (Fig. 3-6). However, in dichloromethane, we were unable to measure a significant decrease in absorption from picosecond to nanosecond time region. In water, the magnitude of the decrease in the transient ESA from C1 was not sufficiently large for the quantitative estimation of the decay constant. However, the AE signal showed a clear rapid decrease ($\tau_{AE} = 430\pm50$ ps). This lifetime is in accord with the value of 410 ± 10 ps obtained from fluorescence lifetime measurements (chapter 5) independently. In the case of C102 in water, the transient absorption actually increases from 100 ps to 5 ns. These results are interpreted to mean that not only are the singlet and triplet ESA transitions similar in energy, but, they also possess comparable oscillator strengths throughout the absorption wavelengths investigated. Thus depending on the quantum yield of formation of the triplet excited state and the extinction coefficients of the excited singlet and triplet states, the transient absorption can either decrease, when the singlet absorption dominates, or
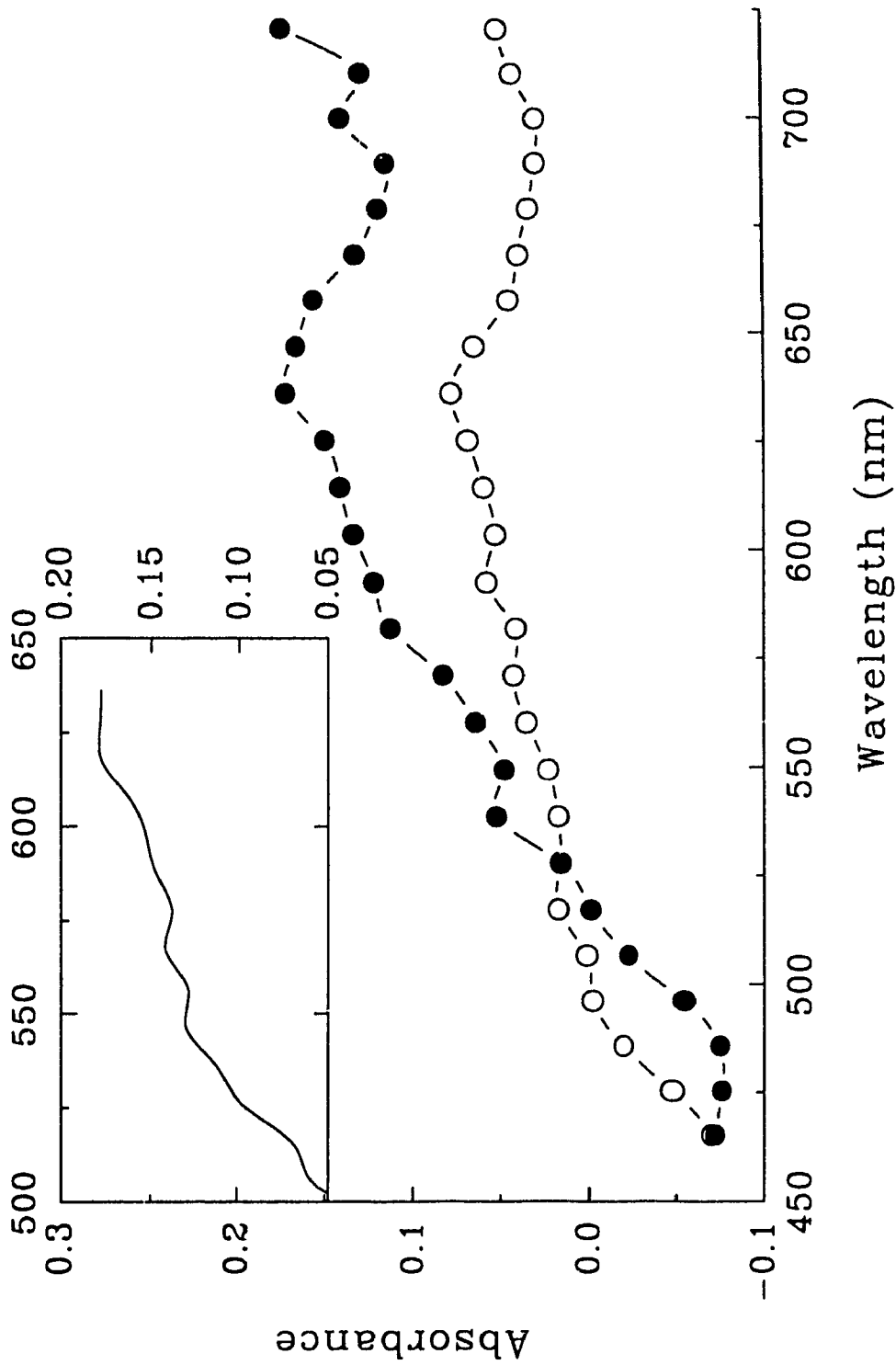
Fig. 3-5   Transient absorption spectra of C1 in (●) : water (4.4x10⁻⁴ M, 0.36 mJ), (O): dichloromethane
(1.0x10⁻⁴ M, 1.03 mJ), and PEG-600 (solid curve in insert frame) (2.9x10⁻⁴ M, 2.6 mJ) at 100 ps
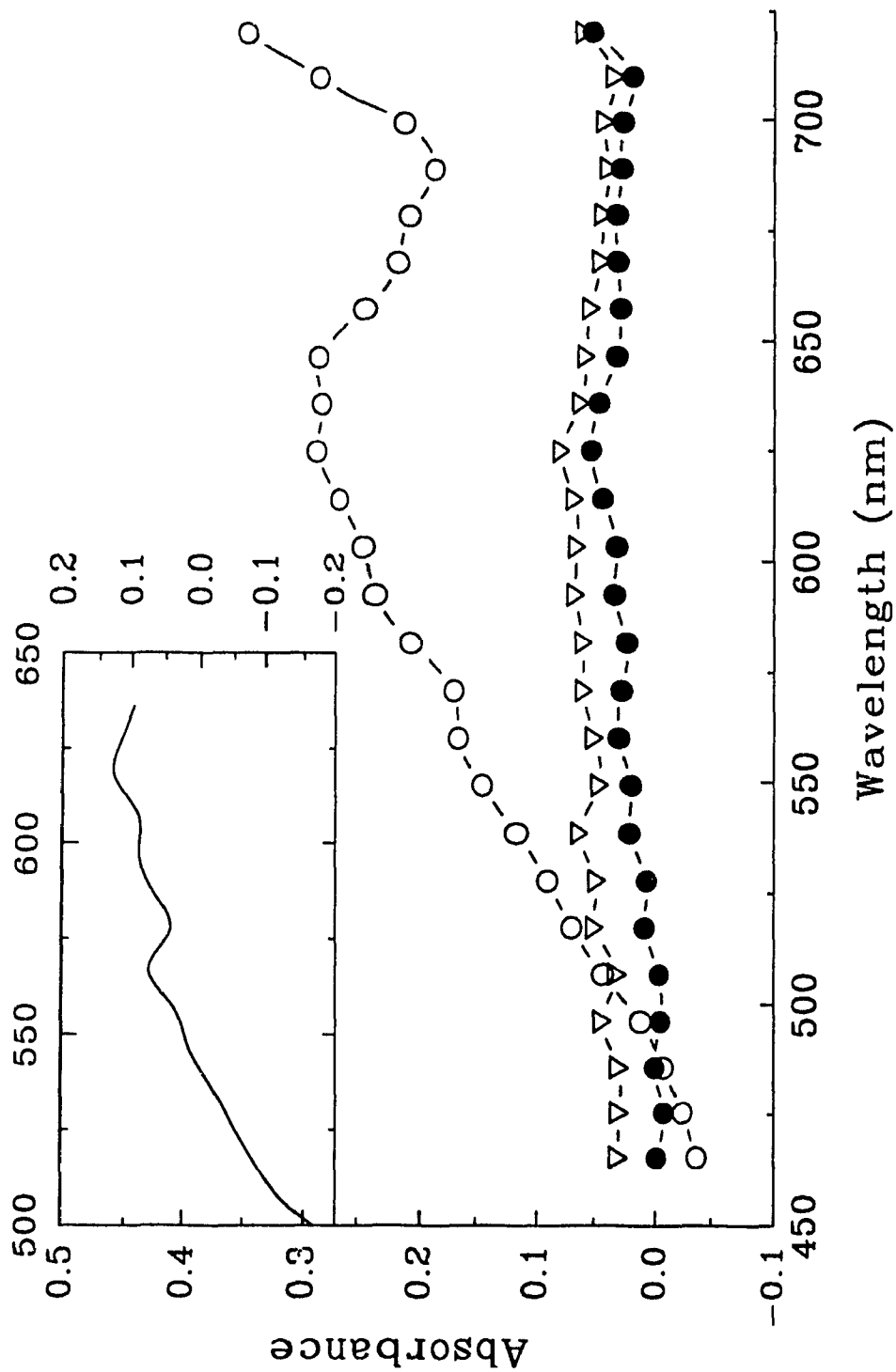
Fig. 3-6   Transient absorption spectra of C102 in water (1.1x10^{-4} M, 1.5mJ) at (●): 100 ps, (▽): 5 ns; and of C1 in water (4.4x10^{-4} M, 0.36 mJ) at (O): 100 ps.   Insert spectrum: C102 in PEG-600 (50 ps, 1.8x10^{-4} M, 1.2 mJ)

77

increase, when the triplet excited state absorption dominates, as described earlier in eq. (8). Such triplet ESA leads in changes in fluorescence quantum yield of these 7-aminocoumarins in polar solvents. The observed increase in transient absorption with C102 in water can be interpreted in terms of a greater yield of the triplet excited state since the structural constraint of this molecule is such that the TICT state, which may offer a competing rapid decay channel, can not be formed. Ideally, the singlet ESA can be identified by applying (i) the intersystem crossing rate k_{ISC} from the rise time of fluorescence using the time-resolved fluorescence spectroscopic technique, (ii) the decay time τ_S of AE from the time-resolved transient absorption measurement, and (iii) the maximum triplet ESA intensity at long delay time after complete depopulation of the excited singlet state ($n_S \rightarrow 0$). From eq. (8), the relationship among these above parameters (for $\tau_S \ll 10$ ns) can be expressed by the following equation:

$$A(\lambda, 10 ns) = 0.434 \sigma_T(\lambda) k_{ISC} \tau_S n_S(0) L \tag{9}$$

Thus, the cross section of the triplet ESA can be found:

$$\sigma_T(\lambda) = \frac{2.304 A(\lambda, 10 ns)}{k_{ISC} \tau_S n_S(0) L} \tag{10}$$

Therefore, ESA intensities at long wavelengths satisfies the following equation:

$$A(\lambda, t) = A(\lambda, 10 ns) - \left[A(\lambda, 10 ns)/n_S(0) - 0.434 \sigma_S(\lambda) L \right] n_S(t) \tag{11}$$

By applying the exponential decay of the population at the excited singlet state of eq. (12)

$$n_s(t) = n_s(0)e^{-t/\tau_s} \tag{12}$$

into eq. (11), the cross section of the singlet excited state can be estimated from the following relation:

$$A(\lambda,t) = A(\lambda,10ns) - \left[A(\lambda,10ns) - 0.434\sigma_s(\lambda)n_s(0)L\right]e^{-t/\tau_s} \tag{13}$$

where the initial population at the singlet excited state can be estimated from the the number of the probe molecules (C102) with a factor of 10^{-5}.

The AE from C1 in dichloromethane was intense, and not surprisingly, in view of the increased fluorescence yield in solvents of moderate polarity (refer to Table 4-1), consisted mainly of non-time-resolved AE of the spontaneous
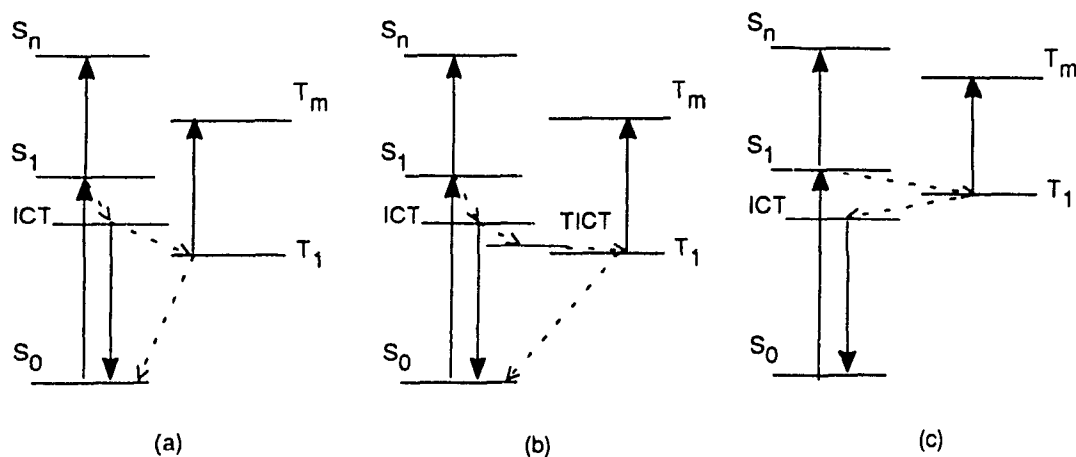
Scheme 3-1 Excited States

fluorescence. It is reasonable to assume in our case, that the similar spectra observed for C1 and the rigid C102 aminocoumarin in highly polar aqueous solution, and for C1 in solvents of lower polarity, are associated with non-fully-twisted ICT state; the (short) lifetime of the ICT state of C1 in aqueous solution (0.4 ns) is determined by the rate of conversion of the ICT state to the TICT state and by the lifetime of the TICT state. The TICT state can be considered as a

nonradiative state with fast rate of conversion to the lowest excited triplet state. The excited states are illustrated in Scheme 3-1, in which scheme (a) and (b) can be assigned to C102 and C1 in polar solvent, respectively. Both scheme (a) and (b) can offer the similar ESA spectrum without distinct TICT contribution for C1 in polar solvent as we observed in experiment. For scheme (c), the fast decay of triplet ESA would be expected, which is not observed experimentally for either 7-aminocoumarins.

3.4.2   C1/β–cyclodextrin complexes

3.4.2.1   Formation of C1/βCD complexes

From uv/vis absorption and steady state fluorescence (excited at isobestic point $\lambda_p = \lambda_{iso}^{ab}$) studies, as shown in Fig. 3-7 and Fig. 3-8, the ground state complexation dominates the mechanism of fluorescence enhancement in presence of β-CD with high ground state association constant (Fig. 3-9a) in the order of 10^4 (M^{-1}) instead of 10^2 (M^{-1}).[24] The kinetic study of the formation of ground and excited state complex[15,16] as discussed in chapter two, has been applied to distinguish the origin of the florescence enhancements in Fig. 3-8.

From Fig. 3-8, the weak contribution of excited state complexation ($K_{sv} \rightarrow$ 0 M^{-1} in comparison to $K \sim 10^4$ M^{-1}) has been calculated and illustrated in Fig. 3-9b. Therefore, the formation of **D-CD** complexes is dominated by static process.[15,16]

3.4.2.2   Picosecond time-resolved amplified emission (AE) and excited state absorption (ESA)

The picosecond time-resolved **AE** & **ESA** spectra of C1 in methanol, in water with or without β-CD (10 mM) at 50 ps, are shown in Fig. 3-10. The
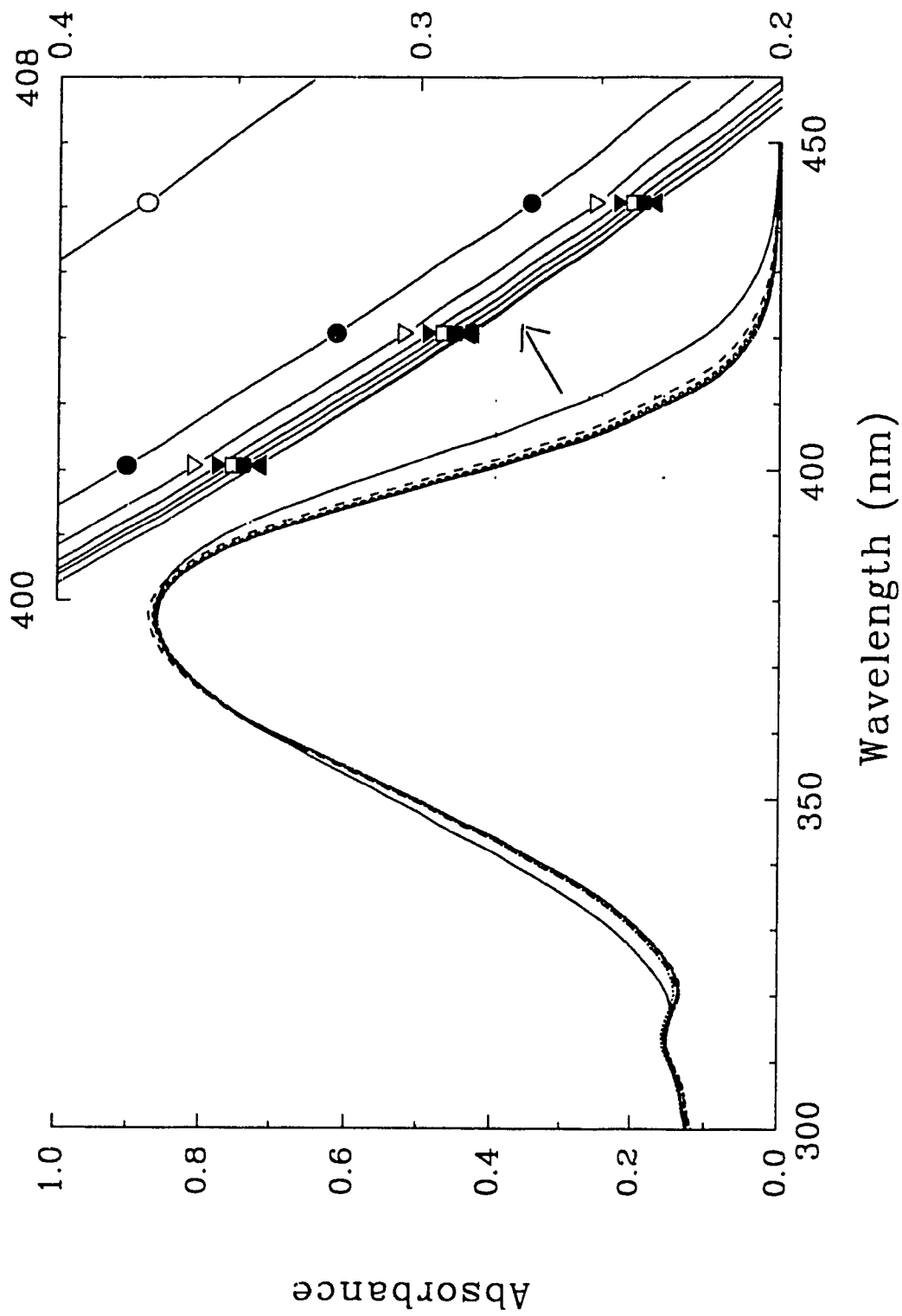
Fig. 3-7 UV/Vis absorption spectra of C1 (10^{-4} M) in water with different concentration of β-CD ($0 \rightarrow 15$ mM)
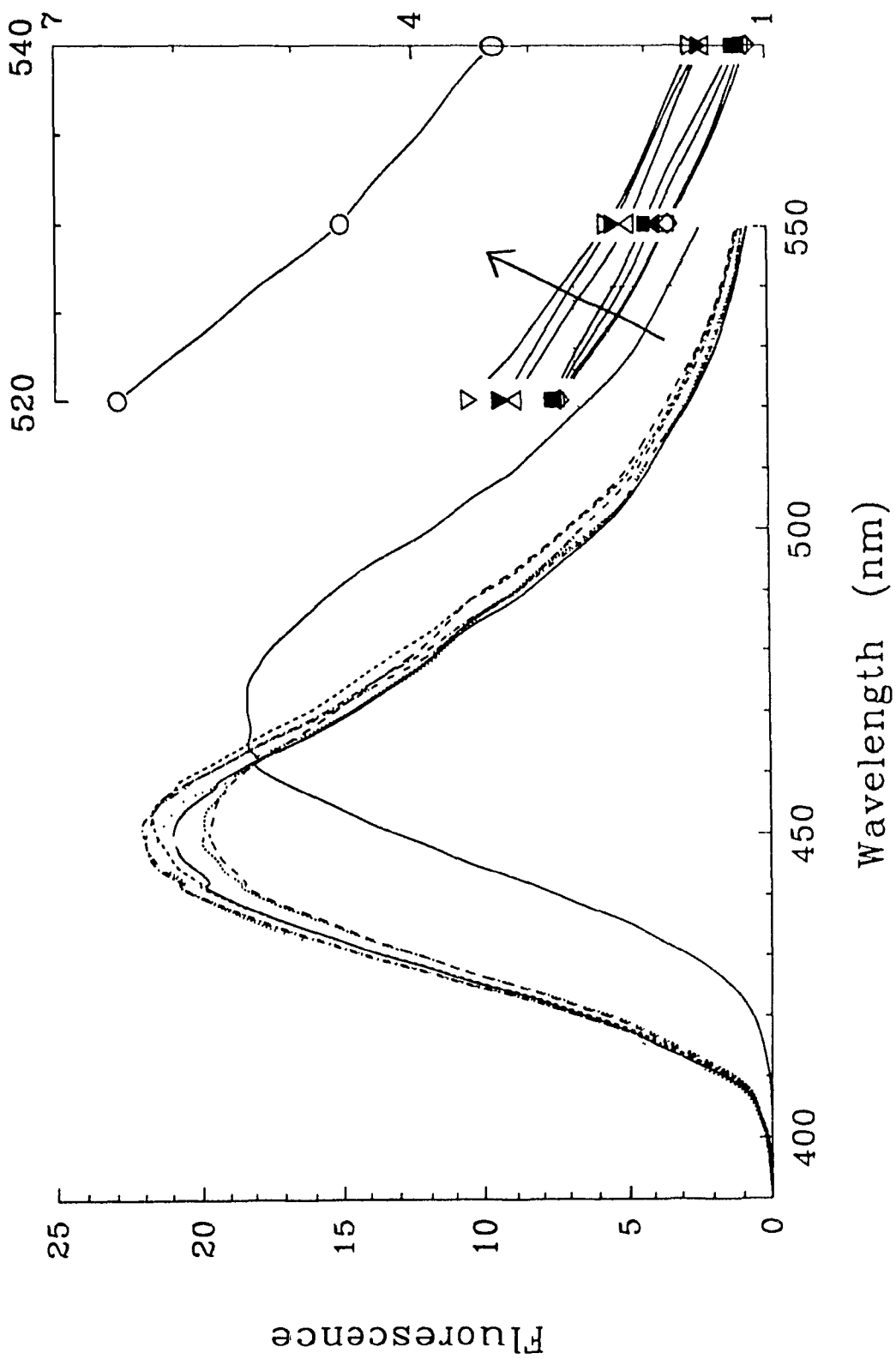
Fig. 3-8   Fluorescence spectra of C1 (10^{-4} M) in water with different concentration of β-CD ($0 \rightarrow 15$ mM)
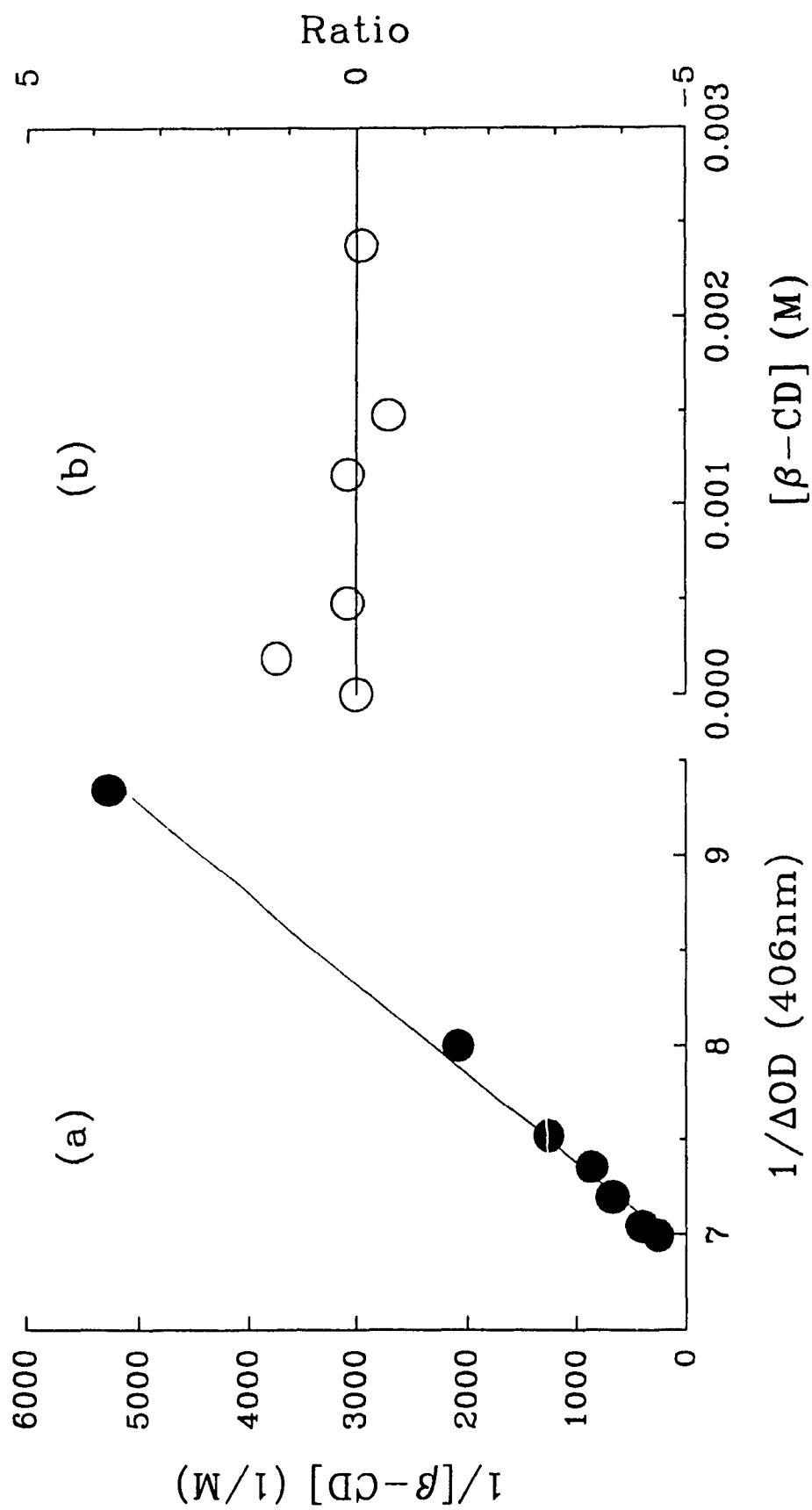
Fig. 3-9   Complexation constant of C1 with β-CD in water (a) in the ground state, 1/[β-CD] = ΔεLK[C1]/ΔOD-K,
K = (1.45±0.05)x10^4, M^{-1}; (b) in the excited state, [I$_0$/(I - I$_{CD}$)(1 - α) -1 = K$_{SV}$[β-CD], K$_{SV}$ → 0
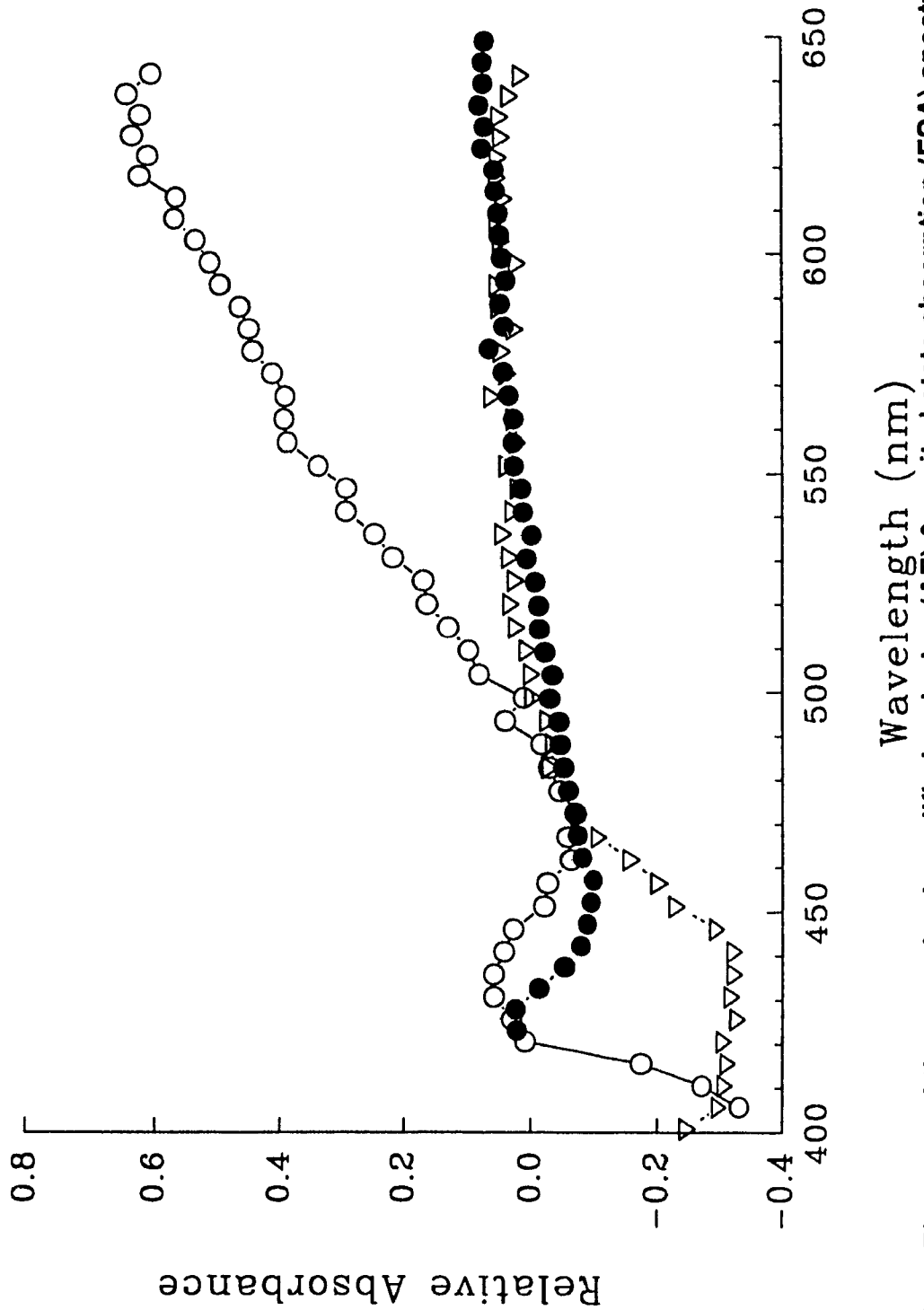
Fig. 3-10   Picosecond time-resolved amplified emission (AE) & excited state absorption (ESA) spectra (50 ps) of C1 (a) in methanol (∇); (b) with β-CD in water ($\bullet$); and (c) without β-CD in water (O)

shift of **AE** peak position due to the environmental polarity known from the steady state study,[6] and shows that C1 included in β-CD (Fig. 3-11) is in an environment of polarity intermediate between methanol and water. Meanwhile, the change of the kinetic decay from **AE & ESA** spectra of these systems (Table 3-3) parallels the tendency of the **AE** peak position change ($\tau_{MeOH} > \tau_{\beta\text{-CD/H}_2\text{O}} > \tau_{H_2O}$) for both C1 and C1F/βCD complexes in aqueous solution. But, as we know from the steady state fluorescence studies (Figs. 3-8, 3-9b), the fluorescence peak position should correspond to the polarity of the empty cavity which is like alcohol,[127,128,130] if the probe molecule occupies the empty CD's cavity. The results obtained from the **AE & ESA** spectra contradict this expectation.

Table 3-3: Comparison of the lifetimes in AE & ESA studies:

Dyes	Solvent	CD's	λ_{AE}, nm	τ, ns
C1	H_2O	None	471	0.43±0.05
C1	H_2O	β-CD	456	0.6±0.2
C1	MeOH	None	440	2.3±0.3
C1F	H_2O	None	None[a]	None[a]
C1F	H_2O	β-CD	530	0.05±0.01
C1F	MeOH	None	523	0.37±0.08

[a] No **AE & ESA** was observed from 0.05 to 10 ns within limits of apparatus.
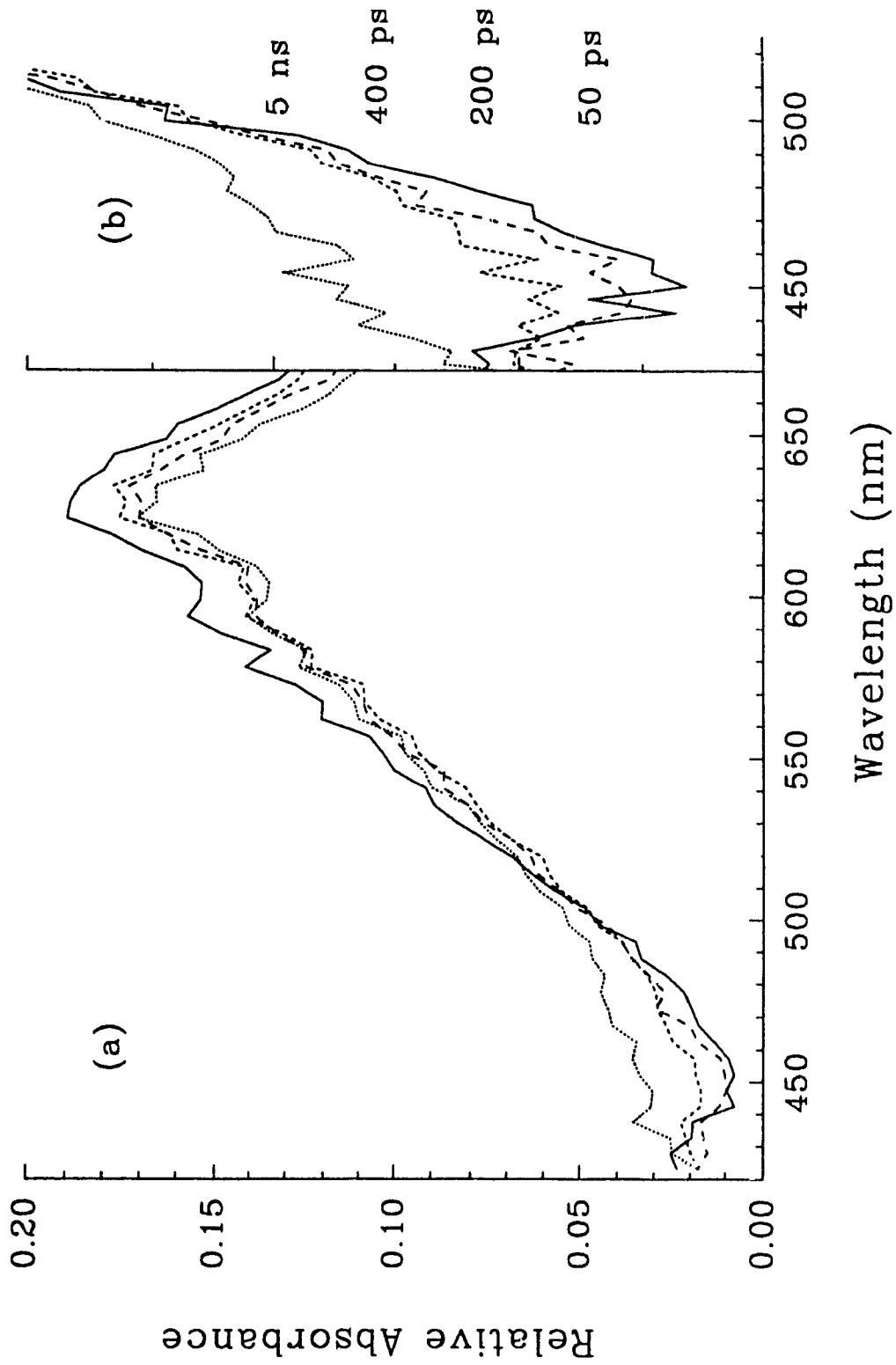
Fig. 3-11 Picosecond time-resolved (a) excited state absorption (ESA) & (b) amplified emission (AE) spectra of C1 with β-CD in water

3.4.2.3　　Time-resolved fluorescence measurements

To answer the above question, additional time-resolved fluorescence studies were carried out. The results show that the decay of the fluorescence of C1/β-CD (~10 mM) in water follows a triexponential decay kinetics with 85% of two similarly short-lived (0.3±0.1 ns and 0.5±0.1 ns) and 15% of long-lived (2.5±0.1 ns) components. The species associated spectra (SAS)[74] are shown on Fig. 3-12, using multiexponential- component kinetics (details see chapter 5). The lifetimes of the short-lived species are similar to that of C1 in water, and that of the long-lived species closes to that of C1 in methanol (Table 3-4).

Table 3-4: Comparison of lifetimes of C1 in time-resolved fluorescence studies:

Solvent	CD's	Kinetics	τ_{FL} (ns)	τ_{AE} (ns)
H_2O	None	Single-exponential	0.416±0.001	0.43±0.05
H_2O	β-CD	Tri-exponential	2.3±0.1	
			0.5±0.1	0.6±0.2
			0.3±0.1	
MeOH	None	Single-exponential	2.100±0.001	2.3±0.3

On the basis of information obtained from the time-resolved measurements, such as kinetic decay time of the emitting state, the coexistence of short-lived and long-lived components was reported in
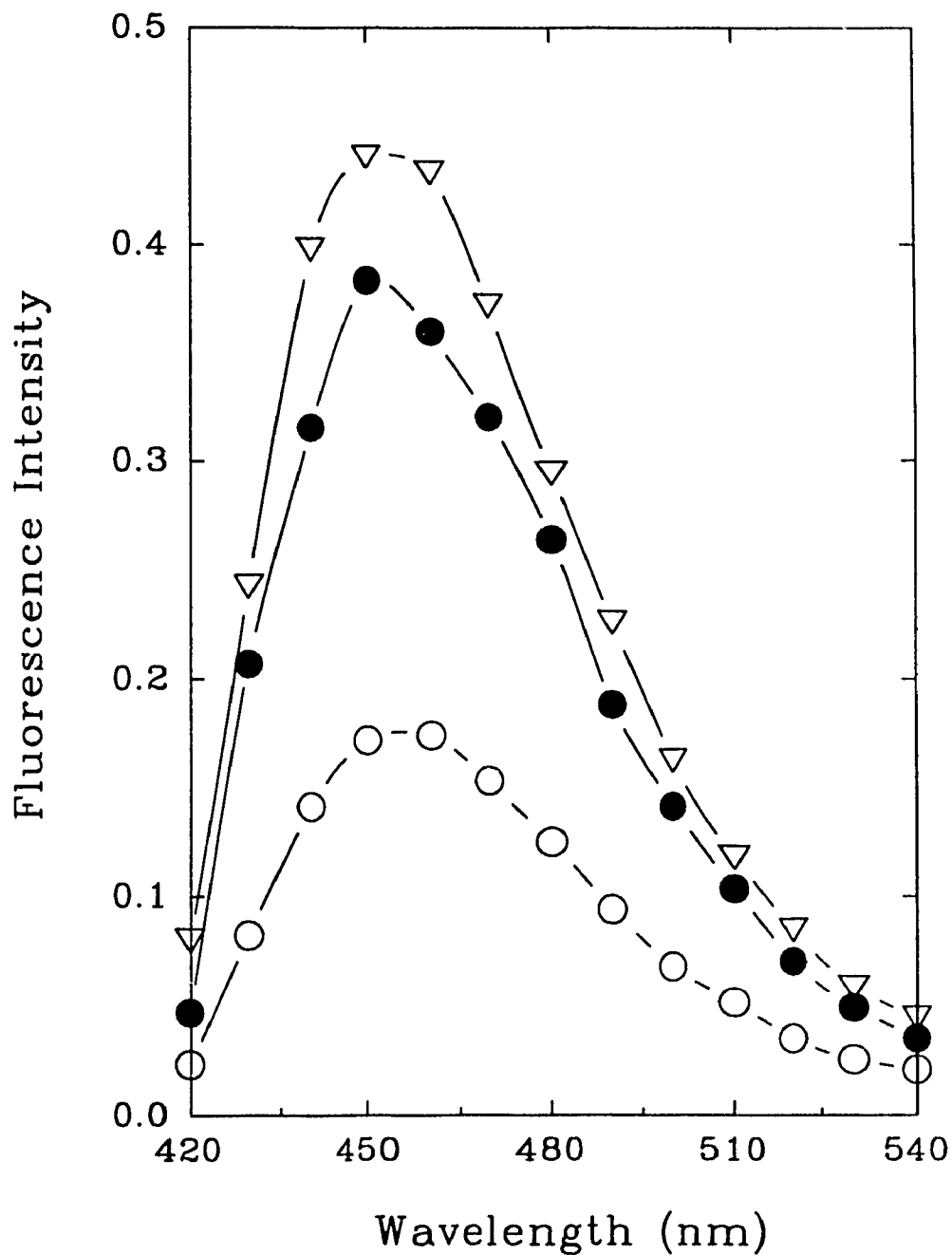
Fig. 3-12 Species associated fluorescence spectra of C1 with β-CD in water with different decay times of 0.5±0.1 ns (●); 0.3±0.1 ns (O); and 2.5±0.1 ns (∇)

pyrene/cyclodextrin/alcohols,[167] and potassium 2-(p-toluidinyl)naphthalene-6-sulfonate/cyclodextrin/surfactant system,[60a] using time-resolved fluorescence techniques. But, until now, there is no report on the kinetics and the dynamics of the formation of 7-aminocoumarin dye/cyclodextrin complexes in aqueous solution using time-resolved transient absorption and fluorescence spectroscopies. In comparison with **AE** & **ESA** results (Tables 3-3, 3-4), the **AE** position of C1 included in β-CD and the lifetime of the excited state, can be explained by the overlapping of three fluorescent components as detected in time-resolved fluorescence measurements. Since the majority (85%) of the complexes are the short-lived species, the lifetimes found in **AE** & **ESA** studies are of the same order as that of C1 in water.

The co-existing short (85%) and long-lived (15%) components in presence of β-CD could be explained by co-existing normal and inverted **D-CD** complexes as illustrated in Figs. 3-13a, b[23] where the normal complex should have a long lifetime due to alcohol-like environment inside the empty CD's cavity. Conversely for the inverted complex, the environment seems similar to that in water and a much shorter lifetime is observed (Tables 3-3, 3-4). But, the reason for forming two short-lived complexes is still arguable[109] considering the hydrophobic nature inside the CD's cavity and charge transfer (CT) properties of coumarin dyes.

However, since the C1 molecules have been completely included inside CD's cavity (complexed) as observed from ground state and steady state fluorescence studies, the more acceptable structure of **D-CD** complexes can be considered as the normal form as illustrated in Fig. 3-13a. The pre-existing H_2O molecules inside CD's cavity are coexisting with dye molecule rather than excluded.[109] As a result, the co-existing H_2O molecules inside the CD's cavity

can build a water-like environment for the short-lived normal complex (Fig. 13c).
In other words, a majority of CD cavities include H_2O molecules to build up a
water-like environment; 15% of CD's cavities exclude H_2O molecules with more
alcohol-like environment as illustrated in Fig. 13a.
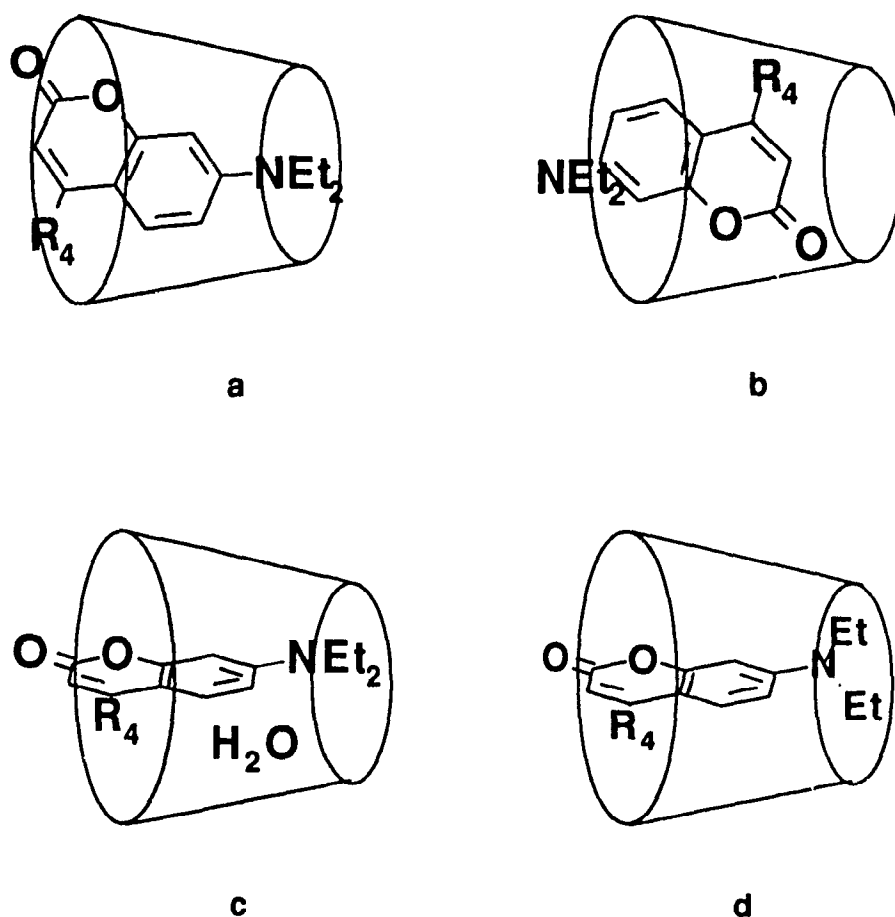
Fig. 3-13 (a) Normal; (b) inverted; (c) normal with H_2O; and (d) unsolvated TICT
C1/β-CD complexes

90

Meanwhile, the origin of the shortest-lived species found in time-resolved fluorescence measurements (Table 3-4), may be due to the unsolvated twisted internal charge transfer state (**TICT**) of C1 in the empty CD cavity (Fig. 13d). But, this is contradictory to the nonradiative characteristics of the TICT state. Therefore, the origin of this shortest lifetime component is still not clear.

3.5   Conclusion

3.5.1   Further studies

3.5.1.1   ESA and AE studies

In the **ESA** study of C1, C102 in methanol, and water, some additional work can be done in future: (i) The effect of the solvated electron absorption which can be subtracted by applying the spectral simulation using the results from the radiation studies;[173] (ii) The explanation about possible TICT contribution to maintain the stable ESA for C1 in aqueous solution could be made clearer by excluding the contribution from the solvated electron; (iii) There is the possibility of calculating the excited singlet state cross sections by integrating the time-resolved transient absorption spectra with respect to time. From eq. (5), the integral of transient absorption with respect to time can be given by:

$$A(\lambda) = \int A(\lambda,t)dt = -0.434\int L\{ [\sigma_e(\lambda) - \sigma_s(\lambda)]n_s(t) + \sigma_T(\lambda)Q_T[n_s(t) - n_s(0)]\}dt$$

$$= L[\sigma_e(\lambda) - \sigma_s(\lambda)] \int n_s(t)dt + L\sigma_T(\lambda)Q_T \int [n_s(t) - n_s(0)]dt \qquad (14)$$

where the integral of the second term is equal to zero. Thus, the integral of the transient absorption can be found as:

$$A(\lambda) = -0.434[\sigma_e(\lambda)-\sigma_s(\lambda)]L\int n_s(t)dt = -0.434[\sigma_e(\lambda)-\sigma_s(\lambda)]Ln_s(0)\tau_s \qquad (15)$$

where τ_S is the lifetime of the excited singlet state.

For the limited cases: (i) at short wavelengths, $\sigma_S(\lambda) = 0$, the stimulated emission cross section can be quantitively estimated by:

$$\sigma_e(\lambda) = -2.304\ A(\lambda)/\ (n_S(0)\tau_S L); \tag{16}$$

(ii) at long wavelengths, $\sigma_e(\lambda) = 0$, the excited singlet state cross section is simply given by:

$$\sigma_S(\lambda) = 2.304\ A(\lambda)/\ (n_S(0)\tau_S L) \tag{17}$$

where the initial population of the excited singlet state can be considered as the number of dye molecules in the solution with a factor f_N ** under assumption of full excitation.

3.5.1.2 Dye-Cyclodextrin complexes

The steady state fluorescence study of C1, C102/β–CD in aqueous solution[74] done in Biology Division, NRC, Ottawa, may offer some valuable information about the difference in complexability of these two dyes with β–CD. The difference can be explained by the following reasons: (i) the molecular size of C102 is comparable to the cavity diameter of β–CD; (ii) the relatively poor cationic character of C102 due to the rigid amino group and less charge separation in comparison with that of the conformational mobile C1 molecules with a potential TICT state.

** This factor f_N can be approximated by: $f_N = \left[E_p / \left(h\nu_p \right) \right] e^{-\varepsilon_{01}(\nu_p)[dye]L}$, where E_p is the pumping energy; $\varepsilon_{01}(\nu_p)$ is the ground state molar absorption coefficient at pumping frequency ν_p; and h is the Planck's constant.

To better understand the formation of D-CD complexes, and proving the coexistence of the water molecules inside the CD's cavity, the dry D-CD solid dissolved into aqueous solution, can be used for further studies. The preparation method of the solid inclusion complex used by Scaiano, et al.,[132b] in studying the xanthone-CD complex, can be introduced to make dry D-CD solid (without water molecules inside the CD's cavity).

For verifying the formation of TICT state D-CD complex (Fig. 3-13d), alcohols can be chosen as the ideal solvent to study the kinetics of the D-CD complexation using single photon counting techniques. The formation of the partial TICT state for C1 in alcohols (methanol) was predicted from MINDO calculation and spectrofluorimetric studies.[94] If two fast-decay components exist in C1/CD methanol solution, but not in C1/CD butanol solution (which is the critical point for the significant TICT formation[90]), along with single decay kinetics for the C102/CD in the similar solvents, it will provide strong evidence for the existence of TICT state of C1 complexed with β–CD in aqueous solution. Meanwhile, a system like C1/CD in chlorinated co-solvents, could be used to verify the possibility, and study the kinetics, and dynamics of exiting H_2O molecule from the CD's cavity[92] using single photon counting techniques.

3.5.2   Conclusion

Time-resolved **AE** has been observed in the transient absorption spectra of C1 in solution using a pump-probe experimental arrangement. The spectral changes consisting of **AE** at short wavelengths, a time-independent wavelength region and **ESA** at longer wavelengths are consistent with a single excited state species. On the basis of the similar transient **ESA** spectra observed for C1 and the "rigid" C102 aminocoumarin in aqueous solution, and for C1 in less polar

solvents, the transient is assigned to an excited **ICT** state[100] rather than to a **TICT** state of C1.[92] These results do no appear to support previous evidence for the formation of a TICT-solvent exciplex in moderately polar to polar solvents.

The independent time-resolved measurements of coumarin dye-CD complex, provide some information about the structure of the **D-CD** complexes. The time-resolved AE spectra of **D-CD** in aqueous solution possess an intermediate peak position and decay time between that of C1 in methanol and aqueous solution. This is evidence that there are water molecules inside CD cavities, which can not be identified by steady state fluorescence studies.[123-25,92,104,133]. The tri-exponential decay of the time-resolved fluorescence spectra observed in C1/βCD in aqueous solution, is an another example of CD inclusion complex and differs from the other cyclodextrin inclusion system.[60a] The majority of the **D-CD** complexes decay much faster than C1 in methanol, but slower than C1 in water, which is consistent with their **AE** results. The further studies will focus on the identification of the co-existing H_2O **D-CD** complex (Fig. 3-13c) and the possible unsolvated TICT **D-CD** complex (Fig. 3-13d).

Chapter 4: SOLVATOCHROMICS of 7-AMINOCOUMARINS

4.1 Introduction

Molecules dissolved in a solvent undergo intermolecular interaction with the solvent in both the ground and excited state,[5,6,65,70,101] which is reflected in changes in ground state absorption and fluorescence spectra with solvents of different polarity. The change can be quantified by a plot of the difference of the maximum absorption and the fluorescent band (represented by the peak frequency) versus solvent polarity function known as a *solvatochromic plot.*[5,6,101] A commonly accepted polarity function is that due to Mataga and Lippert.[5] Exceptions are observed when a conformational change occurs in the excited state such as the formation of a twisted intramolecular charge transfer (TICT) state.[101-103]

The mechanism of this phenomenon has been studied for about thirty years. The intermolecular interaction between solute and solvent can be due to[5c] (i) changing the charge transfer band due to the H-bond formation; (ii) dipole-dipole interaction; (iii) dielectric dispersion of solvent; and (iv) the formation of the TICT state.[101-103] A significant solvatochromic shift was observed for bis(N,N-dialkylamino)phenyl sulfones in homologous alcohol solvents,[174] in which a very high slope for the '*red*' band (TICT) and a more flat slope for the '*blue*' band with polarity of the solvents have been found.

For the 7-aminocoumarin dyes,[101] a linear solvatochromatic plot satisfing the Lippert-Mataga equation is observed in aprotic solvents. Such linear behaviour is not found in protic solvents. The mechanism of the nonlinear

phenomenon is not clear and could be due to the formation of TICT state as pointed out by Rettig and Klock for C1 in alcohols.[94]

In contrast to the thoroughly studied polarity properties of pure liquids,[6a] only little is known about the polarity of mixtures of liquids,[175-177] which are rather useful for studying solvent effects due to continuously adjustable properties of various solvents by changing the mixture ratio. Based on Rettig and Klock's interpretation,[94] and the significantly lower fluorescence quantum yield for C1 and C1F in comparison with that of C102 and C102F in alcohols and water,[87,88,90] and the difference in the solvatochromic plot between the flexible C1(or C1) and the rigid C102 (or C102F) in the co-solvent system is a reflection of the conformational change asscociated with the formation of TICT state in C1 or C1F, but not in the rigid species (C102, C102F).

4.2   **Experimental Section**

4.2.1   Chemicals   .

Cyclohexane (BDH, distilled in glass), n-butyl acetate (Fisher, spectro), acetonitrile (Caledon, distilled), 1-butanol (Fisher, spectro), 1-propanol (Fisher, spectro), methanol (Accusolv spectro), Dichloromethane (CH_2Cl_2) (Anachimia, spectro), and water (NANO Pure, distilled) have been used without further treatment. The 7-diethylamino- 4-methylcoumarin (C1, C460) (Exciton) was recrystallized from methanol-water and sublimed (as described in section 2.2.4); C102 or C480 (2,3,5,6-1H,4H-tetrahydro-8-methylquinolazino [9,9a,1-gh] coumarin) (Exciton); 7-diethylamino- 4-trifluoromethylcoumarin (C1F) (Exciton) and C102F or C530 (2,3,5,6-1H,4H-tetrahydro-8-trifluoromethylquinolazino [9,9a,1-gh] coumarin) (Exciton), were used as received.

4.2.2 Sampling and measurements

For the binary solvent system, the samples were made by titrating two stock solutions of different compositions with the same molar concentration of the coumarin dye. (For detailed information see section 2.2.3)

The ground state absorption and excited state fluorescence spectra were done on Cary 2200 (Varian) uv/vis spectrophotometer and MPF-44 (Perkin-Elmer) spectrofluorimeter (see section 2.2.2) at Dépt. de Chimie, UQAM, respectively. Unfortunately, calibration of the wavelength position was not done in the measurement. But, it can be considered as a constant factor which is acceptable over a small wavelength region.

4.3 Solvatochromics of 7-aminocoumarin Derivatives

4.3.1 in pure solvents

4.3.1.1 Lippert-Mataga relation

According to the Lippert-Mataga relation:[5c]

$$\Delta \upsilon = \upsilon_{ab}^r - \upsilon_{fl}^r = \frac{2}{hc} \frac{(\mu_e - \mu_g)^2}{a^3} (\frac{\varepsilon - 1}{2\varepsilon + 1} - \frac{n^2 - 1}{2n^2 + 1}) + Z \tag{1}$$

where υ_{ab}^r, υ_{fl}^r are the frequencies at peak position on the absorption and fluorescence spectra, respectively. μ_g, μ_e are the dipole moments of the ground and excited states, respectively; n and ε are the refractive index and dielectric constant of the solvent. The constants h and c are respectively, Planck's constant and the velocity of light in vacuum. The Onsager radius a of the solvent cage can be taken as approximately 40% of the long axis of the molecules as suggested by Lippert for elongated nonspherical molecules.[5d] Z is a minor term

related to the sum of the maximum vibronic energy in both ground and excited singlet states.[5c]

The solvatochromic plots of C1 and C102 in different solvents are illustrated in Figs. 4-1, 4-2. The horizontal shift of the solvatochromic plot of C1 in aprotic solvents in comparison with that in protic solvents (Fig. 4-1), is consistent with the H-bonding effect from the H-bond donating protic solvents. The linear fit for the shifts of C1 in aprotic solvents is computed by the method of least square as:

$$\Delta \upsilon_{st} = (4.3 \pm 1.0)F(\varepsilon,n) + (3.0 \pm 0.2) \tag{2}$$

where the function $F(\varepsilon,n)$ is derived from the eq. (1) as defined by:

$$F(\varepsilon,n) = \frac{\varepsilon - 1}{2\varepsilon + 1} - \frac{n^2 - 1}{2n^2 + 1}. \tag{3}$$

This is similar to the linear fit function obtained from C102 in the whole range of solvents as:

$$\Delta \upsilon_{st} = (4.0 \pm 0.7)F(\varepsilon,n) + (3.4 \pm 0.2). \tag{4}$$

Since the excited state dipole moment is much larger that that in the ground state $\mu_e \gg \mu_g$,[5c] the excited state dipole moment can be estimated from the slope in eq. (2) for C1 or eq. (4) for C102, which are of the same order, if the Onsager radius is assumed to be the same for both.

The nonlinear solvatochromic plot of C1 in protic solvents is in sharp contrast with the linear plot for C102, and may be due to their conformational difference in excited state. The difference in the fluorescence quantum yield
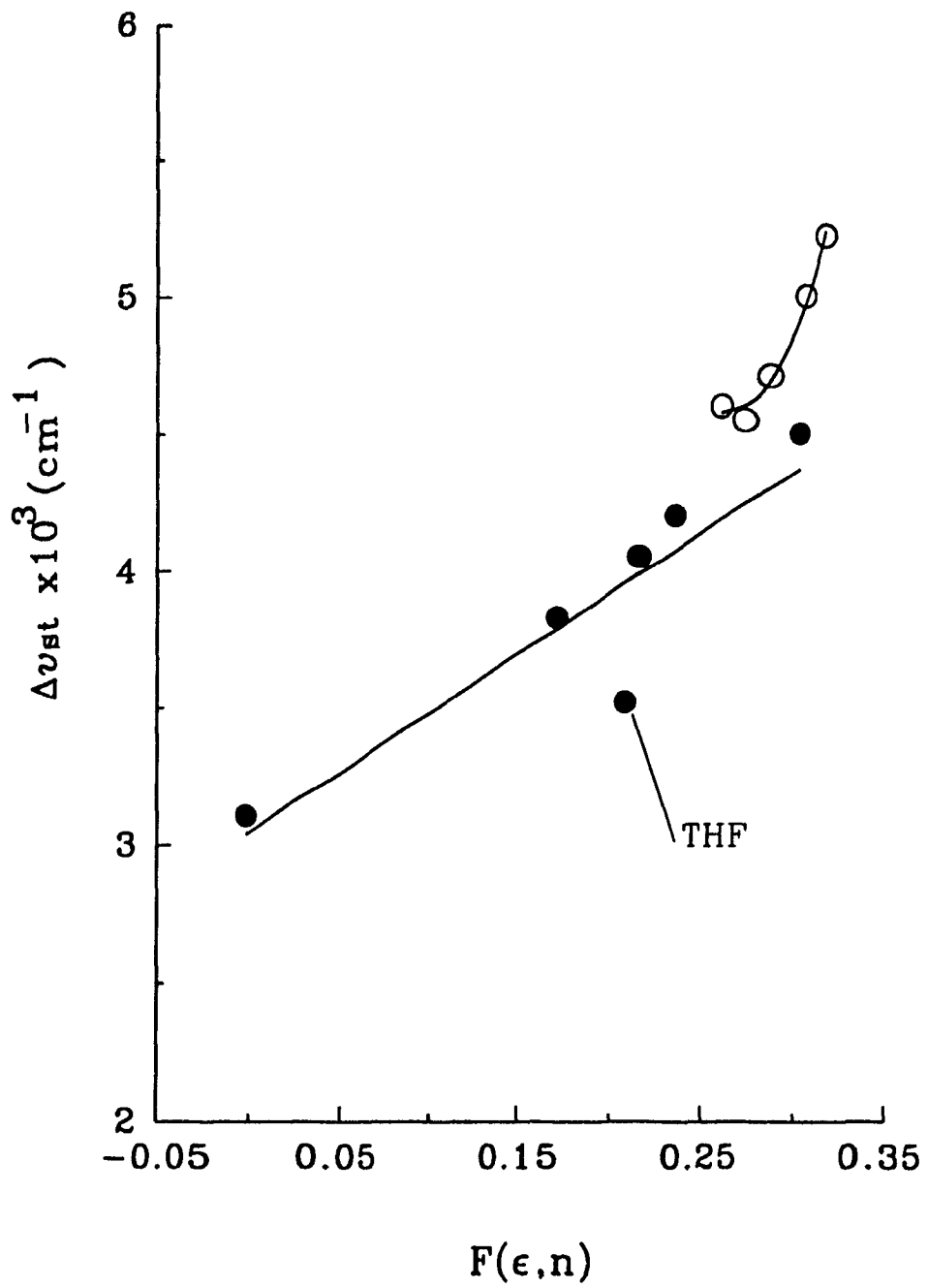
Fig. 4-1   Solvatochromic shift of C1 in aprotic (●) and protic (O)
solvents.
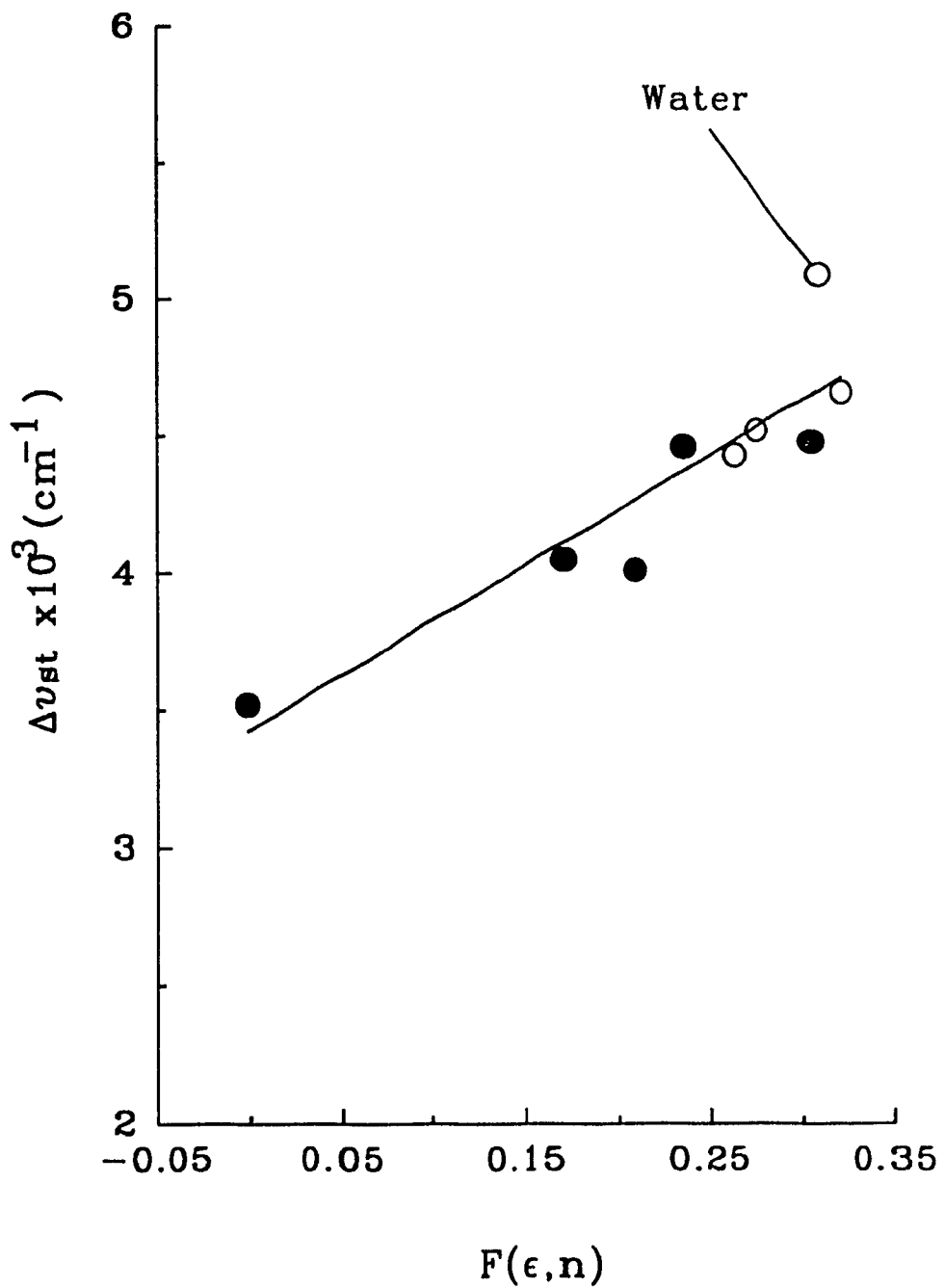
Fig. 4-2 Solvatochromic shift of C102 in aprotic (●) and protic (O) solvents.

studies between these two molecules seems to further support this view.[87,88,90] Such solvatochromic behaviour is similar to the solvatochromic study of the other coumarin dyes (7-N-dimethylamino-4-methylcoumarin, and 7-amino-4-methylcoumarin).[178]

The nonlinear change of $\Delta\upsilon_{st}$ for C1 in protic solvents, but not in aprotic solvents, is attributable to the formation of the TICT state[102] whose dipole moment is much larger than that of the planar ICT state and leads to the change in the slope of the solvatochromic plot as described by eq. (1). The increased dipole moment of the TICT state is due to the full charge separation in contrast to that of the planar ICT state.[103] As observed by Rettig and Klock,[94] the threshold for nonlinearity is between butanol and propanol, which is exactly the same as was observed from with experiment shown in Fig. 4-1 (open circles). Therefore, the question about the origin of the fluorescent state of C1 in protic solvents has been raised, which is the main object in the following discussion.

4.3.1.2 Empirical Polarity $E_T(30)$[6a]

In Fig. 4-3, the solvatochromic shifts of C1 and C102 over the whole range of solvents, are plotted with respect to the empirical polarity $E_T(30)$[6a] instead of F(ϵ,n), where the H-bonding induced solvent polarity change is taken into account. The linear solvatochromic behavior for both C1 and C102 in the whole range of solvents clearly suggests that the origin of the fluorescence is the planar ICT state in all cases.[90] From the Lippert-Mataga equation (eq. (1), such linear solvatochromic shift should be proportional to the empirical polarity $E_T(30)$, and satisfies eq. (5),

$$\Delta\upsilon = \upsilon_{ab}^r - \upsilon_{fl}^r = \frac{2}{hc}\frac{(\mu_e - \mu_g)^2}{a^3}E_T(30) + Z \qquad (5)$$
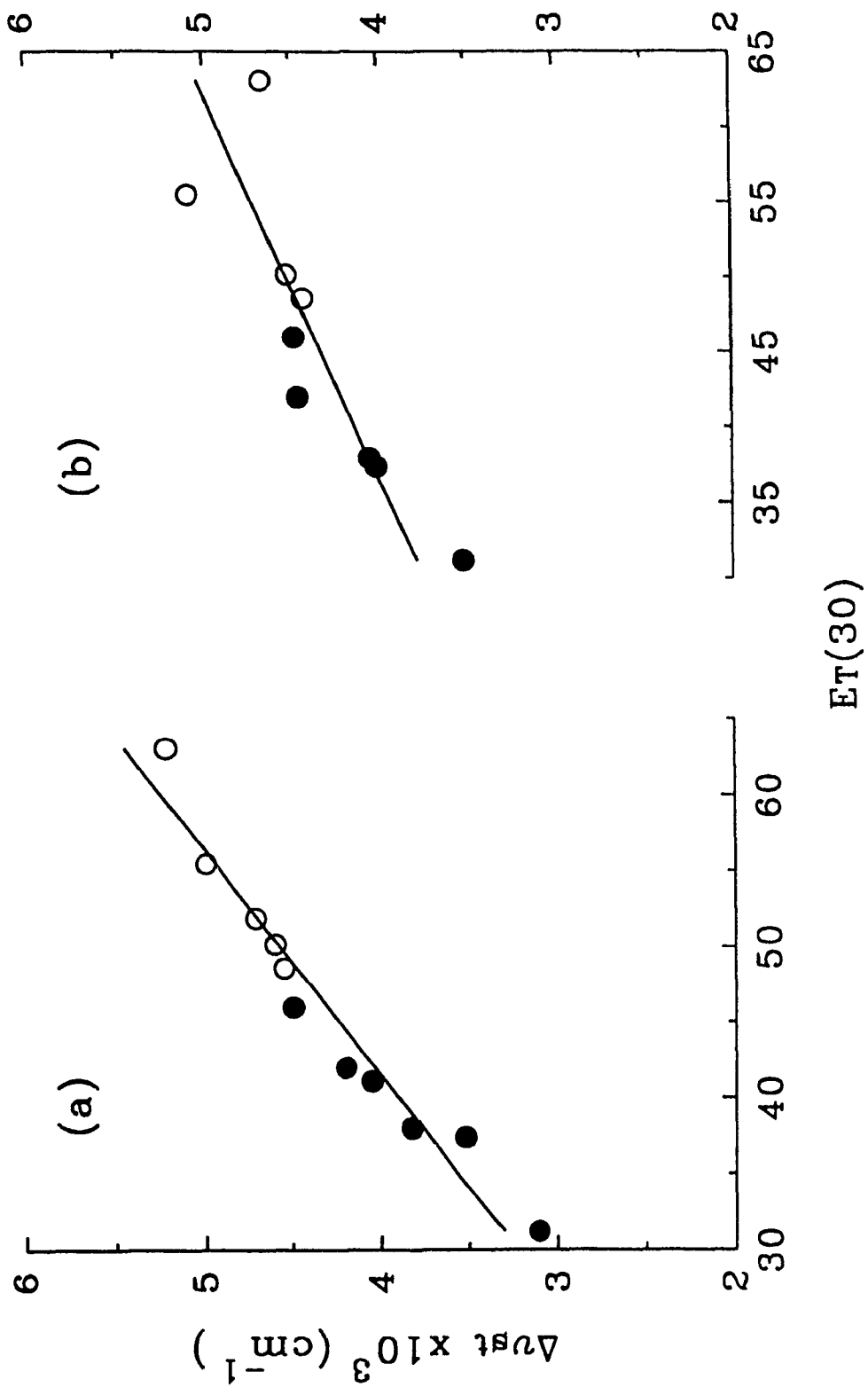
Fig. 4-3 Solvatochromic shifts of (a) C1 and (b) C102 in aprotic (●) and protic (O) solvents with respect to the empirical polarity $E_T(30)$

The trend of the plots for both dyes in the whole range of solvents, seems to be the same, in spite of the larger fluctuation for C102 in water. (This may be due to the aggregation of C102 in water which should be verified again in the near future.) Coupled with the solvatochromic shift, the fluorescence quantum yield of C1 in protic solvent decreases with the polarity of the solvent as listed in Table 3-1, which is due to fast internal conversion among the excited states including TICT states as discussed in the previous chapter.

From ASE study in chapter 2, the H-bonding effects on 7-aminocoumarins have been observed.[15,16] There are three possible modes for forming H-bonded complexes:[179] (i) H-N bond, (ii) intramolecular hydrogen bond, and (iii) intermolecular hydrogen bond. In the presence of hydroxylic molecules in solution, the third mode is the main mechanism for nonlinear solvatochromism for C1 as obsered in Fig. 4-1. If $\Delta\upsilon$ is now plotted against the empirical polarity $E_T(30)$ (see Fig. 4-3a), a linear plot is observed for both C1 and C102. The empirical polarity parameter $E_T(30)$ takes into account of hydrogen bonding effects. In other words, when H-bonding is taken into account, there is no difference in the solvatochromic plots between C1 and C102. Therefore, the fluorescence band of C1 can be assigned to its planar ICT state, rather than the TICT state.

4.3.2 in Binary solvents

A dramatic change of the fluorescence quantum yield was observed in protic solvents for C1, and polar solvents for C1F (Table 4-1),[90] which is consistent with the prediction made by Rettig and Klock.[94] This extraordinary behaviour has been explained as being due to the radiationless decay of TICT state in C1 in comparison with the rigid species C102 (or C102F). Such

expectation still has not been observed directly in experiments (unlike the dual fluorescence of N, N-dimethylaminobenzonitrile (DMABN) in moderate polar solvents[180]).

Since the polarity of a binary solvent can be adjusted continuously with the mixture ratio,[175] this could be an ideal means to study the formation of TICT state of C1 or C1F. The difference between the solvatochromics of C1 or C1F and that of C102 or C102F, can be explained by two factors as: (i) the formation of TICT state, and (ii) the H-bonding induced dipole-dipole interaction.

To take into consideration of the H-bonding effect, the empirical polarity has been applied to this study. The nonlinearities of the empirical polarity $E_T(30)$[6a] of some binary solvents (aprotic/protic, protic/protic) with respect to the molar concentration of the more polar component, were studied systematically and satisfied the empirical function with specific parameters for each binary solvents as:[175]

$$E_T(30) = E_D \ln(\frac{c_p}{c^*} + 1) + E_T^L(30) \tag{6}$$

where E_D and c^* are the parameters for each binary solvent mixture and can be found in Ref. 175, c_p is the molar concentration of the more polar component, and $E_T^L(30)$ is the empirical polarity of the less polar component as listed in Table 4-1.

4.3.2.1   Aprotic solvent mixture (nBuOAc/AN)

For the aprotic solvent mixture such as n-butyl acetate (nBuOAc)-acetonitrile (AN), the solvatochromic plots of C1F and C102F of Fig. 4-4, do not

Table 4-1: Polarities of the solvents used in this study

Solvent	ε^a	n^a	$F(\varepsilon,n)^b$	$E_T(30)^c$
cyclohexane	2.02	1.4262	-0.00165	31.2
n-butyl acetate	5.010	1.394	0.1709	38.0
tetrahydrofuran	7.58	1.4072	0.2096	37.4
dichloromethane	8.93	1.4242	0.2171	41.1
benzonitrile	25.7	1.528	0.2359	42.0
acetonitrile	35.94	1.3441	0.3046	46.0
1-butyl alcohol	17.51	1.3993	0.2635	50.2
2-propanol	19.92	1.3772	0.2762	48.6
ethanol	24.55	1.3614	0.2888	51.9
methanol	32.66	1.3284	0.3086	55.5
water	78.30	1.3330	0.3210	63.1

[a] Dielectric constant and refractive index of solvents from Reference 6a; [b] Equation (3); [c] Empirical polarity of solvents from Reference 185
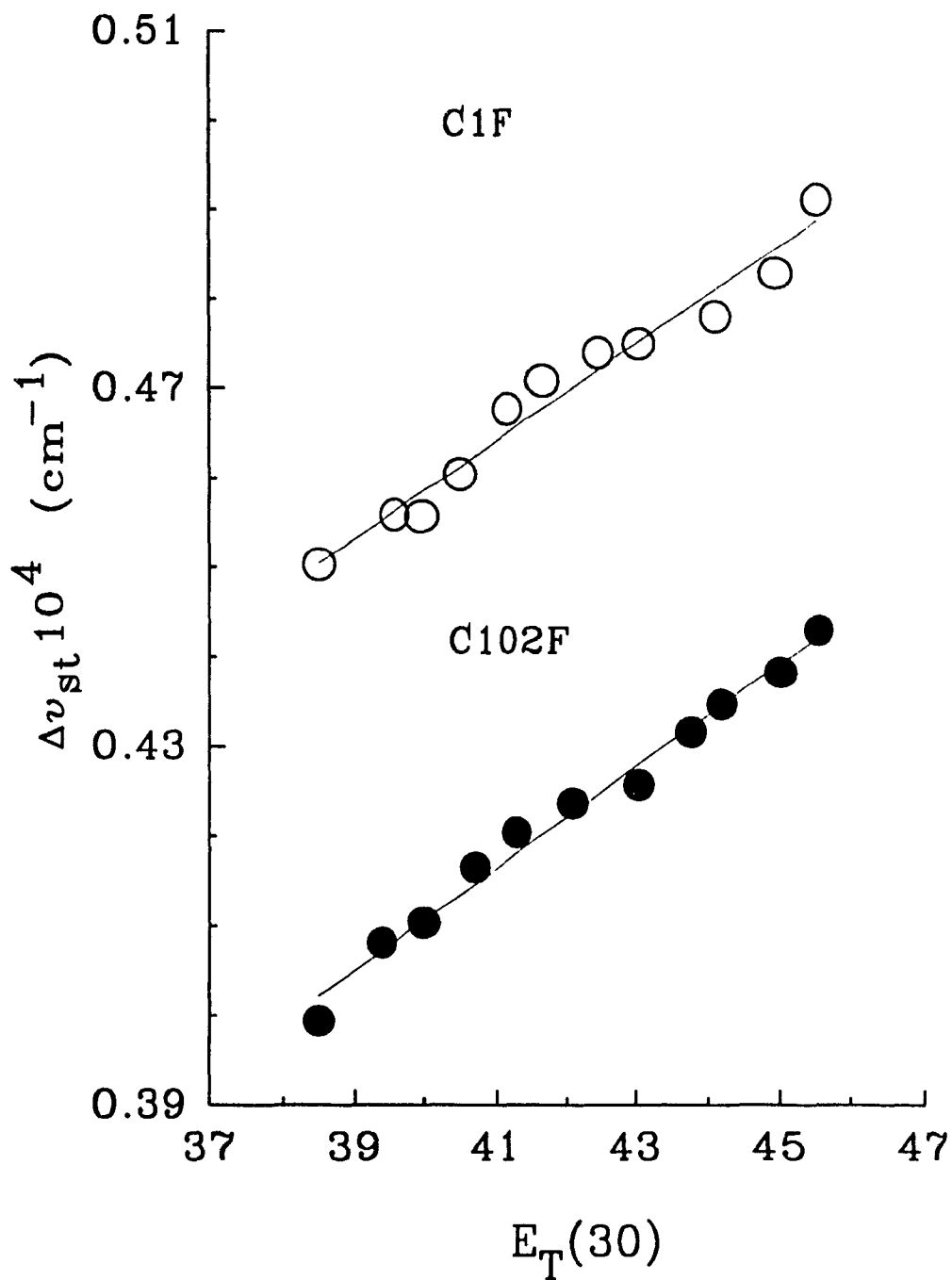
Fig. 4-4 Solvatochromic shifts of C1F (O), C102F (●) in n-butyl acetate (nBuOAc)/acetonitrile (AN).

show any extraordinary behaviour. The empirical polarities of the mixture are proportional to the mole fraction of the more polar component as expected:

$$E_T(30) = X_c \left(E_T^{II}(30) - E_T^{L}(30)\right) + E_T^{L}(30) \tag{7}$$

where $E_T^{I}(30)$, $E_T^{II}(30)$ are the empirical polarities of the less, and more polar components, respectively, and X_c is the mole fraction of the more polar component.

The solvatochromic shifts for both C1F and C102F in n-butyl acetate/acetonitrile, are well fitted by the linear functions as:

$$\Delta \upsilon_{st}(C1F) = (0.054 \pm 0.003)E_T(30) + (2.4 \pm 0.1). \tag{8}$$

and

$$\Delta \upsilon_{st}(C102F) = (0.057 \pm 0.002)E_T(30) + (1.8 \pm 0.1). \tag{9}$$

These linear solvatochromic plots of C1F or C102F (Fig. 4-4) are similar to those of C1 or C102 in different pure aprotic solvents as shown in Figs. 4-1, 4-2. In comparison to eq. (7), the parallel solvatochromic plot as observed from these 7-aminocoumarin dyes indicates that there is no difference in dipole moment of the fluorescent state for either flexible or rigid species, while the Onsager radius for both systems are assumed to be the same. The constant shift of the plot, $\Delta C = 0.06 \times 10^4$, cm^{-1}, is the difference of the Stokes Shift between C1F and C102F in aprotic solvent mixture. The direction of the shift of the plot is contrary to that of the shift for C1 and C102 in aprotic solvents, which is about $- 0.04 \times 10^4$, cm^{-1} from eqs. (2) and (4). It could be due to the difference in maximum vibronic energy of Z in eq. (1) between these two 7-aminocoumarins. The dramatic quantum yield change for C1F in acetonitrile can be explained by the loss due to

107

the nonradiative internal transition from the TICT state to the ground state.[90] The coexisting planar ICT state contributes to the fluorescence quantum yield as discussed for C1.

4.3.2.2   Polar aprotic and protic solvent mixture (AN/MeOH)

Due to the existence of the H-bonding effect,[181] the nonlinear relation between the mole fraction X_c and the empirical polarity $E_T(30)$ has been studied in different solvent mixtures.[175-177,182,183] In this study, the binary system consisting of unreactive acetonitrile (no H-bonding effect)[184] and the H-bond donor, methanol was chosen. The empirical polarity of the mixture can be obtained using Dawber's[176] results from which nonlinearity of the empirical polarity $E_T(30)$ with respect to the mole fraction of the binary solvent due to the H-bonding effect is illustrated on Fig. 4-5. Fig. 4-6 shows the solvatochromic shifts of C1 & C102 and C1F versus corrected polarity $E_T(30)$ of the binary solvent (AN/MeOH). The results shown on Fig 4-6, do not supply enough information to allow interpretation such as: (i) no result with C102F can be compared; (ii) there are missing the data for all these dyes in the binary solvent from $X_{MeOH} = 0$ to the *synergistic maximum* which is defined as the mole fraction at maximum polarity. From the information we have, it is difficult to distinguish the effect of the formation of TICT and the inhomogeneity of the mixture. This needs to be completed through further studies as described in the next section. However, by combining Fig. 4-4 and Fig. 4-6 for C1F which shows the solvatochromic shift continuously from n-butyl acetate to methanol, the extraordinary behavior illustrated in Fig. 4-7, we could obtain some useful information about the effect of the formation of the TICT state, which we believe exist. It will also be interesting to study this for C102F.
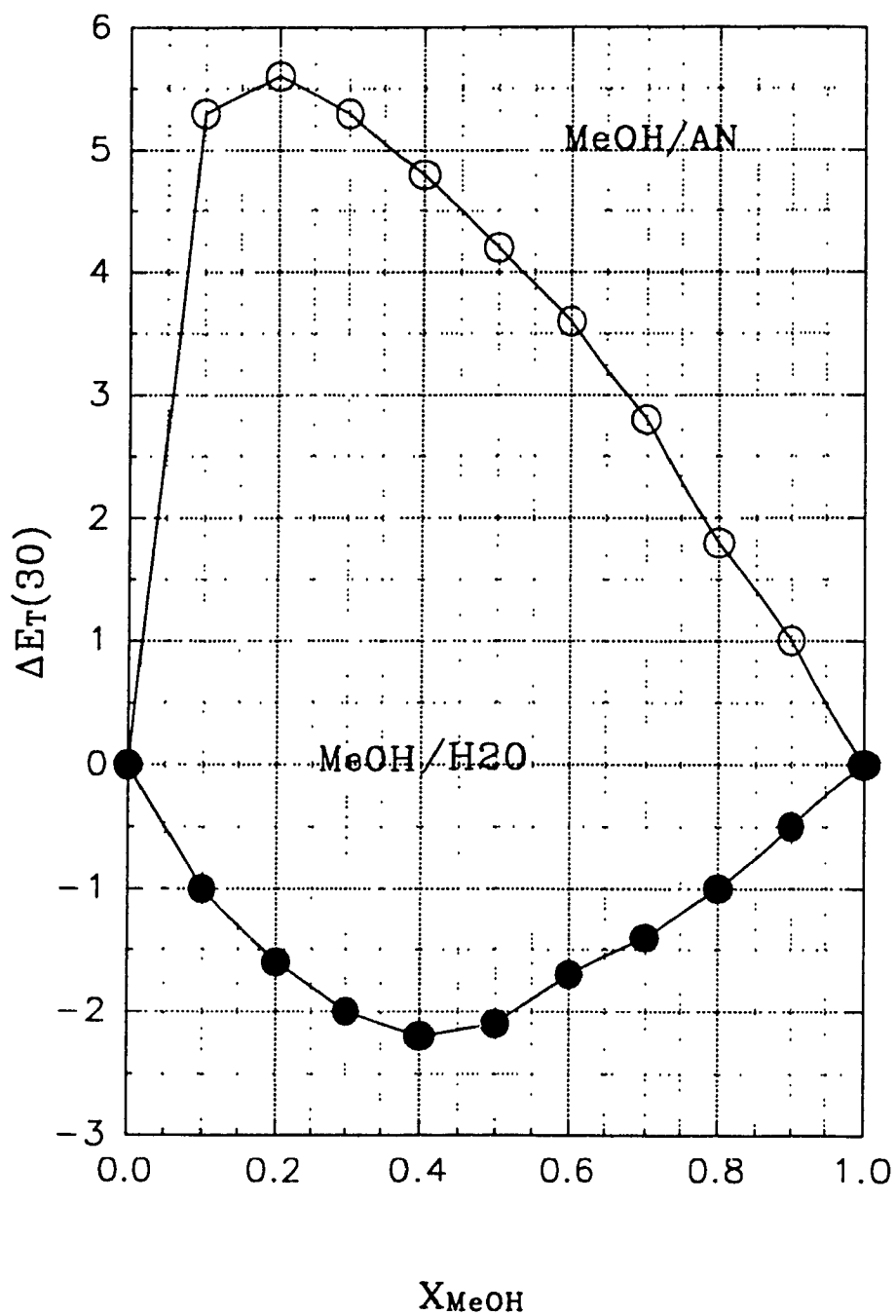
Fig. 4-5 Corrected empirical polarity $E_T(30)$ of acetonitrile (AN)/methanol (O), and methanol/water (●) mixture with mole fraction of methanol.176
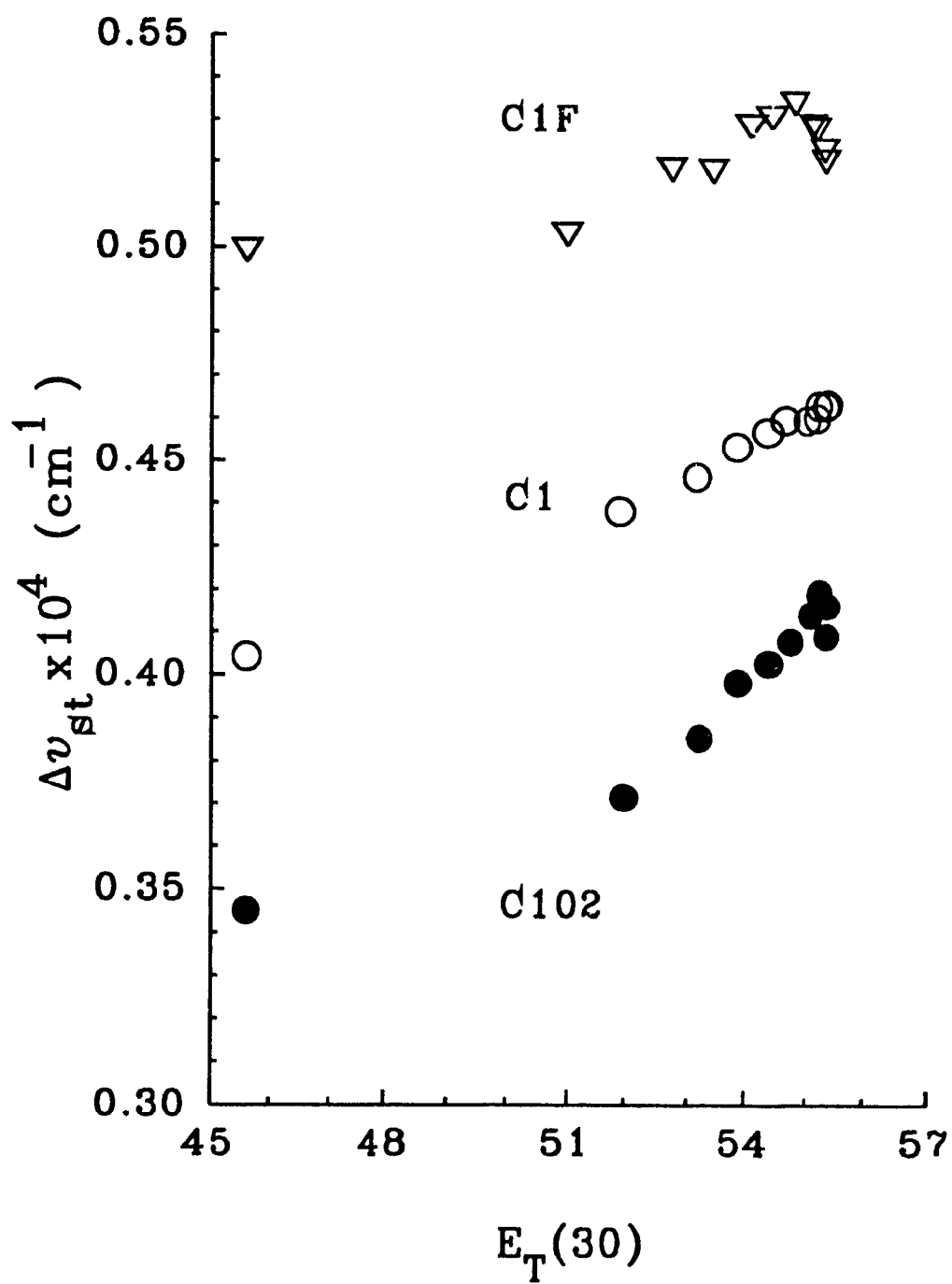
Fig. 4-6 Solvatochromic shifts of C1 (O), C1F (∇), and C102 ($\bullet$) in acetonitrile (AN)/methanol mixture
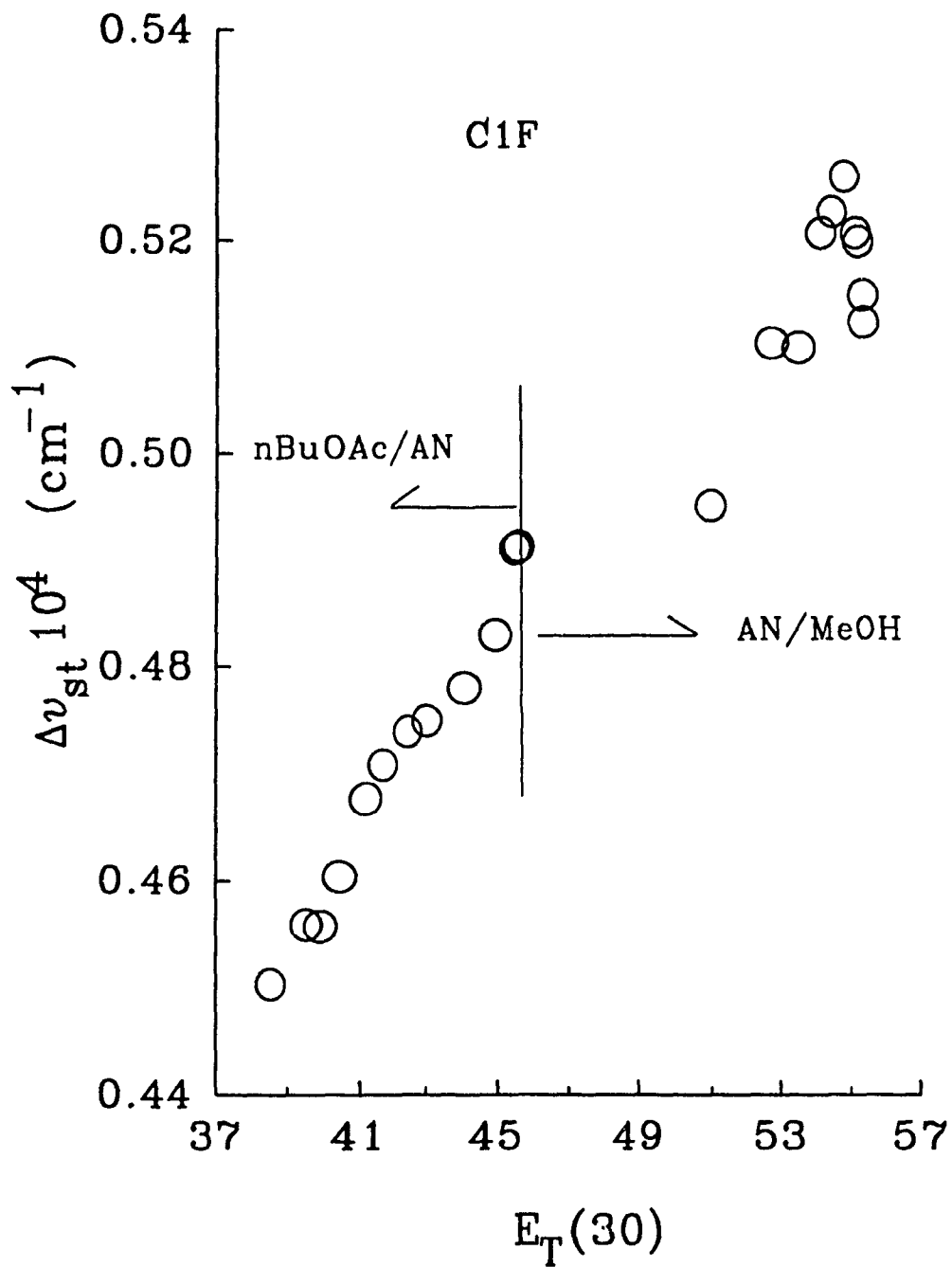
Fig. 4-7 Solvatochromic shift of C1F in nBuOAc/AN, and AN/MeOH mixture

4.4   Conclusion

4.4.1   Further studies

According to Rettig and Klock's study,[94] the quantum yield drop occuring in 1-BuOH for C1 is explained by incomplete formation of the TICT state in which the dimethylamino group is only partially twisted. Therefore, the solvatochromic plots of C1 the propanol/methanol mixture, show an anomalous behaviour in comparison with that of C102. Such extraordinary phenomena (if it would be observed) would offer strong evidence to support the predicted formation of the TICT state for C1. For comparison, since the formation of the TICT state for the N, N-dimethylaminobenzonitrile (DMABN) is well known,[101-103] it can be selected as the probe to study the solvatochromic shift in binary solvents, such as cyclohexane/acetonitrile, acetonitrile/methanol, and cyclohexane/methanol. These three binary solvent systems can be applied to study (i) nonlinearity of the solvatochromic shift due to the formation of the TICT state for the b band in comparison with the linearity for the a band (planary ICT band); (ii) the H-bonding effect on the dipole moment of the TICT band (reflecting on the slope change, nonlinearity). These solvatochromic plots could be applied as the reference to study the formation of TICT for the 7-aminocoumarin dyes. The reason of excluding water as one component, is due to its complicated solvation effect,[6a] that would make the problem more difficult.

4.4.2   Conclusion

The solvatochromic shift study of the 7-aminocoumarin dyes in pure solvents is apparently consistent with the previous observations from other typical TICT compounds (DMABN).[101] Without considering the H-bonding effect, the *nonlinear* solvatochromic plot of C1 in *protic* solvents seems to

suggest of the formation of a partially twisted intramolcular charge transfer (TICT) state.[94,100] However, when the H-bonding effect is taken into account, by plotting solvatochromism of C1 against the empirical polarity ($E_T(30)$) of solvent, a linear plot is obtained. Therefore, there is no evidence for the formation of a TICT state. The fluorescence of C1 originates from the planar ICT state rather than the TICT state. Further studies are proposed, which could offer enough information to distinguish these two effects in experiment directly.

Chapter 5:   IRREVERSIBLE SOLVATION DYNAMICS and KINETICS

5.1   Introduction

Interest in the molecular motions associated with chemical reactic ,s in
solution has prompted an effort to understand the dynamics of solvation. The
effect of macroscopic solvent parameters (i.e., viscosity, polarity) on chemical
dynamics has been extensively studied for many decades.[6] These studies show
that only to, some extent the nature of solvent effects on chemical reactions can
be accounted for in terms of the changes the solvent induces on the potential
energy barrier and relative free energies of the reactants and products.[64,65] In
order to understand dynamic solvent effects on chemical reactions, it is
necessary to determine the time scales of solvent dielectric relaxation as well as
to evaluate the time dependent forces, or dielectric friction, that the polar solvent
exerts on the reacting molecule.

Time-resolved fluorescence spectroscopy of polar fluorescent "probes"
has been used extensively to study microscopic solvation dynamics in a broad
range of solvents.[58,66-70] One of the basic methods of extracting the
polarization function $C(t)$[71] of the fractional change in time-resolved emission
maximum on the time and wavelength resolved fluorescence spectra has been
known, in principle, for about ten years.[72]

For an exponential $C(t)$, the solvation process of a solvating state is
assumed to undergo a continuous relaxation process from the initial excited
state to the final solvated excited state due to the induced rotational and
longitudinal relaxation of solvent molecules.   A mixture of the emissive

unsolvated and solvated species, has been considered as a single solvating species.[72] Therefore, the decay of the time-dependent fluorescence i(λ,t) can be expressed by:

$$i(\lambda,t) = f(\lambda,t)e^{-1/\tau(t)} \tag{1}$$

where τ(t) is the lifetime of the solvating state and should vary with time; and f(λ,t) is the fluorescence profile with time-dependent spectral shape. However, in our recent time-dependent fluorescence TDF measurements of 7-diethylamino-4-methylcoumarin in 1-butanol, we found negative distribution of a preexponential parameter $\alpha_i(\lambda)$ corresponding to a wavelength independent decay time τ_i. The fluorescence decay at specific wavelength i(λ,t) is considered as the sum of all contributions from each individual decay component with decay time τ_i (i=1..n), and satisfies the following exponential relation:

$$i(\lambda,t) = \sum_{i=1}^{n}\alpha_i(\lambda)e^{-1/\tau_i} \tag{2}$$

For an irreversible two-state system, the kinetics were found from these preexponential parameters $\alpha_i(\lambda)$, i=1,2, in which one of the two preexponential parameters appears to be negative in part of spectral region, and the other one remains positive over all.[73,74] This has been accepted as a signature in the study of the kinetics of the irreversible two-state system.[73-78] Apparently, the similar observation (a negative preexponential parameter) found in our experiment indicates the presence of two-state kinetics. In order to verify the multistate kinetics, in this chapter, the following comparisons have been made, which are based on our experimental observations: (i) the decay time of the exponential fit of C(t) and (ii) the spectral shape parameters Γ, b in log-normal shape fitting function (eq. (3)) to the spectrally reconstructed (SR) time-resolved

emission spectra TRES and to the simulated TRES. We find a significant difference in values of the decay times (especially for the fast decay component in 1-octanol) between those of the exponential fit of C(t) of TRES, and those of the global fit of TDF. Such difference raises a question as to the precise time-dependency of C(t). (iii) Under the multistate model, the TRES $i(\upsilon_m,t)$ dependency of C(t), the function $C(\upsilon_m,t)$ has been derived from the gaussian like species associated spectra while the condition of $\left.\dfrac{\partial\ i(\upsilon,t)}{\partial\upsilon}\right|_{\upsilon=\upsilon_m} \equiv 0$ is applied.

In order to obtain the optimum decay times of C(t), the function $C(\upsilon_m,t)$ has been used to fit to the C(t) data of SR TRES instead of using a multiexponential function while the peak positions υ_m of SR TRES, and the SR TRES at peak $i(\upsilon_m,t)$ have been applied in the optimization. The decay times from this optimization are closer to those global fit of TDF than those of the exponential fit of C(t).

5.2 Experimental Section

5.2.1 Chemicals

n-Butyl acetate (Fisher reagent) and dichloromethane (Anachemia spectrograde) were refluxed over CaH_2 for 1 h and distilled prior to use. Methanol (Caledon distilled in glass), 1-butanol (Fisher certified), isooctane (MCB spectro) were used without further treatment. 1-Octanol (BDH reagent) was distilled under reduced pressure. All solvents were checked for fluorescence impurities. The coumarin dye 7-diethylamino-4-methyl-coumarin (C1) (Exciton) was recrystallized from methanol-water and sublimed. 2,2,5,6-1H,4H-Tetrahydro-8-methylquinolazino-[9,9a,1-gh]coumarin (C102) (Exciton) was recrystallized from methanol.

5.2.2 Measurements

The steady state fluorescence spectra were measured with a SLM 8000C spectrofluorimetry. The emission spectra were corrected using correction factors derived from a calibrated tungsten lamp.

The fluorescence decays were obtained with 310 nm excitation pulses (15 ps FWHM) generated at a repetition rate of 825 kHz by a Spectra Physics mode-locked synchronously pumped and cavity dumped laser system whose output was frequency doubled with a KDP crystal. The fluorescence was detected by a Hamamatsu 1564 U microchannel plate after passing through a polarizer set at the "magic angle" to exclude errors from Brownian rotation and a Jobin Yvon H10 monochromator (4 nm band pass) and measured by usual time-correlated single-photon instrumentation.[63] The instrumental response function was 60 ps FWHM measured at a resolution of 10 ps or 1 ps per channel and was recorded before and after each sample decay measurement. The fluorescence decay parameters were obtained after convolution analysis using the Marquardt algorithm, a background signal always being subtracted prior to deconvolution. The adequacy of fit to the decay data was determined by the inspection of the weighted residuals plot, serial variance ratio (SVR), and root mean sum of weighted squares of residuals (RMSR).[186]

5.2.3. Log-normal line shape function[187]

For spectral reconstruction and simulation, the four-parameter function describing an asymmetric line shape was applied

$$i(v) = \begin{cases} i_0 \exp\left\{ -\ln(2)\left(\dfrac{\ln\left[1 + 2b(v - v_m)/\Delta\right]}{b}\right)^2 \right\} & 2b(v - v_m)/\Delta > -1 \\ 0 & 2b(v - v_m)/\Delta \le -1 \end{cases} \tag{3a}$$

where parameters i_0, v_m, and b are the peak height, the peak frequency at maximum intensity, and an asymmetry parameter, respectively. The FWHM, Γ, of this function relates to the width parameter Δ as:[57]

$$\Gamma = \left| \Delta\left(\frac{\sinh(b)}{b}\right) \right| \tag{3b}$$

5.3   Irreversible Dynamics

5.3.1   Two-state system

5.3.1.1   Dynamics and kinetics

Based on Brand's work,[75,76] the time-resolved emission spectrum $i(v,t)$ can be expressed by species associated spectra $\alpha_j(v)$ j=A, B, in forms of
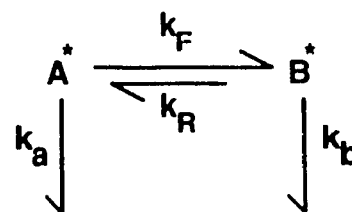
Scheme 5-1

$$i(v,t) = \alpha_A(v)\, N_A(t) + \alpha_B(v)\, N_B(t) \tag{4}$$

where $N(t)_{A,B}$ are the ratios of the population of species A^* or B^* per total excited state population ($N_0 = N_A + N_B$); $\alpha_{A,B}(v)$[73-78] are the fluorescence spectra associated with species A^* and B^*, respectively. In eq. (4), the only time-dependent population ratios $N_A(t)$, $N_B(t)$ satisfy the following differential equations:

$$\begin{cases} \dfrac{d N_A(t)}{dt} = k_R N_B(t) - (k_a + k_F) N_A(t) \\[2mm] \dfrac{d N_B(t)}{dt} = k_F N_A(t) - (k_b + k_R) N_B(t) \end{cases}$$ (5)

and can be expressed by:

$$\begin{cases} N_A(t) = \gamma_1 e^{-\sigma_1 t} + \gamma_2 e^{-\sigma_2 t} \\[2mm] N_B(t) = \delta_1 e^{-\sigma_1 t} + \delta_2 e^{-\sigma_2 t} \end{cases}$$ (6)

where the coefficients γ_1, γ_2, and δ_1, δ_2 are

$$\gamma_1 = [(\sigma_2 - X) + (B_0^* / N_0) k_R]/(\sigma_2 - \sigma_1); \qquad \gamma_2 = 1 - \gamma_1$$ (7a)

and

$$\delta_1 = [(B_0^* / N_0)(\sigma_2 - Y) + k_F]/(\sigma_2 - \sigma_1); \qquad \delta_2 = (B_0^* / N_0) - \delta_1.$$ (7b)

N_0 and B_0^* are the initial populations for A^* and B^*. The decay rates σ_1, σ_2 can be found by solving the differential equation set (8) and are presented by:

$$\begin{cases} \sigma_1 = 0.5\left[X + Y + \sqrt{(X-Y)^2 + 4 k_F k_R}\right] \\[2mm] \sigma_2 = 0.5\left[X + Y - \sqrt{(X-Y)^2 + 4 k_F k_R}\right] \end{cases}$$ (8)

where $X = k_a + k_F$, $Y = k_b + k_R$.

5.3.1.2   Decay associated spectra of an irreversible two-state system

Under the assumptions of (i) $X > Y$, $k_R \to 0$ (for the irreversible process [73-78]), (ii) k_i (i=a,b) $\ll k_F$ (for the fast forward transition, such as solvation process [58,65-70]), and (iii) $N_B(0) = B_0^* / N_0 = 0$ (by ignoring the ground state complexation [15,16]), these coefficients can be simplified

$$X = k_F = \sigma_1 = 1/\tau_1; \qquad\qquad Y = k_b = \sigma_2 = 1/\tau_2$$

$$\gamma_1 = (\sigma_2-X)/(\sigma_2-\sigma_1) = (\sigma_2-\sigma_1)/(\sigma_2-\sigma_1) = 1; \qquad \gamma_2 = 1 - \gamma_1 = 0 \qquad (9)$$

$$\delta_1 = \sigma_1/(\sigma_2-\sigma_1) = -1; \qquad\qquad \delta_2 = -\delta_1 = 1.$$

Thus, the population ratio of each species can be expressed simply by:

$$\begin{cases} N_A(t) = e^{-\sigma_1 t} \\ N_B(t) = e^{-\sigma_1 t} - e^{-\sigma_2 t} \end{cases} \qquad (10)$$

Therefore, from the eqs. (4) and (10), the spectral density $i(\upsilon,t)$ is given by:

$$i(\upsilon,t) = \alpha_A(\upsilon)\, N_A(t) + \alpha_B(\upsilon)N_B(t)$$

$$= [\alpha_A(\upsilon) - \alpha_B(\upsilon)]\, \exp(-\sigma_1 t) + \alpha_B(\upsilon)\exp(-\sigma_2 t)$$

$$= \alpha_1(\upsilon)\exp(-\sigma_1 t) + \alpha_2(\upsilon)\exp(-\sigma_2 t), \qquad (11)$$

where the preexponential coefficients $\alpha_i(\upsilon)$, $i=1,2$ are

$$\alpha_1(\upsilon) = \alpha_A(\upsilon) - \alpha_B(\upsilon)$$

$$\alpha_2(\upsilon) = \alpha_B(\upsilon). \qquad (12)$$

Under above assumptions, the *fractional contribution of the ith decay component to the steady state fluorescence* (decay associated spectra DAS) can be defined by:

$$DAS_i(v) = \alpha_i(v)\tau_i / \sum_{i=1}^{n}[\alpha_i(v)\tau_i]_{ss}(v) = F_i(v)i_{ss}(v) \qquad (13)$$

where the normalized contribution of a specific exponential component to the steady state fluorescence, is defined as $F_i(\lambda) = \alpha_i(\lambda)\tau_i/\sum_i[\alpha_i(\lambda)\tau_i]$, and $i_{ss}(\lambda)$ is the normalized steady state fluorescence spectrum.

From eqs. (12), (13), we can find the correlation between the emission spectra $\alpha_j(\nu/\lambda)$ associated to the species j, j=A, B and DAS:

$$\alpha_A(\lambda) = \alpha_1(\lambda) + \alpha_2(\lambda) = \sum_i [\alpha_i(\lambda)\tau_i]/i_{SS}(\lambda,t) [DAS_1(\lambda)/\tau_1 + DAS_2(\lambda)/\tau_2]$$

$$\alpha_B(\lambda) = \alpha_2(\lambda) = \sum_i [\alpha_i(\lambda)\tau_i]/i_{SS}(\lambda,t) DAS_2(\lambda)/\tau_2 \qquad (14)$$

$$\alpha_A(\lambda)/\alpha_B(\lambda) = [\alpha_1(\lambda) + \alpha_2(\lambda)]/\alpha_2(\lambda) = \alpha_1(\lambda)/\alpha_2(\lambda) + 1.$$

By introducing the steady state fluorescence spectrum

$$I_{SS}(\lambda) = \int_0^\infty i(\lambda,t)dt = \alpha_A(\lambda)\tau_1 + \alpha_B(\lambda)(\tau_2 - \tau_1), \qquad (15)$$

which is the integral of eq. (11) and is equal to $\sum_i [\alpha_i(\lambda)\tau_i]$, i=1,2, we can find the normalized SAS by the steady state spectrum $I_{SS}(\lambda)$ defined as *the fractional contribution of species j (j=A, B) to the steady state fluorescence* as the form of

$$SAS_A(\lambda) = [\alpha_A(\lambda)\tau_1/ I_{SS}(\lambda)] i_{SS}(\lambda) = F_A(\lambda)i_{SS}(\lambda)$$

$$SAS_B(\lambda) = [\alpha_B(\lambda)(\tau_2 - \tau_1)/ I_{SS}(\lambda)] i_{SS}(\lambda) = F_B(\lambda)i_{SS}(\lambda) \qquad (16)$$

$$SAS_A(\lambda)/SAS_B(\lambda) = \alpha_A(\lambda)/\alpha_B(\lambda) \; \tau_1/(\tau_2 - \tau_1)$$

$$= [\alpha_1(\lambda)/\alpha_2(\lambda) + 1] \; \tau_1/(\tau_2 - \tau_1).$$

Here the normalized contribution of the species j, j=A, B to the steady state fluorescence, is defined as $F_A(\lambda) = \alpha_A(\lambda)\tau_1/ I_{SS}(\lambda)$ and $F_B(\lambda) = \alpha_B(\lambda)(\tau_2 - \tau_1)/ I_{SS}(\lambda)$, respectively. The correlation between $DAS_i(\lambda)$, i=1, 2, and $SAS_j(\lambda)$, j=A, B, can be derived from eqs. (14) and (16) as below:

$$SAS_A(\lambda) = DAS_1(\lambda) + DAS_2(\lambda)\tau_1/\tau_2$$

$$SAS_B(\lambda) = DAS_2(\lambda)(1 - \tau_1/\tau_2). \qquad (17)$$

5.3.2 Serial three-state system

5.3.2.1 Dynamics

For a serial three-state system as illustrated in Scheme 5-2. There are two steps to complete the whole process as
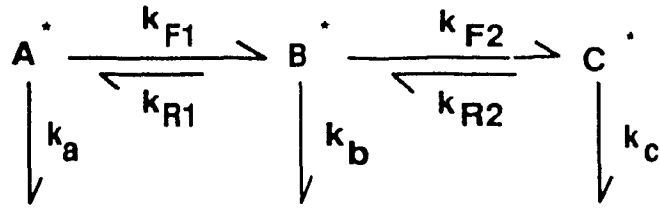
Scheme 5-2

from A^* to B^* for the first step process and followed by the second step process from B^* to C^*. Obviously, the population ratios (population per total population N_O) of species A^*, B^*, and C^* should satisfy the following differential equations:

$$\begin{cases} N_A'(t) = \dfrac{dN_A(t)}{dt} = k_{R1}N_B(t) - (k_a + k_{F1})N_A(t) \\[2mm] N_B'(t) = \dfrac{dN_B(t)}{dt} = k_{F1}N_A(t) + k_{R2}N_C(t) - (k_a + k_{R2} + k_{F2})N_B(t) \\[2mm] N_C'(t) = \dfrac{dN_C(t)}{dt} = k_{F2}N_B(t) - (k_c + k_{R2})N_C(t) \end{cases} \qquad (18)$$

which can be obtained by solving the third derivative equation (19)[156] (details see Appendix B):

$$\frac{d^3N_A(t)}{dt^3} + \alpha\frac{d^2N_A(t)}{dt^2} + \beta\frac{dN_A(t)}{dt} + \gamma N_A(t) \equiv 0 \qquad (19)$$

where $\alpha = k_a + k_{F1} + k_b + k_{R1} + k_{F2} + k_c + k_{R2}$

$\beta = k_a k_b + k_b k_c + k_c k_a + k_{F1}k_{F2}$

$\gamma = k_a k_b k_c + k_c(k_a k_{F2} + k_b k_{F1} + k_c k_{R1} + k_{F1}k_{F2})$

$\qquad + k_{R2}(k_a k_b + k_b k_{F1} + k_c k_{R1})$,

and are in the forms of:

$$\begin{cases} N_A(t) = \beta_1 e^{-\sigma_1 t} + \beta_2 e^{-\sigma_2 t} + \beta_3 e^{-\sigma_3 t} \\ N_B(t) = \delta_1 e^{-\sigma_1 t} + \delta_2 e^{-\sigma_2 t} + \delta_3 e^{-\sigma_3 t} \\ N_C(t) = \gamma_1 e^{-\sigma_1 t} + \gamma_2 e^{-\sigma_2 t} + \gamma_3 e^{-\sigma_3 t} \end{cases} \tag{20}$$

The population ratios of all species can be obtained by solving the third derivative equation and the expressions are complicated. However, since the solvation processes are much faster than the decay of each emissive state (k_{F1}, k_{F2} » k_a, k_b, and k_c), for the irreversible process satisfying the following conditions:

$$k_{F1, F2} \text{ » } k_{R1, R2};$$
$$N_B(0) = N_C(0) = 0; \quad N_A(0) = 1 \tag{21}$$

the population ratios in the initial period as the first-order two-step kinetics, can be expressed by:

$$\begin{cases} N_A(t) = e^{-t/\tau_1} \\ N_B(t) = \dfrac{e^{-t/\tau_2} - e^{-t/\tau_1}}{1 - \tau_1/\tau_2} \\ N_C(t) = e^{-t/\tau_1} - \dfrac{e^{-t/\tau_2} - \tau_1/\tau_2 e^{-t/\tau_1}}{1 - \tau_1/\tau_2} \end{cases} \tag{22}$$

where the decay times $\tau_1 = 1/k_{F1}$, $\tau_2 = 1/k_{F2}$, and $\tau_3 = 1/k_C$, and the kinetic rate constants k_{F1}, k_{F2}, and k_C are defined in Scheme 5-2.

5.3.2.2 Decay-associated spectrum $DAS_i(\upsilon/\lambda)$, i=1..3

Similar to the two-state system, the time-resolved spectral density $i(\upsilon,t)$ can be represented by the species associated spectra (SAS) and the population ratio in the relationship of:

$$i(\upsilon,t) = \sum_{j=A}^{c} \alpha_j(\upsilon) N_j(t)$$

$$= \alpha_A(\upsilon) e^{-t/\tau_1} + \alpha_B(\upsilon) \frac{e^{-t/\tau_2} - e^{-t/\tau_1}}{1 - \tau_1/\tau_2}$$

$$+ \alpha_B(\upsilon) \left[e^{-t/\tau_1} - \frac{e^{-t/\tau_2} - \tau_1/\tau_2 e^{-t/\tau_1}}{1 - \tau_1/\tau_2} \right] \tag{23}$$

Similar to eq. (11), the correlation between the species associated spectra SAS ($\alpha_j(\upsilon)$, J=A..C) and the preexponential coefficients ($\alpha_i(\lambda)$, i=1..3)) can be expressed by:

$$\begin{cases} \alpha_A(\upsilon) = \alpha_1(\upsilon) + \alpha_2(\upsilon) + \alpha_3(\upsilon) \\ \alpha_B(\upsilon) = \alpha_2(\upsilon)(1 - \frac{\tau_1}{\tau_2}) + \alpha_1(\upsilon) \\ \alpha_C(\upsilon) = \alpha_1(\upsilon) \end{cases} \tag{24}$$

The decay associated spectrum to the ith decay component is defined as the *fractional contribution to the total fluorescence* are the same as eq. (13), and the *normalized species associated spectra* by the steady state fluorescence are:

$$SAS_A(\lambda) = [\alpha_A(\lambda)\tau_1/I_{ss}(\lambda)] \, i_{ss}(\lambda)$$

$$SAS_B(\lambda) = [\alpha_B(\lambda)\tau_2/I_{ss}(\lambda)] \, i_{ss}(\lambda) \tag{25}$$

$$SAS_C(\lambda) = \{\alpha_C(\lambda)[\tau_3 - (\tau_1 + \tau_2)]/I_{ss}(\lambda)\} \, i_{ss}(\lambda)$$

where $\tau_1 = 1/k_{F1}$, $\tau_2 = 1/k_{F2}$, and $\tau_3 = 1/k_C$. The total fluorescence $I_{ss}(\lambda)$ is:

$$I_{ss}(\lambda) = \int_0^\infty i(\lambda,t) \, dt = \alpha_A(\lambda)\tau_1 + \alpha_B(\lambda)\tau_2 + \alpha_C(\lambda)[\tau_3 - (\tau_1 + \tau_2)], \tag{26}$$

and is also equal to $\sum_i [\alpha_i(\lambda)\tau_i]$.

From the definitions of α's (eqs. (24), (25) and eq. (11)), the normalized species associated spectra $SAS_j(\lambda)$ and $DAS_i(\lambda)$ are related by:

$$SAS_A(\lambda) = DAS_1(\lambda) + DAS_2(\lambda)(\tau_1/\tau_2) + DAS_3(\lambda)(\tau_1/\tau_3)$$

$$SAS_B(\lambda) = DAS_2(\lambda)(\tau_2 - \tau_1)/\tau_2 + DAS_3(\lambda)(\tau_2/\tau_3) \tag{27}$$

$$SAS_C(\lambda) = DAS_3(\lambda)[\tau_3 - (\tau_1 + \tau_2)]/\tau_3.$$

5.3.3 Parallel three-state system

5.3.3.1. Dynamics and kinetics

For the possible parallel three-state system with two initial states and one final state due to the heterogeneity of the environment, as illustrated in Scheme 5-3, the population
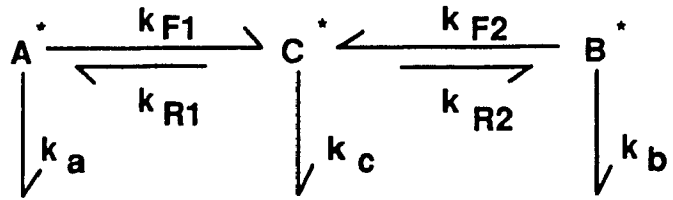
Scheme 5-3

ratios of A^*, B^*, and C^* can be obtained from the following differential equations:

$$\begin{cases} N'_A(t) = \dfrac{dN_A(t)}{dt} = k_{R1}N_C(t) - (k_a + k_{F1})N_A(t) \\[2mm] N'_B(t) = \dfrac{dN_b(t)}{dt} = k_{R2}N_C(t) - (k_b + k_{F2})N_B(t) \\[2mm] N'_C(t) = \dfrac{dN_C(t)}{dt} = k_{F1}N_A(t) + k_{F2}N_B(t) - (k_c + k_{R1} + k_{R2})N_C(t) \end{cases} \tag{28}$$

Similar to the serial three-state system, for the irreversible process satisfying the following conditions:

$$k_{R1,R2} \ll k_{F1,F2} \ll k_a, k_b, \text{ and } k_c$$

$$N_C(0)=0, \text{ and } N_0 = N_0^A + N_0^B \tag{29}$$

the population ratio at each state can be simply expressed by:

125

$$\begin{cases} N_A(t) = \xi e^{-t/\tau_1} \\ N_B(t) = (1-\xi)e^{-t/\tau_2} \\ N_C(t) = e^{-t/\tau_3} - (1-\xi)e^{-t/\tau_2} - \xi e^{-t/\tau_1} \end{cases} \tag{30}$$

where the initial population ratio $\xi = N_0^A/N_0 = 1 - N_0^B/N_0$.

5.3.3.2   Decay-associated spectrum $DAS_i(\upsilon)$, $i=1..3$

From the expression of the emission density $i(\upsilon,t)$

$$i(\upsilon,t) = \sum_{j=A}^{C} \alpha_j(\upsilon)N_j(t) = \sum_{l=1}^{3} \alpha_l(\upsilon)e^{-t/\tau_l} \tag{31}$$

the correlation between SAS and preexponential coefficients can be found:

$$\begin{cases} \alpha_A(\upsilon) = \dfrac{\alpha_1(\upsilon)}{\xi} + \alpha_3(\upsilon) \\ \alpha_B(\upsilon) = \dfrac{\alpha_2(\upsilon)}{(1-\xi)} + \alpha_3(\upsilon) \\ \alpha_C(\upsilon) = \alpha_3(\upsilon) \end{cases} \tag{32}$$

As the serial three-state system, the decay associated spectrum to i^{th} decay component is defined as *the fractional contribution to the total fluorescence* are the same as eq. (13), therefore the normal species associated spectra $SAS_j(\lambda)$, $i=A$, B, and C are defined by:

$$SAS_A(\lambda) = \rho \, \alpha_A(\lambda)\tau_1/I_{ss}(\lambda) \, i_{ss}(\lambda)$$

$$SAS_B(\lambda) = (1-\rho) \, \alpha_B(\lambda)\tau_2/I_{ss}(\lambda) \, i_{ss}(\lambda) \tag{33}$$

$$SAS_C(\lambda) = \alpha_C(\lambda)(\tau_3 - \rho\tau_1 - (1-\rho)\tau_2)/I_{ss}(\lambda) \, i_{ss}(\lambda)$$

In comparison with the DAS and preexponential distribution α's in eqs. (13), (32) and eq. (33), the correlation between DAS and normal SAS can be found as below:

$$SAS_A(\lambda) = (\alpha_1(\lambda) + \rho \, \alpha_3(\lambda))\tau_1/I_{SS}(\lambda) \, i_{SS}(\lambda)$$

$$= \alpha_1(\lambda)\tau_1/I_{SS}(\lambda) \, i_{SS}(\lambda) + \rho \, \alpha_3(\lambda)\tau_1/I_{SS}(\lambda) \, i_{SS}(\lambda)$$

$$= DAS_1(\lambda) + \rho\tau_1/\tau_3 \, DAS_3(\lambda),$$

$$SAS_B(\lambda) = (1-\rho) \, \alpha_B(\lambda)\tau_2/I_{SS}(\lambda) \, i_{SS}(\lambda) \tag{34}$$

$$= \alpha_2(\lambda)\tau_2/I_{SS}(\lambda) \, i_{SS}(\lambda) + (1-\rho) \, \alpha_3(\lambda)\tau_2/I_{SS}(\lambda) \, i_{SS}(\lambda)$$

$$= DAS_2(\lambda) + (1-\rho)\tau_2/\tau_3 \, DAS_3(\lambda),$$

$$SAS_C(\lambda) = \alpha_C(\lambda)(\tau_3 - \rho\tau_1 - (1-\rho)\tau_2)/I_{SS}(\lambda) \, i_{SS}(\lambda)$$

$$= (\tau_3 - \rho\tau_1 - (1-\rho)\tau_2)/\tau_3 \, DAS_3(\lambda)$$

where the total fluorescence $I_{SS}(\lambda) = \sum_i [\alpha_i(\lambda)\tau_i]$, has been applied.

5.4 Time-Dependent $C(\upsilon_m, t)$

5.4.1 Two-state system

For the irreversible two-state system, the species associated spectra (SAS) $\alpha_A(\upsilon)$, $\alpha_B(\upsilon)$ of both species A* and B* can be simplified by assigning a gaussian function[187] instead of a log-normal line shape function.[57,187] For mathematical derivation convenience, the species associated spectra can be expressed simply by:

$$\begin{cases} \alpha_A(\upsilon) = \alpha_A^0 e^{-[\upsilon - \upsilon_m(0)]^2/\delta^2} \\ \alpha_B(\upsilon) = \alpha_B^0 e^{-[\upsilon - \upsilon_m(\infty)]^2/\delta^2} \end{cases} \tag{35}$$

where δ is the band width of the distribution and is assumed to be the same for all species; α_A^0, α_B^0 are the maximum amplitudes; and $\upsilon_m(0)$, $\upsilon_m(\infty)$ are the frequencies at maximum intensity at initial and infinite tume as the peak position of species A* and B* $\left(\upsilon_m(0) = \upsilon_m^A, \ \upsilon_m(\infty) = \upsilon_m^B\right)$, respectively.

From eq. (11), the first derivative fluorescence spectral density with respect to the frequency υ is given by:

$$\frac{\partial\, i(\upsilon,t)}{\partial\upsilon} = \left[\frac{d\alpha_A(\upsilon)}{d\upsilon} - \frac{d\alpha_B(\upsilon)}{d\upsilon}\right]e^{-t/\tau_1} + \frac{d\alpha_B(\upsilon)}{d\upsilon}e^{-t/\tau_2} \qquad (36)$$

Since $\dfrac{d\alpha_A(\upsilon)}{d\upsilon} = -2[\upsilon - \upsilon_m(0)]/\delta^2\alpha_A(\upsilon)$, $\dfrac{d\alpha_B(\upsilon)}{d\upsilon} = -2[\upsilon - \upsilon_m(\infty)]/\delta^2\alpha_B(\upsilon)$,

eq. (36) can be written to:

$$\frac{\partial\, i(\upsilon,t)}{\partial\upsilon} = -\frac{2}{\delta^2}\left\{\begin{array}{l}\{[\upsilon - \upsilon_m(0)]\alpha_A(\upsilon) - [\upsilon - \upsilon_m(\infty)]\alpha_B(\upsilon)\}e^{-t/\tau_1}\\ +[\upsilon - \upsilon_m(\infty)]\alpha_B(\upsilon)e^{-t/\tau_2}\end{array}\right\} \qquad (37)$$

For the frequency at maximum emission ($\upsilon = \upsilon_m$), the first derivative $i(\upsilon,t)$ with respect to the frequency, should be equal to zero:

$$\{[\upsilon_m - \upsilon_m(0)]\alpha_A(\upsilon_m) - [\upsilon_m - \upsilon_m(\infty)]\alpha_B(\upsilon_m)\}e^{-t/\tau_1}$$
$$+[\upsilon_m - \upsilon_m(\infty)]\alpha_B(\upsilon_m)e^{-t/\tau_2} = 0 \qquad (38)$$

and

$$\{[\upsilon_m - \upsilon_m(\infty) + \upsilon_m(\infty) - \upsilon_m(0)]\alpha_A(\upsilon_m) - [\upsilon_m - \upsilon_m(\infty)]\alpha_B(\upsilon_m)\}e^{-t/\tau_1}$$
$$+[\upsilon_m - \upsilon_m(\infty)]\alpha_B(\upsilon_m)e^{-t/\tau_2} = 0 \qquad (39)$$

Dividing the constant $\upsilon_m(0) - \upsilon_m(\infty)$ for all terms, we can get

$$\left\{\left[\frac{\upsilon_m - \upsilon_m(\infty)}{\upsilon_m(0) - \upsilon_m(\infty)} - 1\right]\alpha_A(\upsilon_m) - \frac{\upsilon_m - \upsilon_m(\infty)}{\upsilon_m(0) - \upsilon_m(\infty)}\alpha_B(\upsilon_m)\right\}e^{-t/\tau_1}$$
$$+\frac{\upsilon_m - \upsilon_m(\infty)}{\upsilon_m(0) - \upsilon_m(\infty)}\alpha_B(\upsilon_m)e^{-t/\tau_2} = 0 \qquad (40)$$

where the fraction $\dfrac{\upsilon_m - \upsilon_m(\infty)}{\upsilon_m(0) - \upsilon_m(\infty)} = C(\upsilon_m, t)$ is exactly the same as the definition

of the function $C(t)$.[71] Thus the eq. (40) can be represented by $C(\upsilon_m, t)$ as:

$$\left\{ [C(\upsilon_m, t) - 1]\alpha_A(\upsilon_m) - C(\upsilon_m, t)\alpha_B(\upsilon_m) \right\} e^{-t/\tau_1} + C(\upsilon_m, t)\alpha_B(\upsilon_m)e^{-t/\tau_2} = 0 \,(41)$$

Therefore, the $C(\upsilon_m, t)$ can be described by:

$$C(\upsilon_m, t) = \frac{\alpha_A(\upsilon_m)e^{-t/\tau_1}}{[\alpha_A(\upsilon_m) - \alpha_B(\upsilon_m)]e^{-t/\tau_1} + \alpha_B(\upsilon_m)e^{-t/\tau_2}} = \frac{\alpha_A(\upsilon_m)e^{-t/\tau_1}}{i(\upsilon_m, t)} \tag{42}$$

5.4.2 Serial three-state system

Similarly to the two-state system, a gaussian function can be assigned to the SAS for A^*, B^*, and C^* with different peak position as:

$$\begin{cases} \alpha_A(\upsilon) = \alpha_A^0 e^{-[\upsilon - \upsilon_{1m}(0)]^2/\delta^2} \\ \alpha_B(\upsilon) = \alpha_B^0 e^{-[\upsilon - \upsilon_{1m}(\infty)]^2/\delta^2} = \alpha_B^0 e^{-[\upsilon - \upsilon_{2m}(0)]^2/\delta^2} \\ \alpha_C(\upsilon) = \alpha_C^0 e^{-[\upsilon - \upsilon_{2m}(\infty)]^2/\delta^2} \end{cases} \tag{43}$$

where δ is the band width of the gaussian distribution and is assumed to be the same for all species; α_A^0, α_B^0, and α_C^0 are the maximum amplitudes of species A^*, B^*, and C^*; and $\upsilon_{1m,2m}(0)$ and $\upsilon_{1m,2m}(\infty)$ are the peak positions at initial and infinite of two separated solvation steps ($\upsilon_{1m}(\infty) = \upsilon_{2m}(0)$), which are also the same as the frequencies at maxima of these three species

$$\left(\upsilon_{1m}(0) = \upsilon_m^A, \ \upsilon_{1m}(\infty) = \upsilon_{2m}(0) = \upsilon_m^B, \text{ and } \upsilon_{2m}(\infty) = \upsilon_m^C \right)$$

For monitoring the peak shift with time, the first derivative spectral density with respect to the frequency υ from eq. (23) is

$$\frac{\partial\, i(\upsilon,t)}{\partial\upsilon} = \frac{d\alpha_A(\upsilon)}{d\upsilon}e^{-t/\tau_1} + \frac{d\alpha_B(\upsilon)}{d\upsilon}\frac{e^{-t/\tau_2} - e^{-t/\tau_1}}{1-\tau_1/\tau_2}$$

$$+ \frac{d\alpha_C(\upsilon)}{d\upsilon}\left(e^{-t/\tau_1} - \frac{e^{-t/\tau_2} - \tau_1/\tau_2 e^{-t/\tau_1}}{1-\tau_1/\tau_2}\right) \tag{44}$$

where the first derivative SAS with respect to time are:

$$\begin{cases} \dfrac{d\alpha_A(\upsilon)}{d\upsilon} = -2[\upsilon - \upsilon_{1m}(0)]/\delta^2\alpha_A(\upsilon) \\[2mm] \dfrac{d\alpha_B(\upsilon)}{d\upsilon} = -2[\upsilon - \upsilon_{1m}(\infty)]/\delta^2\alpha_B(\upsilon) = -2[\upsilon - \upsilon_{2m}(0)]/\delta^2\alpha_B(\upsilon) \\[2mm] \dfrac{d\alpha_C(\upsilon)}{d\upsilon} = -2[\upsilon - \upsilon_{2m}(\infty)]/\delta^2\alpha_C(\upsilon) \end{cases} \tag{45}$$

Dividing a constant term $\upsilon_{1m}(0)$-$\upsilon_{2m}(\infty)$ for all, and applying

$$C(\upsilon,t) = \frac{\upsilon - \upsilon_{2m}(\infty)}{\upsilon_{1m}(0) - \upsilon_{2m}(\infty)} \tag{46}$$

into eq. (45), we get

$$\begin{cases} \dfrac{d\alpha_A(\upsilon)}{d\upsilon} = -\dfrac{2[\upsilon_{1m}(0) - \upsilon_{2m}(\infty)]}{\delta^2}[C(\upsilon,t)-1]\alpha_A(\upsilon) \\[2mm] \dfrac{d\alpha_B(\upsilon)}{d\upsilon} = -\dfrac{2[\upsilon_{1m}(0) - \upsilon_{2m}(\infty)]}{\delta^2}[C(\upsilon,t)-\zeta]\alpha_B(\upsilon) \\[2mm] \dfrac{d\alpha_C(\upsilon)}{d\upsilon} = -\dfrac{2[\upsilon_{1m}(0) - \upsilon_{2m}(\infty)]}{\delta^2}C(\upsilon,t)\alpha_C(\upsilon) \end{cases} \tag{47}$$

where $\zeta = \dfrac{\upsilon_{1m}(\infty) - \upsilon_{2m}(\infty)}{\upsilon_{1m}(0) - \upsilon_{2m}(\infty)} = \dfrac{\upsilon_{2m}(0) - \upsilon_{2m}(\infty)}{\upsilon_{1m}(0) - \upsilon_{2m}(\infty)} \equiv Const.$ Therefore, for monitoring

the emission peak position shift with time, the first derivative $i(\upsilon,t)$ of eq. (44)

should be equal to zero, in which the first derivative α's can be replaced by the

equation set (47) as:

$$C(\upsilon_m,t) = \cfrac{[\alpha_A(\upsilon_m) - \rho\alpha_B(\upsilon_m)]e^{-t/\tau_1} + \rho\alpha_B(\upsilon_m)e^{-t/\tau_2}}{\left\{\left[\alpha_A(\upsilon_m) - \cfrac{\alpha_B(\upsilon_m) - \tau_1/\tau_2\alpha_C(\upsilon_m)}{1-\tau_1/\tau_2}\right]e^{-t/\tau_1} + \cfrac{\alpha_B(\upsilon_{r.}) - \alpha_C(\upsilon_m)}{1-\tau_1/\tau_2}e^{-t/\tau_2} \atop +\alpha_C(\upsilon_m)e^{-t/\tau_3}\right\}} \quad (48)$$

In comparison to eq. (23), the spectral shape- and time-dependency of $C(\upsilon_m,t)$ of eq. (48) can be simply expressed by:

$$C(\upsilon_m,t) = \frac{[\alpha_A(\upsilon_m) - \rho\alpha_B(\upsilon_m)]e^{-t/\tau_1} + \rho\alpha_B(\upsilon_m)e^{-t/\tau_2}}{i(\upsilon_m,t)} \quad (49)$$

where $\rho = \dfrac{\zeta}{1-\tau_1/\tau_2} = \dfrac{\upsilon_m^B - \upsilon_m^C}{(\upsilon_m^A - \upsilon_m^C)(1-\tau_1/\tau_2)}.$

5.5 Fluorescence Decay Spectra of C1 and C102

5.5.1 Fluorescence decay spectral measurements

5.5.1.1 Spectral deconvolution

The fluorescence decay kinetics of C1 and C102 in the different solvents were fitted to a sum of exponentials, no physical significance *a priori* being attributed to the recovered lifetimes or preexponential terms. The data for C1 in water could only be satisfactorily fitted, if a very short decay time component with a value less than 0.5 ps was included. In the data analysis, the value of the 0.5 ps component was held at this constant value and represents an upper limit to a very short decay time component. By contrast, the data for C102 in water gave an excellent fit for a single exponential decay.

The "best fit" parameters are presented in Table 5-1, where there is more than one kinetic component (bi- or tri-exponential decays), the shortest

131

Table 5-1: Fluorescence Decay Parameters for C1 and C102 in Different Solvents

Solvent	Fluorescence Maximum, nm		Fluorescence Decay Parameters[a] ns		τ_L [b] ps
	C1	C102	C1	C102	
Water	472.0	492.2	$\tau_1 \leq 0.0005$	5.96 ± 0.01 [c]	
			$\tau_2 = 0.416 \pm 0.001$	SW(500 nm)	0.53[d]
			$\tau_3 = 4.33 \pm 0.07$		
			GF (12)		
Methanol	456.5	476.5	$\tau_1 = 0.0157 \pm 0.0006$	$\tau_1 = 0.022 \pm 0.004$	
			$\tau_2 = 2.10 \pm 0.01$	$\tau_2 = 5.50 \pm 0.01$	9.30[e]
			GF(9)	SW(450 nm)	
1-Butanol	445.5	466.0	$\tau_1 = 0.107 \pm 0.001$	$\tau_1 = 0.109 \pm 0.001$	
			$\tau_2 = 3.75 \pm 0.01$	$\tau_2 = 4.67 \pm 0.01$	118[e]
			GF(14)	GF(11)	
1-Octanol	440.5	457.5	$\tau_1 = 0.190 \pm 0.003$	$\tau_1 = 0.139 \pm 0.001$	
			$\tau_2 = 0.413 \pm 0.003$	$\tau_2 = 0.439 \pm 0.002$	471
			$\tau_3 = 3.80 \pm 0.01$	$\tau_3 = 4.48 \pm 0.01$	± 5[f]
			GF(14)	GF(15)	
Dichloro-methane	424.0	441.0	$\tau = 3.17 \pm 0.01$		
			SW(460 nm)		
n-Butyl Acetate	407.5	432.0	$\tau_1 = 0.37 - 0.86$[g]	$\tau_1 = 0.62 - 0.80$[g]	
			$\tau_2 = 3.28 \pm 0.01$	$\tau_2 = 3.83 \pm 0.01$	
Isooctane			$\tau = 2.89 \pm 0.01$[h]		

[a]GF = global fit (no. of data sets); SW = single wavelength (wavelength). The majority of data is taken with 10 ps channel width except for the data in 1-butanol and 1-octanol where a 20.5 ps channel width was used. In the case of water solutions, where a higher time resolution was required, 1 and 10 ps channel widths were used. [b]Longitudinal relaxation time at 293 K, $\tau_L =$ $\varepsilon_\infty/\varepsilon_0 \tau_D$, where ε_∞, ε_0 is the high-frequency and zero-frequency dielectric constant, and τ_D is the Debye relaxation time. [c]($\chi^2 = 1.045$ SVR = 1.98) Single exponential decay was observed from 460-540 nm. [d]Mason, P.R.; Hasted, J. B.; Moore, L. Adv. Mol Relaxation Processes, 1974, 6, 217. [e]From Ref. 188. [f]Calculated from the arc plot of the first dispersion region (Fig. 5-15) while $\tau_D = 1780$ ps from Ref. 189. [g]The lifetime did not appear to be independent of the emission wavelength. [h]Single wavelength at 420 nm. ($\chi^2 = 1.045$ SVR = 1.98)

component is labeled as τ_1, the next longest component as τ_2, etc. The following trends were observed. (1) The number of components necessary to describe the decay kinetics was the same for both C1 and C102 in the various solvents except for water. (2) The short-lifetime components were similar for both C1 and C102. (3) A single-exponential decay function was observed for the dyes in dichloromethane and isooctane solutions. (4) Double exponential decays were observed in 1-butanol, methanol and n-butyl acetate. In 1-octanol, three exponentials were required to describe the decay. In the alcohols where multi-exponential decays were found, the short-lifetime components had negative preexponential factors at long wavelengths.

4.5.1.2   in Water

The residual plots for the two dyes C1 and C102 are shown in Fig. 5-1 and Fig. 5-2, respectively. The single and biexponential residual plots for C102 are virtually unchanged (Fig. 5-2) and therefore the decay of C102 in water is best described by a single exponential. In contrast, the residual plots for a biexponential decay at channel widths at 10 ps or 1 ps (Fig. 5-1 (a), (b)) for C1 in water show a poor fit at low channel numbers. Inclusion of a third, short component of 0.5 ps in the decay function (Fig. 5-1 (c), (d)), gave an excellent fit. The 0.5 ps decay component is not an experimental or instrumental artifact. The fluorescence results of the same C1 in other solvents such as dichloromethane and isooctane gave excellent fits to single exponential decay behaviors. In methanol, the fluorescence decay of C1 was satisfactorily fit to a double exponential decay model with no evidence of a very short decay (< 1 ps) component. This is a strong evidence that the 0.5 ps component observed for C1 in water does not originate from a solute impurity. This also eliminates a strong-light artifact.
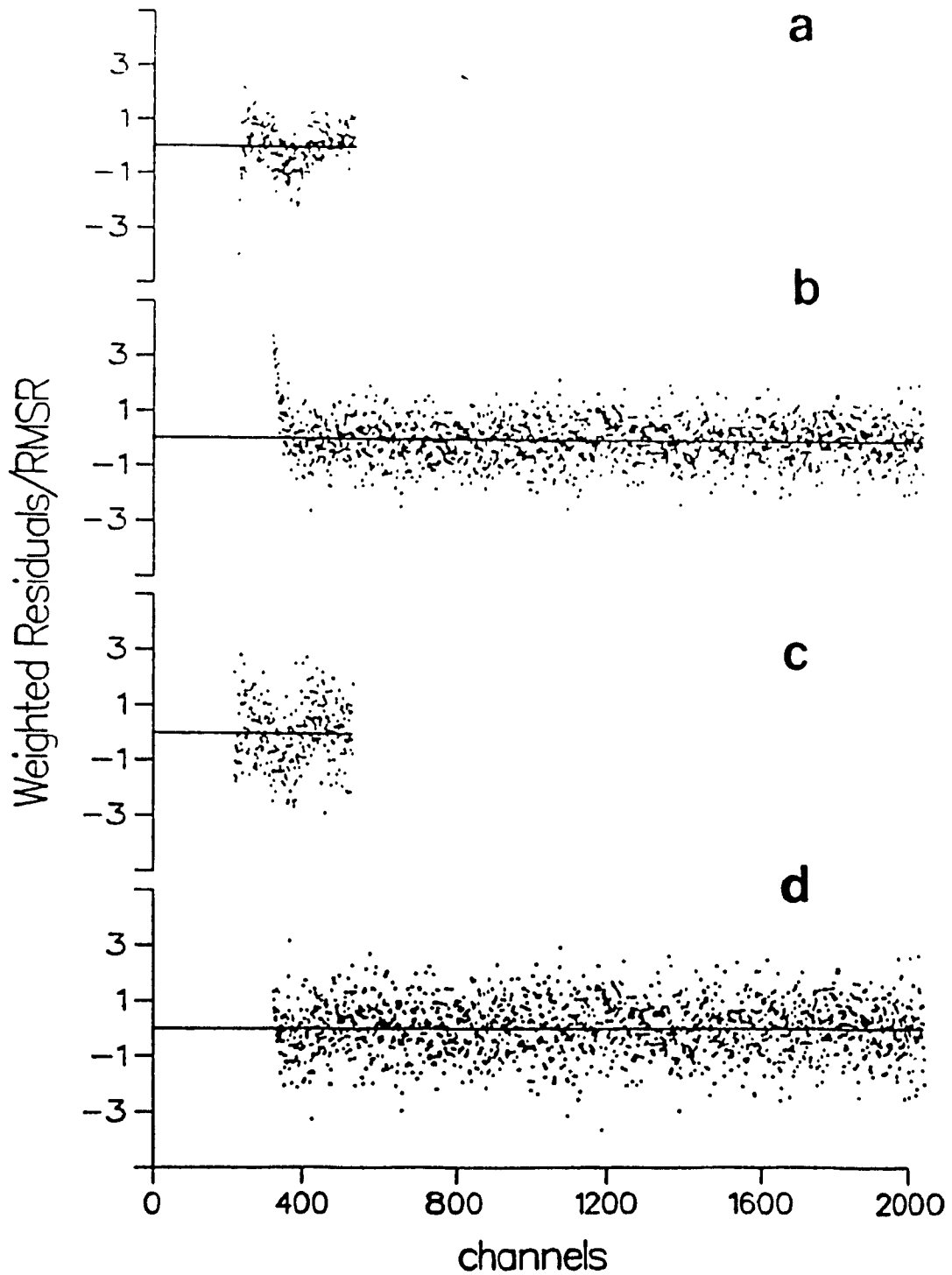
Fig. 5-1   Plot of the weighed residual vs channel number for the fluorescence decay of C1 in water at 430 nm. (a) biexponential fit; 1 ps channel width. (b) biexponential fit; 10 ps channel width. (c) triexponential fit; 1 ps channel width. (d) triexponential fit; 10 ps channel width.
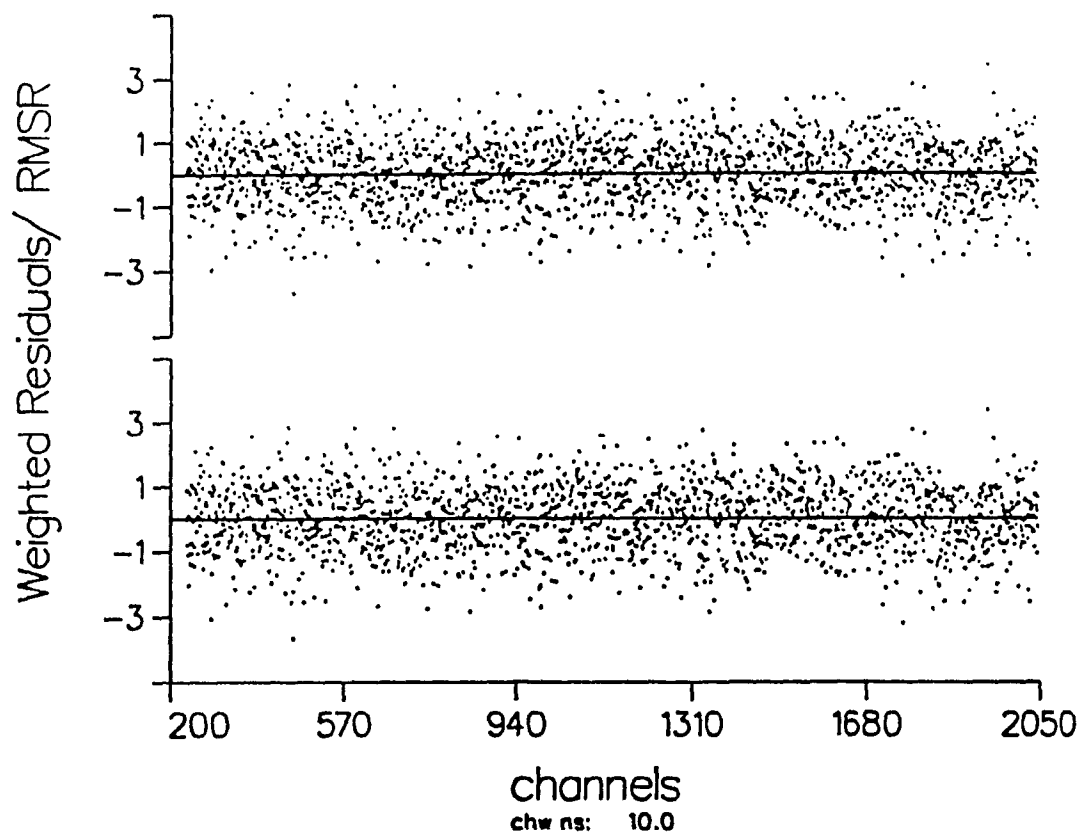
Fig. 5-2 Plots of the weighted residuals vs channel number for a monoexponential fit of the fluorescence decay of C102 in water at 460 nm; 10 ps channel width.

5.5.1.3   in 1-Butanol

In 1-butanol, the lifetime of the short-lived component of the biexponential decays was virtually identical for C1 and C102 (107 ps and 109 ps, respectively). The lifetimes and preexponential factors ($\alpha_i(\lambda)$'s, i=1,2) at different emission wavelengths for C1 are listed in Table 5-2, and the emission spectra associated with each lifetime (decay-associated spectra or DAS) for C1 and C102 are shown in Fig. 5-3. Table 5-2 shows that α_1 (short-lifetime component) is positive at short wavelengths, crosses zero and becomes negative at long wavelengths. At the cross-over point (440-445 nm), the fraction of the short-lived component becomes minute and the decay function fits a single exponential reasonably well. The values of the decay times of a double exponential decay in the cross-over region appear to vary singnificantly from the values at the other wavelengths. This is because the integrated intensity of the short-lifetime component at these wavelengths is extremely small and the error in this component is large for the biexponential fit. The trend of the preexponential factors as a function of wavelength for C1 and C102 are more clearly seen as DAS curves in Fig. 5-3. The DAS curves for the two coumarins have the same shape. The short-lifetime curve is positive at short wavelengths, crosses zero and becomes negative (due to the negative values of $\alpha_i(\lambda)$'s, i=1,2) at long wavelengths, whereas the long-lifetime curve remains positive throughout the emission region. The fluorescence decay kinetics of C1 and C102 in methanol are qualitatively identical to those in 1-butanol (shape of DAS curves, wavelength-independent lifetimes, etc.). The lifetimes for C1 and C102 in the different solvents are summarized in Table 5-1.

Table 5-2: "Best Fit" Fluorescence Decay Parameters for C1 in 1-Butanol at Selected Emission Wavelengths

λ_{em} (nm)	Lifetime (ns)		Preexponential Factor[a]	
	τ_1	τ_2	α_1	α_2
415	0.10	3.81	0.72	0.28
420	0.13	3.80	0.57	0.42
425	0.12	3.78	0.47	0.53
430	0.14	3.77	0.33	0.67
435	0.18	3.77	0.18	0.82
440	-	3.75[b]	-	1.00
	0.52	3.77	0.04	0.96
443	-	3.76[b]	-	1.00
	0.91	3.78	0.02	0.98
445	-	3.76[b]	-	1.00
	0.03	3.75	-0.68	1.68
450	0.05	3.76	-0.84	1.84
455	0.08	3.75	-0.60	1.60
460	0.08	3.75	-1.12	2.12
465	0.09	3.75	-1.13	2.13
470	0.12	3.75	-0.49	1.49
475	0.10	3.74	-1.91	2.91
480	0.11	3.72	-1.39	2.39
490	0.12	3.72	-1.31	2.31
500	0.12	3.72	-1.61	2.61

[a]Normalized to $\alpha_1 + \alpha_2 = 1$. [b]Single exponential fit was satisfactory.

5.5.1.4   in 1-Octanol

In 1-octanol, three exponential terms were required to fit the decay kinetics for C1 and C102. The three DAS curves associated with each of the terms for C1 were similar to those for C102 (Fig. 5-4). The most intense of the
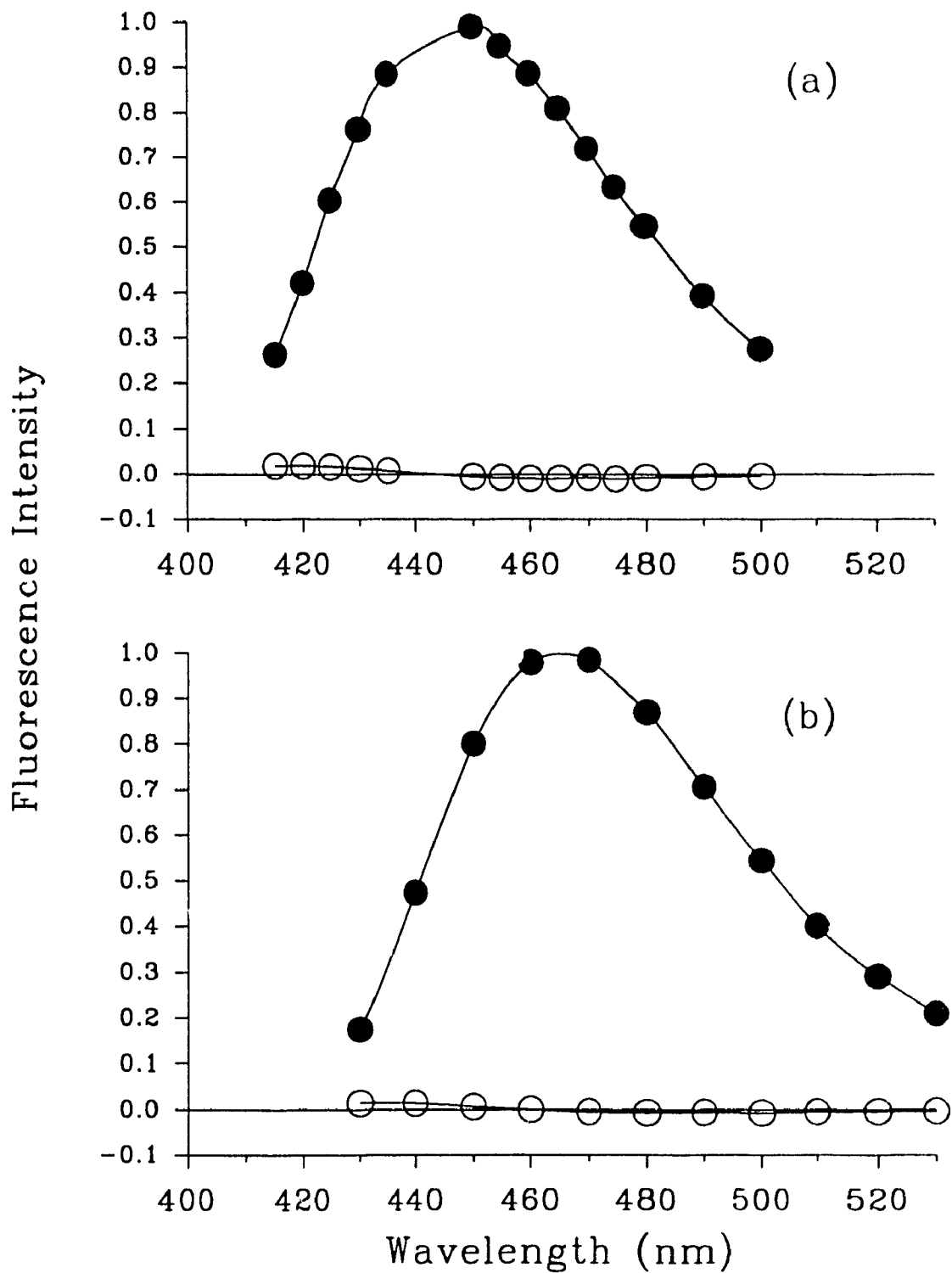
Fig. 5-3   Decay-associated spectra of (*a*) C1 and (*b*) C102 in 1-butanol.
The *upper curve* of the pair of DAS corresponds to the longer-lived
component.   *Upper* (*a*) τ = 3.75 ns; *Lower* (*a*) τ = 0.107 ns;
Upper (*b*) τ = 4.67 ns; *Lower* (*b*) τ = 0.109 ns
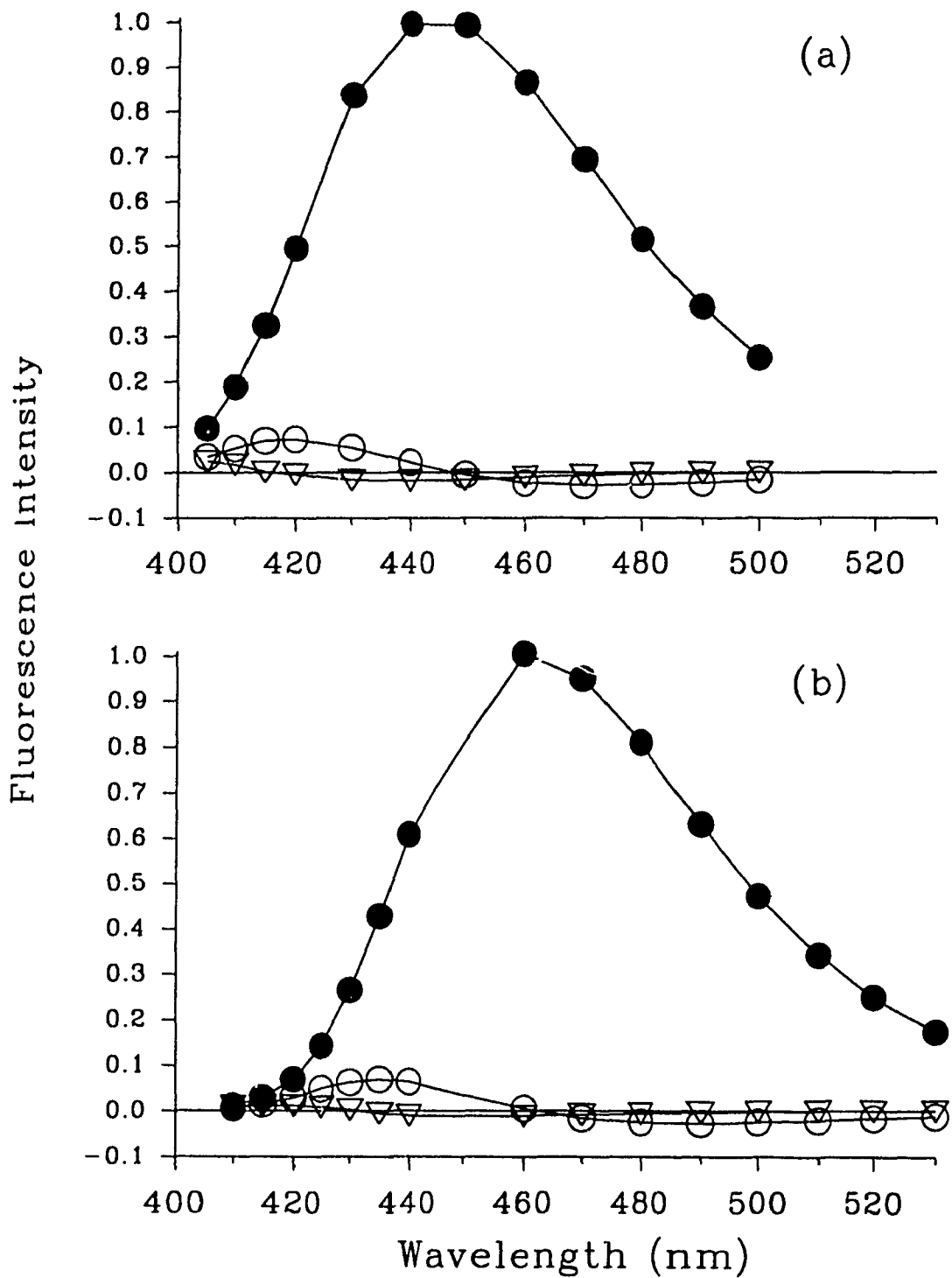
Fig. 5-4   Decay-associated spectra of (a) C1 and (b) C102 in 1-octanol.
In frame (a) for C1, the lifetimes of the curves, in order of diminishing
intensities are: 3.80 ns (●), 0.41 ns (O), and 0.19 ns (∇).   In frame (b, for
C102, the lifetimes are: 4.48 ns (●), 0.44 ns (O), and 0.14 ns (∇).

three DAS curves was positive throughout the wavelength region ($\alpha_i(\lambda)>0$, i=3) and had the longest lifetime. The other two DAS curves contained negative values of $\alpha_i(\lambda)$, i=1,2 at long wavelengths. The more intense of the two negative-going curves had intermediate lifetimes of 0.413 ns (C1) and 0.439 ns (C102), and the negative-going curves had the shortest lifetimes: 0.190 ns (C1) and 0.139 ns (C102). The lifetimes of the short-lifetime components are similar for C1 and C102 in 1-octanol, but are clearly different from those in 1-butanol. These results obviously indicate a solvent-dependency rather than a probe dependency.

5.5.1.5   in Aprotic Solvents

The fluorescence decay of C1 in isooctane gave a single exponential (τ = 2.90±0.01 ns; χ^2=0.997; SVR=2.01) since no significant solvation was expected. C1 in dichloromethane also displayed single exponential kinetics with the same lifetime throughout the emission wavelength range of 400-480 nm (τ = 3.17±0.01 ns, χ^2=1.013, SVR=1.83 at 460 nm). Both C1 and C102 in n-butyl acetate (see Table 5-1) gave biexponential kinetics with negative preexponential factors for the short-lived components at long wavelengths. However the lifetimes of the short-lived component varied slightly with the emission wavelength. This was probably due to the very low contribution of this component to the total fluorescence.

5.5.2   Discussions

The multiexponential decay kinetics (with long and short components) observed for C1 (or C102) in the polar solvents cannot be due to impurities since only single exponential decays with comparable decay time values were observed from solutions of C1 (C102) of identical purity in dichloromethane or

isooctane. A feature of a kinetically coupled A/B system is that the kinetics are biexponential with lifetimes which are **independent of the emission wavelength**, as is observed in the present case. By contrast, relaxation described by a single excited state undergoing a continuum solvation process should give multiexponential and emission wavelength dependent fluorescence decays. This has been observed for the case of 12-(9-anthroyloxy)stearic acid in hydrocarbon solvents.[62] The DAS curves are signatures of the kinetics of a two-state system.[73-78] In the case of a coupled irreversible system ($A^* \to B^*$, $k_B \ll k_A + k_{AB}$) as illustrated in Scheme 5-1, the DAS curve corresponding to the long-lived component remains positive throughout the emission wavelength region (contribution by species B^* only). The short-lived component is due to a difference in the spectra of species A^* and B^*.[73-78] Therefore, in the specific wavelength region where the contribution of the two species are comparable, the DAS will be near zero. Thus the DAS of the short-lifetime component curve is positive at where species A^* predominates, crosses through zero and becomes negative in the spectral region where the B^* fluorescence predominates. The results in the polar solvents (Fig. 5-1) are in exact accord with the signature in which the A^* emission spectra predominate at short wavelengths and the B^* emission spectra predominate at the long wavelengths.

The values of the short-lifetime component for C1 and C102 in the polar solvents provide further evidence that the decay kinetics are intimately related to the solvation process. The differences in lifetimes (of the short-lived component) in the different polar solvent do not correlate with the probe molecule but rather to the solvent polarity. The lifetimes of the short-lived component are more likely correlating to the longitudinal relaxation times τ_L of the solvent (Table 5-1).

The fluorescence decays of C1 and C102 in 1-octanol required triexponential functions to fit the experimental results. The similarity in the shape of the DAS curves (Fig. 5-1) for the both coumarins suggests that the third component is not a random adventitious observation but rather results from a property of the solvent. The shapes of the DAS show that the initial and final states are kinetically coupled. The 400 ps component correlates with the longitudinal relaxation time for 1-octanol. The values of the shortest time component are similar for the two different probe molecules in the same solvent. Therefore, they may be related to some sort of solvent relaxation process such as solvent heterogeneity since 1-octanol contains a large hydrophobic side-chain. The results of the DAS emissions do provide encouragement to the view that the method is capable of detecting subtle differences in the solvation process.

The fluorescence decays for C1 and C102 in water show a marked divergence from that in the other solvents. The fluorescence decay of C1 fit to three exponentials whereas the decay of C102 fit well to a single exponential. The 4.33 ns component contains only positive α's and accounts for between 1-8 % of the total fluorescence in the emission spectra. Rationalization of the origin of this component is speculative. We suggest that the ≤ 0.5 ps component may be associated with twisting of the diethylamino group to form a TICT state, in the relaxation process. Such a possibility does not exists in C102 and would account for the difference in the fluorescence decay behavior between the two coumarins.

5.6 Spectral Reconstruction of TRES

From the fluorescence-decay measurements, the fluorescence density $i(\upsilon,t)$ can be obtained from the global fitting results using a multi-exponential function[63] as

$$i(\upsilon,t) \ = \ \sum_{i=1}^{n} \alpha_i(\upsilon)exp(-t/\tau_i) \tag{50}$$

where $\alpha_i(\upsilon)$, $i=1..n$ is the preexponential coefficient of the ith decay component with decay time of τ_i. The *fractional contribution of the ith decay component to the steady state fluorescence* called the decay associated spectrum DAS as shown in Fig. 5-3, and Fig. 5-4, is defined by eq. (13) as:

$$DAS_i(\upsilon)=\alpha_i(\upsilon)\tau_i \ / \sum_{i=1}^{n} \ [\alpha_i(\upsilon)\tau_i] \ i_{SS}(\upsilon) \tag{50}$$

Here $i_{SS}(\upsilon)$ is the normal steady state fluorescence spectrum.

5.6.1 C1 and C102 in 1-butanol

The SR time-resolved emission spectra (TRES) of C1 and C102 in 1-butanol illustrated in Fig. 5-5a, and Fig. 5-5b, were calculated by eq. (50) using the preexponential coefficients and the decay times listed in the Table 5-3 from our global fitting[73] of the experimental TDF. Obviously, the TRES of both C1 and C102 in 1-butanol can be reconstructed (lines in Fig. 5-5a, and Fig. 5-5b) very well using the log-normal line function (eq. (3)), in which the frequency at fluorescence maximum (υ_m) at each specific time, was used to calculate the fractional frequency shift $C(t)$ of eq. (52)
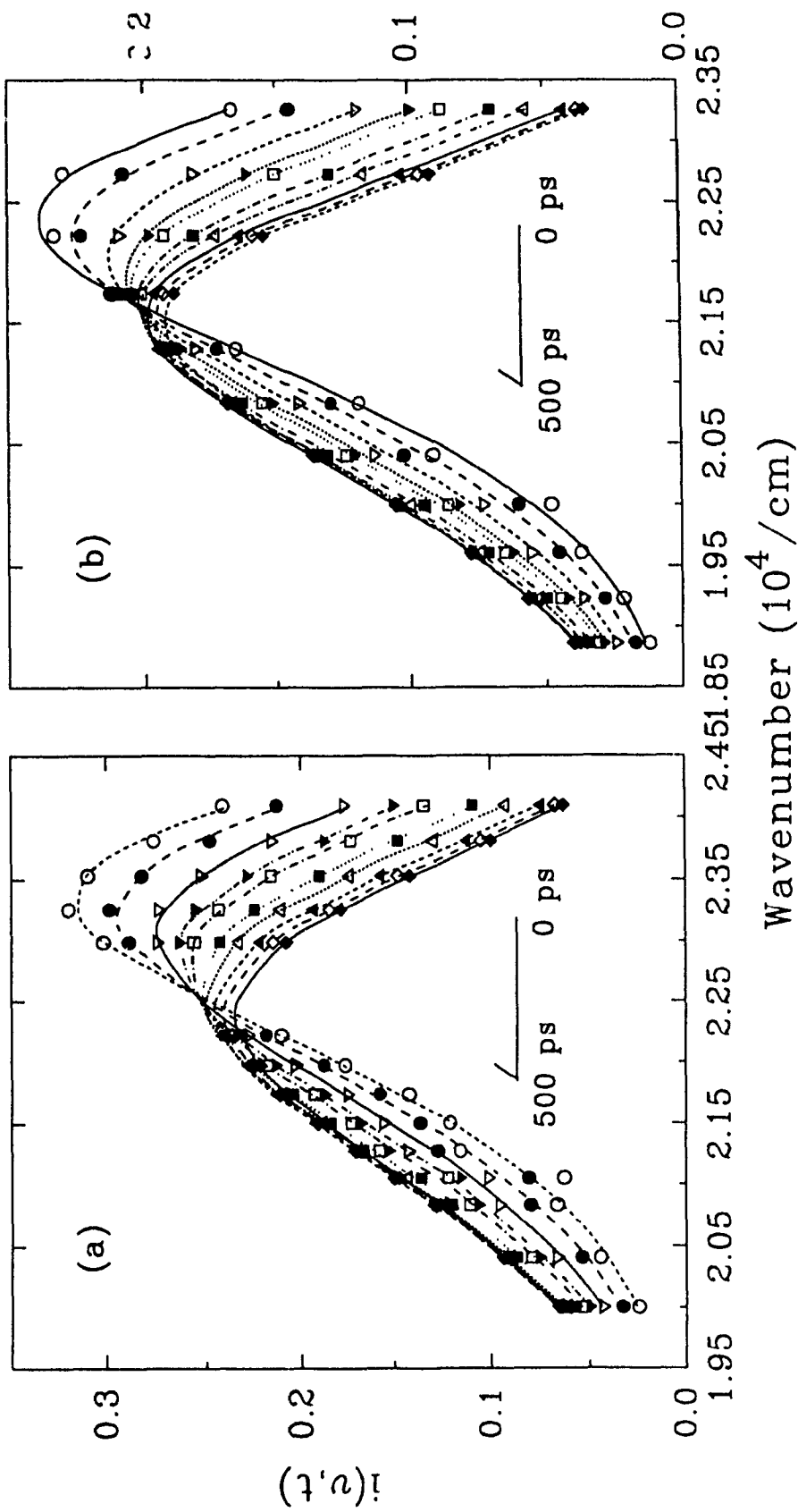
Fig. 5-5　TRES (*a*) of C1; (*b*) of C102 in 1-butanol, at 0, 20, 50, 80, 100, 150, 200, 300, 400, and 500 ps; (right to left). Symbols represent the *experimental* data and are fitted by various curves using log-normal functions.

$$C(t) = \frac{v_m(t) - v_m(\infty)}{v_m(0) - v_m(\infty)}$$ (52)

as plotted in Fig. 5-7a and Fig. 5-7b. The Decay of the C(t) follows a single exponential decay with decay time of 109 ± 4 ps for C1 and of 97 ± 2 ps for C102, respectively.

5.6.2   C1 & C102 in 1-Octanol

Similarly, the spectral densities of C1 and C102 in 1-octanol were obtained using eq.(50) in which the parameters in the Table 5-3 from the global fit of the TDF were applied. The TRES were fitted well using the log-normal function of eq. (3) as illustrated in Fig. 5-6a, 5-6b, respectively. The decay of the fractional frequency shifts C(t) of eq.(52) are calculated, and fitted to a biexponential function with decay times of 128 ± 4, 469 ± 9 ps for C1 and of 65 ± 2, 472 ± 5 ps for C102, as illustrated respectively in Fig. 5-7a and Fig. 5-7b. There is no significance on the shapes of these two C(t) fitted by either single or double exponential founction. The decay time from the single exponential fit of these two C(t) are: 248 ± 6 ps for C1 and 235 ± 13 ps for C102, respectively.

5.7   **Simulation of TRES under Irreversible Multi-State Model**

5.7.1   Kinetics

The negative decay associated spectra (DAS) of C1 or C102 in alcohols as illustrated in Fig. 5-3, and Fig. 5-4, indicate the existence of the kinetic correlation among the individual states (j=A..Z). The fluorescence density can be described by the total contribution of each individual species as:

$$i(\upsilon,t) = \sum_{j=A}^{Z} \alpha_j(\upsilon)N_j(t)$$ (53)
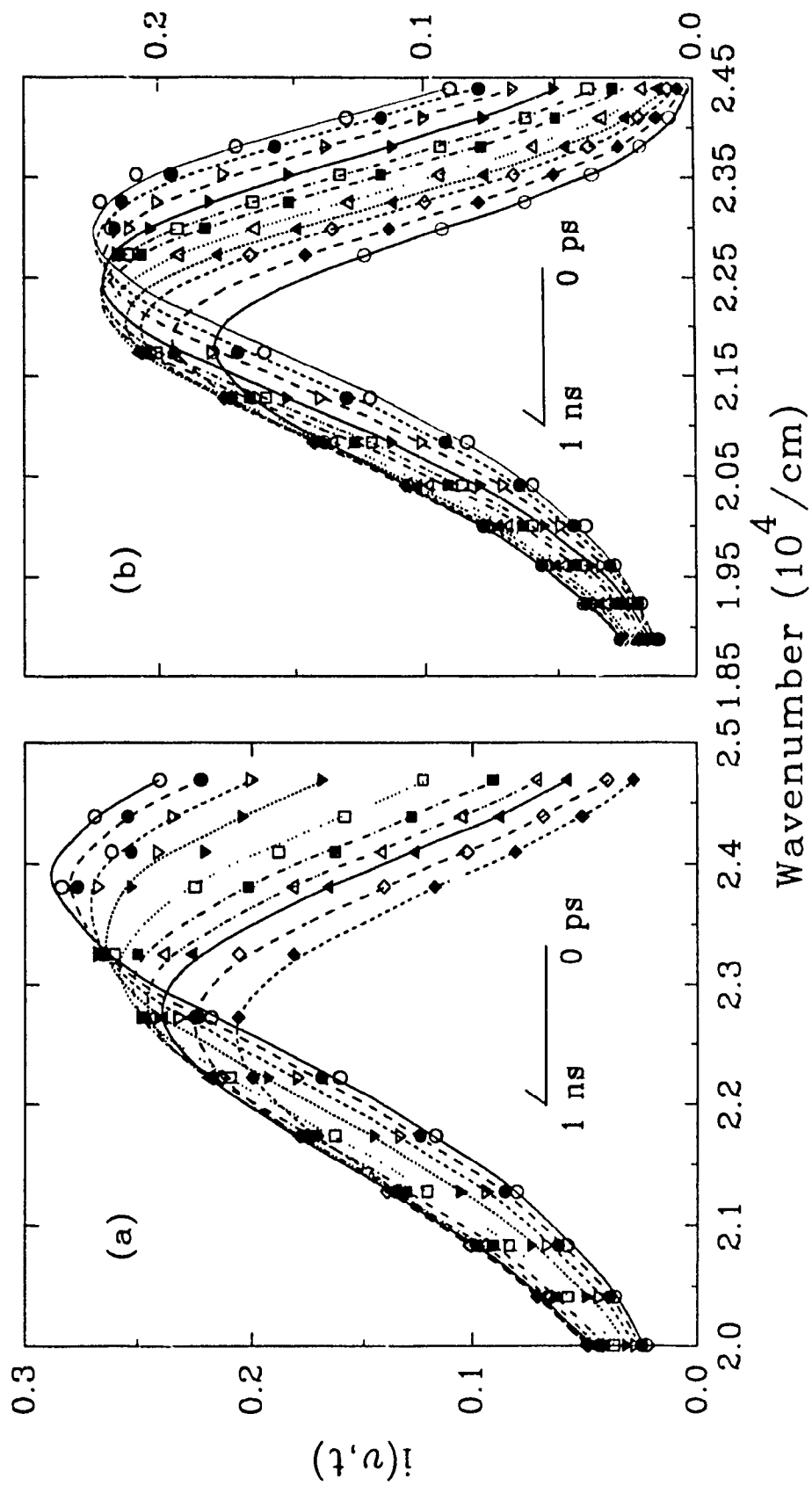
Fig. 5-6   TRES (a) of C1; (b) of C102 in 1-octanol at 0, 20, 50, 100, 150, 200, 300, 400, 500, 700 ps, and 1 ns, (right to left). Symbols represent the *experimental* data and are fitted by various curves using log-normal functions.
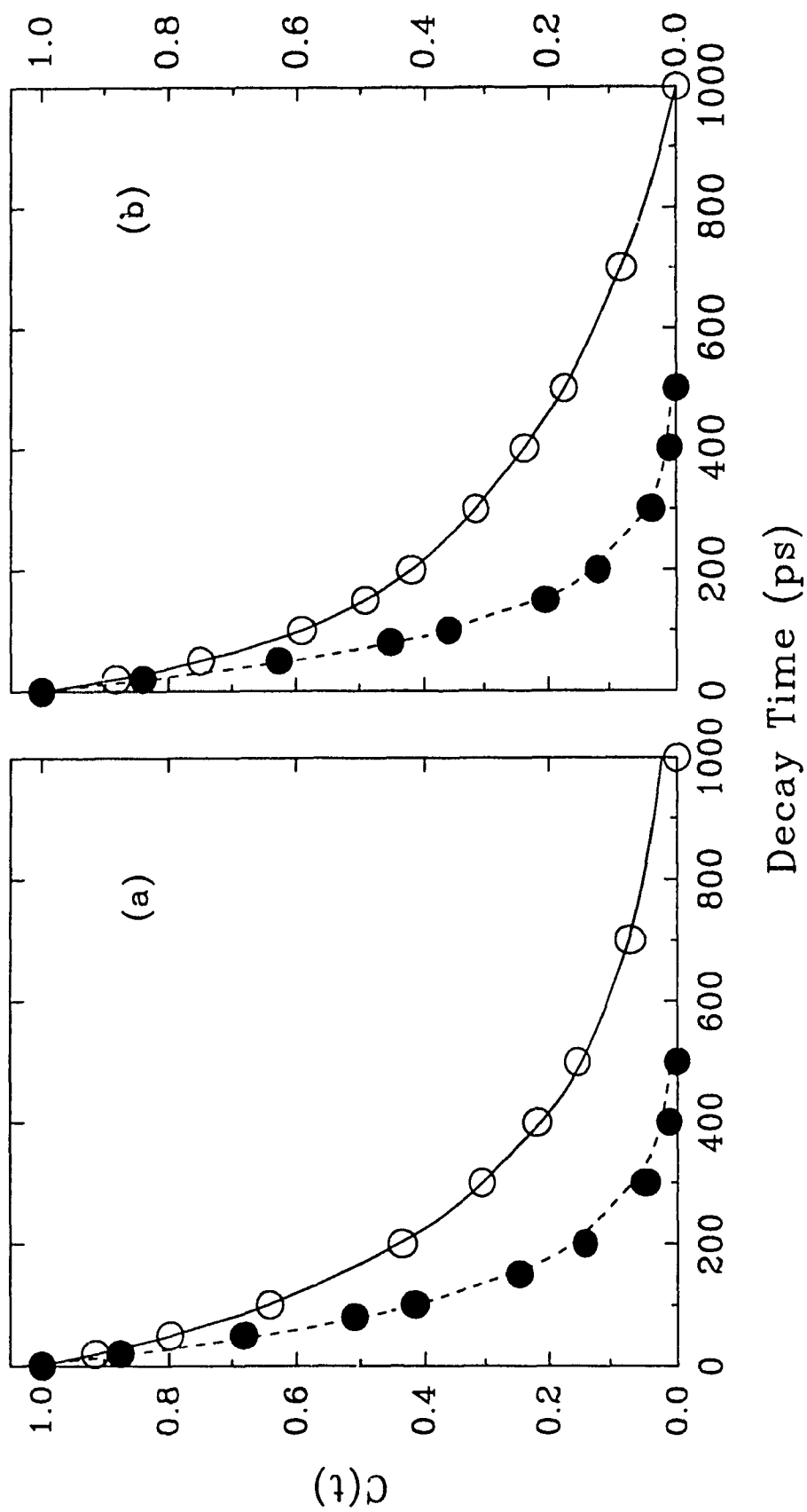
Fig. 5-7 C(t) calculated from SR TRES of (a) C1 in 1-butanol (●) and in 1-octanol (○), fitted by an exponential function (solid curve) ; (b) C102 in 1-butanol (●) and in 1-octanol (○), fitted by an exponential function (solid line)

Table 5-3: Comparison of the decay times obtained from different methods

Methods	Probe	Function	1-Butanol $\tau_1\pm\Delta\tau_1$ (ps)	1-Octanol $\tau_1\pm\Delta\tau_1(\%)^f$ (ps)	$\tau_2\pm\Delta\tau_2(\%)^f$ (ps)
$\tau_L{}^a$			118		471±5
$C(t)^b$	LDS-750		61		
TDF^c	C1		107±1	190±3	413±3
	C102		109±1	139±1	439±2
C(t) (Spectral Reconstruction)	C1	monoexp.	104±4	248±6	
		biexp.		128±3(41)	469±9(60)
	C102	monoexp.	97±2	235±13	
		biexp.		65±2(31)	472±5(69)
C(t) (Simulation)	C1	monoexp.	114±3	292±13	
		biexp.		120±4(40)	488±12(60)
	C102	monoexp.	104±2	292±19	
		biexp.		72±3(32)	481±7(68)
TRES^d (Spectral Reconstruction)	C1	$C(\upsilon_m,t)^e$	105±1	142±3	433±5
	C102	$C(\upsilon_m,t)^e$	101±1	98±3	446±5

a. Longitudinal solvent relaxation times from Ref. 188, 189, and Fig. 5-15. b. Ref 190. c TDF Time-Dependent Fluorescence. d. Applying eq. (59) for 1-butanol, and eq (60) for 1-octanol e TRES: Time-Resolved Emission Spectra. f. Values in parentheses are the preexponential fractions of the bi-exponential fittings.

where $N_j(t)$ is the population ratio of the jth (j=A..Z) species. From eq. (50) and eq. (53), the *species associated spectra* (SAS) $\alpha_j(\upsilon)$, j=A..Z, are correlated to the *preexponential coefficients* $\alpha_i(\upsilon)$, i=1..n by the following equations:

(i).   Two-state system (Section 5.3.1.2, and eq. (14))

$$\begin{cases} \alpha_A(v) = \alpha_1(v) + \alpha_2(v) \\ \alpha_B(v) = \alpha_2(v) \end{cases} \tag{54}$$

(ii)   Serial three-state system (Section 5.3.1.3, and eq. (24))

$$\begin{cases} \alpha_A(v) = \alpha_1(v) + \alpha_2(v) + \alpha_3(v) \\ \alpha_B(v) = \alpha_2(v)(1 - \frac{\tau_1}{\tau_2}) + \alpha_3(v) \\ \alpha_C(v) = \alpha_1(v) \end{cases} \tag{55}$$

It has to be pointed out that the similar DAS behaviour can be also found for a parallel three-state system, in which the correlation between SAS and the preexpoential coefficients can be expressed by:

$$\begin{cases} \alpha_A(v) = \frac{\alpha_1(v)}{\xi} + \alpha_3(v) \\ \alpha_B(v) = \frac{\alpha_2(v)}{(1-\xi)} + \alpha_1(v) \\ \alpha_C(v) = \alpha_3(v) \end{cases} \tag{56}$$

where $\xi = N_0^A/N_0$, $1-\xi = N_0^B/N_0$ and $N_0 = N_0^A + N_0^B$ are the initial population ratios of two individual species (see Section 5.3.1.4 and eq. (32)). Unfortunately, the parallel three-state kinetics can not be confirmed from our TDF results due to unknown initial population ratios in two heterogeneous states.

5.7.2   Simulation of TRES

From the bi-, and tri-exponential decay characteristics of TRES of C1 & C102 in alcohols,[73] the SAS of two (eq. (54)), and three (eq. (55)) species can be calculated from their preexponential coefficients. These SAS were fitted well by the log-normal function of eq. (3). Therefore, the TRES can be simulated

under the irreversible multi-state kinetics by combining the contribution from each species as:

(i)   Two-state (eq. (11))

$$i(\upsilon,t) = \alpha_A(\upsilon)e^{-t/\tau_1} + \alpha_B(\upsilon)(e^{-t/\tau_2} - e^{-t/\tau_1}) \tag{57}$$

(ii)   Serial three-state (eq. (23))

$$i(\upsilon,t) = \alpha_A(\upsilon)e^{-t/\tau_1} + \alpha_B(\upsilon)\frac{e^{-t/\tau_2} - e^{-t/\tau_1}}{1-\tau_1/\tau_2} + \alpha_C(\upsilon)\left(e^{-t/\tau_1} - \frac{e^{-t/\tau_2} - \tau_1/\tau_2 e^{-t/\tau_1}}{1-\tau_1/\tau_2} \right) \tag{58}$$

The parameters of the log-normal SAS of the SR TRES as listed in the Table 5-4, were applied into the simulations. In Fig. 5-8, Fig. 5-9, the simulated TRES were illustrated whose frequencies at maxima can be found from each curve fitting result using the log-normal function. These frequencies at maxima are applied into eq. (52) to get the frequency fraction C(t) as shown in Fig. 5-10. The mono- and bi-exponential decay of the C(t) are observed for both dyes in 1-butanol, and 1-octanol, respectively. The decay times of 109±5 ps for C1, of 100±1ps for C102 in 1-butanol, and of 120±4, 488±12 ps for C1, of 72±3, 481±7 ps for C102 in 1-octanol, are obtained as listed in the Table 5-3. Similar to the C(t) of SR TRES of both coumarins in 1-octanol, there is no significance on the shape of C(t) fitted by either single and double exponential founction. The decay times from the single exponential fitting are 292±13 ps for C1 and 292±19 ps for C102, respectively.

5.7.3   Comparison between SR and simulated TRES

In the above simulation (in Table 5-3), we find the agreement in (i) the decay times obtained from decay of C(t); (ii) spectral shapes, of reconstructed TRES and simulated TRES under irreversible multi-state kinetics. Such
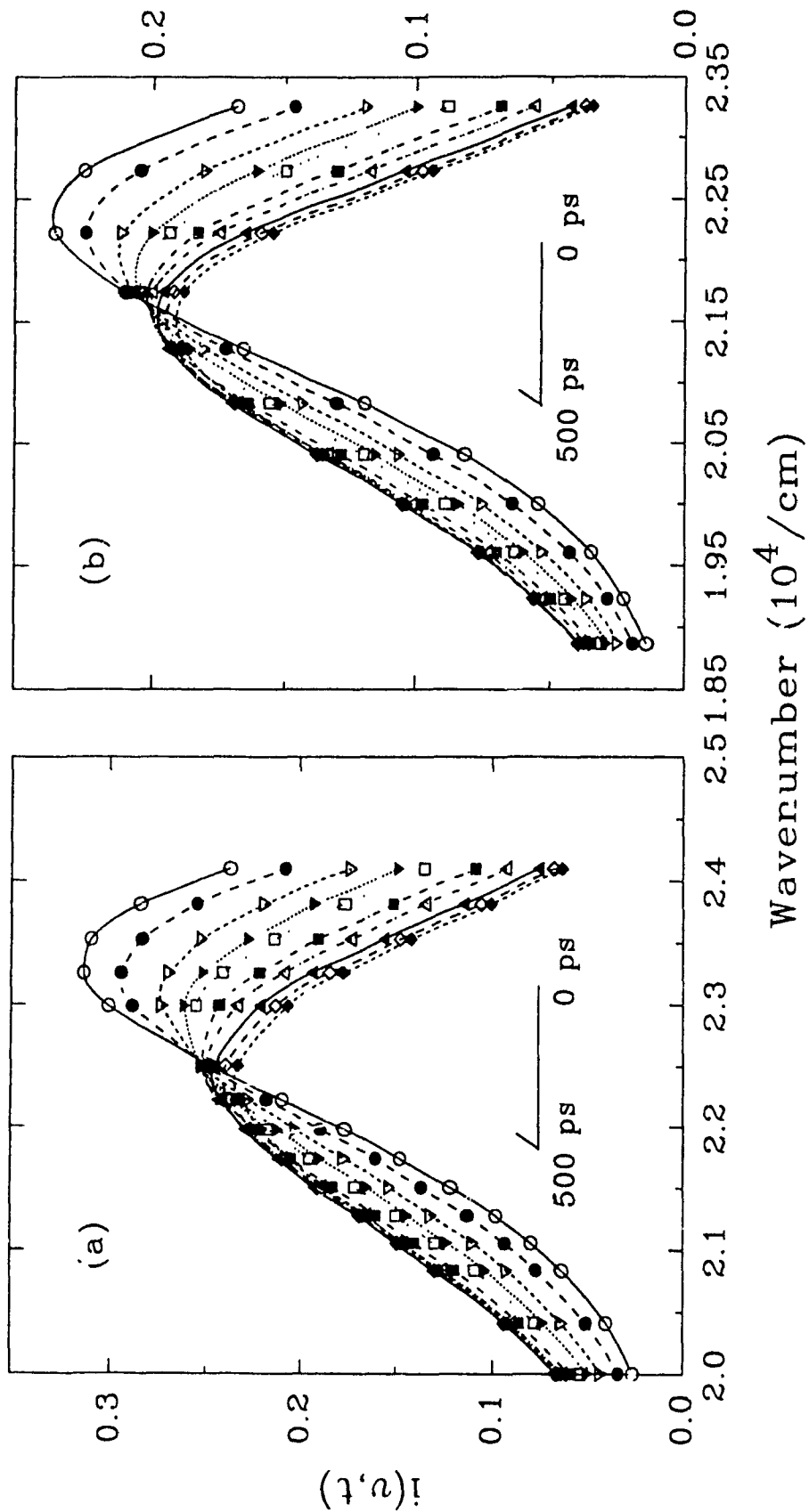
Fig. 5-8 *Simulated* TRES (*a*) of C1; (*b*) of C102, in 1-butanol at 0, 20, 50, 80, 100, 150, 200, 300, 400, 500 ps (right to left); Symbols represent the data from simulation and are fitted by various curves using log-normal functions.
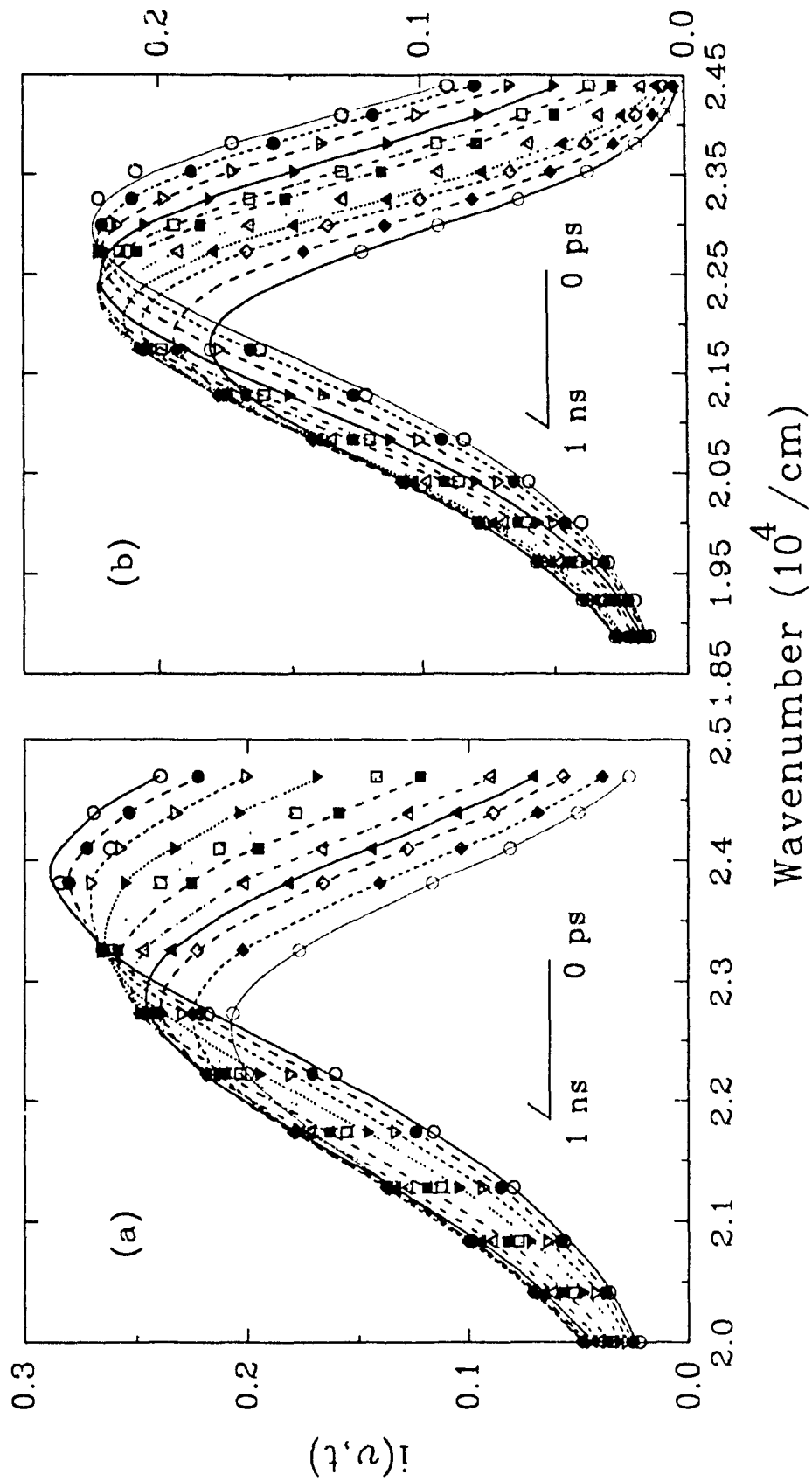
Fig. 5-9 *Simulated* TRES (*a*) of C1; (*b*) of C102, in 1-octanol at 0, 20, 50, 100, 150, 200, 300, 400, 500, 700 ps, and 1 ns (right to left). Symbols represent the data from simulation and are fitted by various curves using log-normal functions.
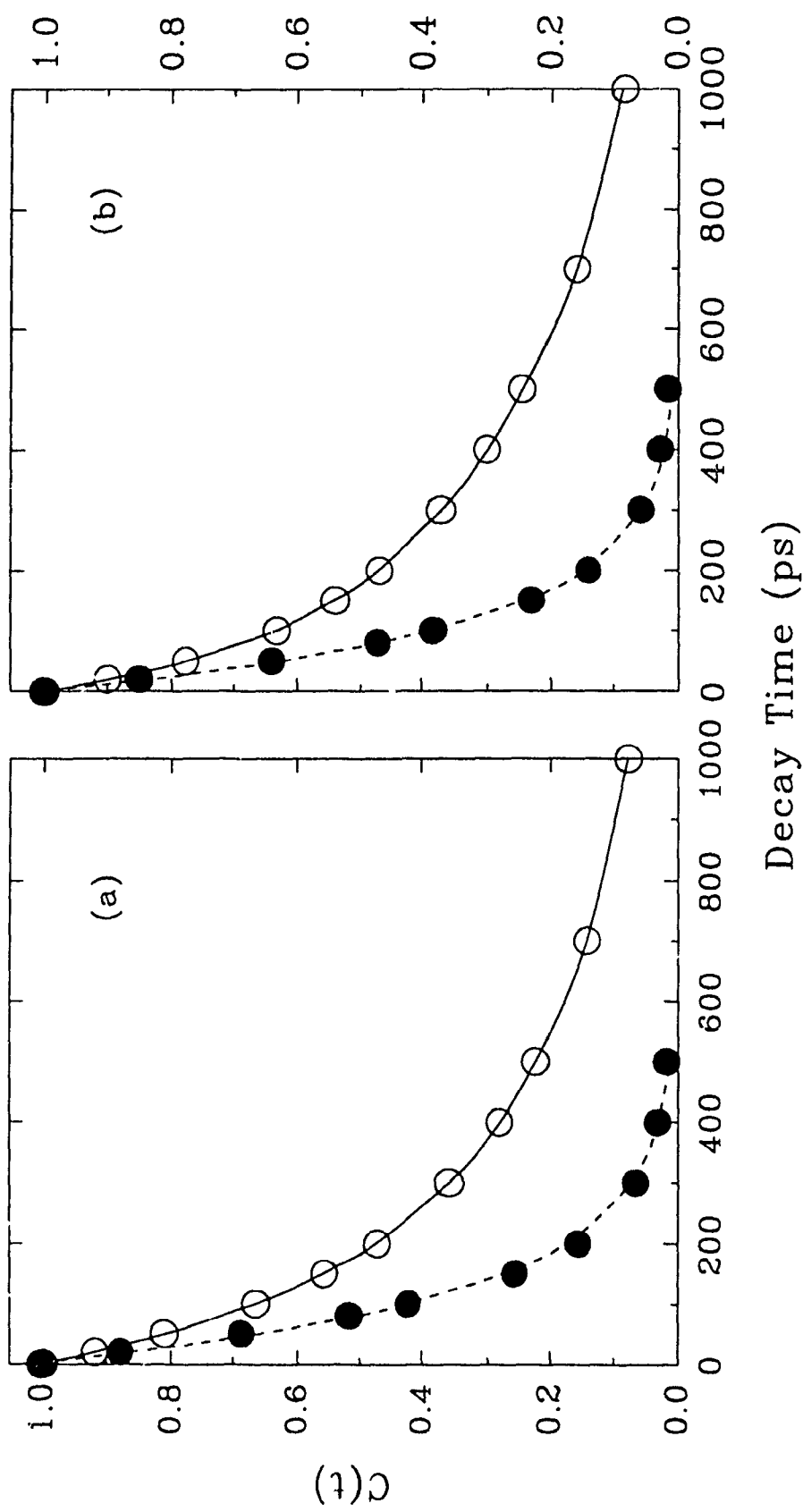
Fig. 5-10 C(t) calculated from simulated TRES of (a) C1 in 1-butanol (●) and in 1-octanol (O); (b) C102 in 1-butanol (●) and in 1-octanol (O), decay exponentially (solid curve).

Table 5-4   Parameters of the log-normal line shape[a] Species Associated Spectrum (SAS) used in Simulations

Solvent	Dye	Species ($\tau \pm \Delta\tau$ ps)	i0	$-b/\Delta$	b	ν_m (10^4/cm)	Γ^b
1-Butanol	C1	A* (107±1)	0.3149	1.1449	0.2984	2.3338	0.2645
		B* (3752±1)	0.2680	0.9196	0.2696	2.2399	0.2967
	C102	A* (109±1)	0.23?	0.7729	0.2128	2.2352	0.2774
		B* (4674±2)	0.2140	1.0700	0.2966	2.1501	0.2813
1-Octanol	C1	A* (190±3)	0.2883	0.6017	0.2005	2.3877	0.3355
		B* (413±3)	0.3000	0.9173	0.2629	2.2970	0.2899
		C* (3800±1)	0.2672	0.8087	0.2383	2.2476	0.2975
	C102	A* (139±1)	0.2249	1.0612	0.3159	2.2960	0.3027
		B* (439±2)	0.2588	1.0986	0.2910	2.2266	0.2686
		C* (4479±2)	0.2239	1.0158	0.2822	2.1674	0.2815

[a]. As defined by eq. (3).   [b]. FWHM of emission spectrum as defined by eq (3) from Ref 57

consistency indicates that the individual species are kinetically related, a conclusion previously reached on the basis of the negative character of DAS. Fig. 5-11, and Fig. 5-12 respectively illustrate the time-dependency of the FWHM of the SR TRES (Γ of eq. (3)) of C1 and C102 in 1-butanol and 1-octanol. This observation contradits to the single state model, in which the *unique change* of both Γ (FWHM) and asymmetric parameter (b in eq. (3)) is expected.[57] Therefore, the time-dependency of these parameters further supports the previous conclusion of the multi-state kinetics.

For both C1 and C102 in 1-octanol, we find a difference in decay times between those from exponential fitted C(t) and those from global fitting of TDF (refer to Table 5-3). Whatever, ideally, there should be no singnificant difference in these decay times. Therefore, there is a doubt about the real time-dependency of C(t) which is the objective of the next section.

5.7.4 Spectral shape dependency of $C(\upsilon_m, t)$

From the definition of C(t) which monitors the frequency shift at emission maximum, the nonexponential time-dependent $C(\upsilon_m, t)$ can be derived under the irreversible multi-state kinetics (Section 5.4). To simplify the derivation of $C(\upsilon_m, t)$, the gaussian shape distribution with *constant band width* was assigned to each SAS ($\alpha_j(\upsilon)$, j=A..Z)), therefore, the nonexponential time-dependent $C(\upsilon_m, t)$ can be expressed by the eqs. (42) and (49) as below:
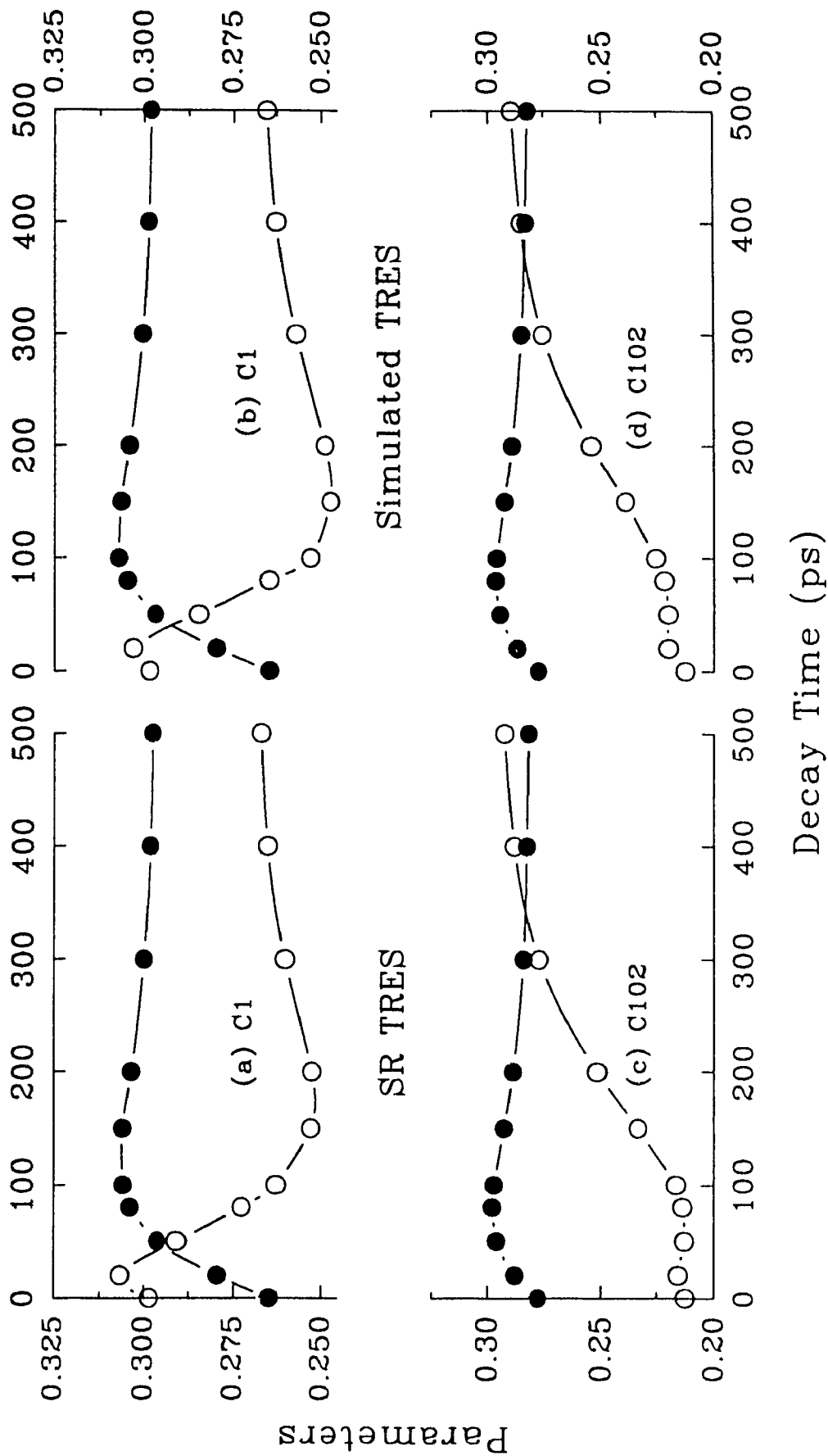
Fig. 5-11　The FWHM (Γ) of eq. (3) (●); and asymmetric parameters (b) (O) of SR TRES of (a) C1 and (c) C102; and of simulated TRES of (b) C1 and (d) C102, in 1-butanol.
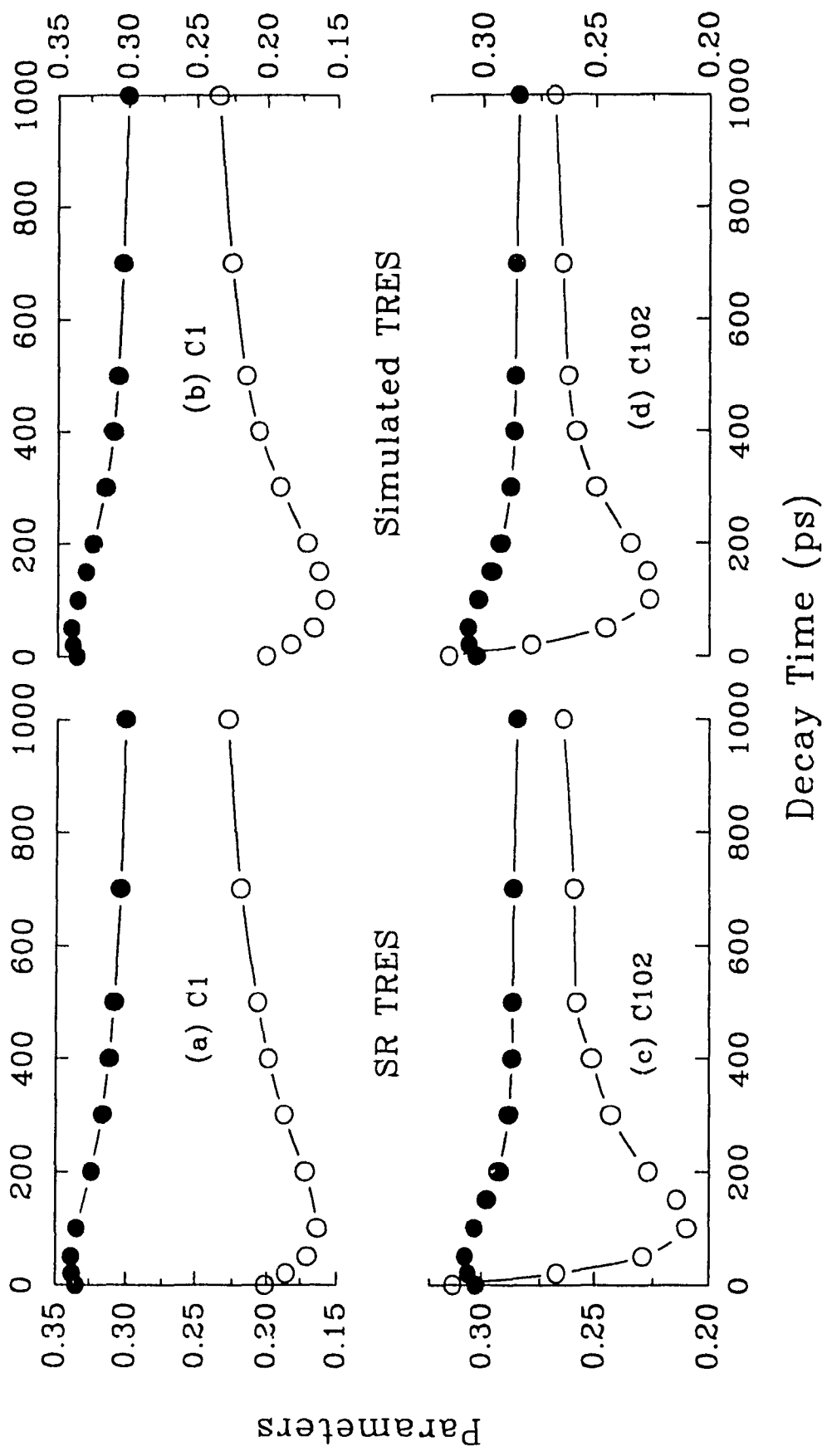
Fig. 5-12 The FWHM (Γ) of eq. (3) (●); and asymmetric parameters (b) (O) of SR TRES of (*a*) C1 and (*c*) C102; and of simulated TRES of (*b*) C1 and (*d*) C102, in 1-octanol.

157

$$C(\upsilon_m, t) = \frac{\alpha_A(\upsilon_m) \, e^{-t/\tau_1}}{i(\upsilon_m, t)} \qquad \text{(Two-State)} \quad (59)$$

$$\left\{ \begin{array}{l} C(\upsilon_m, t) = \dfrac{[\alpha_A(\upsilon_m) - \rho\alpha_B(\upsilon_m)] e^{-t/\tau_1} + \rho\alpha_B(\upsilon_m) e^{-t/\tau_2}}{i(\upsilon_m, t)} \\[4mm] \rho = \dfrac{\upsilon_m^B - \upsilon_m^C}{(\upsilon_m^A - \upsilon_m^C)(1 - \tau_1/\tau_2)} \end{array} \right. \qquad \text{(Three-State)(60)}$$

where υ_m^A, υ_m^B, and υ_m^C are the frequencies at maximum emission of species A*

and B*, and C*, respectively. $i(\upsilon_m, t)$ is the fluorescence maximum at an instant

time.

In the limiting case of b=0, the log-normal function of eq. (3) turns to be a

gaussian function. Therefore, it is acceptable to use the above equations (eq.

(59) and eq. (60)) to monitor the frequency shifts of TRES at maxima at short

times. In this study, these spectral shape dependent functions have been

applied to test the irreversible multi-state model. In order to find the optimum

decay times from C(t) data, the following values have been applied into the

functio.? $C(\upsilon_m, t)$ (eq. (59) or eq. (60)): (i) the spectral shape paremeters of the

species associated spectra (SAS) $\alpha_j(\upsilon)$, j=A..Z; (ii) the frequency at maximum

fluorescence (υ_m) and the amplitude of TRES $i(\upsilon_m, t)$ at maximum obtained from

the log-normal fits of the SR or the sumulated TRES; (iii) the amplitude of SAS

at υ_m ($\alpha_j(\upsilon)=\alpha_j(\upsilon_m)$), j=A..Z); and (iv) the decay times (τ_i, i=1..n) obtained from

the global fit of TDF. Fig. 5-13 shows the fit of C(t) data to function $C(\upsilon_m, t)$. The

results listed in Table 5-3, appear to be closer to the results from the global fit of

the time-dependent fluorescence decay (TDF) than those from the exponential fit

of C(t). Ideally, the decay times from this optimization should be the same as the

results from the global fit of the TDF. The origin of this difference can be
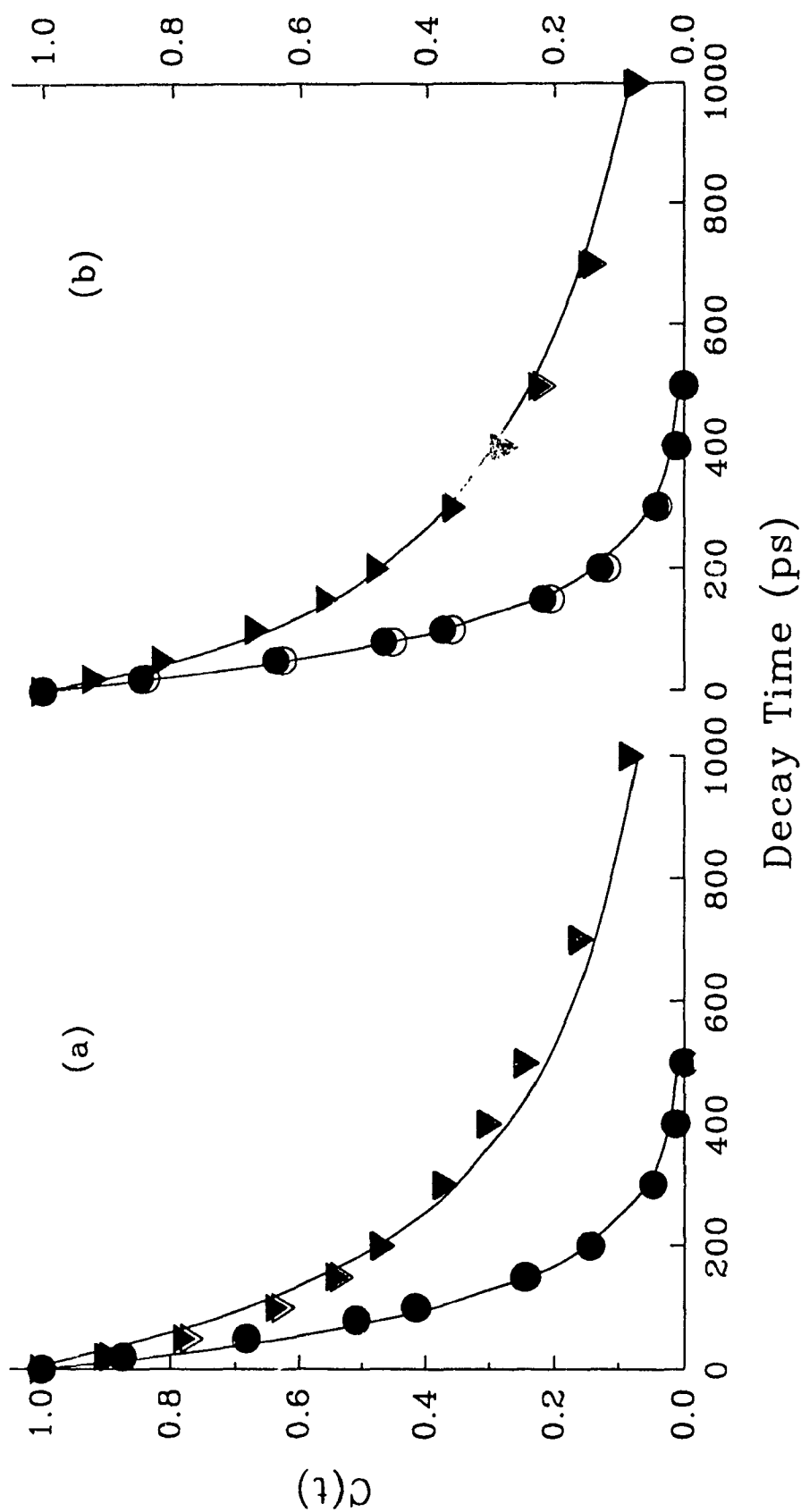
Fig. 5-13   C(t) data of (a) C1, and (b) C102 in 1-butanol from (●): SR TRES, (○): simulated TRES; or in 1-octanol from (▼): SR TRES, (▽): simulated TRES; are fitted by solid curves using C(υ_m,t) of eq. (59) or eq. (60).

explained by considering the factor resulting from the simplification made in deriving these spectral shape dependency $C(\upsilon_m, t)$.

The difference in decay times from the optimization of $C(t)$ using the spectral shape dependent $C(\upsilon_m, t)$ and multi-exponential fit of $C(t)$ is due to: (i) the simplification of the fraction of the preexponential factor as express by eq. (61), which has been set as a constant in the multi-exponential fit of $C(t)$, but not in the case of $C(\upsilon_m, t)$; (ii) in 1-octanol, no significant difference in the shape of $C(t)$ using either single or double exponential function. As a result, it introduces large uncertainty and difference in the decay times by comparing to those from the global fit of TDF. In Table 5-4, the values of FWHM of each SAS are variable within a moderate region (~15%). The variation of FWHM does not show significant effect on the decay times from $C(t)$, but does show the effect in 1-octanol, in which the $C(t)$ data are no longer following the exponential function.

From the expression of $C(\upsilon_m, t)$ of eq. (60), the fraction of the preexponential contribution can be described by:

$$\begin{cases} f_1 = \dfrac{\alpha_A(\upsilon_m) - \rho\alpha_B(\upsilon_m)}{i(\upsilon_m, t)} \\ f_2 = \dfrac{\rho\alpha_B(\upsilon_m)}{i(\upsilon_m, t)} \end{cases} \tag{61}$$

where constant ρ is the same as defined in eq. (60). These two fractions (f_i, i=1,2) of two dyes in 1-octanol are illustrated in Fig. 5-14. The average values of f_i, i=1,2 from 0 to 100 ps ($\bar{f_1}$=0.45±0.08, $\bar{f_2}$=0.59±0.08 for C1 and $\bar{f_1}$=0.28±0.09, $\bar{f_2}$=0.70±0.07 for C102) due to the weight of contribution are close to the preexponential constants of bi-exponential functions as listed in parentheses of Table 5-3.
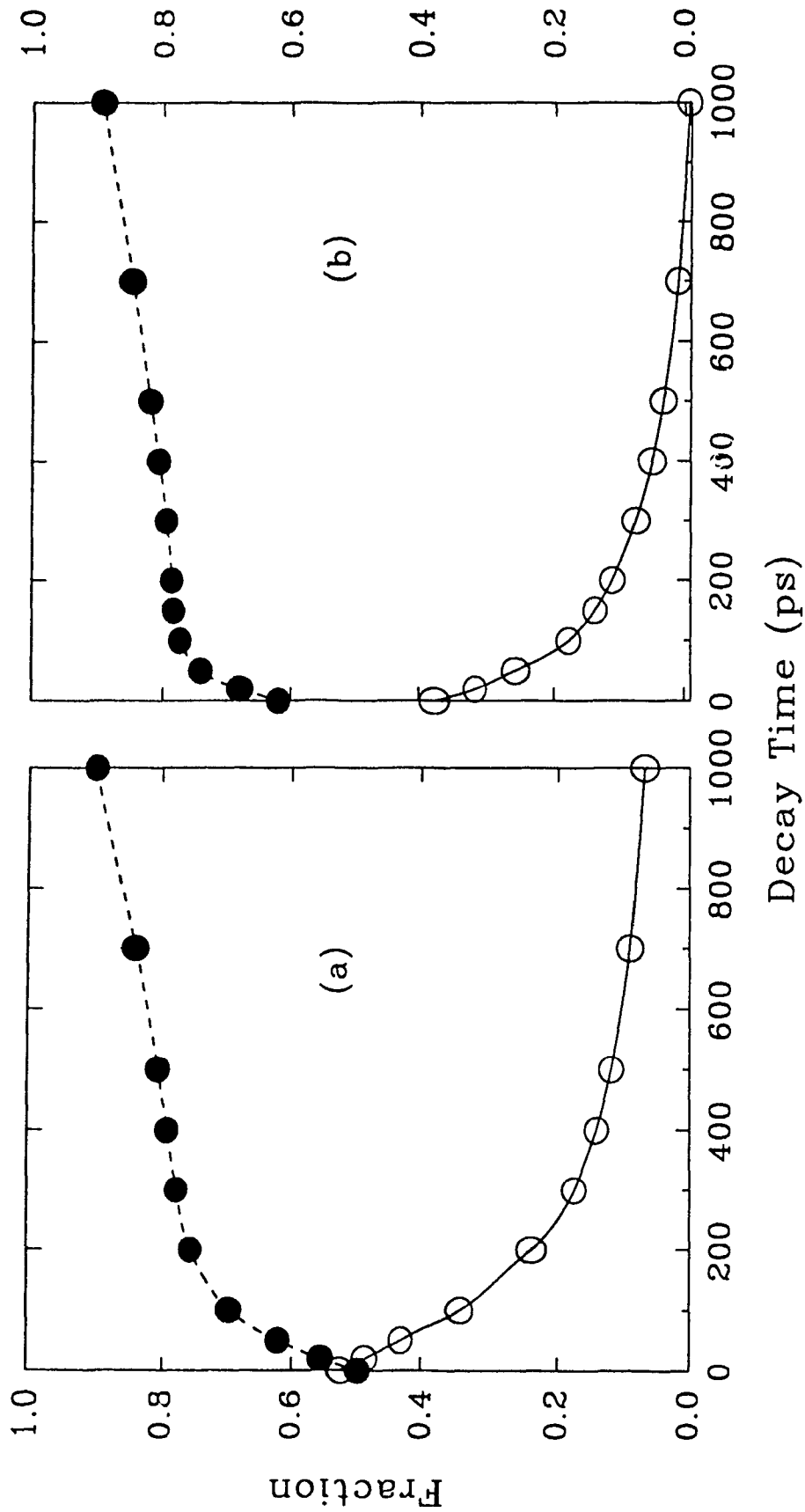
Fig. 5-14 Preexponential fraction f_1 (O) and f_2 (●) of SR TRES (a) C1 and (b) C102 in 1-octanol, are calculated using eq. (61)
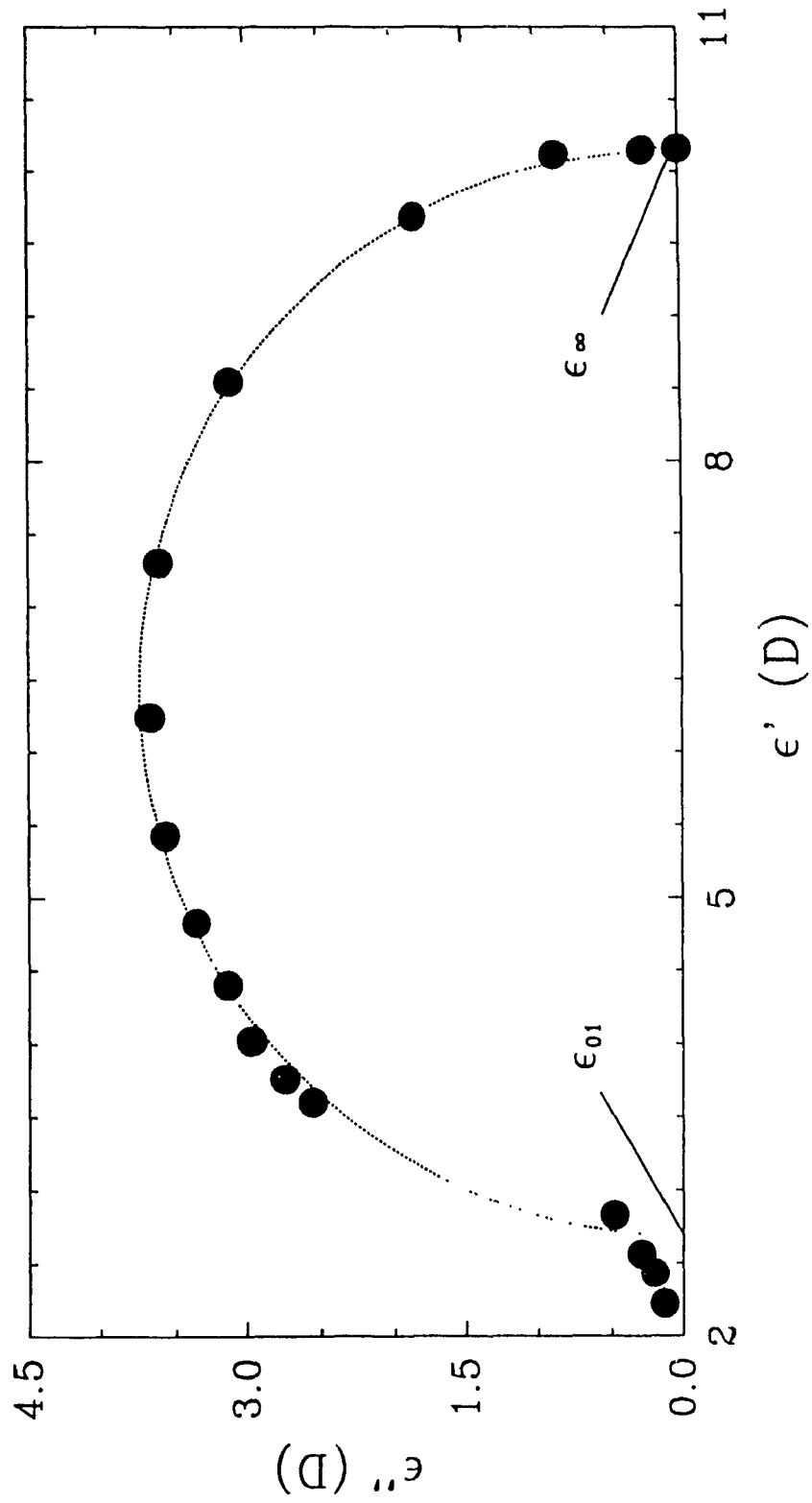
Fig. 5-15   Arc plot of dispersive dielectric constant ε'' vs dielectric constant ε' of 1-octanol from Ref. 27 (O), the high- and low-frequency dielectric constant (ε_∞=10.17 D, ε_{01}=2.69 D) are obtained from the best Arc fit expressed by the function $\varepsilon''^2 = 14.0 - (\varepsilon'-6.43)^2$ (broken curve).

5.8   Conclusion

5.8.1   Further studies

The absence of a short-lived component in the fluorescence decay of C102 in water is consistent with a subpicosecond[68] solvation time component which could not be detected with the time resolution of these measurements. Further experiments to obtain more definitive data on these subpicosecond components have to be done in near future.

The *overdamped* behaviour defined as the slower decay of C′t) at very earlier time from 0 to 0.1 ps , and fast in later time region from 0.1 to 1.0 ps in acetonitrile[65] were predicted from the simulation studies[65,191] and were observed experimentally.[192] The mechanism of this behaviour was explained by the heterogeneity of the inertial relaxation process of the solvent.[65,191,193] But, from the kinetic point of view, for the multi-state system, the *overdamped* behaviour of C(t) can also be found for the system with large difference in energy betwe 1 initial and final excited state in comparison to FWHM of their spectra. It would be interesting to measure the TRES of C102 in acetonitrile in the subpicosecond region to investigate the fast solvation dynamics. Alternatively, the possible difference from that of C1 in the same solvent could offer some information about the fast conversion of TICT state as discussed in Scheme 3-1b.

5.8.2   Conclusion

The DAS emission measurements have enabled us to clearly demonstrate that a two-state kinetic model related to the solvation process applies to the alcohol solvents but not dichloromethane (or isooctane as

expected). n-Butyl acetate may be a borderline case. In this solvent, negative preexponentials were observed, but, the lifetime was not wavelength-dependent as required by the two-state model. The results from 1-octanol solutions have revealed an additional kinetic process not previously noted in the fluorescence decay of photophysical probe molecules and indicates that DAS measurements are capable of uncovering subtle differences in the solvation process. The fluorescence decay of C1 in water displayed a less than 0.5 ps component which may be associated with rotation of the diethylamino group.

For the fast solvation processes of the two 7-aminocoumarin dyes (C1, C102) in 1-butanol and 1-octanol, a kinetic correlation among the individual excited solvation states has been observed from the negative DAS. The decay times of different states were obtained from C(t) data of SR TRES and simulated TRES by the *irrversible multi-state model*. The result from the optimization of C(t) using the function $C(v_m, t)$ appears to be more precise than those of exponential fitting with uncertanty. This can be understood by the *irreversible multi-state model*. The same time-dependency (*not the unique change for a single continuum shift state*) of the spectral shape parameters (FWHM, and asymmetry) from the log-normal fit of both SR TRES and simulated TRES according to the *irreversible multi-state model* does give strong evidence for the existence of a kinetic correlation among different states instead of a single excited state undergoing a continuum solvation process.

Chapter 6: PICOSECOND EXCITED STATE CHARACTERISTICS of NITROBENZENE DERIVATIVES in SOLUTION

6.1 Introduction

Interest in the photochemistry of nitrobenzene derivatives has grown considerably for more than three decades.[104] Nitrobenzene and substituted nitrobenzenes display a remarkably wide variety of photochemical reactions.[105] These include intermolecular[194] and intramolecular benzylic,[153] and homobenzylic[104] hydrogen abstraction, photoaddition to olefines,[195] photoredox,[196] heterolytic photocleavage of the benzylic C-C bond[197,198] in aqueous solutions, and photosubstitution.[199]

The photophysical properties of the nitro compounds have been extensively studied[106] not only for photochemical reactivities and fundamental understanding of photophysics,[14] but also owing to the recently widespread interest in the nonlinear optical (NLO) characters[107] for potential applications in optical storage and information processing.[108] Among the nitro compounds, nitrobenzene derivatives are well known to be nonfluorescent and strong in excited state absorption (ESA), due to the fast singlet-triplet intersystem crossing.[143,154] Between the 1950's and the 1960's, Nagakura's group ascribed the red-shifted electronic absorption band of nitrobenzene to an intramolecular charger transfer (ICT) transition.[142] This ICT transition involves an electron transfer from the benzene ring (Donor) to the nitro group (Acceptor),[142c] and is affected by subsitutents on the nitrobenzene ring.[144] Since the effect of substituent on the energy of the charge transfer state is

proportional to that of the ionization potential (IP) of donor,[14] the lower IP is, the more significant CT character could be appearing on both ground and excited state absorption spectra. For nitromesitylene[142] and 4-nitro-4'-methoxystilbene,[145] the *solvent polarity effect* (i.e., dipole-dipole interaction) on ground[142] and excited state absorption spectra[145] were reported. Experimentally, we find a similar effect of solvent polarity on ESA spectra of two dimethoxynitrobenzenes. With increased solvent polarity. we find the *blue-shift* of the '*red*' ESA band of these compounds in nanosecond time region, which is similar to that of 4-nitro-4'-methoxystilbene.[145] In spite of this quasi-static ICT behaviour, in subnanosecond time region, we also find a remarkably dynamic *blue-shift* of the '*red*' ESA band of these dimethoxynitrobenzenes in alcohols. Such time-dependent *blue-shift* can be quantified by plotting the function C(t) which represents the fractional shift in frequency of ESA peak against time. We find that decay time from an exponential fit of C(t) shows solvent (polarity and viscosity) dependency rather than a dependence on the structure of the probe molecule. The decay time of C(t) is comparable to the longitudinal relaxation time τ_L of the solvent.[190] To my knowledge, this is the first observation of dynamic solvation linked ESA spectra. Alternatively, this study implies that a novel spectroscopic method has been found to study solvation dynamics.

The ICT characteristic triplet ESA spectra were also reported in *p*-nitroaniline at low temperature, in which the *red-shift* of one triplet ESA band of different substituted anilines was interpreted as an ICT between donor and acceptor.[148] In this study, we find that (i) this interpretation was based on an inadequate comparison of the triplet ESA spectra between *p*-nitroaniline and aniline derivatives (except nitro substituted anilines); (ii) the fine structure on the

'*blue*' band is more likely due to vibronic interaction of locally excited benzene ring, rather than the symmetric stretching of locally excited nitro group.

In infrared absorption study of alkylnitrobenzenes, the intensity, or the band position of the symmetric and asymmetric stretching[201] of the nitro group (Scheme 6-1) varied with the type and the position of substituents on the nitrobenzene ring,[106] and the dipole moment of the molecule.[106,202] Generally, for alkylnitrobenzenes, the oscillator strength (f) for the asymmetric stretching of NO_2 is larger than that for the symmetric band (i.e., for nitrobenzene, $f_{as}=2.72 \times 10^4$ and $f_s=1.86 \times 10^4$ $1/(M\ cm^2)$).[203] The variation in the ratio of the oscillator strength ($R=f_s/f_{as}$) for the symmetric (f_s) and the asymmetric (f_{as}) stretching bands of NO_2 with the position of alkyl substituent attaching on the nitrobenzene ring is in the order:[204]
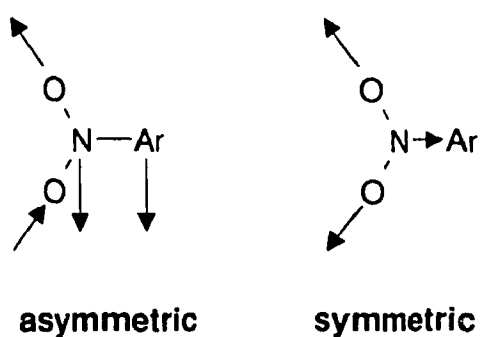
asymmetric   **symmetric**

Scheme 6-1

$$R(para\text{-}) > R(meta\text{-}) > R(ortho\text{-}) > R(2,6\text{-})$$

This trend reflects the symmetry of the vibronic mode including the factor of twsting of nitro group. Within the framework of the Herzberg-Teller model under certain approximation, the ground state vibrational frequencies can be applied to study the excited state vibronic interaction. The validity of this application was verified in study of the phosphorescence spectrum of benzene which is particularly rich in vibronic structure,[147] In this chapter, we have studied the ESA spectra of alkylnitrobenzenes with two transient absorption bands at long and short wavelengths. By considering the following factors: (i) position of the substituent on the nitrobenzene ring; (ii) solvent polarity, we find the effect on

the intensity of these two ESA bands. The vibronic coupling between excited triplet states in characteristics of locally excited benzene ring[146a] is manifested as fine structure on '*blue*' band (~430 nm) for the most alkylnitrobenzenes. This observation is similar to the low temperature triplet ESA spectra of *p*-nitroaniline[148] and aniline.[149] The frequency spacing of the structured '*blue*' band is comparable to the vibrational frequency of the CH bending, or stretching of the benzene ring (~1174, 1550 cm^{-1}).[146] In contrast to this structured '*blue*' band, the structured '*red*' band (~610 nm) which was not found in aniline,[149] can be assigning to the locally excited NO_2 group. The frequency spacing of the structured '*red*' band is the same as the vibrational frequency of the asymmetric stretching of NO_2 group (~1540 cm^{-1}).[205] The intensity ratio of '*blue*' and '*red*' ESA bands depends on the twist of the NO_2 group from the plane of the benzene ring.

To monitor the photochemical process, we studied the ESA of the *o*-nitrobenzyl (ONB) system. The general photoreactivity of ONB with intramolecular hydrogen abstraction has stimulated considerable interests in the exploitation of this reaction in the development of photochromic compounds,[152] photolabile protecting groups,[206] and phtotresists.[207] The photorearrangment reaction (Scheme 6-2) can be proceed from the short-lived photo excited singlet state S_1^* ($\tau < 10$ ps)[45,208] to an *o*-quinonoid intermediate *o*-Q, or from the *n*-π^* excited triplet state[209] T_1^* to biradical (BR), which has been postulated[210] as an intermediate in the formation of *o*-Q. The BR can also give the cyclization product (CP) directly as has been observed in the case of geometrical constrained *o*-nitrobenzyl system.[153] Thus, detection of the biradical, a key intermediate in the triplet pathway for the rearrangement, would provide an

important way in which the mechanism could be delineated since the triplet excited state may or may not lead to reaction product.[45,212]

Scheme 6-2
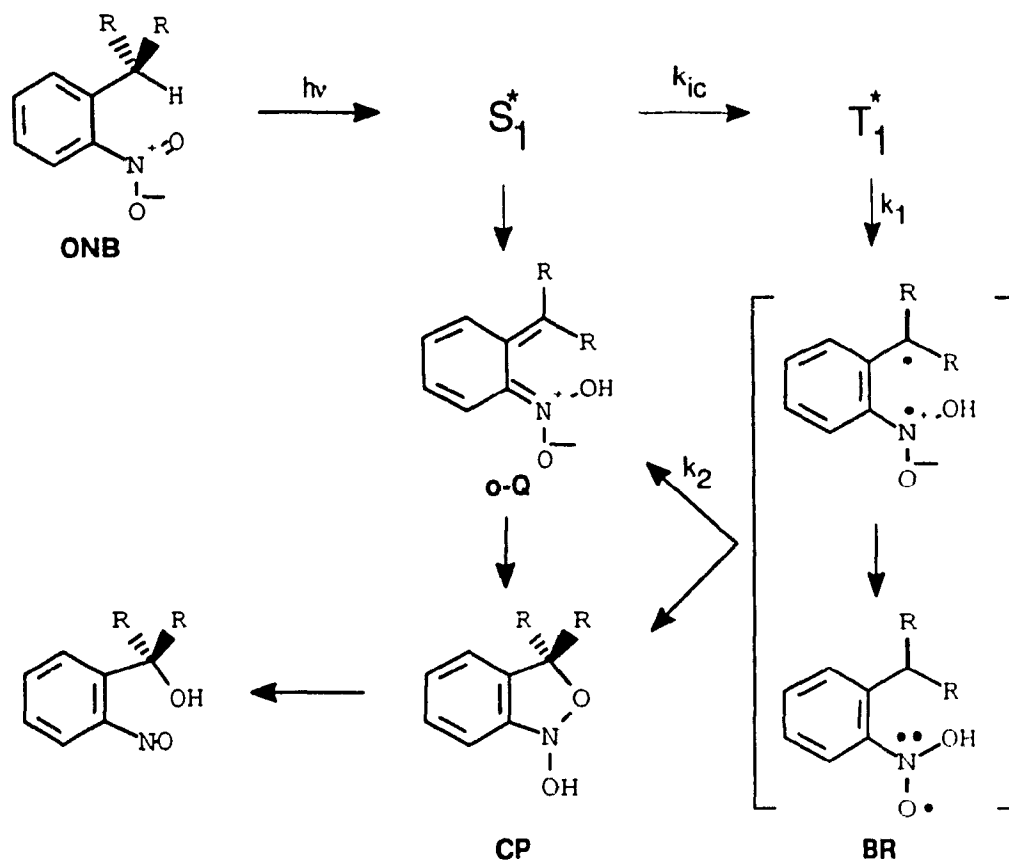
In the previous studies of these alkylnitrobenzenes in our laboratories, the ESA spectra were assigned to the triplet state by quenching with addition of 5-methyl-5-(hydroxymethyl)-1,3-cyclohexadiene (CHD, **12** in Fig. 6-1).[47,154,209-211] In this chapter, the studies on the nitrobenzene derivatives (structures shown on Fig. 6-1) are presented in the following three categories.

(1) For dimethoxynitrobenzenes (**1, 2** in Fig. 6-1), with increased solvent polarity, the *blue-shift* of the '*red*' ESA band shows a significant ICT character. The decay time of the exponential fit of C(t) of DMONB in alcohol is comparable to the longitudinal relaxation time of the solvent, and is consistent with our
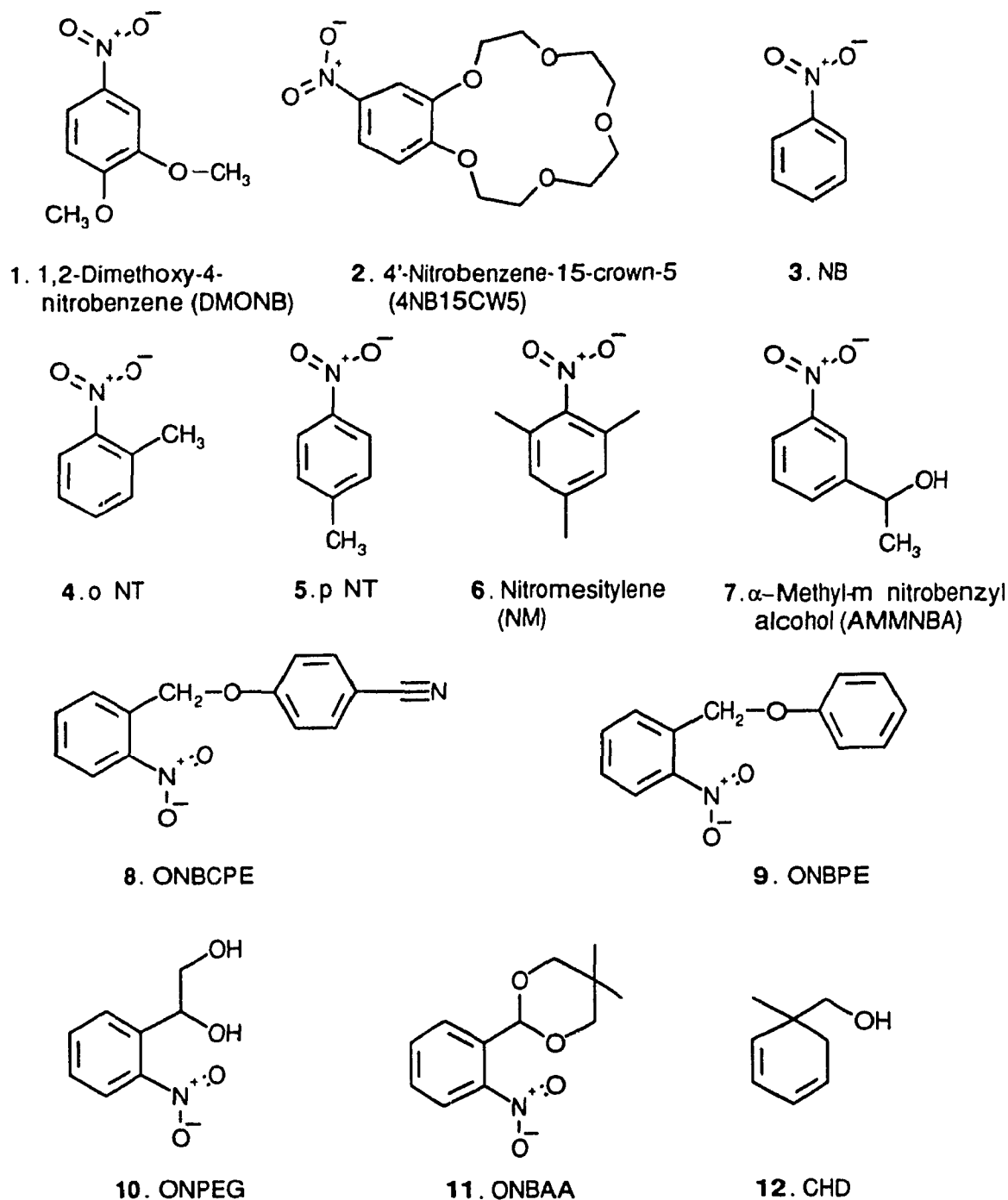
Fig. 6-1   Molecular Structures of Nitrobenzene Derivatives and CHD

solvation dynamic studies using TDF technique.[74,75] To my knowledge, this is

the first observation of dynamic solvation linked ESA spectra. This solvent-

dependent ESA shift implies an alternative method to study solvation dynamics

that does not require some of the constraints imposed on fluorescence probes and might provide additional insight on unexpected relaxation processes observed by other methods (chapter 5).

(2)   For alkylnitrobenzenes (**3 - 7** in Fig. 6-1), the structure and solvent effects on ESA spectra are observed, in which the structured '*blue*' and '*red*' bands correspond to vibrational modes of the benzene ring and asymmetric stretching of NO_2; the relative intensities and the structures of the two ESA bands depend upon the conformation of the **C-N** bond of the substituted nitrobenzenes, such as in nitromesitylene (**6** in Fig. 6-1).[200]

(3)   For *o*-nitrobenzyl derivatives, ONB (**8 - 11** in Fig. 6-1), the identification of the biradical absorption band at 460 nm is done by resolving a series of ESA spectra of ONB into their component bands. The ESA spectra are recorded from about 50 ps to 10 ns. From the kinetics of the component bands corresponding to the triplet excited state, the BR, and the *o*-quinonoid intermediate, the relative contributions of the singlet and triplet excited-state pathways in the formation of the *o*-quinonoid intermediate, are able to established.[154]

6.2   **Experimental Section**

6.2.1   Chemicals

6.2.1.1   Dimethoxynitrobenzenes

1,2-Dimethoxy-4-nitrobenzene (DMONB) (**1** in Fig. 6-1) of Aldrich, was recrystallized from methanol. The recrystallization procedure is similar to the procedure described in section 2.2.4. 4'-nitrobenzene-15-crown-5 (4NB15CW5) (**2** in Fig. 6-1) of Aldrich was used as received.

6.2.1.2 Alkylnitrobenzenes

Nitrobenzene, o-, and p-nitrotoluenes (3 · 5 in Fig. 6-1) provided by Professors D. Gravel and R. Giasson (Université de Montréal), 2,4,6-trimethyl nitrobenzene (nitromesitylene) (6 in Fig. 6-1) of Aldrich, α-methyl-m-nitrobenzyl alcohol (AMMNBA) (7 in Fig. 6-1) provided by Professor Yates (University of Toronto), were used without further treatment.

6.2.1.3 o-Nitrobenzyl derivatives

o-Nitrobenzyl-p-cyanophenyl ether (ONBCPE) (8 in Fig. 6-1), o-nitrobenzyl-p-phenyl ether (ONBPE) (9 in Fig. 6-1), o-nitrophenylethylene glycol (ONPEG) (10 in Fig. 6-1), and o-nitrobenzaldehyde acetal (ONBAA) (11 in Fig. 6-1) provided by Professors D. Gravel and R. Giasson (Université de Montréal), were used without further treatment.

6.2.1.4 Solvents

Cyclohexane (BDH distilled), tetrahydrofuran (THF) (Aldrich, Gold label), 2-propanol (Fisher, certified A.C.S.), tert-butyl alcohol (Fisher, certified A.C.S.), 1-butanol (Fisher, certified A.C.S.), methanol (Accusolo, distilled), poly(ethylene glycol) (PEG, M.W.: 200) (Aldrich), Poly(ethylene glycol) (PEG, M.W.: 600) (Aldrich), and deionized water (NANO Pure), were used without further treatment. 1-Octanol (BDH reagent) was distilled under reduced pressure. n-Butyl acetate (nBuOAc) (Fisher reagent), and acetonitrile (Caledon, distilled), were refluxed over CaH_2 for 1 h and distilled. The triplet quencher 5-methyl-5-(hydroxymethyl)-1,3-cyclohexadiene (CHD) (12 in Fig. 6-1) was provided by Professors D. Gravel and R.Giasson (Université de Montréal).

6.2.2 Measurements

The ESA spectra of the above species in different solvents were done using the picosecond transient absorption spectroscopic technique, as mentioned in Chapter 3. Briefly, the third harmonic Nd: YAG laser pulses at 355 nm of 30-40 ps duration were used for the excitation and continuum pulses with a useful window between 390 and 730 nm for probing the transient absorption from 0 ps to 10 ns with pumping energy between 1.9 -2.7 mJ. The optical densities of all samples at 355 nm in 2 mm cell were between 0.3 - 1.0. There are three calibrated spectral regions being used for most measurements as listed in Table 3-2. In order to keep the number of photon on the optimum level for the detector (5000 - 10000), various neutral density filters, a special filter (0.8 mm Corning 7-51 + 1 mm Schott BG24), and a short-wavelength sharp cut-off filter (Schott, KV-380, or KV-400), were chosen and put in front of the monochromator to protect the detector from uv light and overflow of photons. The role of the special filter is to balance the spectral distribution of the contiuum light pulse. The control program automatically rejected signals less than 1000 counts. The spectra were treated on a PDP-11 computer and transferred to IBM data format which can be read using the program CRVFIT written in our laboratories.

6.2.3 Deconvolution of ESA

The absorption spectra were fitted to absorption bands described by Cauchy-Gauss product functions of the type

$$F(x - x_o) = A \frac{e^{-C^2(x-x_o)^2}}{1 + B^2(x - x_o)^2} \tag{1}$$

where x is the wavelength of the band in nm; x_0 is the wavelength of the peak of the band in nm; B is the Cauchy factor; C is the Gauss factor; and A is the band amplitude, by using the program (CRVFIT) developed on the basis of Pitha and Jones' work[212] which employed the Marquardt optimization method. In order to eliminate the fluctuation on the two edges of spectra, the spectral deconvolutions were done in the restricted spectral region excluding the initial and final channels. But, the spectral region should be kept the same for each series spectra. The average pumping energy of each set of spectra with the same decay time, was used to divide the spectral area of each component from the deconvolution. The spectral area per pumping energy was applied in the quantitative analysis in kinetics.

6.2.4　　　Time-dependent fraction in frequency at absorption maxima C(t)

The shifts of ESA bands fitted by Cauchy-Gauss function were calculated using the time-dependent fraction of the frequency at absorption maxima C(t)

$$C(t) = \frac{\upsilon_m(t) - \upsilon_m(\infty)}{\upsilon_m(0) - \upsilon_m(\infty)} \tag{2}$$

where $\upsilon_m(0)$, $\upsilon_m(t)$, and $\upsilon_m(\infty)$ are the zero-, instantaneous, and infinite time frequencies at absorption maxima. The expression of C(t) is similar to the function discussed in the previous chapter (Chapter 5).

6.3　　Triplet ESA of 1,2-Dimethoxy-4-nitrobenzene and 4'-Nitrobenzene-15-crown-5: New Method for Study Solvation Dynamics

By introducing methoxy group onto the nitrobenzene ring, both ionization potential of the benzene ring (the electron-donor chromophore) and the charge transfer energy should be depressed. Therefore, such effect could be reflected

in the ESA spectra, such as the excited state ICT interaction. Indeed, we observe significant ICT phenomena on the ESA spectra of two dimethoxynitrobenzenes. (i) Only in cyclohexane, we find a decay of both ESA bands. (ii) Both ESA bands can be assigned to triplet ESA by quenching with addition of 5-methyl-5(hydroxymethyl)-1,3-cyclodiene (CHD, **12** in Fig. 6-1). (iii) The *blue-shift* of the *'red'* ESA band shows the solvent polarity dependency rather than the dependence on the probe molecule. (iv) In alcohols, a dynamic *blue-shift* of the *'red'* ESA band is observed. The rate constant of this dynamic *blue-shift* of the *'red'* band depends on the solvent polarity and viscosity. (v) For 4NB15CW5, the salt effect on ESA spectra is observed and shows a selectivity to the presence of metal ions.

6.3.1 The lower excited CT state

6.3.1.1 4NB15CW5, DMONB in cyclohexane

There are two transient absorption bands (~425, and ~510 nm) in the ESA spectra of both 4NB15CW5 and DMONB in cyclohexane as illustrated in Fig. 6-2, and Fig. 6-3. The decay rate constant of the *'blue'* band is $(0.21\pm0.03)\times10^9$ s^{-1} for DMONB, and $(0.42\pm0.10)\times10^9$ s^{-1} for 4NB15CW5, respectively. These decay rate constants are comparable to those of the *'red'* band of $(0.28\pm0.02)\times10^9$ s^{-1} for DMONB, and $(0.42\pm0.09)\times10^9$ s^{-1} for 4NB15CW5, respectively. The comparable decay rate constants of these two bands indicate that both bands originate from the same kinetic state. The decay of both ESA bands are associated with the probe compound.
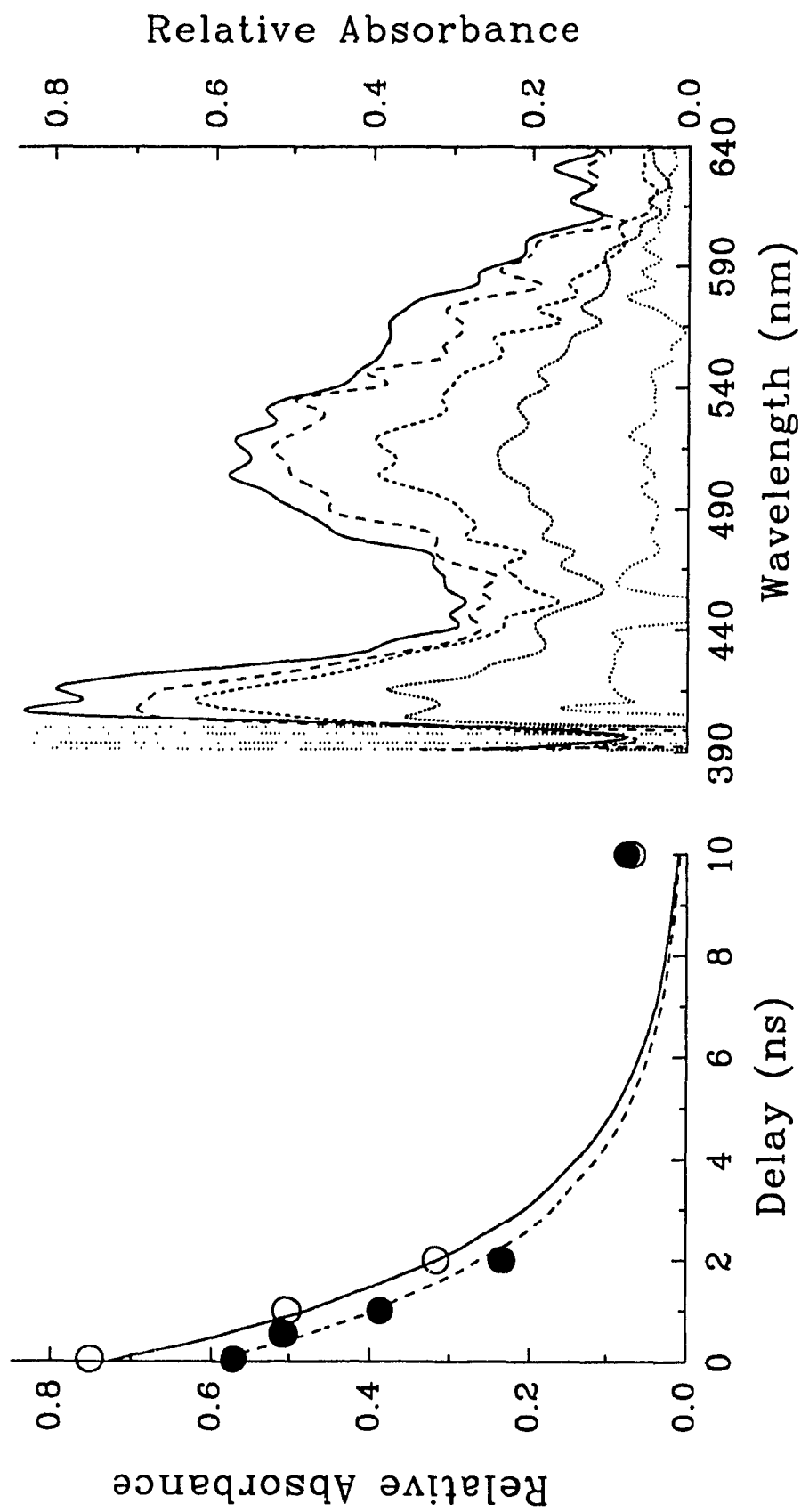
Fig. 6-2 Right frame: ESA spectra of 4NB15CW5 in cyclohexane at 50, 550 ps, 1, 2 ns, and 10 ns (from top to bottom). Left frame: the decay of two transient absorption bands at ~414 nm (O) and ~515 nm (●) with the same decay rate constant of $(0.42\pm0.10) \times 10^9$ s^{-1}
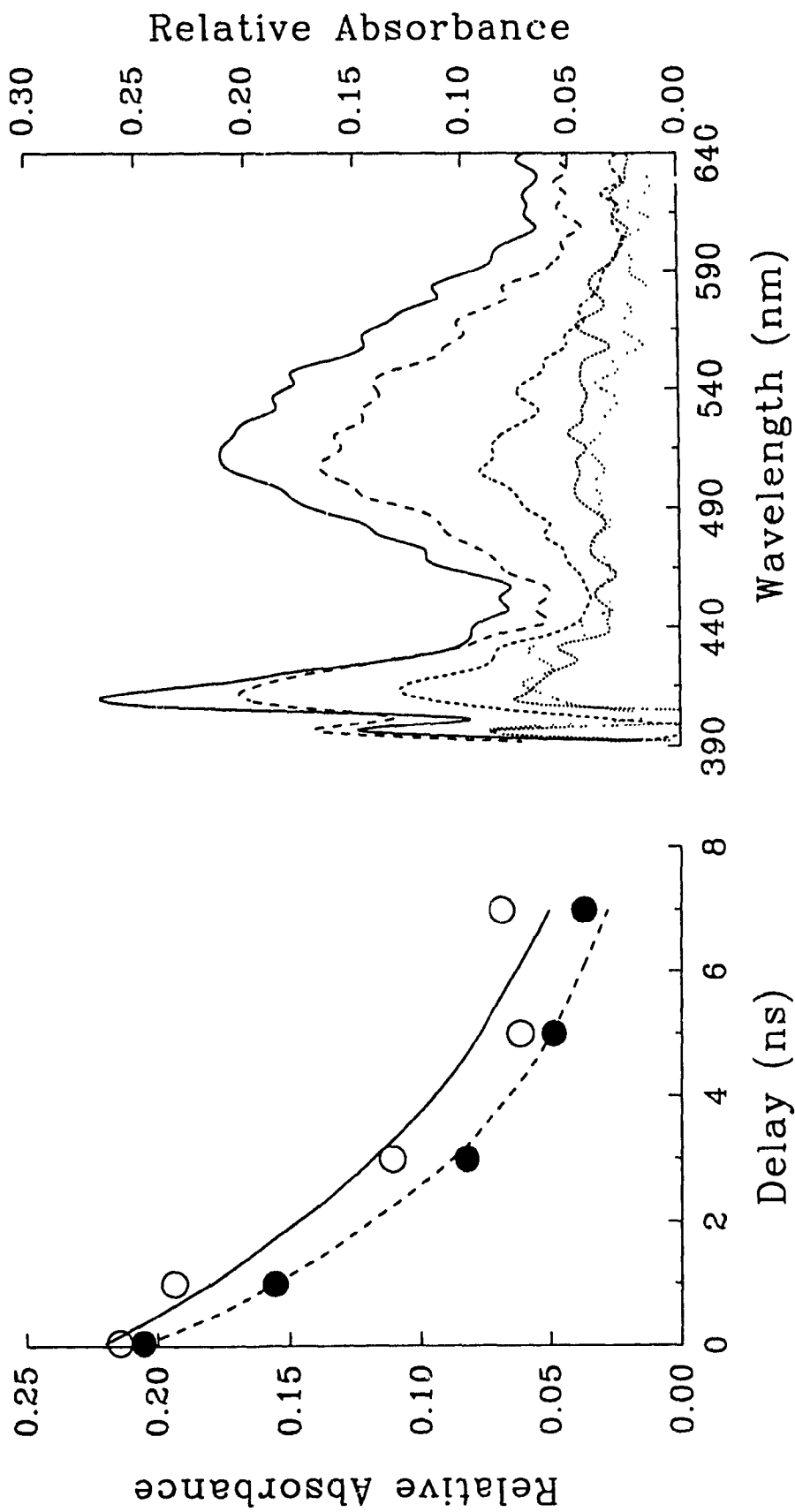
Fig. 6-3   Right frame: ESA spectra of DMONB in cyclohexane at 50 ps, 1, 3, 5, and 10 ns (from top to bottom). Left frame: decay of two transient absorption bands with decay rate constant of (0.21±0.03) x10⁹ s⁻¹ at ~414 nm (O) and (0.28±0.02) x10⁹ s⁻¹at ~521 nm (●), respectively.

6.3.1.2   4NB15CW5, DMONB in acetonitrile

In acetonitrile, the ESA spectra of both compounds are significantly different from those in cyclohexane. There is the *blue-shift* of the transient absorption band at long wavelengths (~480 nm) whose intensity does not change from 30 ps to 10 ns as the *'blue'* band at ~ 430 nm (see Fig. 6-4). By adding 3.7 M of triplet state quencher, CHD, to the 4NB15CW5/acetonitrile solution, both ESA bands start to decay with decay rate constants of $(2.3\pm0.8)\times10^9$ s^{-1} (~430 nm) and $(1.6\pm0.5)\times10^9$ s^{-1} (~480 nm), respectively. This quenching behavior indicates that the two ESA bands originate from a common lower excited triplet state.

Additionally, the ESA spectrum of DMONB (ground state optical density: OD~0.7 in 2 mm cell at 355 nm) in acetonitrile was not observable due to the intense Raman Scattering, which grossly distorted the spectrum.

6.3.2   Polarity-dependent ESA

In some moderately polar solvents, such as THF and n-butyl acetate, the *blue-shift* of the *'red'* band with no decay from 30 ps to 10 ns, is also observed in comparison with that in cyclohexane. With respect to the polarity of solvent, this band seems to shift further towards the blue region. In water, it shows an extreme case of merging of the *'red'* band into the *'blue'* band as shown in Fig. 6-5.

This solvent-dependent behaviour implies that this transient absorption band correlates to the solvated excited state. Such quasi-static solvent-dependent behaviour was also reported in 4-nitro-4'-methoxystilbene in microsecond time region.[145] On the basis of the Lippert-Mataga theories,[5,6b]
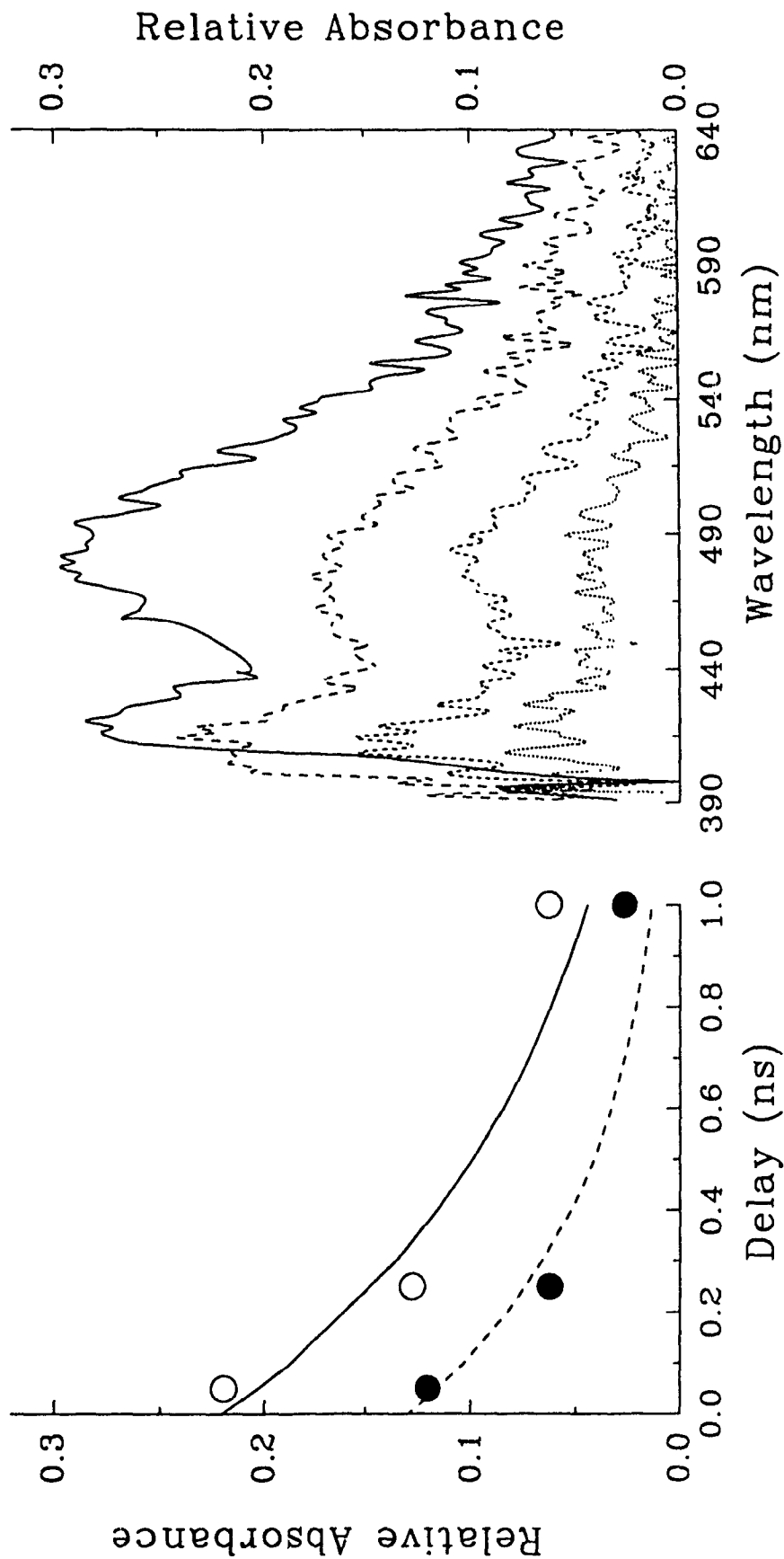
Fig. 6-4   Right frame: ESA spectra of 4NB15CW5 in acetonitrile: in absence of quencher at 50 ps (solid curve), in presence of 3.7 M quencher CHD at 50 ps (long dash), 250 ps (short dash), and 1 ns (dot).   Left frame: decay of two transient absorption bands with decay rate constant of (2.3 ± 0.8) $\times10^9$ s^{-1} at ~414 nm ($\bigcirc$) and (1.6 ± 0.5) $\times10^9$ s^{-1} at ~515 nm ($\bullet$), respectively.
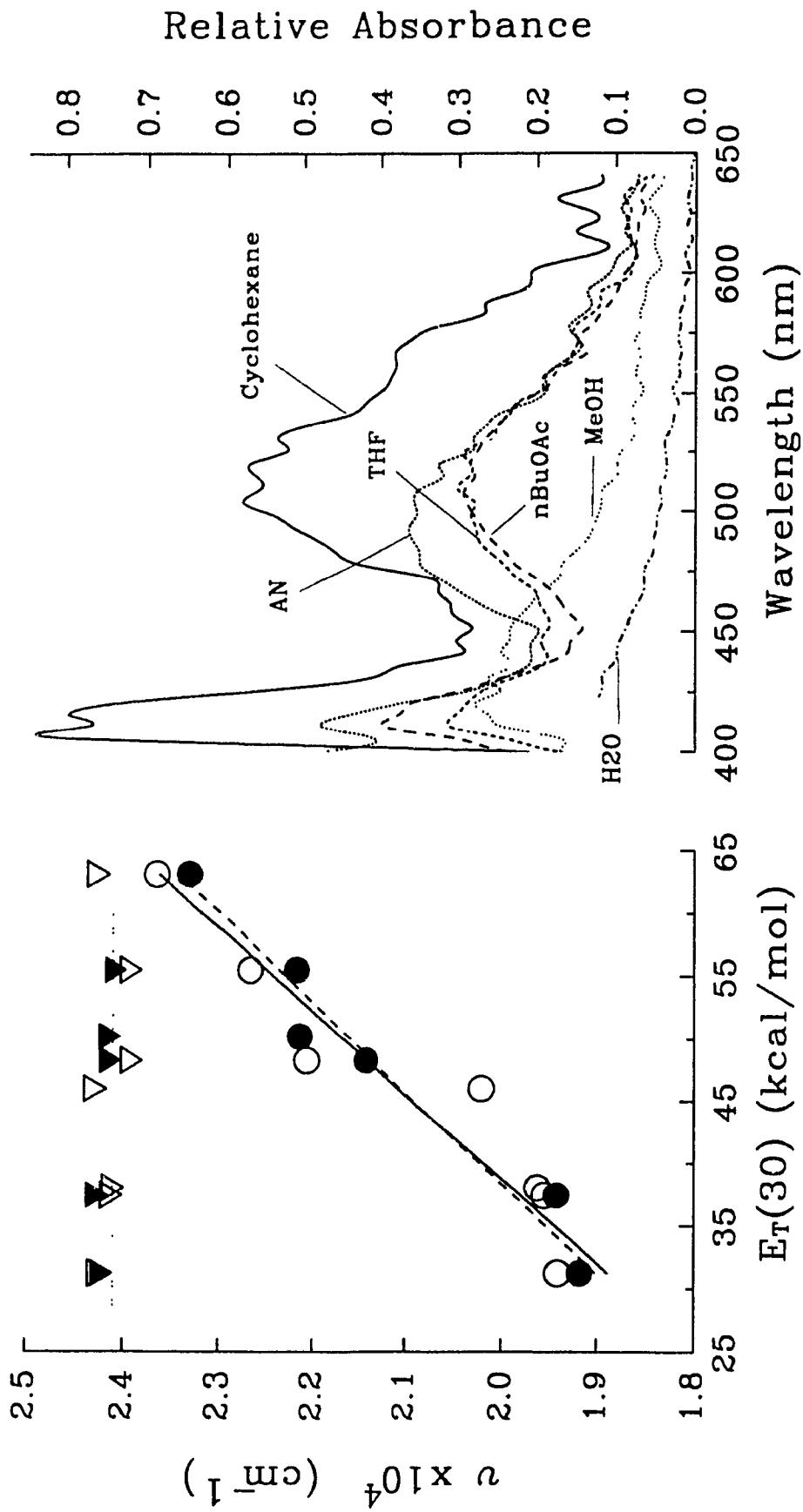
Fig. 6-5   Right frame: ESA spectra of 4NB15CW5 in cyclohexane (solid), THF (mediate dash), acetonitrile (short dash), methonal (dot), and water (dash-dot) at 50 ps.   Left frame: The blue shift of the 'red' band of 4NB15CW5 (O) and DMONB (●) and invariable 'blue' band of 4NB15CW5 (▽) and DMONB (▼) with respect to emipirical parameter $E_T(30)$ of solvent.

the empirical parameter $E_T(30)$[6a,185] of solvent is used to study the solvation related phenomena.[6b] Similar to the solvatochromic study, the plot (see Fig. 6-5) of the triplet ESA peak frequency vs. the empirical parameter $E_T(30)$ of solvent does show linear correspondence for both dimethoxynitrobenzenes.

Table 6-1: **ESA peak positions of 4NB15CW5 and DMONB in different solvents determined by CRVFIT**

Solvent	$E_T(30)$[a] kcal/mol	4NB15CW5			DMONB		
		Delay ps	λ_L[b] nm	λ_S[c] nm	Delay ps	λ_L[b] nm	λ_S[c] nm
Cyclohexane	31.2	50	515.1	412.6	50	521.3	413.1
THF	37.4	50	509.5	415.0			
n-Butyl-acetate	38.0	50	511.4	414.7	50	514.7	412.3
Acetonitrile	46.0	50	494.8	412.0	d		
1-Octanol	48.3	1000	453.3	418.3	5000	467.5	416.0
1-Butanol	50.2				5000	454.3	415.4
Methanol	55.5	50	441.2	418.2	1000	451.1	415.5
Water	63.1	50	423	412.5	50	429.5	e

[a] Reference 185. [b] Peak position of the 'red' band. [c] Peak position of the 'blue' band. [d] Too strong Raman Spark. [e] Only fitted to a single band.

From the solvatochromic study in the chapter 4, such linear relation indicates CT characteristics. In other words, it shows a correlation of excited triplet state with the solvation process. The triplet ESA peak positions of both compounds in different solvents are deconvoluted from their ESA spectra (section 6.2.3) using program CRVFIT (see Table 6-1). In spite of this quasi-static shift of ESA spectra with solvent polarity in nanosecond time region, we

also observe the dynamic *blue-shift* of the *'red'* ESA band in the picosecond time region. This dynamic behavior is discussed in the following section.

6.3.3 Time-dependent ESA shift in alcohols

Table 6-2: The shift time of the *'red'* ESA band of DMONB in different solvents.

Solvent	$E_T(30)^a$ kcal/mol	η^b cp	$\tau_L{}^c$ ns	$\tau_{ESA}{}^d$ ns
PEG-600	~53.5			0.56±0.06
1-Octanol	48.3	10.6	0.471±0.005	0.2±0.1
ter-butyl alcohol	43.3	3.316		0.19±0.06
1-Butanol	50.2	2.948	0.118	0.076±0.006

[a] Reference 185. [b] CRC Handbook of Chem. & Phys.. [c] Longitudinal relaxation time of solvent. Reference 74, 68. [d] Obtained from the single exponential fit of ESA peak shift — C(t).

The significant solvatochromic shift of the *'red'* band is not just a quasi-static behavior (within 10 ns). In alcohols, the dynamic *blue-shift* of this *'red'* band was observed at picosecond time scale. Fig. 6-6 and Fig. 6-7, respectively show the dynamic shifts of the ESA spectra of DMONB in 1-octanol and PEG600, and 4NB15CW5 in 1-octanol, in subnanosecond time region. The shift times (listed in Table 6-2) of these *'red'* bands of DMONB in PEG600, 1-octanol, *tert*-butyl alcohol, and 1-butanol, are determined using a single exponential fit of their C(t) data as illustrated in Fig. 6-6, and Fig. 6-8. The
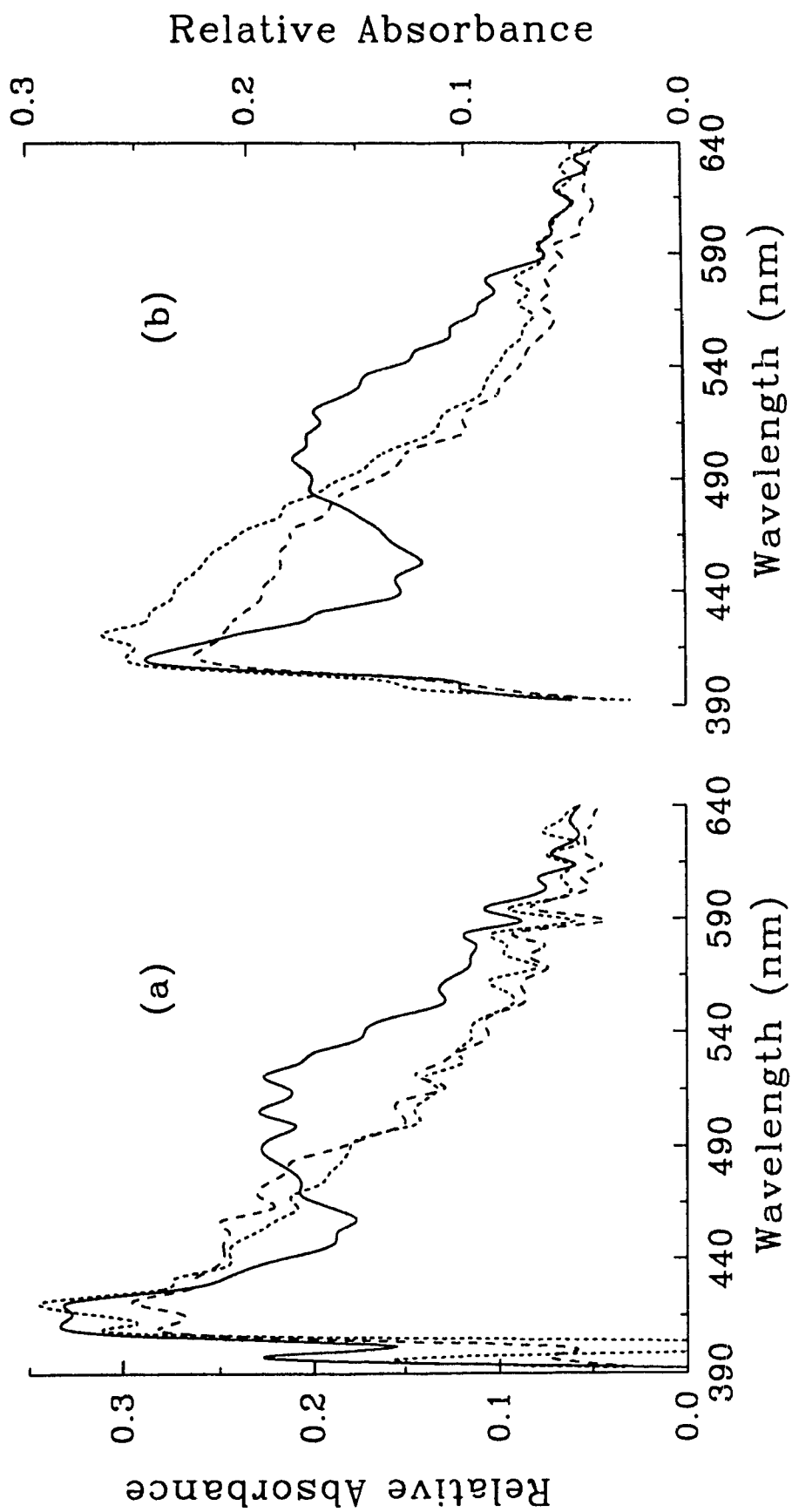
Fig. 6-6   The dyamic *blue-shift* of ESA spectra of (*a*) 4NB15CW5 and (*b*) DMONB in 1-octanol at 50 ps (solid), 1 ns (long dash), and 5 ns (short dash).
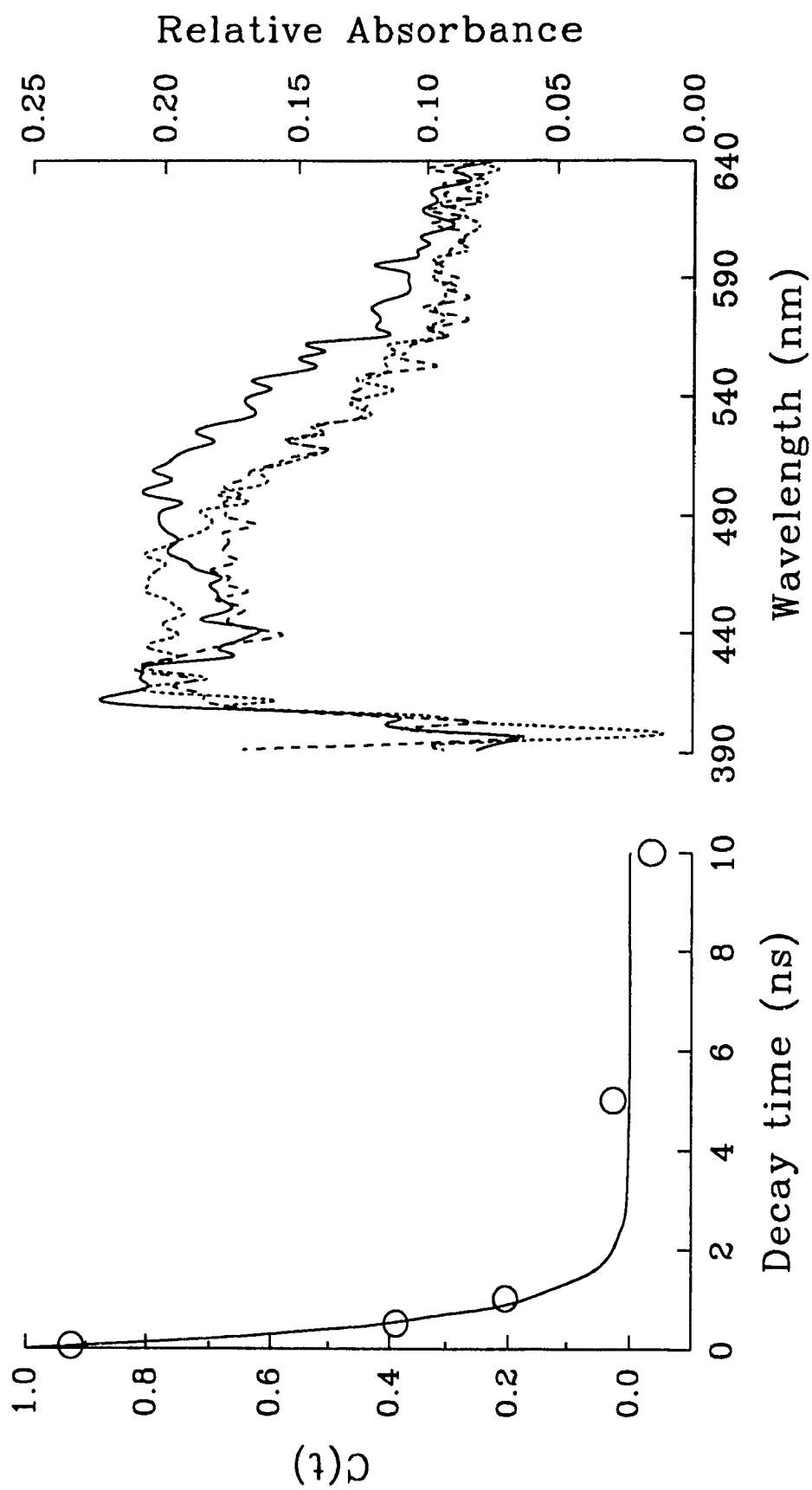
Fig. 6-7 Right frame: Dynamic *blue-shift* of ESA spectra of DMONB in PEG-600 at 50 ps (solid line), 500 ps (long dash), and 1 ns (short dash). Left frame: decay of the fraction in frequency of the *'red'* band with decay rate constant of $(1.8 \pm 0.2) \times 10^9 \, s^{-1}$
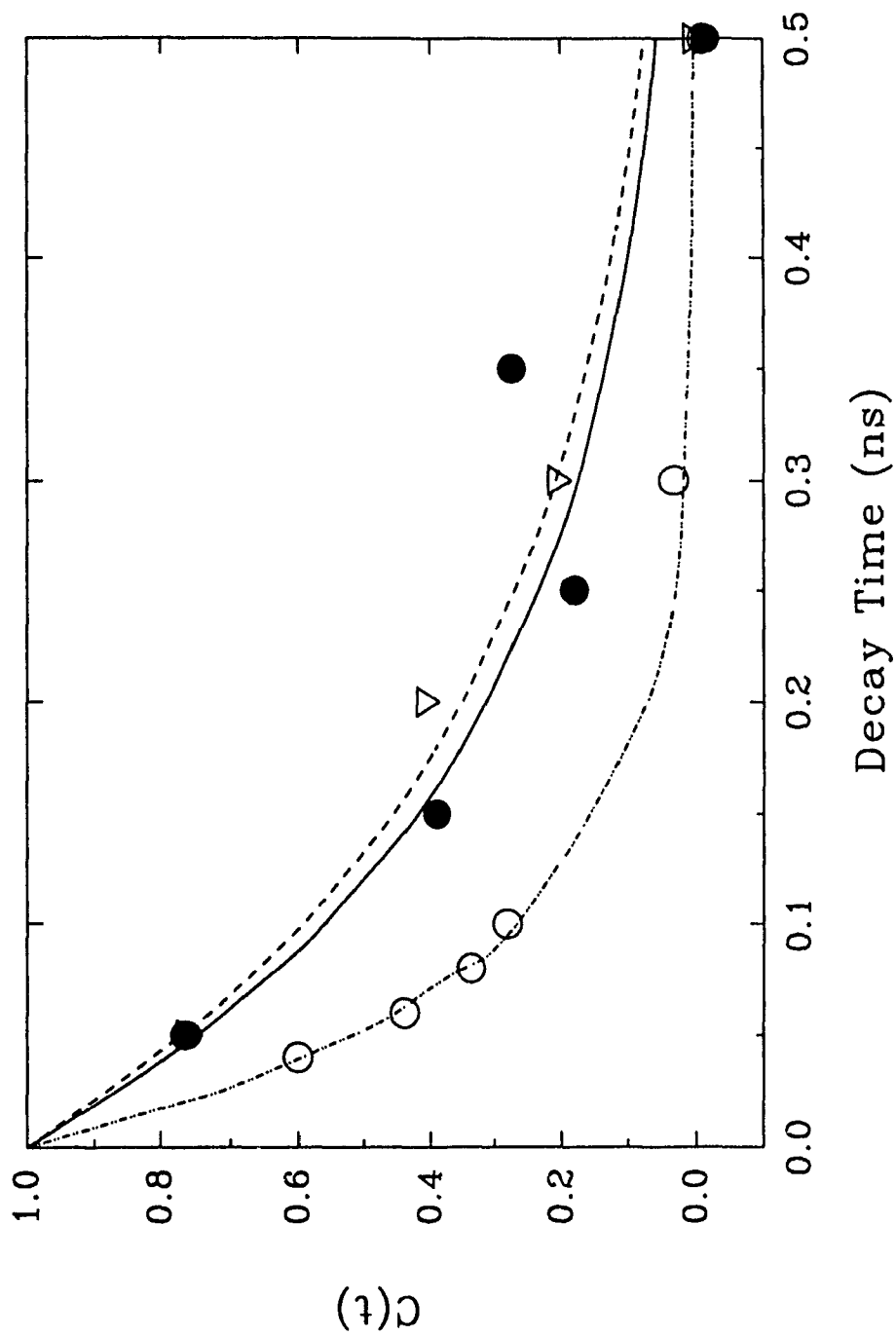
Fig. 6-8   Decay of the fraction in frequency of the 'red' band of DMONB with decay rate constant of $(13\pm1)\times10^9$ s^{-1}in 1-butanol (O, fit to dash-dot curve), $(5.8\pm4.2)\times10^9$ s^{-1} in 1-octanol (●, fit to solid curve), $(5.2\pm1.5)\times10^9$ s^{-1} in *ter*-butyl alcohol (∇, fit to dash curve).

definition of C(t) is similar to that in the *chapter 5* and is given in section 6.2.4. Due to the time-resolution limitation of present appratus with ~30 ps FWHM, the time-dependent ESA shift of these compounds in aprotic solvents (i.e., THF, nBuOAc, AN, etc.) was not detected, and are expected to occur at subpicosecond time scale.

6.3.4 Metal ion effect on the ESA of 4NB15CW5 in acetonitrile

Table 6-3: ESA shift of 4NB15CW5 with metal ions in acetonitrile

Salt	Conc.	Delay (ns)	λ (nm)	$\Delta\lambda_{max}$ (nm)	Ion Size (nm)
		0.05	495.1		
$LiClO_4$	0.06 M	1.0	491.3	16.8	17
		10.0	478.3		
$NaClO_4$	0.05 M	0.05	492.7	11.6	12
		10.0	481.1		
		0.05	491.5		
$KClO_4$	*saturated*	1.0	488.4	5.8	6
		10.0	485.7		

The preliminary study of the metal ion effect on the ESA of 4NB15CW5 is done in acetonitrile. From the time-resolved ESA spectra of 4NB15CW5 in acetonitrile with various metal ions, a slightly shift of the *'red'* band is observed at nanosecond time scale. In acetonitrile, such dynamic *blue-shift* is not

observed in absence of metal ions from 30 ps to 10 ns. The metal ion dependent ESA band positions at different time are deconvoluted from ESA spectra as listed in Table 6-3.

The trend of the maximum band shift ($\Delta\lambda_{max}$) seems to correlate with the size of the metal ion as ~17 nm for Li^+, ~12 nm for Na^+, and only about 6 nm for K^+, respectively.[135] In comparison with the solvent polarity dependency of this ESA band presented before, the interaction between lithium ion seems much stronger than that of potassium ion despite of smaller size of the lithium ion. The parent molecule, the 15-crown-5, is more selective for the larger potassium ion is than that for lithium ion.[135] Apparently, the selectivity of 4NB15CW5 for the metal ion at excited state shows a converse trend to the ground state property of its parent molecule, 15CW5. The ground state absorption spectra of 4NB15CW5 with different salts in acetonitrile (Fig. 6-9) show the similar behaviour as that of ESA spectra. Therefore, both ground and excited states complexation processes might not occur in the cavity of the crown as known in 15CW5.[135] It can not exclud the interaction between the anion-liked nitro group and the metal ions. This has to be verified in the further study of the effect of metal ion on ESA of DMONB in both ground and excited states.

6.3.5   Discussion

Outlining the ESA results of two compounds, four important phenomena are observed. These are: (i) decay of both ESA bands ('blue' and 'red') in cyclohexane, and stabilized in the most solvent at nanosecond time scale; (ii) blue-shift of the 'red' ESA band with solvent polarity, but not the 'blue' band; (iii) dynamic blue-shift of the 'red' ESA band in subnanosecond time region affected
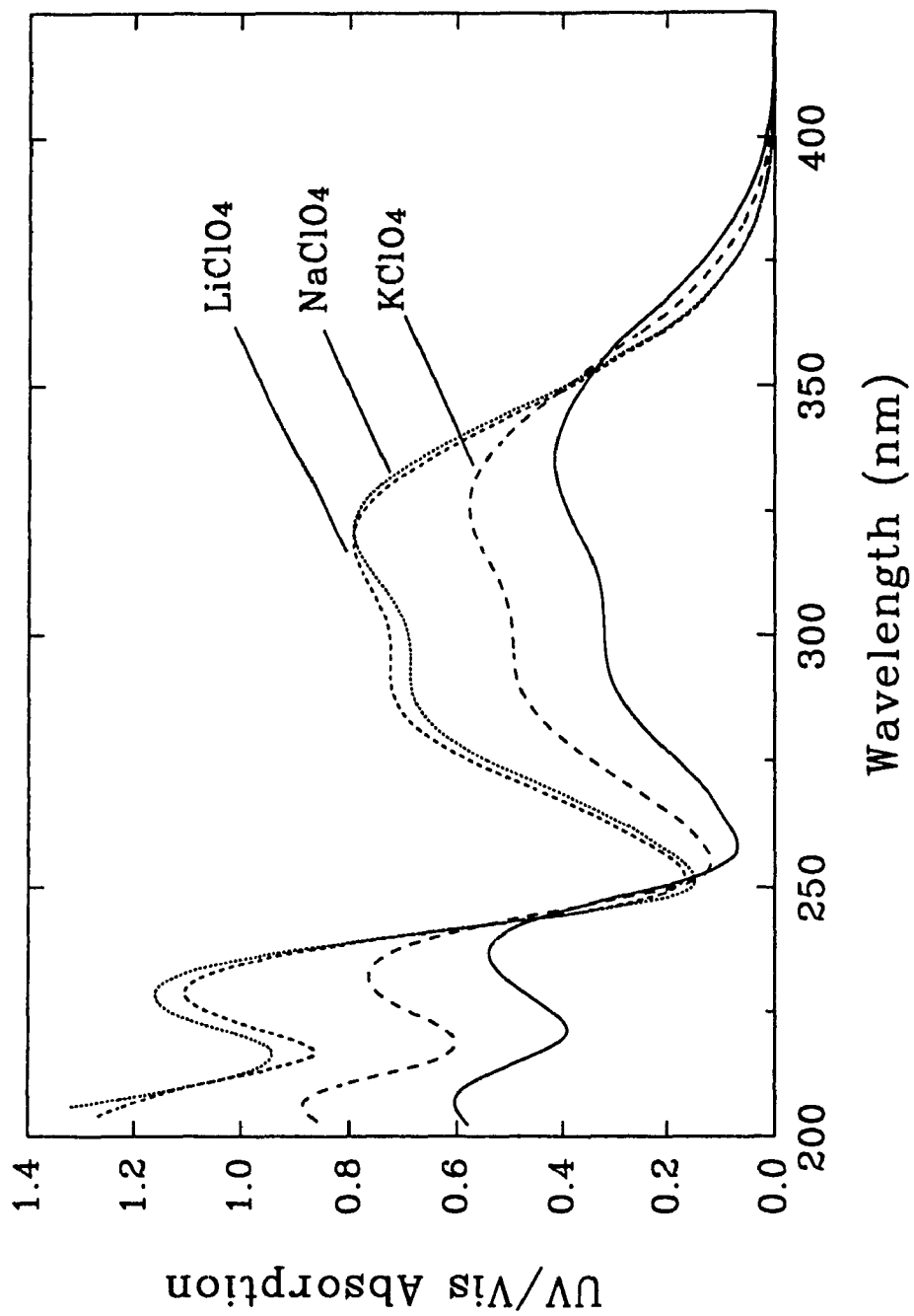
Fig. 6-9 Ground state absorption spectra of 4NB15CW5 in acetonitrile (solid curve) with different salts.

by two factors: polarity, viscosity of solvent; and (iv) salt effects on the *blue-shift* of the *'red'* ESA band of 4NB15CW5 in acetonitrile in nanosecond time region.

In cyclohexane, the decay of both ESA bands shows that the two ESA bands originate from the same excited triplet state. The lifetime of this lowest triplet state is about 2.3 ns for 4NB15CW5, and is about 4.7 ns for DMONB, respectively. But, the decay of both transient absorption bands is not observed in other solvents such as THF, n-butyl acetate, acetonitrile etc., for both probing compounds. This raises a question about the property of this triplet state. Fortunately, the observation of the solvatochromic shift of the *'red'* ESA band (Fig. 6-5) gives strong evidence for the CT characteristics of the triplet state, which is stabilized by the dipole-dipole interactions of the surrounding polar media. This shift is also observed by adding different metal ions into 4NB15CW5/acetonitrile solution.
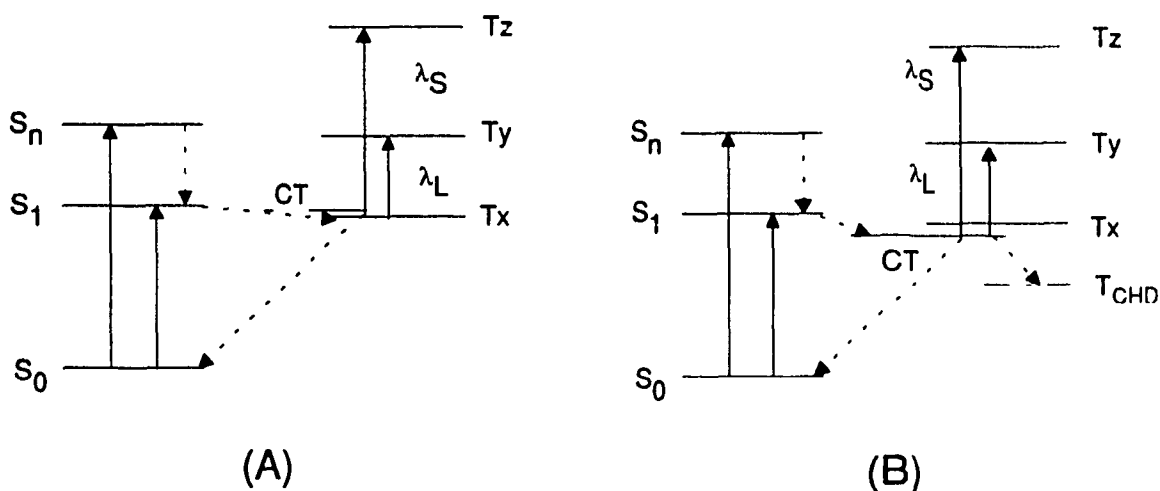
Scheme 6-3 Energy diagram

Scheme 6-3 schematically shows the transitions among the excited triplet states involving the lowest CT state. With increased surrounding polarity, the CT state drops from slightly higher energy in less polar solvent to lower energy than
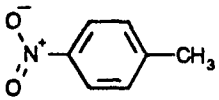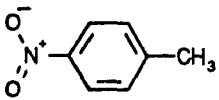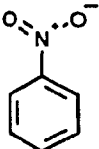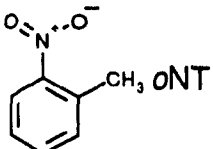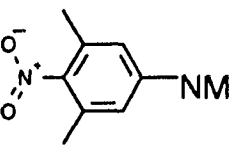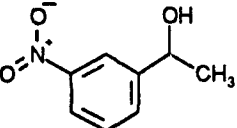
does the lowest excited triplet state T_x in moderately polar and polar solvents. Therefore, the conversion from the excited singlet state (S_1) to this CT state should be more significant. As a result, with increasing solvent polarity, the 'red' band due to the transition from this CT state to the excited triplet state T_y, must shift towards the short wavelength region. From the study of two ESA bands for alkylnitrobenzenes in the next section, this triplet T_y state is characterized by the locally excited nitro group and is not sensitive to the polarity of surrounding media. By contrast, the upper excited triplet state T_z characterized by the excited dimethoxybenzene, seems more sensitive to the surrounding media. Thus, the change of the transition energy between the CT state and the T_z state can not be identified. The quenching of both ESA bands from 4NB15CW5 in acetonitrile (Fig. 6-4) can be explained by the intermolecular energy transfer from the lowest CT state to the excited triplet state T_{CHD} of the quencher (CHD).

The significant solvent effect on the ESA spectra of both dimethoxynitrobenzenes found in this study, is the first observation of strong ICT characteristic ESA spectra. The dynamic *blue-shift* of the 'red' ESA band of both compounds in various alcohols shows a significant solvation related ESA phenomenon, which depends strongly upon the solvent polarity and viscosity. Alternatively, this observation implies a novel method to study the solvation dynamics using transient absorption technique.

6.4   Triplet ESA of Alkylnitrobenzenes
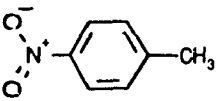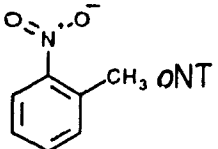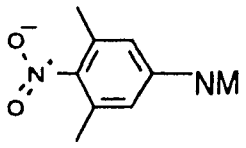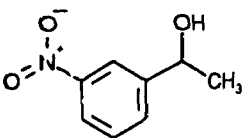
On the basis of the previous observation of quenching of ESA spectra of alkylnitrobenzenes with addition of CHD (No. **12** in Fig. 6-1) in solution, in our laboratories, the triplet state characteristics of these ESA bands are

Table 6-4: Peak position of 'red' and 'blue' ESA bands and the frequency spacing between two resolvable peaks on the structured ESA bands of alkylnitrobenzenes

Molecular Structure	Solvent	'red' Band			'blue' Band		R^d
		$\lambda_p{}^a$ (nm)	$\Delta\upsilon^b$ (cm^{-1})	FWHM^c (cm^{-1})	$\lambda_p{}^a$ (nm)	$\Delta\upsilon^b$ (cm^{-1})	As/AL
pNT	AN/H$_2$O (2:5)^e	662.8			437.8 463.7	1275	1.9
pNT	THF	647.0		3.4x10^5	437.8 460.9	1145	1.6
NB	AN	634.2			427.0 447.4	1069	1.2
oNT	THF	653			429.4 453.8	1254	0.6
NM	AN	578.5 633.9	1510	2.9x10^5	432.8		0.3
AMMNBA	AN	576.4 629.3	1443	3.5x10^5	430.8 459.6	1454	1.1

$^a\lambda_p$: Peak position in nm. ^{b} Frequency spacing between two resolvable peaks on the ESA bands. ^{c} FWHM: Frequency width at half maximum of the whole 'red' band. ^{d} Ratio of the ESA band areas. ^{e} Volume ratio.

Table 6-5: Kinetic Rate Constants of Alkylnitrobenzenes

Molecular Structure	Solvent	$k_L \pm \Delta k_L$ $(\lambda_p)^a$ 10^9 s^{-1}	$k_S \pm \Delta k_S$ $(\lambda_p)^b$ 10^9 s^{-1}
pNT	AN/H2O (2:5)^c	0.83±0.23 (663.7 nm)	1.11±0.02 (437.8 nm) 0.92±0.14 (463.7 nm)
oNT	THF	1.9±0.5 (653 nm)	$2.3\pm0.7\begin{pmatrix}429.4\ nm\\453.8\ nm\end{pmatrix}$
NM	AN	2.3±0.2 (633.9 nm) 2.5±0.2 (578.5 nm)	0.44±0.28 (432.8 nm)
AMMNBA	AN	$1.31\pm0.01\begin{pmatrix}576.4\ nm\\629.3\ nm\end{pmatrix}$	1.1±0.1(430.8 nm) 0.8±0.1(459.6 nm)

^{a} Decay rate constants of ESA at long wavelengths (λ_p: wavelength at peak position). ^{b}Decay rate constants of ESA at short wavelengths (λ_p: wavelength at peak position). ^{c}AN: acetonitrile, volume ratio of acetonitrile/water =2/5.

confirmed.[47] Through a systematic analysis of the ESA spectra of some alkylnitrobenzenes in solution, the following important features have been observed (refer to Table 6-4 and Table 6-5). (1) The structured 'blue' band at short wavelengths appears to be distinct in p-, o-nitrotoluenes and nitrobenzene from that in nitromesitylene. (2) In comparison to the 'red' band at long wavelengths, the relative intensity of the 'blue' band varies with the position of the substituents on the nitrobenzene ring, (i.e., significantly in p-nitrotoluene, but

not in nitromesitylene and tri-*tert*-butyl nitrobenzene). (3) The structured *'red'* band has been observed in nitromesitylene and α-methyl-m-nitrobenzyl alcohol. (4) The blue edge of the *'red'* band, shifts towards the short wavelength region, i.e., from ~600 nm for nitrobenzene to ~550 nm for nitromesitylene in acetonitrile. (5) The full width at half maximum (FWHM) of the *'red'* band seems to vary with the position of the substituents on the nitrobenzene ring. Addition to the substituents effect, (6) the solvent effect on the decay rate constant (Table 6-5) and on the shape of the ESA spectrum has also been found in this study.

6.4.1   Substituents effect

6.4.1.1   Nitromesitylene in acetonitrile

The ESA spectra of nitromesitylene in acetonitrile are illustrated in Fig. 6-10, in which a transient absorption *'red'* band at ~615 nm is similar to that in alkylnitrobenzenes (Fig. 6-11, Fig. 6-12). The similar observation from the low temperature ESA study of *p*-nitroaniline,[147] not from that of aniline,[149] indicates that the origin of this *'red'* band is due to the contribution from the nitro group on the benzene ring. The single exponential decay of this *'red'* band with decay time of 2.4±0.2 ns, is found by an exponential fit of the band area. The structured *'red'* ESA band of nitromesitylene (Fig. 6-10), can be resolved into two separated bands whose peak positions do not depend on time. The frequency spacing between these two peaks (578.5 nm and 633.9 nm) is resolved by the spectral deconvolution as described in section 6.2.3. Therefore, these fine structures reflect the transitions between the lower excited triplet state to the vibronic states of the upper excited triplet state, or to two very close upper excited triplet states. In comparison to the ground state infrared absorption
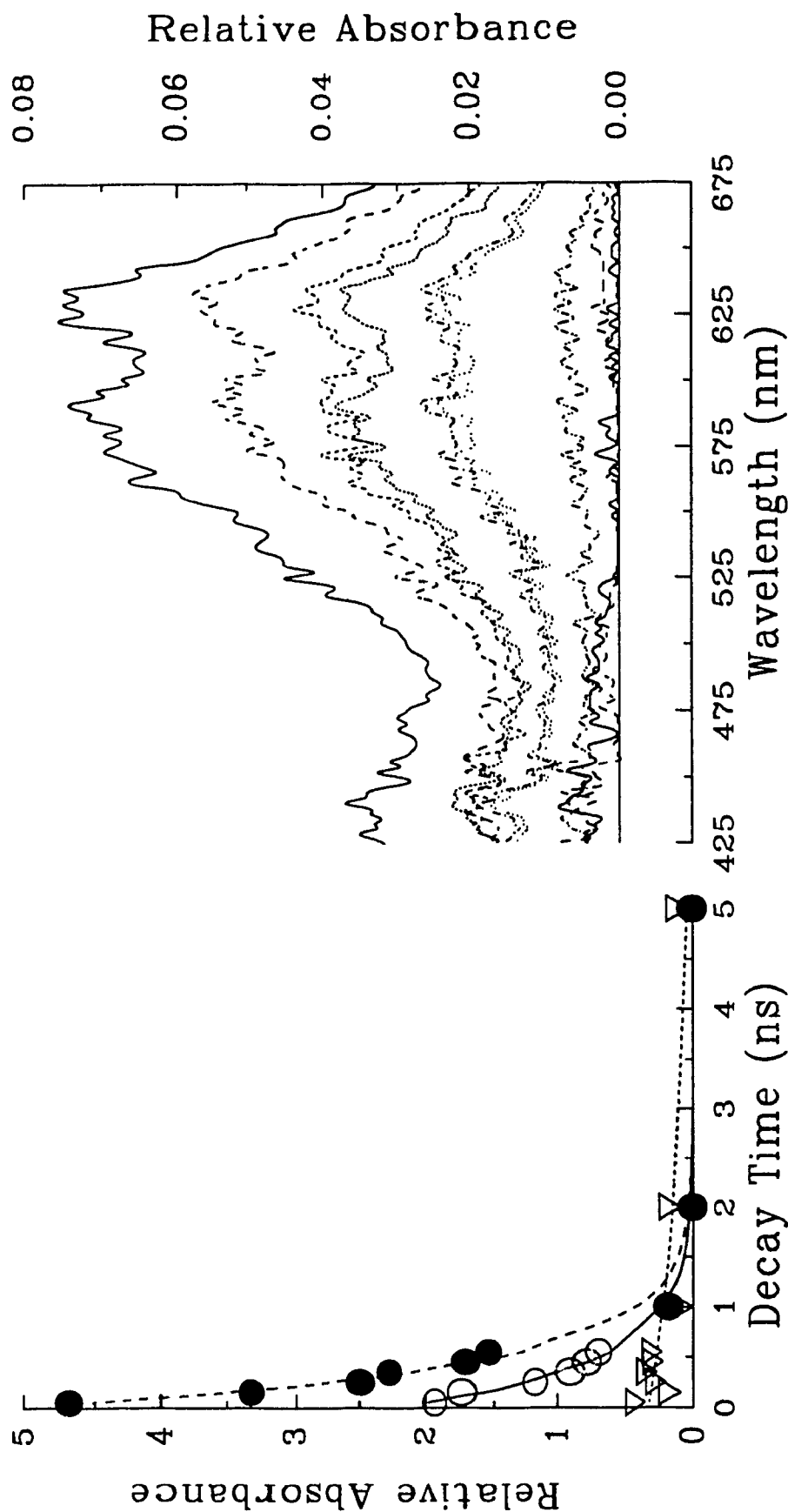
Fig. 6-10   Right frame: The ESA spectra of nitromesitylene in acetonitrile at different delay times: 50, 150, 250, 350, 450, 550 ps, 1, 2, and 5 ns (from top to bottom).   Left frame: The decay of transient absorption areas of the three bands with decay rate constants of $(0.44\pm0.28)\times10^9$ s^{-1} at 432.8 nm (∇), $(2.5\pm0.2)\times10^9$ s^{-1} at 578.5 nm ($\bullet$), and $(2.3\pm0.2)\times10^9$ s^{-1} at 633.9 nm (O), respectively.
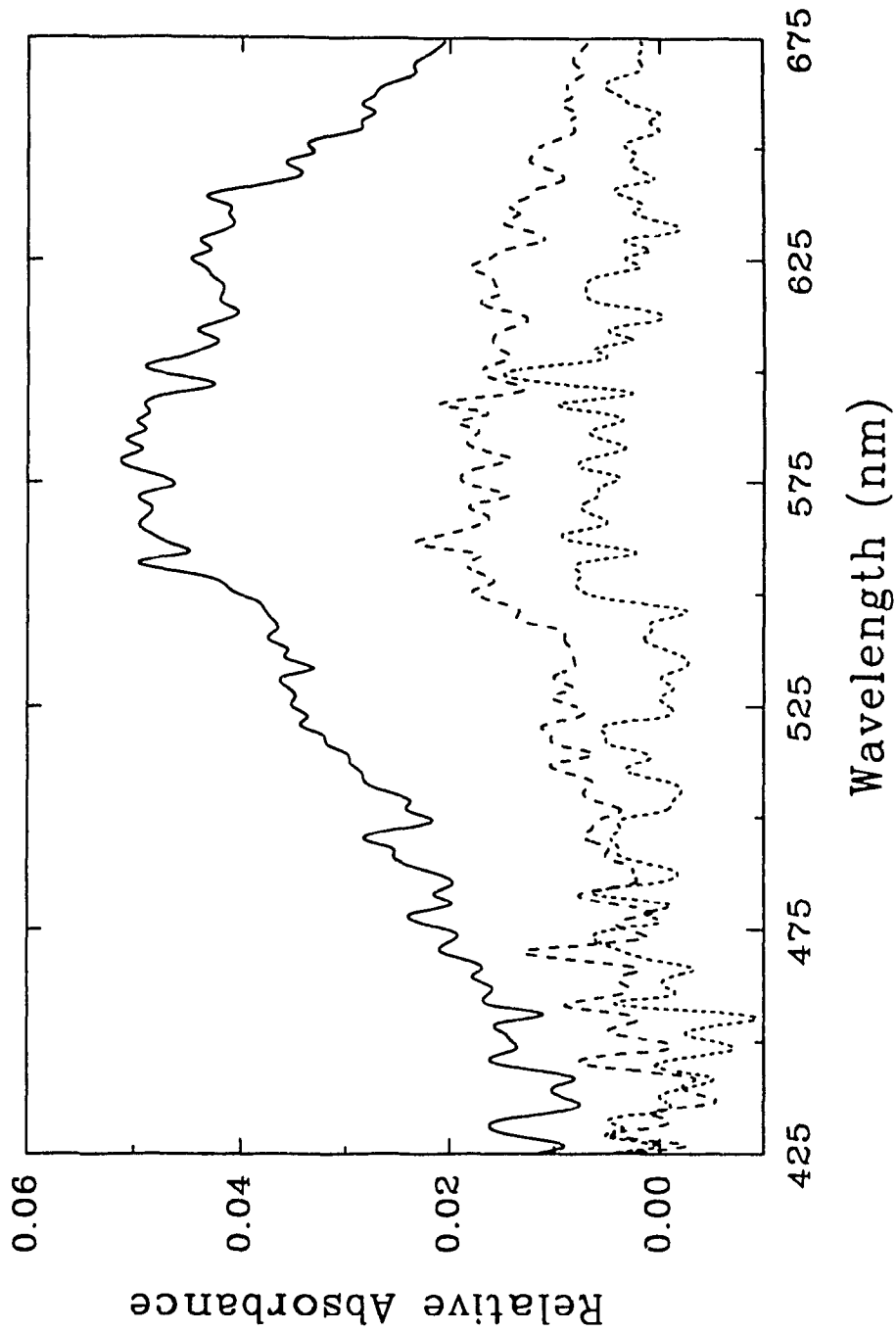
Fig. 6-11   The ESA Spectra of Tri-*ter*-butyl nitrobenzene in cyclohexane at 50 ps (solid curve), 2 ns (dash curve) and 5 ns (dot curve)
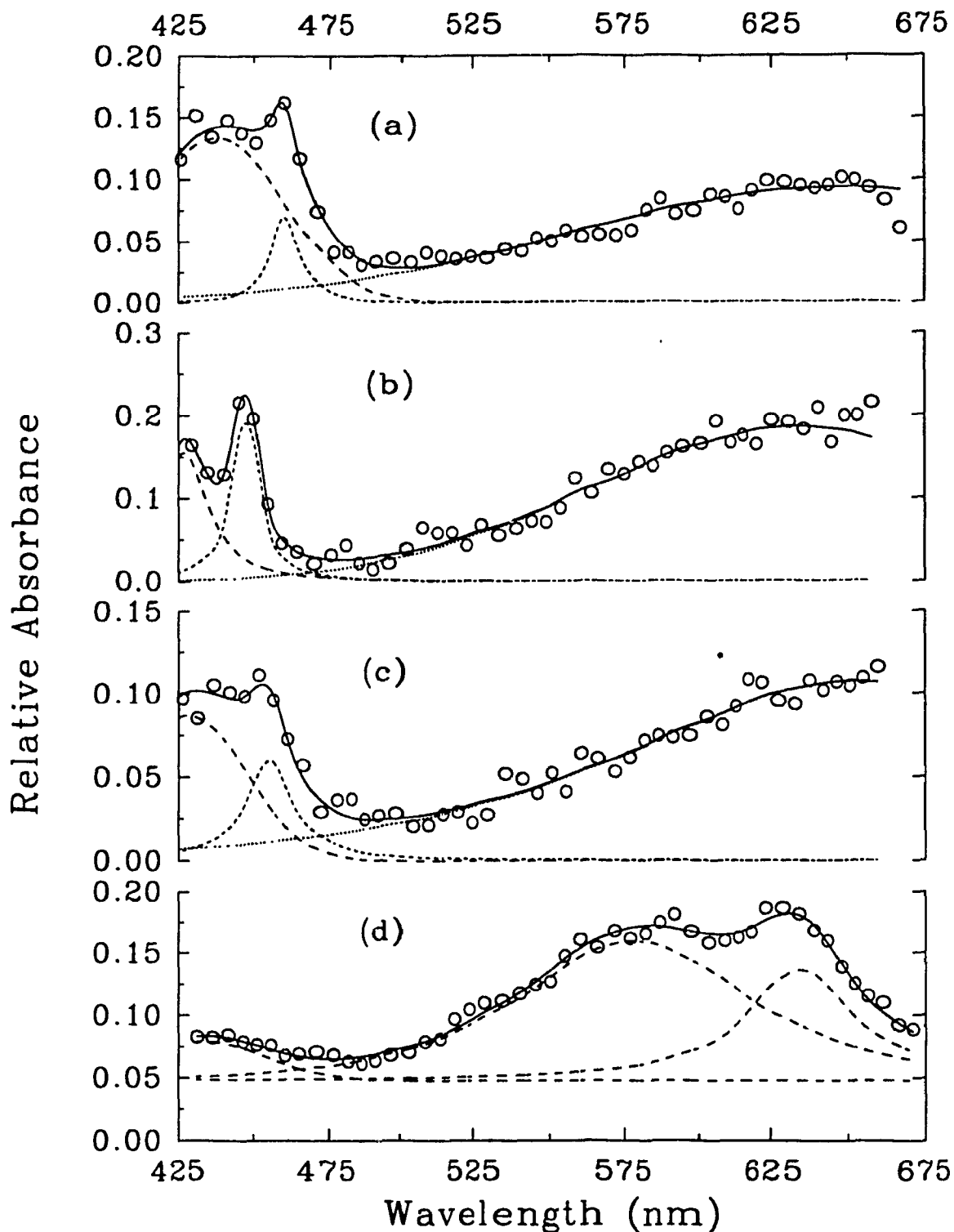
Fig. 6-12   The curve fit of ESA spectra (O) of (a) pNT/THF, (b)
Nitrobenzene/acetonitrile at 100 ps, (c) oNT/THF, and (d)
nitromesitylene/acetonitrile at 50 ps. The dash, short dash and dot
represent the components of the transient absorption bands

studies, this frequency spacing $\Delta\upsilon$ is found to be the same as the vibrational frequency of the asymmetric stretching of the nitro group.[205] This is not a random agreement. Actually, it is the reflection of the characteristics of the '*red*' band characterized by locally excited nitro group.

6.4.1.2   o- and p-Nitrotoluenes and nitrobenzene

In contrast with the ESA spectra of nitromesitylene in acetonitrile, the structured transient absorption '*blue*' band at ~ 420 nm is observed from o-, p-nitrotoluenes in THF, nitrobenzene in acetonitrile at 100 ps, and AMMNBA in acetonitrile at 50 ps (see Fig. 6-12), respectively. The area ratio $R=A_S/A_L$ of the '*blue*' (~ 440 nm) A_S to the '*red*' band (~ 620 nm) A_L varies with the position of substituents attached to the benzene ring (Table 6-4) and is in the order

$$R(pNT) > R(NB) > R(oNT) > R(nitromesitylene) \tag{A}.$$

In the previous section (6.4.1.1), the comparison between the frequency spacing of the structured '*red*' band and the ground state asymmetric stretching of NO_2 shows that this fine structure on the triplet ESA band may reflect excited state vibronic interaction of NO_2. If it is true, the excited state vibronic interaction of NO_2 could be similar to its ground state with strong resonance of the asymmetric stretch of NO_2. By comparison with the infrared spectra of alkylnitrobenzenes, this structure dependency of the ratio of the '*blue*' and the '*red*' band areas parallels the trend of the ground state vibrational absorption intensity of the asymmetric stretching of NO_2, and the oscillator strength ratio ($R=f_S/f_{as}$) of the symmetric (f_S) and the asymmetric (f_{as}) stretching band of NO_2 with the position of alkyl substituent attached to the nitrobenzene ring which appears in the same order:[204]

R(*para-*) > R(*meta-*) > R(*ortho-*) > R(2,6-) (B)

This agreement indicates a significant contribution from the vibronic interaction of the asymmetric stretching of NO_2 group to this '*red*' ESA band. By considering the contribution of the locally excited nitro group to the '*red*' band (~ 620 nm) as for *p*-nitroaniline,[148] there is a question about the '*blue*' band which could have strong contributions from locally excited benzene as for aniline.[149] Similar to the '*red*' band, the frequency spacing (1069 ~ 1454 cm^{-1}) of the fine structure on the '*blue*' band (~ 440 nm) is comparable to the vibrational frequency of CH bending ($\Delta\upsilon \approx 1174\ cm^{-1}$), or the ring stretching of the benzene ($\Delta\upsilon \approx 1550\ cm^{-1}$).[150]

The ratio of the '*blue*' to '*red*' ESA band areas reflects a difference in the probability of the transitions from the lowest to two upper excited triplet states. For nitromesitylene, the characteristics of locally excited NO_2 seems to be more significant due to the twisting of the nitro group out of the plane.[200] In comparison to the relatively small twisting of a nitro group for nitrobenzene and *p*-nitrotoluene, the NO_2 group of nitromesitylene in solution is twisted by 90 ° from the ring plane due to the steric hindrance of the adjacent methyl groups.[200] With twisting of NO_2 off the plane of the benzene ring, the symmetry of the upper excited state could be similar to that of the lower excited state. Therefore, the excited state transition moment between the lowest and the upper excited triplet state as the '*red*' band, can be much larger than that of the '*blue*' band. Thus, the ESA spectra with more significant characteristics of local NO_2 should be observed. By contrast, for those alkylnitrobenzenes with untwisted or slightly twisted NO_2, the transient absorption of the '*blue*' band, should be more significant. This is actually what we observed in Fig. 6-12, and from the agreement between the trends (A) and (B).

198

6.4.2 Solvent effect on ESA of nitromesitylene and α-methyl-m-nitrobenzyl alcohol (AMMNBA)

6.4.2.1 Nitromesitylene

(i)   As presented before, two sets of ESA spectra of nitromesitylene in *acetonitrile* were analyzed using program CRVFIT. The fast decay band at ~615 nm (Fig. 6-10) due to the locally excited nitro group was resolved. The two peaks of the 'red' band are spaced about 1510 cm^{-1} appart (see Table 6-4). The transient absorption at short wavelengths (~ 430 nm) was not reproducible in two sets of spectra. The cause is not known but may be due to hyroxylic impurities in the the solvent resulting in the transient absorption in this wavelength region as is observed in acetonitrile/water mixture.

(ii)   In *acetonitrile/water mixture*, two time-dependent transient absorption bands are found from the spectra (Fig. 6-13). These are: (1) a decay band at ~613 nm with a relatively small decay rate constant of $(0.47 \pm 0.17) \times 10^9$ s^{-1} in comparison to $(1.9 \pm 0.4) \times 10^9$ s^{-1} in acetonitrile; and (2) two gradually enhanced bands at ~400 nm and ~493 nm with the similar rate constant $(0.57 \pm 0.15) \times 10^9$ s^{-1} as listed in Table 6-6. Since the rate constants of both short bands (~ 400 and 493 nm) are very close from the exponential fitting of their transient absorption areas per average pumping energy, it is reasonable to treat these two bands as being kinetically identical.

(iii)   In contrast with the ESA in acetonitrile, the ESA in *water* is very weak. This is due to the trivial factor of low concentration and low absorption of the sample. From the ESA spectra (Fig. 6-14), the transient absorption at 600 nm can be considered as part of the baseline as mentioned before. Similar to the ESA in acetonitrile/water mixture, the transient absorption band of
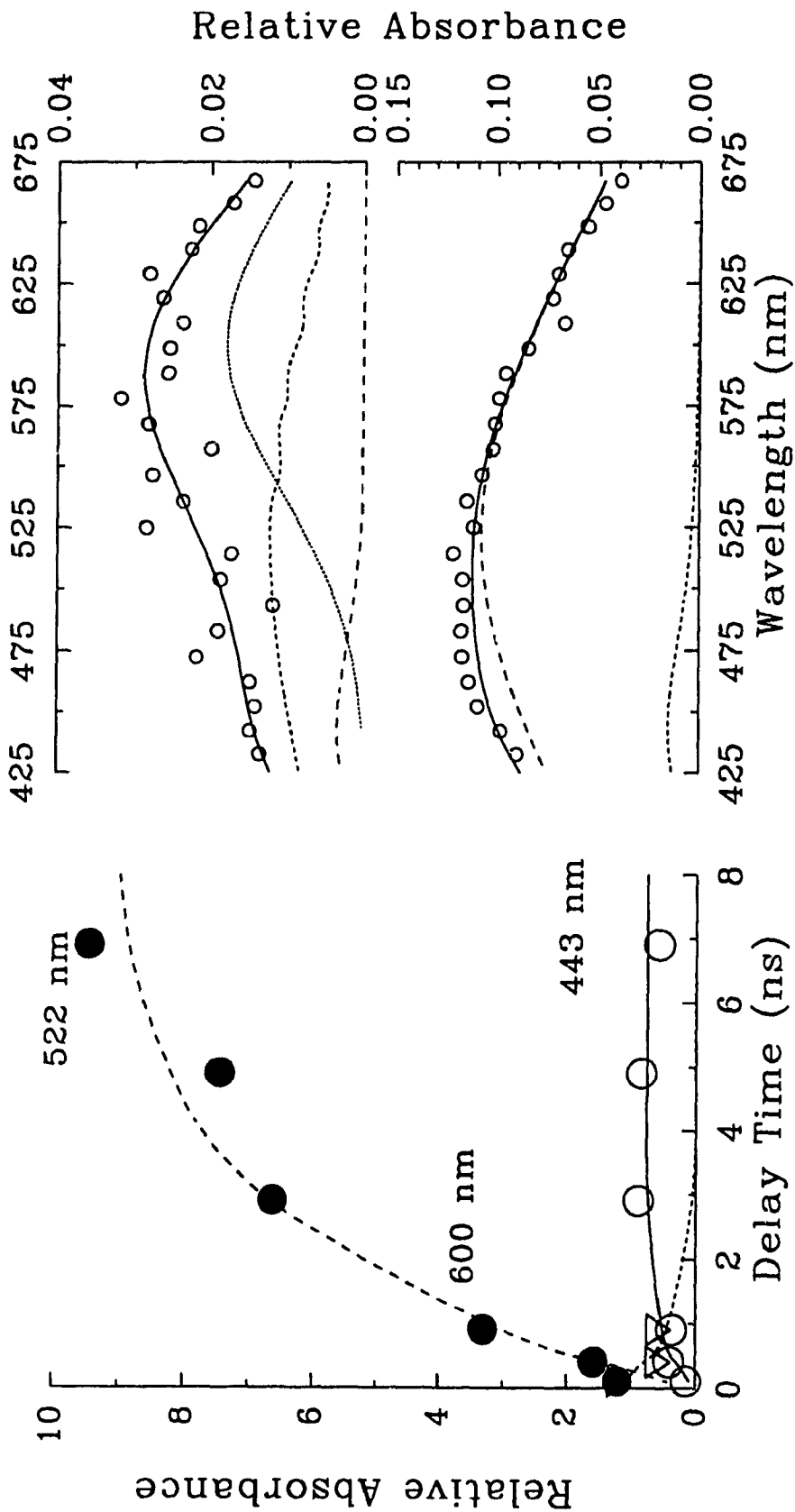
Fig. 6-13 The ESA spectra (O) of Nitromesitylene in AN/H_2O Mixture (1:2) illustrated in *Right top frame*: at 50 ps, fit to three components with trail at short wavelengths; in *Right bottom frame*: at 7 ns, fit to three components. The left frame shows the kinetics of these three transient absorption bands with rate constant (0.39 ± 0.23) x10^9 s^{-1} at 400 nm (∇) and (0.60 ± 0.15) x10^9 s^{-1} at 493 nm ($\bullet$), and with decay rate constant (0.47 ± 0.17)x10^9 s^{-1} at 613 nm (O).
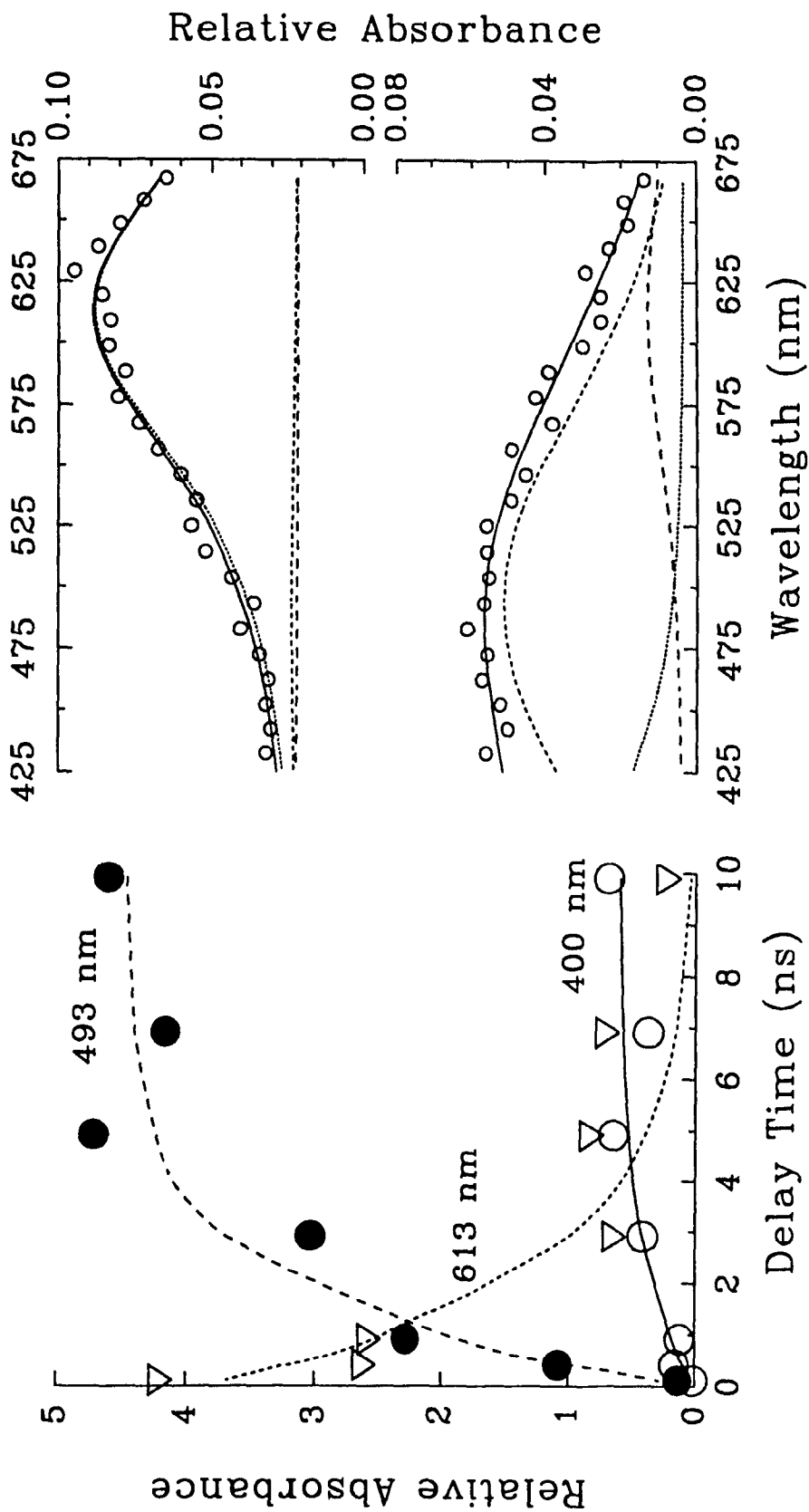
Fig. 6-14   The ESA spectra (○) of Nitromesitylene in H₂O illustrated in Right top frame: at 50 ps, fit to three components with trail at short wavelengths; in Right bottom frame: at 7 ns, fit to three components.   The left frame shows the kinetics of these three transient absorption bands with rise rate constant $(1.2\pm0.3) \times 10^9$ s^{-1} at 443 nm (○) and $(0.43\pm0.08) \times 10^9$ s^{-1} at 522 nm (●), and with decay rate constant $(1.1\pm0.7) \times 10^9$ s^{-1} at 600 nm (▽).

nitromesitylene in AN at short wavelengths was fitted by two separated components ($\sim$443 and 522 nm) with the same kinetic rate constant. Therefore, these two components can be considered as a single component with the rate constant of $(0.32 \pm 0.08) \times 10^9$ s^{-1}. The large deviation (70%) in the rate constant $(1.1 \pm 0.7) \times 10^9$ s^{-1} of the decay band at 600 nm, is not surprising in view of the poor signal/noise.

Table 6-6: Comparison of the Kinetic Rate Constants of Nitromesitylene in Different Solvents

Solvent		$k_L \pm \Delta k_L$ (λ, nm)[a] 10^9 s^{-1}	$k_S \pm \Delta k_S$ (λ, nm)[b] 10^9 s^{-1}	R=As/AL
Cyclohexane		8.5±1.5 (600±5)	12±10 (233~434)	*see the following section (iv)*
Acetonitrile	A	2.3±0.2 (634)	0.44±0.28 (433)	0.3
		2.5±0.2 (579)		
	B	1.9±0.4 (615)		
		0.1±0.4 (573)		0
Acetonitrile/water (1:2)[c]		0.5±0.2 (614)	0.57±0.15 (493;400)	1.3
Water		1.1±0.7 (600)	0.32±0.08(522;443)	8.3

[a] Decay rate constants of ESA at long wavelengths (peak position, nm). [b] Decay rate constants of ESA at short wavelengths (peak position, nm). [c] Volume ratio = V_{AN}/V_{H_2O}=1/2.

The increase in the transient absorption of nitromesitylene in water (see Fig. 6-13 and Fig. 6-14), is not clear, which could be due to the H-bonding interaction between NO_2 and solvent molecules. Therefore, the intensity of the

'red' band which exhibits NO_2 group character should be reduced dramatically.
The origin of the high ratio ($R=A_S/A_L$) observed from pNT in acetonitrile/water
mixture (see Table 6-4), is still not clear. By comparison with the time scale of
the solvation process, this observation also indicates that there is no
contributions from the solvated electronic absorption to both 'blue' and 'red'
bands.

Table 6-7: Spectral Deconvolution Results of ESA Spectra for Nitromesitylene in Cyclohexane

Time	'blue' band			'red' band		
(ps)	λ (nm)[a]	B[b]	C[c]	λ (nm)[a]	B[b]	C[c]
50	403.4	0.0032	0.00456	594.2	0.00002	0.01171
100	434.3	0.0032	0.00456	603.8	0.00002	0.01171
200	232.7	0.0032	0.00456	592.6	0.00002	0.01171
350	396.6	0.0032	0.00456	599.6	0.00002	0.01171
500	358.3	0.0032	0.00456	607.3	0.00002	0.01171
Mean	365±79	0.0032	0.00456	600±6	0.00002	0.01171

[a] Wavelength at peak position. [b] Cauchy factor of eq. (1). [c] Gauss factor of eq. (1).

(iv)   An intense transient at short wavelengths is observed from the ESA
spectra of nitromesitylene cyclohexane as illustrated in Fig. 6-15. From the
spectral deconvolution of these time-dependent ESA spectra by fixing the
spectral shape parameters (i.e., Cauchy and Gauss factors of eq. (1)) as listed in
Table 6-7, we find great uncertainties in (a) the peak position (359±79 nm); (b)
the decay rate constant (12±10 ns^{-1}) of this 'blue' band. By contrast, the 'red'
band is located in a reasonable wavelength region (600±6 nm) with exponential
decay rate constant of 8.5±1.5 ns^{-1}. The rate constant of the decay of the 'red'
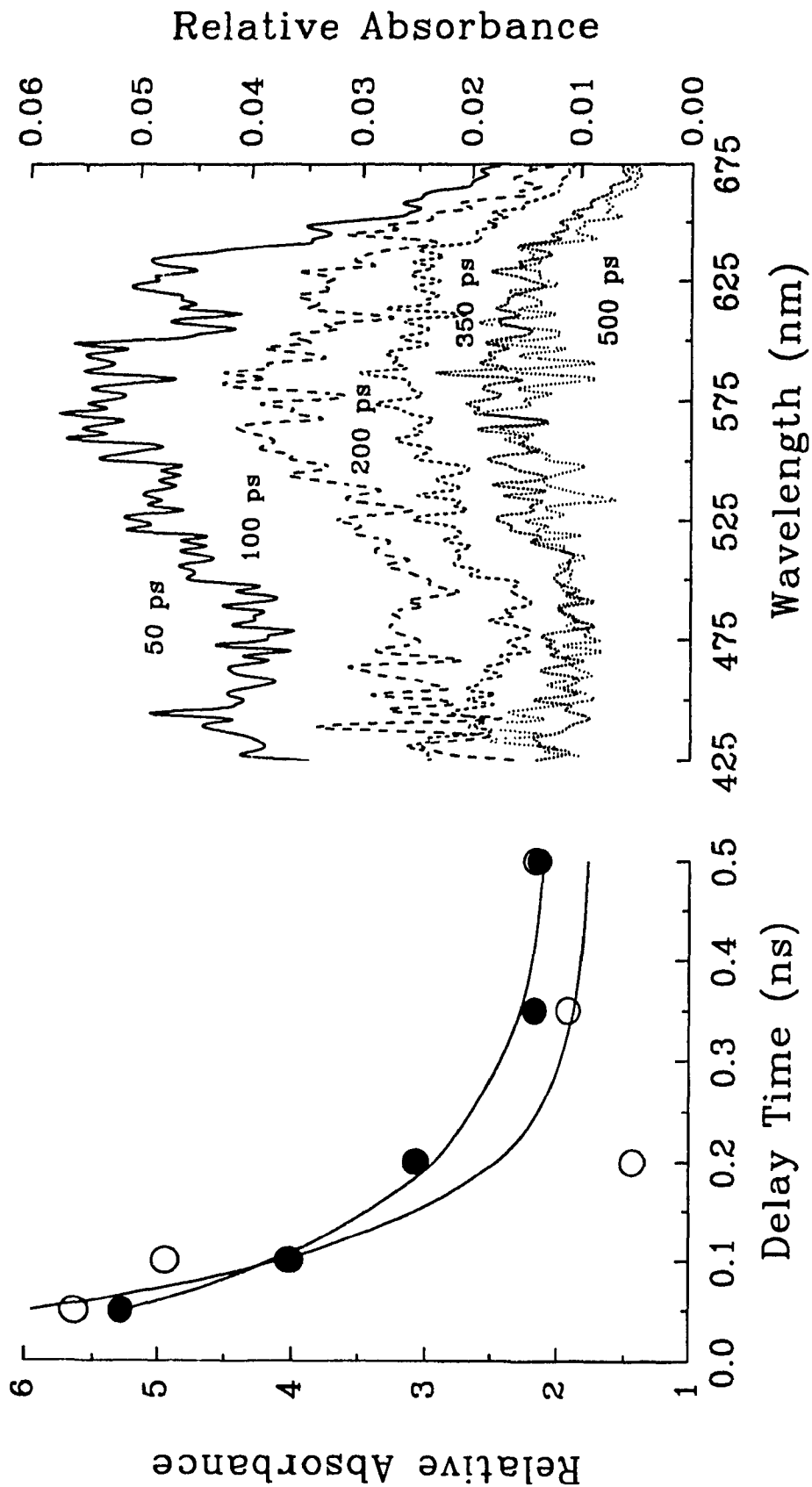
Fig. 6-15 **Right Frame: ESA spectra of nitromesitylene in cyclohexane. Left frame: Exponential decay of the 'blue' band (O) (k_S=12±10 1/ns) and 'red' band (●) (k_L=8.5±1.5 1/ns)**

band in cyclohexane is much larger than that for the 'red' band in acetonitrile as listed in Table 6-6. This could imply the solvent polarity effect on the lifetime of the lowest triplet state. The peak positions of both ESA bands might shift towards the short wavelength region with solvent polarity. This may be the reason for the weak transient absorption at short wavelengths for nitromesitylene in acetonitrile. It will be interesting to measure the ESA spectra of nitromesitylene in different aprotic solvents for verification of these possible solvent effects.

By viewing the ESA spectra of nitromesitylene in different solvents, four significant observations can be noted: (1) the ratio of the transient absorption area (or intensity) of the 'blue' and 'red' bands is small in pure acetonitrile (not in cyclohexane) due to the twisting of the nitro group out of the benzene ring.[200] It shows significant locally excited NO_2 characteristics;[143] (2) in presence of water molecules, the rate constant for the rise of the 'blue' band is slower than that in pure acetonitrile. This could originate from the external H-bonding interaction between nitro group and water molecules. This new transient band at ~480 nm has the same kinetics as the 'red' band; (3) the polarity dependent decay rate constant of the 'red' band tends to be the fastest in cyclohexane. It seems that the lowest triplet state is stabilized by the dipole-dipole interactions in polar solvent and tends to have more ICT characteristic state; (4) the fine structure on the 'red' band with frequency space of ~ 1510 cm^{-1} in acetonitrile (AN) and AN/H_2O is due to the asymmetric stretching of locally excited NO_2 group; (5) the origin of the uncertainty of the 'blue' band in cyclohexane is still not clear. we can not exclude the possible of a blue-shift of this 'blue' band due to solvent polarity.

6 4.2.2   α-methyl-*m*-nitrobenzyl alcohol (AMMNBA)

(i)   The time-resolved transient absorption spectra of AMMNBA in *acetonitrile* (Fig. 6-16), were analyzed by program CRVFIT. There are four resolvable peaks (630, 576 nm, and 460, 431 nm) on two fast decay ESA bands at long and short wavelengths. The decay rate constants of these two ESA bands are $(1.31\pm0.05)\times10^9$ s^{-1}, and $(1.0\pm0.3)\times10^9$ s^{-1} for the *'red'*, and *'blue'* bands, respectively. These components can be considered kinetically identical due to their comparable decay rate constants. After 2 ns, there is a rising component appearing around 566 nm. Obviously, the origin of this ESA band is not the same as the decay components. It may or may not be the effect of impurities.

(ii)   In acetonitrile/water (1:2) mixture and pure water, no difference on the ESA spectra of AMMNBA can be found. Both *'red'* and *'blue'* bands decay exponentially with the similar rate constants. The results are listed in Table 6-8.

By comparison with nitromesitylene, we have not observed a significant solvent effect on the ESA spectra of AMMNBA. There are two structured transient absorption bands at ~ 420 nm and ~ 600 nm, respectively. This is consistent with our previous observation from other alkylnitrobenzenes. The origin of the *'blue'* band, and the *'red'* band, can be respectivly assigned by the transitions between the lowest triplet state to the upper excited triplet state characterized by (i) locally excited benzene, and (ii) locally excited NO_2. The appearance of both structured ESA bands for AMMNBA displaying the characteristics between *o*NT's and nitrobenzene's, can be explained as follows. (1) In AMMNBA, the nitro group is less hindered than in *o*NT and is slightly more hindered than in NB. Therefore, the contribution from the locally excited benzene should be more significant than that in *o*NT. (2) The hydroxyl group
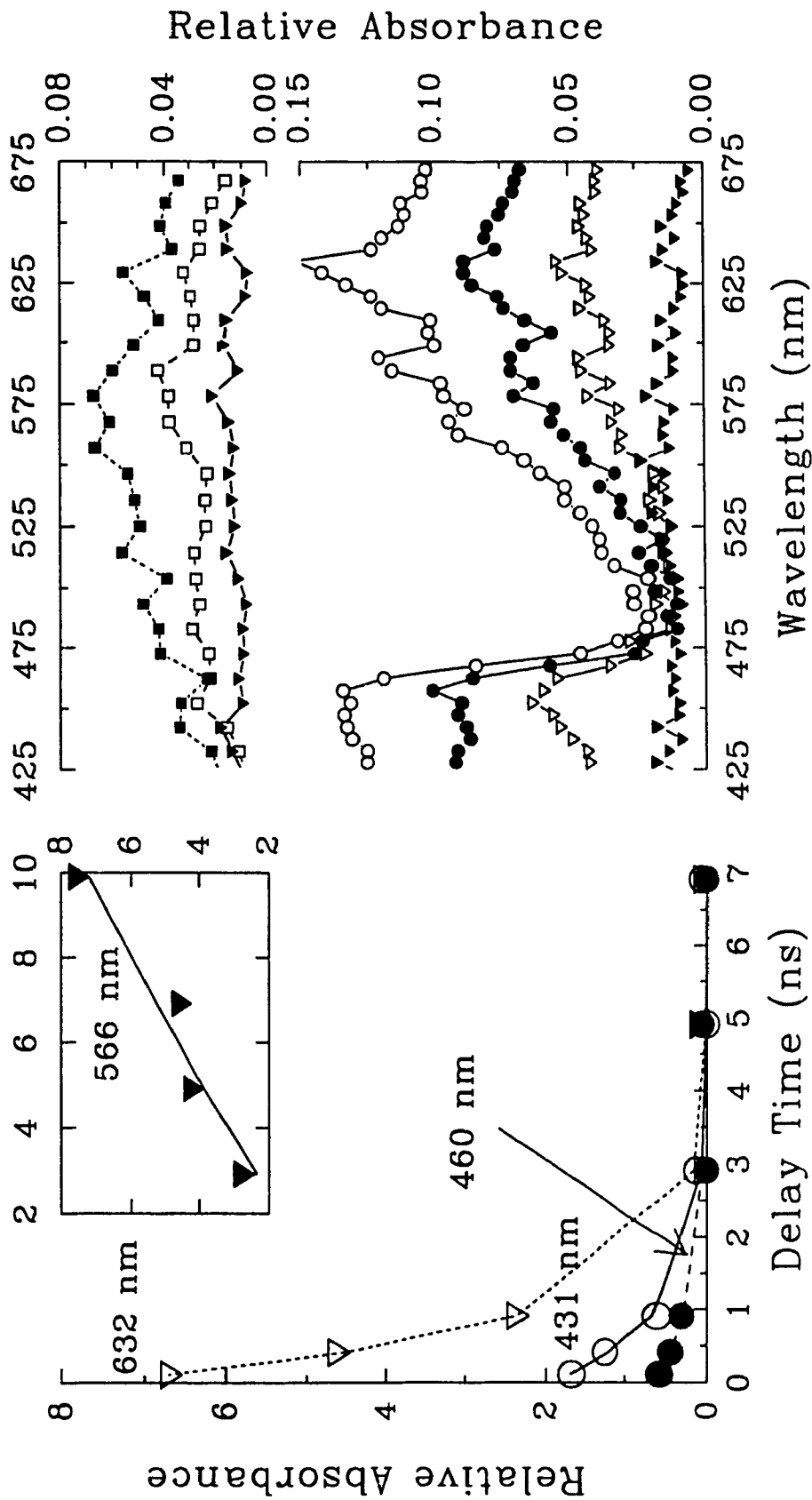
Fig. 6-16   Right frame: The ESA spectra of AMMNBA in AN at 110 ps (O), 410 ps (●), 910 ps (∇), 2.9 ns (▼), 4.9 ns (□), and 9.9 ns (■). Left frame: The decay of three components with decay rate constants of (1.31±0.05) x10⁹ s⁻¹) at 632 nm (∇; (1.1±0.1) x10⁹ s⁻¹ at 460 nm (●), (0.8±0.3) x10⁹ s⁻¹ at 431 nm(O) , and slow rise at 566 nm (▼) in insert frame, respectively.

attached on the *meta* substituent, can form hydrogen bonding or dipole-dipole interactions with the surround molecules. Such interaction provides a shell for the NO_2 group, and reduce its sensitivity to the surrounding media. Thus, the external H-bonding interaction between NO_2 group and the surrounding media should be weaker than that in both *p*NT (see Table 6-4) and nitromesitylene (Table 6-6).

Table 6-8: Comparison of the Kinetic Rate Constants of AMMNBA in Different Solvents

Solvent	$k_L \pm \Delta k_L$ (λ, nm)[a] 10^9 s^{-1}	$k_S \pm \Delta k_S$ (λ, nm)[b] 10^9 s^{-1}	R=As/AL (100 ps)
THF/water (4:1)[c]	1.8±0.4 (613)	1.4±0.2 (433.5)	0.7
Acetonitrile	$1.31\pm0.05 \begin{pmatrix} 576.4 \\ 629.3 \end{pmatrix}$	1.1±0.1 (430.8) 0.8±0.1 (459.6)	1.1
Acetonitrile/water (1:2)[c]	1.5±0.4 (607.3)	1.4±0.3 (430.3) 1.3±0.2 (460.2)	1.1
water	0.9±0.1 (607.6)	1.1±0.2 (433.8) 1.4±0.3 (459.6)	1.1

[a] Decay rate constants of ESA band at long wavelengths (peak position, nm). [b] Decay rate constants of ESA band at short wavelengths (peak position, nm). [c] Volume ratio.

6.4.3 Discussions

In the above ESA study of alkylnitrobenzenes, it is significant that (1) that the ratio of two transient absorption band areas varies with (*a*) the position of the

substituent and (*b*) the *solvent*; (2) the fine structure of either '*blue*' or '*red*' ESA band reflects the excited state vibronic interaction of the locally excited benzene ring or the NO_2 group. These fine structures on the '*blue*' and '*red*' ESA bands correspond to vibronic interaction of locally excited benzene and NO_2, respectively. The ESA of the excited state alkylnitrobenzenes (see Fig. 6-12) are similar to *p*-nitroaniline,[148] but not to aniline, whose ESA spectra only show a single transient absorption band at short wavelengths.[149] The agreement (1) between the frequency spacing of the structured '*red*' band and the asymmetric stretching of NO_2; (2) the comparable frequency between frequency spacing of the structured '*blue*' band and the CH bending or stretching of the benzene ring; (3) the trends of the transient absorption ratio ($R=A_S/A_L$) and the oscillator strength ratio of symmetric and asymmetric stretching of NO_2; further support the assignment of the '*red*' band to a state with locally excited NO_2 characteristics, and the '*blue*' band to a state having e localized benzene ring characteristics. The ratio of these two ESA band areas can be affected by the position of the substituent on the nitrobenzene. Especially, when the nitro group is twisted out of the plane due to steric hindrance, the tansition moments of the '*red*' ESA band could be more significant due to change in symmetry. As a result, the structure of the '*red*' band appears to be more identical to the '*blue*' band.

For the protic solvent such as water, the H-bonding interaction between nitro group and H_2O becomes more significant. Therefore, in the ESA spectra, the intensity of the '*red*' band with the locally excited NO_2 character, appears to be much weaker than those in the absence of water molecules. This is true in the study of the solvent effects on the ESA spectra of nitromesitylene (Fig. 6-10, Fig. 6-13), *p*NT (Table 6-4). In comparison with nitromesitylene and *p*NT, for

nitrobenzene in H_2O, a relative strong 'red' band (~ 575 nm) instead of a 'blue'

band is observed in the initial period (Fig. 6-17). For nitromesitylene in H_2O, a

new ESA band at ~ 480 nm builds up and posseses the same kinetic rate

constant as the decay of the 'red' band. This is possible due to the formation of

a new H-bonding state as nitrobenzene in water (Fig. 6-17). For AMMNBA, the

OH group on the m-substituent could have the function to block the

intermolecular interaction between surrounding protic molecules (e.g., water)

and NO_2. Thus, the sensitivity of AMMNBA to the external protic molecules is

reduced. As a result, no significant solvent effect on ESA spectra can be

observed.

6.5 Identification of the Biradical Intermediate in the Intramolecular Rearrangement

6.5.1 Biradical of intermediate in intramolecular rearrangement

6.3.1.1 ONBCPE in acetonitrile

In thye studies of ONBCPE in acetonitrile (0.8-1.0 x 10^{-2} M), the time-

resolved transient absorption spectra (Fig. 6-18) display two bands (400 ~ 425

nm, and 600 ~ 650 nm) of similar intensities at picosecond times (300 ~ 400 ps),

and at longer delay times, a single band at ~425 nm. These excited state

behaviors were also reported from the ESA of ONBCPE, and ONBPE in THF.[45]

The single triplet excited state absorption band (~ 425 nm) appeared at times

comparable to the pulse duration (~30 ps) and persisted beyond our time

resolution (~10 ns) was attributed to intramolecular H-abstraction reaction from

the excited singlet state (Scheme 6-2), which were similar to the o-quinonoid

absorption characters.[209] Therefore, the intermediates were identified to be o-
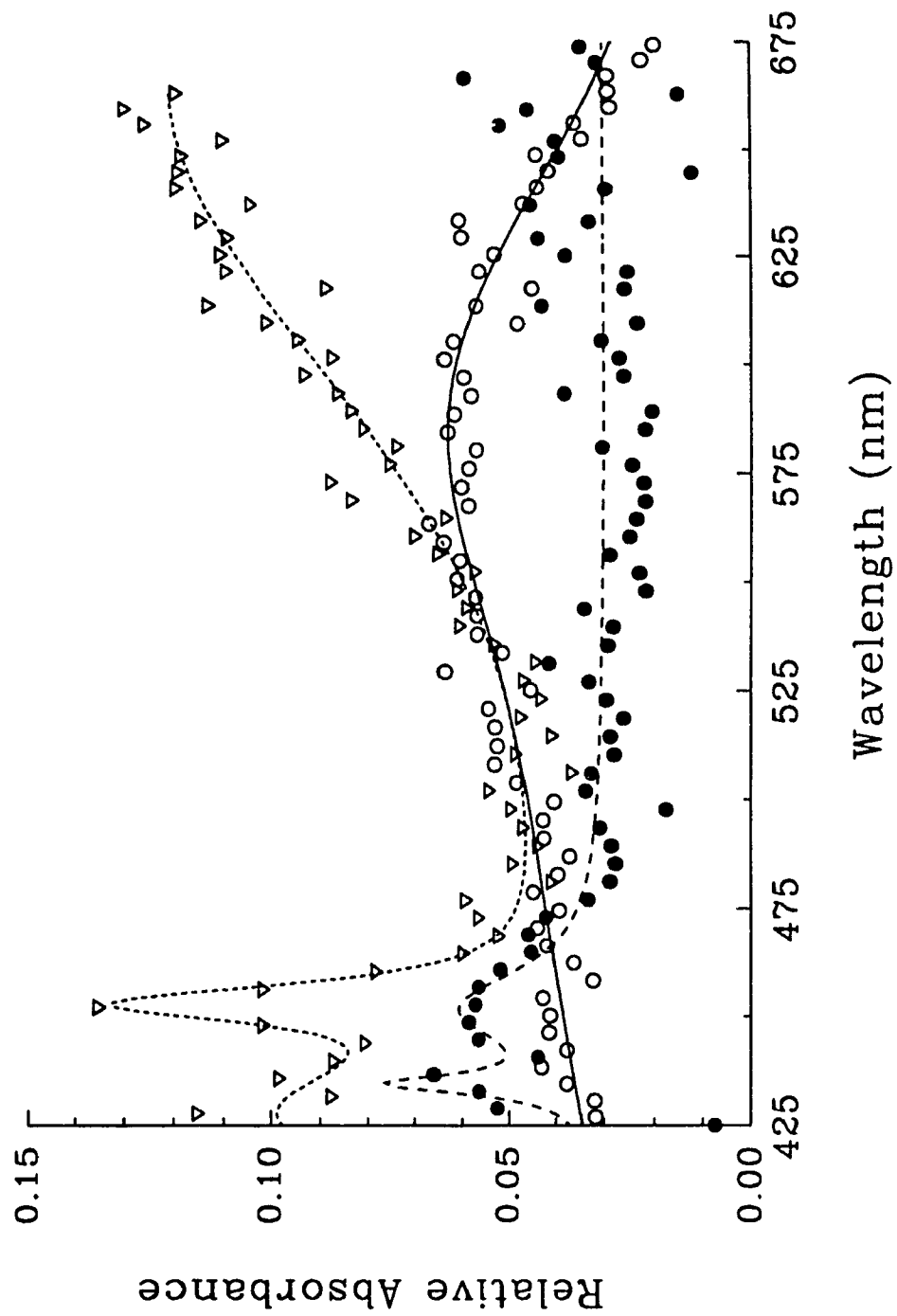
Fig. 6-17   ESA spectra of nitrobenzene in: (∇) AN, ($\bullet$) THF, and (O) H_2O at 100 ps, respectively.
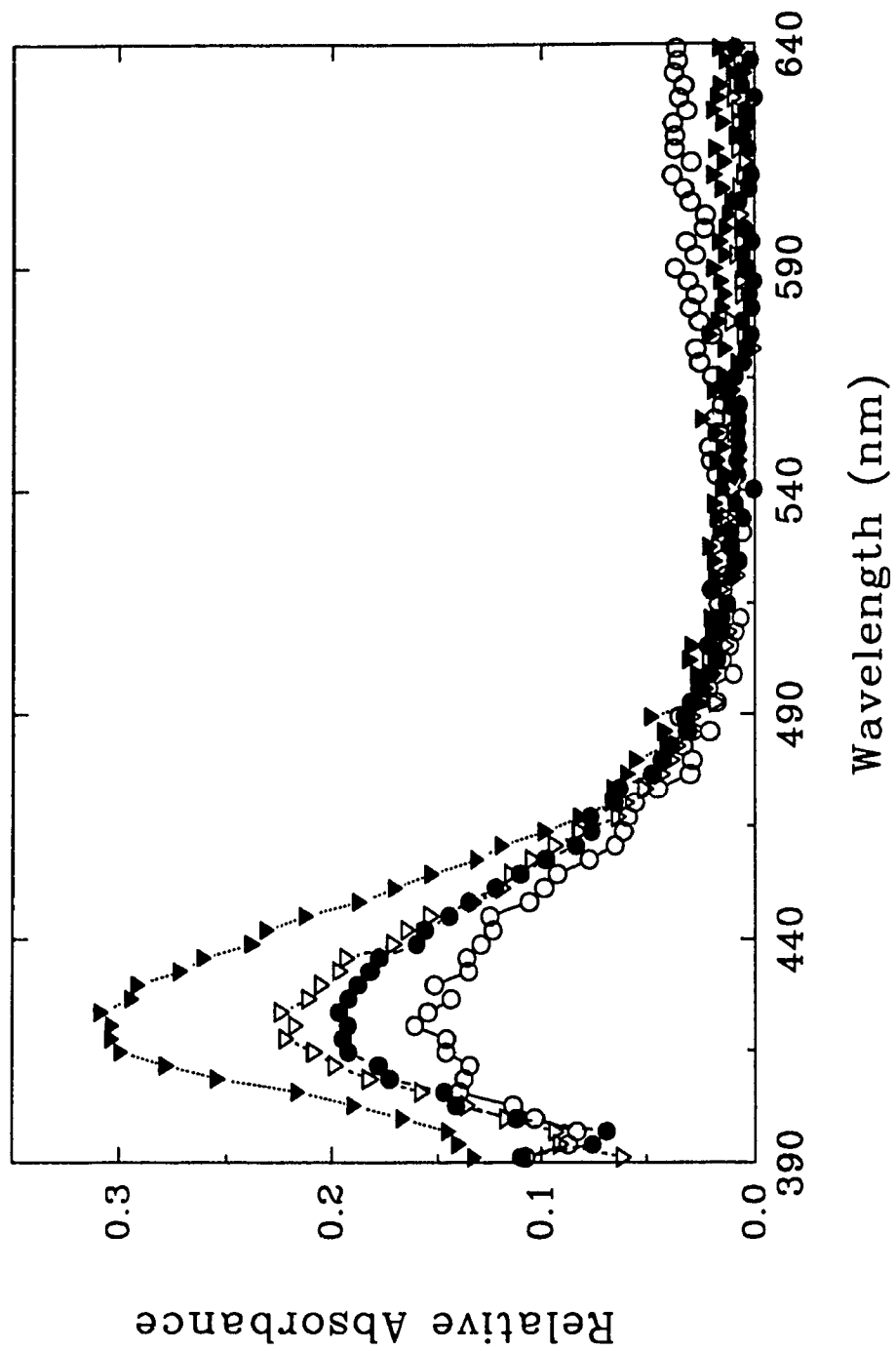
Fig. 6-18 Time-Resolved Transient Absorption Spectra 50 ps (O); 1 ns (●); 5 ns (▽) and 10 ns (▼), of ONBCPE in Acetonitrile; 2 mm path length cell.

quinonoid intermediate.[154] Thus the principle features of the transient absorption spectra are the following: (1) at picosecond times, two absorption bands: one at ~425 nm due to superimposed o-Q and T_1^* absorption, and the other at ~ 650 nm due to T_1^* absorption; (2) at times ≥ 10 ns, a single absorption band at ~ 425 nm due to o-Q.

In addition, a biradical route to o-Q via T_1^* (Scheme 6-2) should result in an *increase* absorption of the o-Q at ~ 425 nm at a rate identical with that of the decay of its biradical precursor. Experimentally, in the 400 ~ 500 nm region, we find what appears to be a single absorption band which gains in intensity from 1 to 10 ns (see Fig. 6-18) which is consistent with a triplet pathway in which o-Q is formed from the biradical. A similar observation has been reported for o-nitrobenzyl esters by Schnabel and co-workers.[212] The apparent shift in the baseline of the spectrum at 10 ns is an experimental artifact due to thermal lensing effect which appears at 8 ~ 10 ns after excitation. This was verified by flash excitation studies of the solution, of different solvents by themselves at different intensities.

6.5.1.2   Deconvolution of the ESA of ONBCPE in acetonitrile

(i)   ~425 nm band at 10 ns

To further analyze the band structure of the absorption in the ~425 nm region, we began by fitting the spectra at 10 ns to the function described by eq. (1), since there does not appear to be significant time-dependent between 8 and 10 ns. The fit should describe a single species due to o-Q. We obtained optimization of the band at 421±3 nm, and Cauchy and Gauss factors of B=0.012±0.005 and C=0.022±0.02, respectively from six ESA spectra.

(ii)   421 nm and 460 nm bands

Spectra corresponding to a delay time of 1 ns (Fig. 6-19) were next
selected for optimization with the 421 nm band position and band factors B and
C fixed to the previously optimized values. These spectra correspond to
absorption due to o-Q and possible the biradical. Contribution from the triplet
excited state is not expected to be significant because of its short lifetime (~300
ps, vide infra). Optimizations were carried out for different number of bands but
significant contribution were found only for bands at 421 nm and a new band at
460±17 nm optimized from seven ESA spectra. In the presence of 6-methyl-6-
(hydroxymethyl)-1,5-cyclohexadiene (CHD), a diene which is known to quench
the triplet lifetime of ONBCPE,[45] the amount of the 421 nm band at 10 ns was
reduced by ~40% compared with the band area from ONBCPE without the
quencher (Fig. 6-20). The quenching constant K (0.58 M^{-1}) can be obtained
from the slope of the straight line in the insert frame of Fig. 6-20.

**Table 6-9:   Optimized Fitting Parameters for Transient Absorption
Spectra Bands from ONBCPE in Acetonitrile[a]**

Delay time	Peak position (nm)	Gauss factor C	Cauchy factor B
50 ps	649±7 (4)	0.008±0.004	0.005±0.004
1 ns	460±17 (7)	0.014±0.005	0.0005±0.0005
10 ns	421±3 (6)	0.022±0.002	0.012±0.005

[a] Values in parentheses are the number of samples. The band shape Cauchy and Gauss factors
are defined in eq. (1).
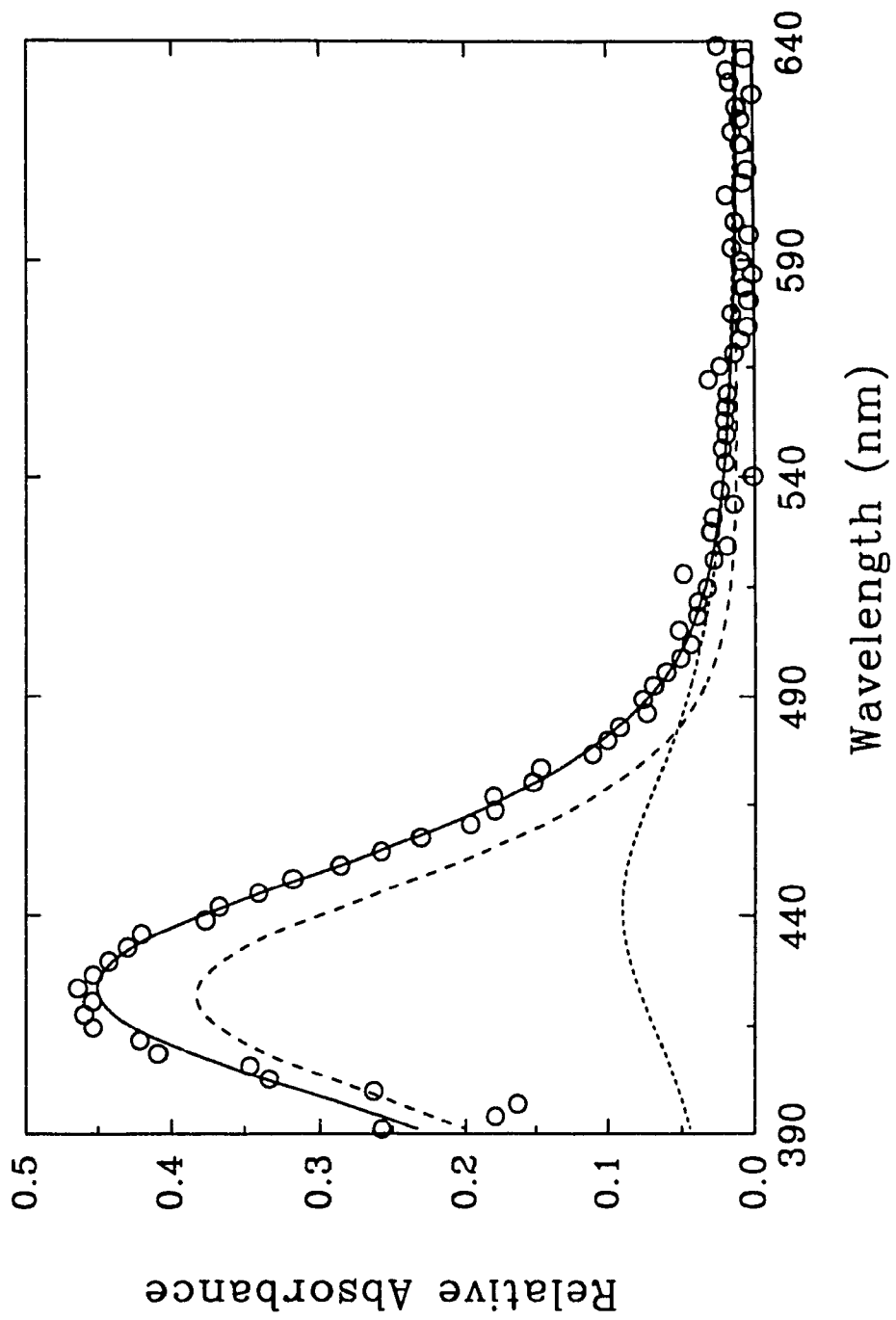
Fig. 6-19 Curve Fit of the **421** nm (dash) and **460** nm (dot) Transient Absorption Bands from ASE spectra (O) of ONBCPE in Acetonitrile at 1 ns.
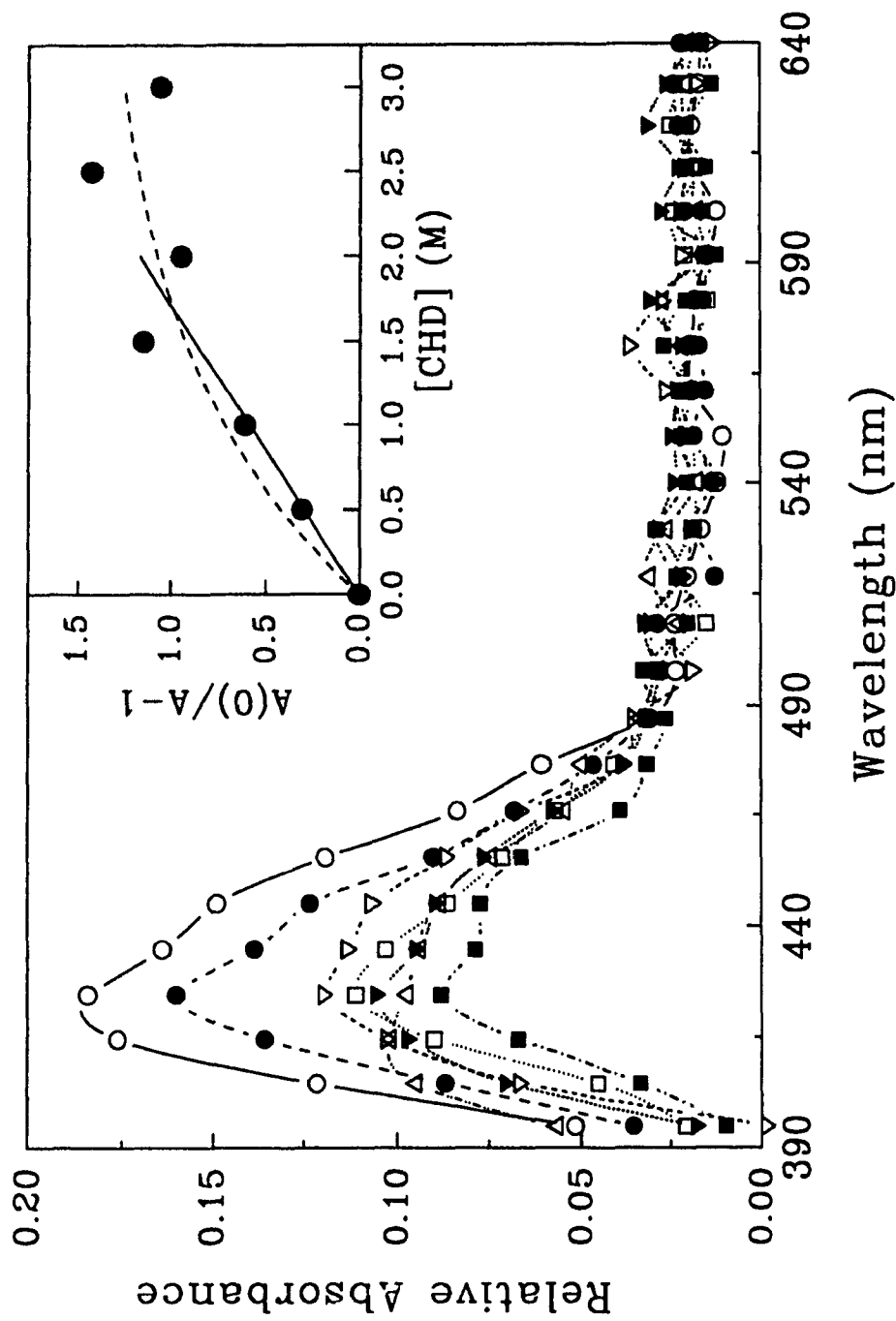
Fig. 6-20 Main frame: The ESA spectra of ONBCPE with (○) zero M; (●) 0.5 M; (▽) 1.0 M; (▼) 1.5 M; (□) 2.0 M; (■) 2.5 M; (△) 3.0 M of Triplet Quencher CHD in Acetonitrile at 10 ns. Insert frame: The transient absorption area ratio A(0)/A-1 vs. concentration of quencher whose first five points show linearly to [CHD] (sol'd line) and trend to saturate for the last four points (dash curve).

(iii)   ~ 650 nm Band

At times < 1 ns, we were unable to resolved a third band in the 400 ~ 450 nm wavelength region due to the triplet excited state.[45] The weakness of the absorption band at 460 nm and that of the T_1^* was, however, optimized at 649±7 nm from four ESA spectra. The optimization parameters for ESA of ONBCPE in acetonitrile are summarized in Table 6-9.

6.5.2   Kinetics

The absorption at the 460 nm band overlaps with that expected for a 'blue' band of the triplet excited state. Therefore, if the 460 nm band was due to the biradical derived from triplet and the two bands were similar in intensities, little or no absorption changes would result during decay of the triplet. However, as the o-quinonoid is formed from the biradical, decay of the 460 nm band is expected together with increase of the 421 nm band of the o-quinonoid. Kinetically, the intramolecular hydrogen abstraction from the triplet excited state leading to the o-quinonoid intermediate via the biradical can be represented by the series of two first-order reactions with rate constants k_1 and k_2 (see Scheme 6-2). Other competing reactions by T_1^* and BR, will reduce the yields of BR and o-Q (Γ_{BR} and $\Gamma_{o\text{-}Q}$, respectively) from the triplet excited state. The populations of the three species can be expressed by the following equations:[210]

$$\begin{cases} T_1^*(t) = \alpha_0 e^{-k_1 t} \\ BR(t) = \beta_{BR}\left(e^{-k_1 t} - e^{-k_2 t}\right) \\ o - Q(t) = o - Q(0) + \beta_{o\text{-}o}\left(1 + \frac{k_2 e^{-k_1 t} - k_1 e^{-k_2 t}}{k_1 - k_2}\right) \end{cases} \qquad (3)$$

217

where $\alpha_0 = T_1^*(0)$ is the yield of T_1^* at t=0; $\beta_{BR} = \Gamma_{BR}\alpha_0 k_1/(k_2-k_1)$; o-Q(0) is the initial concentration of the o-quinonoid from the singlet excited state; and $\beta_{o\text{-}Q} = \Gamma_{o\text{-}Q}\alpha_0$. In the case where the rate of decay of the triplet state is much greater than that for the formation of o-Q, ($k_1 \gg k_2$), decay of the biradical could be described by a single-exponential function. Therefore, eq. (3) can be simply expressed by:

$$
\begin{cases}
T_1^*(t) = \alpha_0 e^{-k_1 t} \\
BR(t) = \Gamma_{BR}\alpha_0 e^{-k_2 t} \\
o - Q(t) = o - Q(0) + \Gamma_{o\text{-}Q}\alpha_0\left(1 - e^{-k_2 t}\right)
\end{cases}
\tag{4}
$$

The area of the band component for the o-quinonoid (λ_{max}=421 nm) at different delay time was fitted to o-Q(t) of eq. (4) with minimization function σ^{**} using a modified Simplex optimization algorithm.[215] In all, 35 spectra from 7 sets were used for the global fit which gave a $1/k_2$ rise time of 7.7±1.2 ns. The areas of the T_1^* and the BR band components were substantially smaller than those of the o-Q. To reduce the random error for these weaker signals, the results for a given delay time from several sets were averaged. The fit of the results from 23 spectra for T_1^* to $T_1^*(t)$ of eq. (4) gave a $1/k_1$ decay time of 294±112 ps. The kinetics of the BR is expected to rise and decay according to BR(t) of eq. (4) with the same k_1 and k_2 as those obtained from the kinetic treatment of the o-Q and T_1^*. The calculated curve from eq. (3) and the experimental points (derived from 23 spectra) for the 460 nm band component

---

$$
\sigma^{**} = \sum_{i=1}^{n}\sqrt{\sum_{j=1}^{m_i}\left(\frac{n_i(t_j)-F(t_j)}{n_i(t_j)}\right)^2 \Big/ (m_i - 1)}
$$
, where ni(tj) is the jth data of the ith set; mi is the total number of data in the ith set; F(tj) is the optimized data for all sets at tj; and n is the total number of sets.

attributed to the BR, together with the results for the o-Q and the T_1^*, are shown in Fig. 6-21. These results support the assignment for the BR.

Table 6-10: Deconvolution Results of o-Nitrobenzyl Derivatives

Compound	Solv	λT_1^* (nm)	λ_{BR} (nm)	$\lambda_{o\text{-}Q}$ (nm)	τ_1 (ns)	τ_2 (ns)
ONBCPE	AN	649±7(4)	460±17(7)	421±3(6)	.29±.11(23)	7.7±1.2(35)
ONBPE	AN	653±5(2)	444	427±2	0.17	5
	THF	665±2	451±4	425±2	0.2	4±2
ONBAA	THF		449	420		
ONPEG	THF		482	429		

Similarly, the optimizations of ESA of ONBPE in acetonitrile and THF (not ONBAA in THF, ONPEG in THF) by eq. (1) offered some similar information as observed from ONBCPE in acetonitrile. The kinetic transition times were obtained by the same treatment as those of ONBCPE. The signals of BR band for ONBPE were so weak that it was hard to deconvolute the BR band from some sets of ESA spectra of ONBPE in acetonitrile, THF, and ONBCPE in THF. For both ONBAA, and ONPEG in THF, the signals of the triplet excited state were difficult to identify which were comparable to the noise. The uncompleted results of these o-nitrobenzyl derivatives in the two solvents listed in Table 6-10, were obtained from insufficient or uncompleted time-coverage numbers of
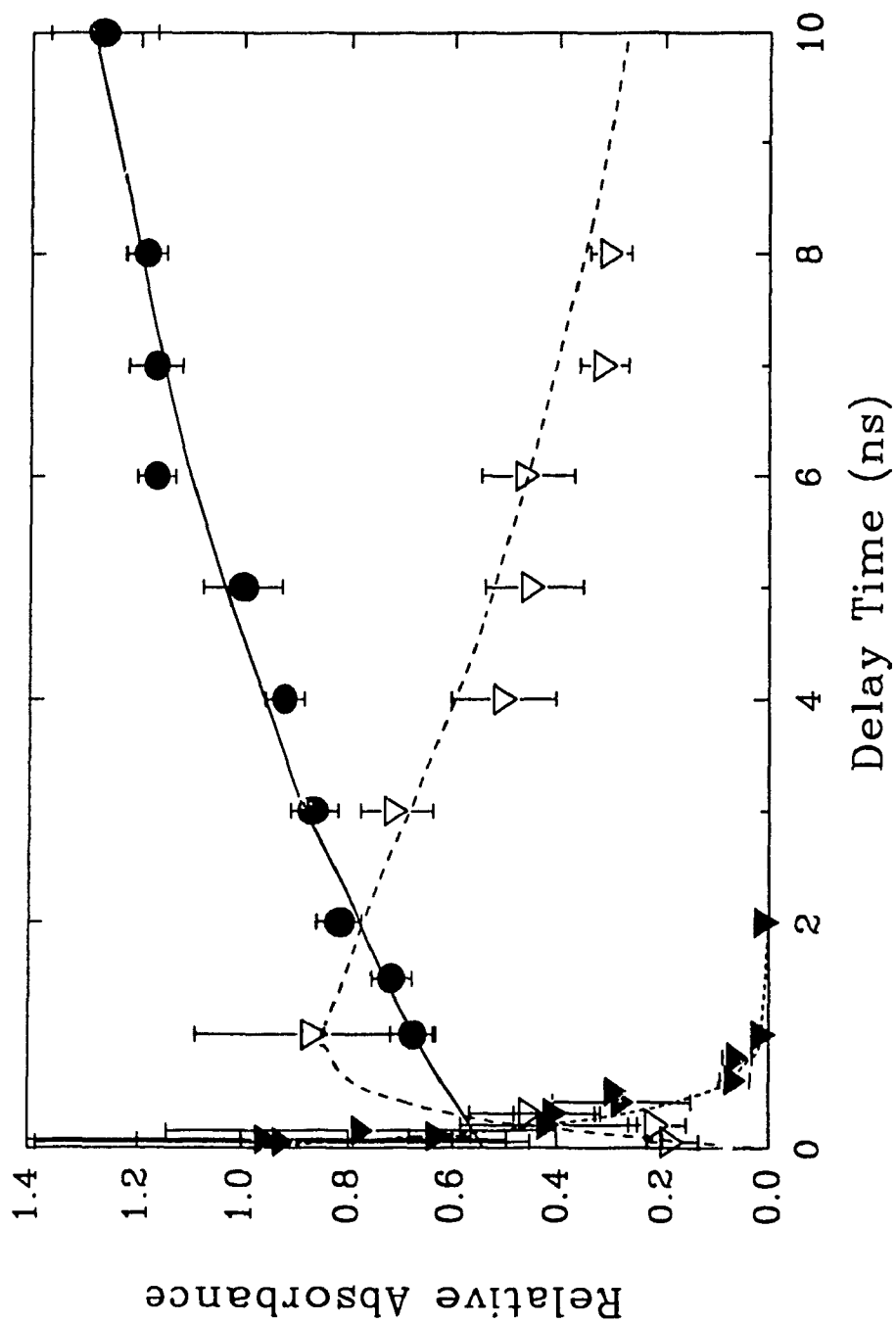
Fig. 6-21   Kinetics of the 649, 460, and 421 nm bands due to the Triplet Excited State, the Biradical, and the o-quinonoid intermediate, repectively. Eq. (3) was used to calculate three respective kinetic curves, with $k_1=3.4 \times 10^9$ s^{-1} and $k_2=0.13 \times 10^9$ s^{-1}. ($\bullet$) 649 nm T^* band; ($\triangledown$) 460 nm biradical band; ($\blacktriangledown$) 421 nm o-quinonoid band

spectra. The order of the band fit was the same as that for ONBCPE in acetonitrile.

6.5.3   Pumping energy effect

To eliminate the possibility that the 460 nm band was a consequence of nonlinear processes, the excitation energy Ep was varied to determine if there was a threshold energy, or a quadratic (Ep^2), or higher power, energy dependence for the 460 nm band. We obtained the relative band areas of ONBCPE in acetonitrile at 10 ns. Fig. 6-22 shows the linear relation between the area of 460 nm band and the excitation energy, excluding the highest excitation energy. The latter may originate from saturation, a diminution of the triplet lifetime due to triplet-triplet annihilation, or other effects; and in any event it is incompatible with an Ep^2 or higher power.

6.5.4   The yield of o-quinonoid formation

The yield of the o-quinonoid formed from singlet excited state (o-Q(0)) as a fraction of the total o-quinonoid (o-Q(∞)) formed can also be obtained from the kinetics. The value for o-Q(0) can be obtained by band fitting at 1ns, where the contribution due to absorption from T_1^* is negligible, and the value of o-Q(∞)) can be obtained from the plot of o-Q(t) of eq. (4). We obtained a value of o-Q(0)/o-Q(∞) = 0.43±0.05—that is , approximately 40 % of the o-quinonoid is formed from the singlet pathway. From the relative area obtained from the decay of the biradical and the rise of the o-quinonoid, we obtained a limiting value for the relative oscillator strengths f ($f = 4.139 \times 10^{-9} \int \varepsilon(\upsilon)d\upsilon$) of the two species, f_{o-Q}/f_{BR} ≥4.6±1.1. The inequality corresponds to a yield of the o-quinonoid from the biradical of < 1.
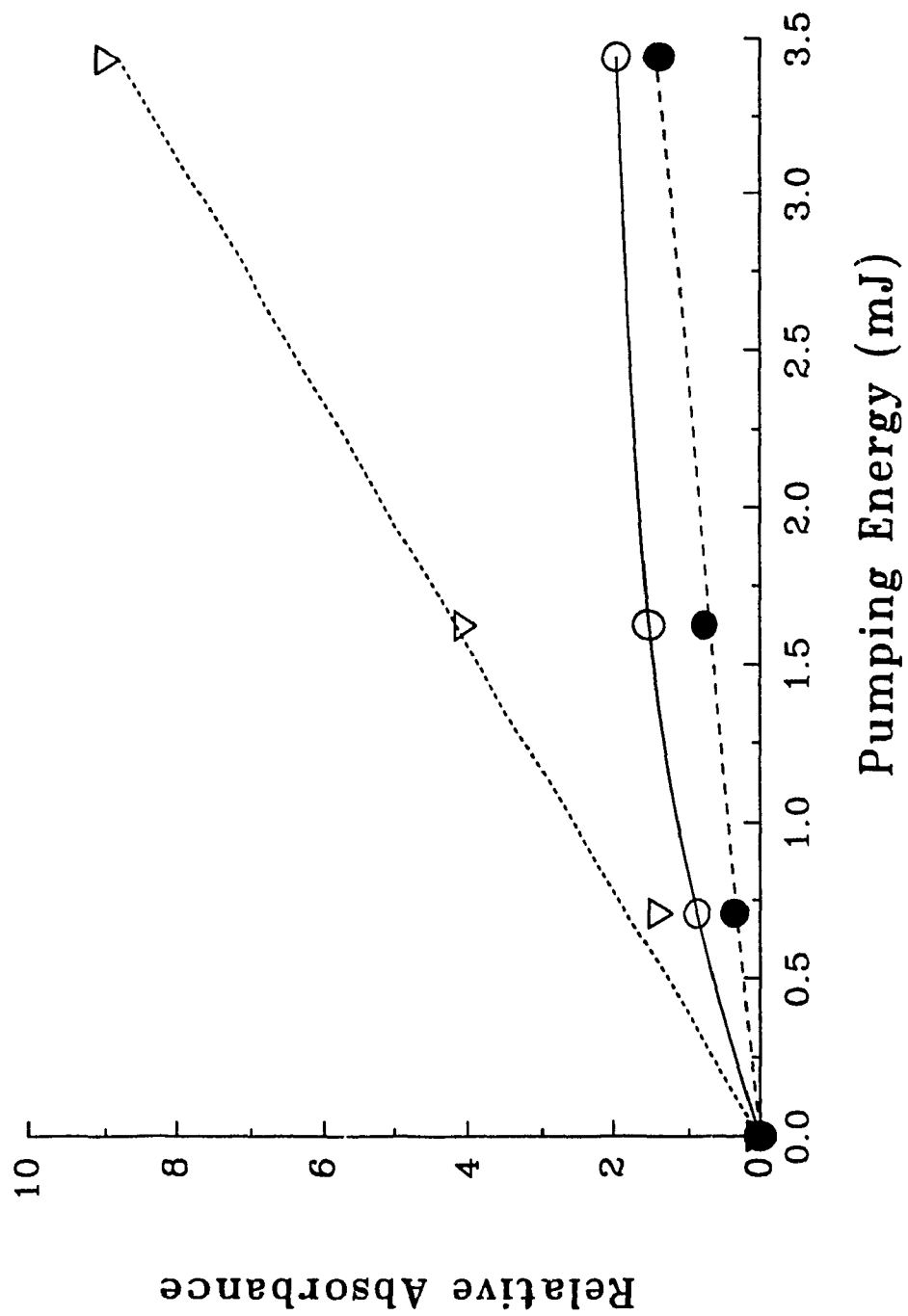
Fig. 6-22   The Transient Absorption Areas of Three Bands vs. Pumping Energy at 1 ns.   (∇) 649 nm T_1' Band; ($\bullet$) 460 nm Biradical Band; (O) 421 nm o-quinonoid Band.

6.6   Conclusion

6.6.1   Further studies

6.6.1.1   Solvation dynamics

The solvation correlated ESA shift provides an alternative method to study the solvation dynamics. The solvation dynamics should be systematically studied in various solvents to determine the scope of this method. Since the solvation relaxation is completed at subpicosecond or picosecond time scale, the femtosecond technique will be required to study the time-dependent *blue-shift* of ESA of these dimethoxynitrobenzenes in aprotic solvents, methanol, and water. Meanwhile, the effect of the viscosity, temperature (thermodynamics) studies can be also carried out.

The identification of the excited and ground state molecular recognition of 4NB15CW5 with metal ions has to be worked out. The *blue-shift* of the ESA of 4NB15CW5 with metal ions seems much slower than the solvation process, which would provide some information about the salt effect on the solvation dynamics. It can be identified by comparing the ESA spectra of these two compounds with and without addition of salts.

6.6.1.2   Alkylnitrobenzenes

For the ESA study of alkylnitrobenzenes, the following phenomena have not been verified. (1) The '*red*' ESA band could shift with (i) the position of substituents on the nitrobenzene ring, (e.g., λ_p (*p*NT) > λ_p (nitromesitylene) as listed in Table 6-4); (i) polarity of solvent. (2) The effect of hydroxyl group on substituents or in solvent, on ESA spectra. (3) The transient at short wavelengths is observed significantly in cyclohexane (Fig. 6-15) which is weak in

acetonitrile (Fig. 6-10) and is diminished in water (Fig. 6-14). The transient at short wavelengths could be real, and may be due to the *blue-shift* of the 'blue' band with solvent polarity. (4) The quantitative analysis of the twisting of NO_2 for these alkylnitrobenzenes, should provides clear evidence about its correlation to the trend of the ratio of the ESA band areas.

6.6.2   Conclusion

6.6.2.1   ESA of DMONB and 4NB15CW5

From the ESA results, the following important features are observed for both compounds. These are (1) decay of both ESA bands ('*blue*' and '*red*') in cyclohexane, and stable in the most solvents at nanosecond time scale; (2) quenching of these triplet ESA spectra with addition of 5-methyl-5(hydroxymethyl)-1,3-cyclohexadiene (CHD); (3) at nanosecond time scales, a quasi-static blue-shift of the '*red*' ESA band, not the '*blue*' band with increasing of solvent polarity; (4) in alcohols, a dynamic *blue-shift* of the '*red*' ESA band affected by two factors: polarity, viscosity; and (5) with addition of salts in solution, a slowly dynamic *blue-shift* of the '*red*' ESA band of 4NB15CW5 in acetonitrile at nanosecond time scale.

The energy diagram of these compounds in different solvents is schematically illustrated in Scheme 6-3. The triplet state characteristics of these ESA spectra has been confirmed by the quenching of both ESA bands with addition of CHD (No. **12** in Fig. 6-1). The lowest excited triplet state in less polar solvent (e.g., cyclohexane) contributes to the dual transient absorption bands with the same decay rate constant. The observation of a linear solvatochromic shift of the '*red*' ESA band (Fig. 6-5) in most solvents gives strong evidence of the charge transfer characteristics of the lowest excited state. It is stabilized by

224

the dipole-dipole interactions of the surrounding polar media. With increased solvent polarity, the drop in the energy of the CT state turns to be more significant than that for the lowest excited triplet state T_x and even to be lower than the T_x. Therefore, the CT characteristic '*red*' band shifts towards the short wavelength region due to the environment insensitive triplet state T_y. By contrast, the stable '*blue*' ESA band reflects that the upper excited triplet state T_z is more sensitive to the surrounding media. As a result, the transition energy between the CT state and the triplet state T_z does not change or only change slightly with solvent polarity. The preliminary test of the salt effect on ESA of 4NB15CW5 has been done, which shows excited state molecular recognition and salt effect on the solvation dynamics.

At subpicosecond time scale, the dynamic *blue-shift* of the '*red*' ESA band is observed. The shift time from the exponential fit of $C(t)$ is comparable to the longitudinal relaxation time of alcohol.[74,68] Such correlation to the dynamic solvation has been confirmed. No such time-dependent phenomenon has been reported. This observation implies an alternative method for studying the solvation dynamics using transient absorption technique.

6.6.2.2   ESA of alkylnitrobenzenes

Several significant observations can be drawn from the above ESA studies of alkylnitrobenzenes: (1) the ratio of two ESA band areas varies with (*a*) the position of *substituents* and (*b*) *solvent*; (2) the fine structure of the '*blue*' and/or the '*red*' ESA bands, reflects the excited state vibronic interaction of the benzene ring on the '*blue*' band, and the NO_2 group on the '*red*' band. The steric hindrance on the twisting of nitro group, could enhance the characteristics of locally excited NO_2 and relatively reduce the characteristics of localized

benzene ring. The structure (position of the substituent attached to the benzene ring) dependency of the ratio of two ESA band areas ($R=A_S/A_L$) posses the same trend as that of the ratio of the oscillator strength of the symmetric and asymmetric stretching of the amino group from infrared measurements.[106,201] Such agreement provides strong evidence of locally excited NO_2 characteristics of the 'red' ESA band as for p-nitroaniline,[148] but, not for aniline.[149] The effect of hydroxylic solvent on the ESA spectra could be due to the H-bonding between nitro group and media. This should be confirmed in further study.

6.6.2.3   Identification of biradical intermediate

From the transient absorption spectra of ONBCPE and some other derivatives, an absorption band at 460 nm has been resolved by CRVFIT. It has been assigned to the biradical BR (Scheme 6-2) on the basis of the kinetics of the biradical species and of the formation of the o-quinonoid intermediate o-Q absorbing at 421 nm, and is further supported by intensity and diene quenching experiments.   To our knowledge, this identification represents the first optical detection of the biradical intermediate in o-nitrobenzyl system.   These results also show that, in the case of ONBCPE, o-Q is formed from both the singlet as well as the triplet excited state, with approximately 40% of the total reaction originating from the singlet excited state.   The present and past[45] results on ONBCPE together with those of Schnabel and co-workers on the o-nitrobenzyl esters[208] establish that, at least in these two instances, dual singlet and triplet excited-state pathways are operative.   The generality of the phenomenon and the factors determining the partitioning of the two pathways remains to be investigated.

Appendix A: Derivation of ASE Gain from ASE Spectra

In laser physics, the intensity $I(\lambda)$ of the amplifed spontaneous emission ASE can be described by the gain coefficient $G(\lambda)$ and the width (L) of the amplification media in the form of:[29]

$$I(\lambda) = \frac{C}{G(\lambda)}\left(e^{G(\lambda)L} - 1\right) \tag{A.1}$$

where C is a wavelength dependent parameter including the instrumental response function which is independent to the excitation slit width and can be cancelled from the ratio of their ASE spectra with different excitation slit width. In order to obtain the gain spectrum, the ratio R of ASE intensities with partial and full excitation width are used in experiment. There are two cases being used in this project:

1.   With half of full width

In this case, the ASE intensity ratio R can be expressed by:

$$R = I_L(\lambda)\Big/ I_{1/2L}(\lambda) = \frac{e^{G(\lambda)L} - 1}{e^{G(\lambda)1/2L} - 1} = e^{G(\lambda)1/2L} + 1 \tag{A.2}$$

Therefore, the gain can be obtained as:

$$G(\lambda) = \frac{2}{L}\ln(R - 1) \tag{A.3}$$

2.   2/3 of full width

Similary, from eq. (A.1), the ASE intensity ratio R can be given in the form of:

$$R = I_L(\lambda)\Big/ I_{2/3L}(\lambda) = \frac{e^{G(\lambda)L} - 1}{e^{G(\lambda)2/3L} - 1} = \frac{X^3 - 1}{X^2 - 1} = \frac{X^2 + X + 1}{X + 1} \tag{A.4}$$

where $X = e^{1/3LG(\lambda)}$ can be solved from the following second order equation:

$$(X+1)R = X^2 + X + 1 \tag{A.5}$$

as a function of R. Thus, the gain coefficient can be expressed by the following relations:

$$X = e^{1/3LG(\lambda)} = \frac{1}{2}\left[R - 1 + \sqrt{(R-1)^2 + 4(R-1)}\right]$$

$$G(\lambda) = \frac{3}{L}\ln\left\{\frac{1}{2}\left[R - 1 + \sqrt{(R-1)^2 + 4(R-1)}\right]\right\} \tag{A.6}$$

Appendix B: Derivation of the Third Order Differential Equation

From eq. (18) of chapter 5, the population of B^* can be expressed in terms of the populations of A^* and C^* as below:

$$N_B(t) = \{N'_A(t) + X N_A(t)\}/k_{R1} \tag{B.1}$$

and the first derivative $N_B(t)$ in eq. (18) with respect to time is:

$$N'_B(t) = \{N''_A(t) + X N'_A(t)\}/k_{R1} \tag{B.2}$$

which should be equal to $N'_B(t)$ in eq. (18) as:

$$N'_B(t) = \{N''_A(t) + X N''_A(t)\}/k_{R1} = k_{F1}N_A(t) + k_{R2}N_C(t) - Y N_B(t) \tag{B.3}$$

where the population $N_B(t)$ can be replaced by eq. (B.1) as:

$$\{N''_A(t) + X N''_A(t)\}/k_{R1} = k_{F1}N_A(t) + k_{R2}N_C(t) - Y \{N'_A(t) + X N_A(t)\}/k_{R1} \tag{B.4}$$

By rearrangment of eq. (B.3), the population of C^* can be expressed by:

228

$$N_C(t) = \{[N''_A(t) + X\, N'_A(t)]/k_{R1} - k_{F1}N_A(t) + Y\, [N'_A(t) + X\, N_A(t)]/k_{R1}\}/k_{R2}$$

$$= [\, N''_A(t) + (X+Y)N'_A(t) + (XY - k_{R1}k_{F1})N_A(t)\,] / (k_{R1}k_{R2}) \qquad (B.5)$$

Similarly, we can get

$$N'_C(t) + Z\, N_C(t) = [\, N'''_A(t) + (X+Y)N''_A(t) + (XY - k_{R1}k_{F1})N'_A(t)\,]/(k_{R1}k_{R2})$$

$$+ Z\, [\, N''_A(t) + (X+Y)N'_A(t) + (XY - k_{R1}k_{F1})N_A(t)\,]/(k_{R1}k_{R2})$$

$$= k_{F2}N_B(t) = \{N'_A(t) + X\, N_A(t)\}k_{F2}/k_{R1}. \qquad (B.6)$$

and

$$[\, N'''_A(t) + (X+Y)N''_A(t) + (XY - k_{R1}k_{F1})N'_A(t)\,]/k_{R2}$$

$$+ [\, N''_A(t) + (X+Y)N'_A(t) + (XY - k_{R1}k_{F1})N_A(t)\,]/k_{R2}$$

$$= \{N'_A(t) + X\, N_A(t)\}k_{F2} \qquad (B.7)$$

$$N'''_A(t) + (X+Y+Z)N''_A(t) + [XY + (X+Y)Z - k_{R1}k_{F1} - k_{F2}k_{R2}]N'_A(t)$$

$$+ [\, (XY - k_{R1}k_{F1})Z - X\, k_{F2}k_{R2}\,]N_A(t) = 0 \qquad (B.8)$$

or

$$N'''_A(t) + \alpha N''_A(t) + \beta N'_A(t) + \gamma N_A(t) = 0 \qquad (B.9)$$

where $X = k_a + k_{F1}$; $Y = k_b + k_{R1} + k_{F2}$; $Z = k_c + k_{R2}$

$$\alpha = X + Y + Z = k_a + k_{F1} + k_b + k_{R1} + k_{F2} + k_c + k_{R2}$$

$$\beta = XY + (X+Y)Z - k_{F1}k_{R1} - k_{F2}k_{R2} = k_ak_b + k_bk_c + k_ck_a + k_{F1}k_{F2}$$

$$\gamma = (XY - k_{F1}k_{R1})Z - Xk_{F2}k_{R2}$$

$$= k_ak_bk_c + k_c(k_ak_{F2} + k_bk_{F1} + k_ck_{R1} + k_{F1}k_{F2}) + k_{R2}(k_ak_b + k_bk_{F1} + k_ck_{R1})$$

REFERENCES

1. Jablonski, A., *Z. Phys.*, **1935**, *94*, 38.

2. Mulliken, R. S.; Person, W. B., *Ann. Rev. Phys. Chem.*, **1962**, *13*, 107.

3. a) Bennett, R. G.; Kellogg, R. E., in *Progress in Reaction Kinetics*, Pergamon, London, **1967**, *4*, 217. b) Wagner, P. J.; Kochevar, I., *J. Am. Chem. Soc.*, **1968**, *90*, 2232. c) Balzani, V.; Bolletta, F.; Scandola, F., *J. Am. Chem. Soc.*, **1980**, *102*, 2152. d) Carmichael, I.; Hug, G. L., *J. Phys. Chem. Ref. Data*, **1986**, *15*, 1.

4. Michl, J.; Bonacic-Koutechy, V., *Electronic Aspects of Organic Photochemistry*, Interscience, New York, **1990**.

5. a) Lippert, E., *Z. Naturforsch*, **1955**, *10a*, 541. b) Mataga, N.; Kaifu, Y.; Koizumi, M., *Bull. Chem. Soc. Jpn.*, **1955**, *28*, 690. c) Mataga, N.; Kubota, T., *Molecular Interactions and Electronic Spectra*, Marcel Dekker, New York, **1970**. d) Lippert, E., *Z. Naturforsch. Teil*, **1955**, *10*, 541.

6. a) Reichardt, C. *Solvents and Suivent Effects in Organic Chemistry*, VCH Verlagsgesellschaft mbH, Weinheim, **1988**, 359. b) Suppan, P., *J. Photochem. & Photobiol.*, **1990**, *A50*, 293.

7. Burgess, C.; Knowles, A., *Standards in Absorption Spectrometry*, Chapman and Hall, London, **1981**.

8. Miller, J. N., *Standards in Fluorescence Spectrometry*, Chapman and Hall, London, **1981**.

9. Wehry, E. L., *Modern Fluorescence Spectroscopy*, **1981**, *3*.

10. Lakowicz, J. R.; *Principles of Fluorescence Spectrosocpy*, Plenum, New York, **1983**.

11. Schäfer, F. P., *Dye Lasers*, Springer-Verlag, Berlin, **1977**.

12. Maeda, M., *Laser Dyes*, Academic, Tokyo, **1984**.

13. Weller, A., in *Progress in Reaction Kinetics,* Porter, G.; Stevens, B.; Phil., D., eds., **1961**, *1*, 189.

14. Birks, J. B., *Photophysics of Aromatic Molecules,* Interscience, London, **1970**.

15. Yip, R. W.; Wen, Y. X., *Can. J. Chem.,* **1991**, *69*, 1413.

16. Yip, R. W.; Wen, Y. X., *Can. J. Chem.,* **1991**, *69*, 2142.

17. Georghiou, S., in *Reference 9.*

18. Weinryb, I.; Steiner, R. F. *"The Luminescence of the Aromatic Amino Acids",* in *Excited States of Proteins and Nucleic Acids,* Steiner, R. F.; Weinryb, I.; eds. Plenum Press, New York, **1971**, chapt.5.

19. Guilbault, G. G., *Practical Fluorescence,* 2nd., Marcel Dekker, New York, **1990**.

20. Lumry, R.; Hershberg, M. *Photochem. Photobiol.,***1978**, *27*, 819.

21. Skalski, B.; Rayner, D. M.; Szabo, A. G. *Chem. Phys. Lett.,* **1980**, 170, 587.

22. Eaton, D. F., *Tetrahedron,* **1987**, *43*, 1551.

23. Scypinski, S.; Drake, J. M. *J. Phys. Chem.,* **1985**, *89*, 2432.

24. Zhang, X.; Chen, J.; Wan, C.; Liu, L.; Xu. G.; Tang, Y., *Wuli Huaxue Xuebao* (in Chinese), **1986**, *2*, 493 (CA. 106: 110372n).

25. Patonay, G.; Shapira, A.; Diamond, P.; Warner, I. M., *J. Phys. Chem.,* **1986**, *90*, 1963.

26. Abdel Mottaleb, M. S. A.; Antonious, M. S.; Abo-Aly, M. M.; Ismaiel, L. F. M.; EL-Sayed, B. A.; Sherief, A. M. K. *J. Photochem. Phtotobiol.,* **1989**, *A 50*, 259.

27. Aloisi, G. G.; Eliser, F. *J. Phys. Chem.,* **1990**, *94*,5813.

28. Silfvast, W. T.; Deech, J. S. *Appl. Phys. Lett.,* **1967**, *11*,, 97.

29. a) Shank, C. V.; Dienes, A.; Silfvast, W. T. *Appl. Phys. Lett.,* **1970**, *17*, 307. b) Shank, C. V. *Rev. Mod. Phys.,* **1975**, *47*, 649.

30. Ganiel, U.; Hardy, A.; Neumann, G.; Treves, D., *IEEE J. Quan. Electron.* **1975**, *QE-11*, 881.

31. a) Nair, L. G. *Prog. Quant. Electr.*, **1982**, *7*, 153. b) Duarre, F. J.; Hillman, L. W., *Dye Laser Principle with Application*, Academic, Boston, **1990**.

32. Marowsky, G.; Tittel, F. K.; Wilson, W. L.; Frenkel, E. *Appl. Opt.*, **1980**, *19*, 38.

33. Chou, P.; McMorrow, D.; Aartsma, T. J.; Kasha, M. *J. Phys. Chem.*, **1984**,*88*, 4596.

34. Fabeni, P.; Linari, R.; Pazzi, G. P.; Ranfagni, A. *Appl. Opt.*, **1987**, *26*, 5317.

35. Heldt, J.; Heldt, J. R.; Szczepanski, J.; Diehl, H. A. *Appl. Phys.*,**1988**,*B 46*, 339.

36. a) Masilamani, V.; Sivaram, B. M. *J. Lumin.*, **1982**, *27*, 137. b) Masilamani, V.; Chandrasekar, V.; Sivaram, B. M.; Sivasankar, B.; Natarajan, S. *Opt. Commun.*, **1986**, *59*, 203. c) *Opt. Commun.*, **1987**, *62*, 389. d) Ramalingam, A.; Palanisamy, P. K.; Masilamani, V.; Sivaram, B. M. *J. Photochem. & Photobiol.*, **1989**, *A 49*, 89.

37. a) Norrish, R. G. W.; Porter, G., *Nature*, **1949**, *164*, 658. b) Porter, G., *Proc. Roy. Soc. (London) A.*, **1950**, *200*, 284.

38. Hilinski, E. F.; Rentzepis, P. M., *Acc. Chem. Res.*, **1983**, *16*, 224.

39. Yip, R. W.; Koppi-Tommola, J., *Rev. Chem. Intermediates*, **1985**, *6*, 33; and References cited therein.

40. Demas, J. N., *Excited State Lifetime Measurements*, Academic, New York, **1983**.

41. a) Cundall, R. B.; Dale, R. E., eds., *Time-Resolved Fluorescence Spectroscopy in Biochemistry and Biology*, Plenum, New York, **1983**. b) Ware, W. R., in *Photochemistry in Organized and Constrained Media*, Ramamurthy, V. ed., VCH, New York, **1991**, 563.

42. O'Connor, D. V.; Phillips, D., *Time-correlated Single Photon Counting*, Academic, London, **1984**.

43. a) Cavabagh, R. R.; Beckerle, J. D.; Casassa, M. P.; Heilweil, E. J.; Stephenson, J. C., in *Picosecond and Femtosecond Spectrosocpy from*

Laboratory to Real World, **1990**, *SPIE 1209,* 86. b) Laubereau, A.; Kaiser, W., *Rev. Modern Phys.,* **1978**, *50,* 608.

44. a) Mataga, N., in *Photochemical Processes in Organic Molecular Systems* Honda, K. ed., North-Holland, Amsterdam, **1991**, 3. b) Lu, P. Y.; Yu, Z. X.; Alfano, R. R.; Gersten, J. I., *Phys. Rev. A.,* **1982**, *26,* 3610.

45. Mathries, R. A.; Brito Cruz, C. H.; Polland, W. T.; Shank, C. V., *Science,* **1988**, *240,* 777.

46. a) Zewail, A. H.; Bernstein, R. B., *Chem. & Engin. New,* **1988**, *Nov. 7.* b) Dantus, M.; Rosker, M. J.; Zewail, A. H., *J. Chem. Phys.,* **1988**, *89,* 6128. c) Simon, J. D.; Peters, K. S., *Acc. Chem. Res.,* **1984**, *17,* 277.

47. Yip, R. W.; Sharma, D. K.; Giasson, R.; Gravel, D., *J. Phys. Chem.,* **1985**, *89,* 5328.

48. Eisenthal, K. B., *Ann. Rev. Chem. Phys.,* **1977**, *28,* 207.

49. Ohtani, H.; Lobayashi, T.; Suzuki, K.; Nagakura, S., *Bull. Chem. Soc. Jpn.,* **1980**, *53,* 43.

50. Kenney-Wallace, G. A., in *Laser Applications in Physical Chemistry,* Evans, P. K. ed., Marcel Dekker, New York, **1989**, 377.

51. a) Williams, L. R.; Nelson, K. A., *J. Chem. Phys.,* **1988**, *87,* 7346. b) Miyasaka, H.; Masuhara, H.; Mataga, N., *Laser Chem.,* **1983**, *1,* 357.

52. a) Sharma, D. K.; Yip, R. W.; Williams, D. F.; Sugamori, S. E.; Bradley, L. L. T., *Chem. Phys. Lett.,* **1976**, *41,* 460. b) Sharma, D. K.; Yip, R. W., *Opt. Commun.,* **1979**, *30,* 113. c) Sala, K. L.; LeSage, R.; Yip, R. W., *Appl. Spectro.,* **1984**, *38,* 87.

53. a) Chakrabarti, S. K.; Ware, W. R., *J. Chem. Phys.,* **1971**, *55,* 5494. b) Ware, W. R., in *Creation and Detection of the Excited State,* Lamolar, A. A., ed., Marcel Dekker, New York, **1971**, *IA,* 2130

54. Wang, Y.; Eisenthal, K. B., *J. Chem. Phys.,* **1982**, *77,* 6076.

55. Declemy, A.; Rulliere, C.; Kottis, Ph., *Chem, Phys. Lett.,* **1983**, *101,* 401.

56. Blanckard, G. J., *J. Phys. Chem.,* **1988**, *92,* 6303.

57. Maroncelli, M.; Fleming G. R., *J. Chem. Phys.,* **1987**, *86,* 6221.

58   Barbara, P.: Jarzeba, W., *Adv. Photochem.*, **1990**, *15*, 1.

59.   Pena, A. M. de la; Ndou, T. Zung, J. B.; Warner, I. M., *J. Phys. Chem.*, **1991**, *95*, 3330; and References cited therein.

60.   a) Jobe, D. J.; Verrall, R. E.; Palepu, R.; Reinsborough, V. C., *J. Phys. Chem.*, **1988**,*92*, 3582. b) Huang, H. F.; Bright, F. V., *J. Phys. Chem.*, **1990**, *94*, 8475. c) Bright, F. V.; Catena, G. C.; Huang, H. F., *J. Am. Chem. Soc.*, **1990**, *112*, 1343. d) Zhang, J.; Bright, F. V., *J. Phys. Chem.*, **1991**, *95*, 7900.

61.   a) Yamazaki, I.; Winnik, F. M.; Winnik, M. A.; Tazuke, S., *J. Phys. Chem.*, **1987**, *91*, 4213. b) Alcala, J. R.; Gratton, E.; Prendergast, F. G., *Biophys. J.*, **1987**, *51*, 925.

62.   Berberan-Santos, M. N.; Prieto, M. J. E.; Szabo, A. G., *J. Phys. Chem.*, **1991**, *95*, 5471.

63.   Zuker, M.; Szabo, A. G.; Bramall, L.; Krajcarski, D. T.; Selinger, B., *Rev. Sci. Instrum.*, **1985**, *56*, 14.

64.   Calef, D. F.; Wolynes, P. G., *J. Chem. Phys.*, **1983**, *78*, 4145.

65.   van der Zwan, G.; Hynes, J. T., *J. Phys. Chem.*, **1985**, *89*, 4181.

66.   Bagchi, B. *Ann. Rev. Phys. Chem.*, **1989**, *40*, 115.

67.   Kosower, E.M.; Huppert, D. *Ann. Rev. Phy. Chem.* **1986**, *37*, 127.

68.   a) Simon, J.D. *Acc. Chem. Res.* **1988**, *21*, 128; b) Peggy, A. T.; Simon, D.; Desai, M. A.; Good, W. R.; Silvers, C. D.; Moog, R. S., *Picosecond and Femtosecond Spectroscopy from Laboratory to Real World*, SPIE, **1990**, *1209*, 2.

69.   Maroncelli, M.; MacInnis, J.; Fleming, G.R. *Science* **1989**, *243*, 1674

70.   a) Weaver, M. J.; McManis III, G. E. *Acc. Chem. Res.*, **1990**, *23*, 294;

       b) Weaver, M. J., *Chem. Rev.*, **1992**, *92*, 463.

71.   a) Bakhshiev, N. G. *Opt. Spectrosc.*, **1965**, *19*, 196 ; b) Bakhshiev, N.G.; Mazurenko, Y.T.; Piterskaya, I.V. *Opt. Spectry.* **1966**, *21*, 307; c) Mazurenko, Y. T.; Bakhshiev, N. G. *Opt. Spectry.*, **1970**, *28*, 490; d) Mazurenko, Y. T.; Udaltsov, V. S. *Opt. Spectry.*, **1978**,*44*, 417; e) *Opt. Spectry.*, **1978**, *48*, 756.

72. Nagarajan, V.; Berarley, A. M.; Tong, T. J.; Babara, F. P. *J. Chem. Phys.,* **1987,** *86,* 3183.

73. Knutson, R.; Walbridge, D. G.; Brand, L. *Biochemistry,* **1982,***21,*4671.

74. Davenport, L; Knutson, J. R.; Brand, L. *Biochemistry,* **1986,** *25,* 1186.

75. Yip, R. W.; Wen, Y. X.; Szabo, A. G. *J. Phys. Chem.,* submitted.

76. Yip, R. W.; Wen, Y. X., *J. Int. Chem. Kinetics,* submitted.

77. Szabo, A. G.; Yamashita, S. in *Fluorescent Biomolecules,* eds. Jansen, D.; Reichardt, C. Plenum, **1989,** 406.

78. Willis, K.J.; Szabo, A.G.; Drew, J.; Zuker, M.; Ridgeway, J.M. *Biophys. J.* **1990,** *57,* 183.

79. Weber, G., *Biochem.* **1979,** *18,* 3075

80. Macgregor, R. B.; Weber, G., *Nature,* **1986,** *319,* 70.

81. Seliskar, C. J.; Brand, L., *J. Am. Chem. Soc.,* **1971,** *93,* 5414.

82. Detoma, R. P.; Brand, L., *Chem. Phys. Lett.,* **1977,** *47,* 231.

83. Bismuto, E.; Jameson, D. M.; Gratton, E., *J. Am. Chem. Soc.,* **1987,** *109,* 2354.

84. Lakowicz, J., in *Principles of fluorescence spectroscopy,* Plenum, New York, **1983,** chapt. 7.

85. Kosower, E. M.; Kanety, H., *J. Am. Chem. Soc.,* **1983,** *105,* 6236.

86. Rettig, W., *Appl. Phys.,* **1988,** *B45,* 145.

87. Jones, II, W.; Jackson, W. R.; Kanoktanaporn, S.; Halpern, A. M., *Optics Comm.,* **1980,** *33,* 315.

88. Jones, II, W.; Jackson, W. R.; Halpern, A. M., *Chem. Phys. Lett.,* **1980,** *72,* 391.

89. Drexhage, K. H., in *Reference 11.*

90. Jones II, G.; Jackson, W. R.; Choi, C.-Y.; Bergmark, W. R., *J. Phys. Chem.,* **1985,** *89,* 294.

91. Krasovitskii, B. M.; Bolotin, B. M., *Organic Luminescence Materials,* VCH, Weinheim, **1988.**

92. Nag, A.; Chakrabarty, T.; Bhattacharyya, K., *J. Phys. Chem.*, **1990**, *94*, 4203.

93. Nag, A.; Bhattacharyya, K., *Chem. Phys. Lett.*, **1990**, *169*, 12.

94. Rettig, W.; Klock, A. *Can. J. Chem.*, **1985**, *63*, 1649.

95. Mohan, D.; Taneja, L.; Gaur, A.; Sharma, A. K.; Singh, R. D., *J. Lumin.*, **1991**, *50*, 127.

96. Bowden, M. J., in *Materials for Microlithography*, Tompson, L. F.; Willson, C. G.; Frechet, J. M. J., eds. ACS Symposium Series, Washington, **1984**. *v.226*, 39.

97. Braun, A. M., *Photochemical Conversions*, International Organization for Chemical Science in Development, UNESCO, Presses Polytechniques Romandes, Lausanne, **1983**.

98. Rebek, J. F., *Experimental Methods in Photochemistry and Photophysics*, Part 2, Wiley, Chichester, **1982**.

99. Cowley, D. J., *Nature*, **1986**, *319*, 14.

100. Yip, R. W.; Wen, Y. X. *J. Photochem. Photobiol.*, **1990**, *A 54*, 263.

101. Lippert,E.; Rettig, W.; Bonacic-Koutecky, V.; Heisel, F.; Miehe, J. A., *Adv. Chem. Phys.*, **1987**, *68*, 1.

102. Grabowski, Z. R.; Rotkiewicz, K.; Siemiarczuk, A.; Cowley, D. J.; Baumann. W. *Nouv. J. Chimie*, **1979**, *3*, 443. and references cited therein.

103. Rettig, W. *Angew. Chem. Int. Ed. Engl.* **1986**, *25*, 971.

104. a) Döpp, D. O., *Topics in Current Chemistry*, **1975**, *55*,51. b) Feuer, H.; Nielsen, A. T., *Nitro Compounds*, VCH, New York, **1990**.

105. Morrison, H. A., in *The Chemistry of Nitro and Nitroso Groups*,Feuer, H., Ed.; Interscience, New York, **1969**, Part I, Chapt. 4, p. 164.

106. Rao, C. N. R., in *The Chemistry of Nitro and Nitroso Groups*, Feuer, H., Ed.; Interscience, New York, **1969**, Part I, Chapt. 2, p.80.

107. Eaton, D. F., *Science*, **1991**, *253*, 281.

108. a) Nicoud, J. F.; Twieg, R. J., in *Nonlinear Optical Properties of Organic Molecules and Crystals*, Chemla, D. S.; Zyss, J., Eds., Academic Press, Orlando, **1987**, *1*, Chapt. II-3, p. 227. b) Rettig, W., *Appl. Phys.*, **1988**, *B45*,145.

109. Bergmark, W. R.; Davis, A.; York, Clayton, Macintosh, A.,; Jones II, G., *J. Phys. Chem.*, **1990**, *94*, 5020.

110. a) Schneider, H. J., *Angew. Chem. Int. Ed. Engl.*, **1991**, *30*, 1417, and references cited therein. b) Rebek, Jr. J., *Angew. Chem. Int. Ed. Engl.*, **1990**, *29*, 245, and references cited therein.

111. Vögtle, F., *Supramolecular Chemistry*, Wiley, Chichester, **1991**.

112. Lehn, J. M., *Angew. Chem. Int. Ed. Engl.*, **1988**, *27*, 89.

113. Inoue, Y.; Gokel, G. W., Eds., *Cation Binding By Macrocycles (Complexation of Cationic Species by Crown Ether)*, Marcel Dekker, New York, **1990**.

114. *Biominetic and Bioorganic Chemistry*, a) Boschke, F. L., Ed., part I: *Top. Curr. Chem.*, **1985**, *128;* b) Vögtle, T.; Webber, E., Eds., part II: *ibid*, **1986**, *132;* c) Vögtle, T.; Webber, E., Eds., part III: *ibid*, **1986**, *136*.

115. Patai, S.; Rappopont, Z., Eds., *Crown Ethers and Analogs*, Wiley, Chichester, **1989**.

116. D'Souze, V. T.; Bender, M. L., *Acc. Chem. Res.*, **1987**, *20*, 146.

117. a) Diederich, F., *Angew. Chem. Int. Ed. Engl.*, **1988**, *27*, 362. b) Schneider, H. J.; Blatter, T., *Angew. Chem. Int. Ed. Engl.*, **1988**, *27*, 1163.

118. Schurig, V.; Nowotny, H. P., *Angew. Chem. Int. Ed. Engl.*, **1990**, *29*, 939, and references citied therein.

119. Mertes, M. P.; Bowman, K.; Mertes, K. B., *Acc. Chem. Res.*, **1990**, *23*, 413, and references citied therein.

120. *Host-Guest Molecular Interactions: From Chemistry to Biology.* (Ciba Foundation symposium *158*), Wiley, Chichester, **1991**.

121. Kimura, K.; Yamashita, T.; Yokoyama, M., *J. Phsy. Chem.*, **1992**, *96*, 5614.

122. Bourson, J.; Borrel, M. N.; Valeur, B., *Analy. Chim. Acta.,* **1992,** *257,* 189.

123. Valeur, B.; Pouget, J.; Bourson, J., *J. Lumin.,* **1992,** *52,* 345.

124. Wasielewski, M. R., *Chem. Rev.,* **1992,** *92,* 435.

125. Alaprie, J. P.; Vo-Dinh, T., *Talanta,* **1991,** *38,* 529.

126. Ueno, A.; Kuwabara, T.; Nakamura, A.; Toda, F., *Nature,* **1992,** *356,* 136.

127. Bend, M. L.; Komiyama, M., *Cyclodextrin Chemistry,* Springer-Verlag, Berlin, **1978.**

128. Saenger, W., in *Inclusion Compounds, 2,* Atwood, J. L.; Davies, J. E.; MacNicol, D. D., eds., Academic, London, **1984,** Chapter 8.

129. Bhone, C.; Barra, M.; Boch, R.; Abuin, E. B.; Scaiano, J. C., *J. Photochem. Photobiol.,* **1992,** *A65,* 249.

130. Saenger, W., *Angew. Chem. Int. Ed. Engl.,* **1980,** *19,* 344; and References cited therein.

131. a) Dominique, D., *Cyclodextrins and Their Industrial Uses,* Ed. Sante, Paris, **1987.** b) Uneo, A.; Osa, T., in *Photochemistry in Organized and Constrained Media,* Ramamurthy, V. ed., VCH, New York, **1991,** 739.

132. a) Barra, M.; Bohne, C.; Scaiano, J. C., *J. Am. Chem. Soc.,* **1990,** *112,* 8075. b) Barra, M.; Bohne, C.; Scaiano, J. C., *Photochem. Photobio.,* **1991,** *54,* 1.

133. a) Moriwaki, F.; Kaneko, H.; Ueno, A.; Osa, T., *Bull. Chem. Soc. Jpn.,* **1987,** *60,* 3619. b) Kano, K.; Matsumoto, H.; Yoshimura, Y.; Hashimoto, S., *J. Am. Chem. Soc.,* **1988,** *110,* 204. c) Chahine, J. M. E. H.; Bertigny J. P.; Schwaller, M. A., *J. Chem. Soc. Perkin. Trans. II,* **1989,** 629. d) Nishijo, J.; Yasuda, M.; Nagai, M., *Chem. Pharm. Bull.,* **1991,** *39,* 5.

134. Nakamura, A.; Saitoh, K.; Toda, F., *Chem. Phys. Lett.,* **1991,** *187,* 110.

135. a) Pedersen, C. J., *J. Am. Chem. Soc.,* **1967,** *89,* 2495, 7017. b) Pedersen, C. J., *Org. Synth.,* **1972,** *52,* 66. c) Pedersen, C. J.; Frensdorff, H. K., *Angew. Chem. Int. Ed. Engl.,* **1972,** *11,* 16.

136. Vögtle, F.; Weber, E., in *Reference 92,*, p.207. and references cited therein.

137. a) Melson, G. A., *Coordination Chemistry of Macrocyclic Compounds,* Plenum, New York, **1979**. b) Izatt, R. M.; Christensen, J. J., *Progress in Macrocyclic Compounds,* Wiley, New York, **1979**.

138. Behr, J. P.; Lehn, J. M.; Vierling, P., *Helv. Chim. Acta,* **1982**, *65,* 18.

139. Zhu, C. Y.; Izatt, R. M.; Bradshaw, J. S.; Dalley, N. K., *J. Inclu. Phen. Mol. Recog. Chem.,* **1992**, *13,* 17.

140. Ha, Y. L.; Chakraborty, A. K., *J. Phys. Chem.,* **1992**, *96,* 6410.

141. Lehn, J. M., *Science,* **1985**, *227,* 849.

142. a) Nagakura, S.; Tanaka, J., *J. Chem. Phys.,* **1954**, *22,* 236. b) Nagakura, S., *Pure Appl. Chem.,* **1963**, *7,* 79. b) Nagakura, S.; Kojima, M.; Maruyama, Y., *J. Mole. Spec.,* **1964**, *13,* 174.

143. a) Selishar, C. J.; Khalil, O. S.; McGlynn, S. P., in *Excited States,* Lim, E. C., Ed., Academic Press, New York, **1974**, *1,* p. 231. b) Ohtani, H.; Kobayashi, T.; Suzuki, K.; Nagakura, S., *Bull. Chem. Soc. Jpn.,* **1980**, *53,*43.

144. Kobayashi, T.; Nagakura, S., *Bull. Chem. Soc. Jpn.,* **1974**, 47, 2563.

145. Görner, H.; Schulte-Frohlinde, D., *Ber. Bunsenges. Phys. Chem.,* **1978**, *82,* 1102.

146. a) Wagnière, G. H., in *The Chemistry of Nitro and Nitroso Groups,* Feuer, H., Ed.; Interscience, New York, **1969**, Part I, Chapt. 1, p.1. b) Hamer, J.; Placek, L.; Ahmad, M., in *Nitro Compounds,* Urbanski, T. ed., Pergamon, New York, **1964**, 395. c) Van Veen, A.; Verkade, P. E.; Wepster, B. M., *Rec. Tra. Chim. Pays-Bas,* **1957**, *76,* 801. d) Smith, D. C.; Pan, C.-Y.; Nielsen, J. R., *J. Chem. Phys.,* **1950**, *18,* 706.

147. Nieman, G. C., *J. Chem. Phys.,* **1969**, *50,* 1660, 1674.

148. Wolleben, J.; Testa, A. C., *J. Phys. Chem.,* **1978**, *81,* 429.

149. Cadogan, K. D.; Albrecht, A. C., *J. Phys. Chem.,* **1969**, *73,* 1868.

150. a) Ziegler, L. D.; Hudson, B. S., in *Excited States,* Lim, E. C., ed., Academic, New York, **1982**, *5,* p.42. b) Turner, D. W., in *Adv. in Phys.*

Organic Chem., **1966,** *v. 4,* 57. c) Spangler, J. D.; Kilmer, N. G., *J. Chem. Phys.,* **1968,** *48,* 698. d) Pertruska, J., *J. Chem. Phys.,* **1961,** *34,* 1111, 1120.

151. Vasil'eva. V. N., in *Nitro Compounds,* Urbanski, T. ed., Pergamon, New York, 1964, 403.

152. Dessauer, R.; Paries, J. P., in *Advances in Photochemistry;* Noyes, W. A.; Jr. Hammond, G. S.; Pitts, J. N., eds., Interscience, New York, **1963,** *1,* 275.

153. de Mayo, P.; Reid, S. T., *Q. Rev.,* **1961,** *15,* 393.

154. Yip, R. W.; Wen, Y. X.; Gravel, D.; Giasson, R.; Sharma, D. K., *J. Phys. Chem.,* **1991,** *95,* 6079.

155. Birks, J. B.; Dyson, D. J.; Munro, I. H. *Proc. R. Soc. A,* **1963,** *275,*575.

156. Korn, G. A.; Korn, T. M. *Mathematical Handbook for Scientists and Engineers,* McGraw-Hill, New York, **1968,** 266.

157. Anderson B. D.; Rytting, J. H.; Lindenbaum, S.; Higuchi, T. *J. Phys. Chem.* **1975,** *79,* 2340.

158. Andreoli- Ball, L.; Costas, M.; Paquet, P.; Patterson, D.; Victor, M. S. *Pure Appl. Chem.* **1989,** *61,* 1075.

159. Korppi-Tommola, J.; Yip, R. W. *Can. J. Chem.* **1981,** *59,* 191.

160. Korppi- Tommola, J. *J. Mol. Struct.* **1977,***40,* 13.

161. Bensi, H. A.; Hildebrand, J. H., *J. Am. Chem. Soc.,* **1949,** *71,* 2703.

162. Sumiyoshi, T.; Katayama, M. *Bull. Chem. Soc. Jpn.* **1990,** *63,* 1293; 1584.

163. Wen, Y. X. *'Organic Bichannel Optical Processor',* a research proposal presented to the Dept. of Chem. & Biochem., Concordia University for fulfillmemt of the degree of Ph. D., **1993.**

164. Armstrong, D. W.; Alak, A.; Bui, K.; De Mond, W.; Ward, T.; Riehl, T. E., *J. Inclusion Phenom.,* **1984,** *2,* 533.

165. Ihara, Y.; Nakanishi, E.; Nango, M.; Koga, J., *J. Bull. Chem. Soc. Jpn.,* **1986,** *59,* 1901.

166. (a) Yoshida, N.; Seiyama, A.; Fujimoto, M. *J. Phys. Chem.*, **1990**, *94*, 4246; (b) Wenz, G.; Keller, B. *Angew. Chem. Int. Ed. Engl.*, **1992**, *31*, 197.

167. (a) Nelson, G.; Patonay, G.; Warner, I. M., *Anal. Chem.*, **1988**, *60*, 274; (b) *Talanta*, **1989**, *36*, 199.

168. Okada, T.; Mataga, N.; Baumann, W. *J. Phys. Chem.* **1987**, *91*, 760.

169. Rullière, C.; Grabowski, Z. R.; Dobkowski, J. *Chem. Phys. Lett.* **1987**, *137*, 408.

170. Patoney, G.; Rollie, M. E.; Warner, I. M., *Anal. Chem.*, **1985**, *57*, 569.

171. Sahar, E.; Treves, D. *IEEE J. Quantum Electron*, **1977**, *13*, 962.

172. a) Sahyun, M. R. V.; Sharma, D. K., *Chem. Phys. Lett.*, **1992**, *189*, 571. b) Dempster, D. N.; Morrow, T.; Quinn, M. F. *J. Photochem.* **1973/74**, *2*, 329.

173. _____ *Radiation Res. Rev.*, **1968**, *1*,183.

174. Rettig, W.; Chandross, E. A., *J. Am. Chem. Soc.*, **1985**, *107*, 5617.

175. Langhals, H., *Angew, Chem. Int. Ed. Engl*, **1982**, *21*, 724.

176. Dawber, J. G.; Ward, J.; Williams, R. A., *J. Chem. Soc. Faraday Trans. 1*, **1988**, *84*, 713.

177. Dawber, J. G., *J. Chem. Soc. Faraday Trans.* **1990**, *86*, 287.

178. Coosemans, L.; De Schryver, F. C.; Van Dormael, A. *Chem. Phys. Lett.*, **1979**, *65*, 95.

179. Inoue, H.; Hida, M.; Nakashima, N.; Yoshihara, K. *J. Phys. Chem.* **1982**, *86*,3184.

180. Lippert, E.; Lüder, W.; Boos, H. in *Advan. Mol. Spectrosc.*, Mangini, A. ed., Pergamon Press, Oxford, **1962**, 443.

181. Maksimovié, Z. B.; Reichardt, C.; Spirié, A. *Z. Anal. Chem.*, **1974**, *270*, 100.

182. (a) Balakrishnan, S.; Easteal, A. J. *Aust. J. Chem.*, **1981**, *34*, 933; (b) *Aust. J. Chem.*, **1981**, *34*, 943.

183. Kosower, E. W.; Giniger, R.; Radkowsky, a.; Hebel, D.; Shusterman, A. *J. Phys. Chem.*, **1986**, *90*, 5552.

184. Langford, C. H.; Tong, J. P. K. *Pure & Appl. Chem.*, **1977**, *49*, 93.

185. Reichardt, C. *Angew. Chem. Int. Ed. Engl.* **1979**, *18*, 98.

186. McKinnon, A.E.; Szabo, A.G.; Miller, D.R. *J. Phys. Chem.* **1977**, *81*, 1564.

187. Siano, D. B.; Metzler, D. E., *J. Chem. Phys.*, **1969**, *51*, 1856.

188. Bagchi, B.; Oxtoby, D. W.; Fleming, G. R. *Chem. Phys.*, **1984**, *86*, 257.

189. Castner Jr., E. W.; Bagchi, B.; Maroncelli, M.; Webb, S. P.; Ruggiero, A. J.; Flemming, G. R. *Ber. Bunsenges. Phys. Chem.*, **1988**, *92*, 363.

190. Garg, S. K.; Smyth, C. P. *J. Phys. Chem.*, **1965**, *69*, 1294.

191. Castner, E. W. Jr.; Maroncelli, M.; Fleming, G. R., *J. Chem. Phys.*, **1987**, *86*, 1090.

191. Chandra, A.; Bagchi, B., *J. Chem. Phys.*, **1991**, *94*, 3177.

192. Rosenthal, S. J.; Xie, X.; Du, M.; Fleming, G. R., *J. Chem. Phys.*, **1991**, *95*, 4715.

193. Hill, N. E.; Davies, M., in "*Dielectric Properties and Molecular Behavior*", Hill, N. E.; Vaughan, W. E.; Price, A. H.; Davies, M., eds., van Nostrand-Reinhold, New York, **1969**.

194. Hurley, R.; Testa, A. C., *J. Am. Chem. Soc.*, **1968**, *90*, 1949.

195. Charlton, J. L.; Laio, C. D.; de Mayo, P., *J. Am. Chem. Soc.*, **1971**, *93*, 2463.

196. Wan, P.; Yates, K. *J. Org. Chem.*, **1983**, *48*, 136.

197. Wan, P.; Muralidharan, S., *J. Am. Chem. Soc.*, **1988**, *110*, 4336.

198. Craig, B. B.; Weiss, R. G.; Atherton, S. J., *J. Phys. Chem.*, **1987**, *91*, 5906, and reference cited therein.

199. Cornelisse, J.; Lodder, G.; Havinga, E., *Rev. Chem. Intermed.*, **1979**, *2*, 231.

200. a) Sinha, H. K.; Yates, K., *J. Chem. Phys.*, **1990**, *93*, 7085. b) Sinha, H. K.; Yates, K., *J. Can. Chem.*, **1991**, *69*, 550. c) Politzer, P.; Lane, P.; Jayasuriya, K.; Domelshith, L. N., *J. Am. Chem. Soc.*, **1987**, *109*, 1899.

201. a) Van Veen, A.; Verkade, P. E.; Wepster, B. M., *Rec. Tra. Chim.*, **1957**, *76*, 801. b) Hamer, J.; Plack, L.; Ahmad, M., *in Nitro Compounds*, Urbanski, T., ed., MacMillan, New York, **1964**, 395.

202. Kinagasa, T.; Watarai, S., *Nippon Nagku Zusshi*, **1962**, *83*, 476. (*C.A.* **1962**, *58*, 13318b.)

203. Kinagasa, T.; Watarai, S., *Nippon Nagku Zusshi*, **1962**, *83*, 472. (*C.A.* **1962**, *58*, 13317e)

204. Conduit, C. P., *J. Chem. Soc.*, **1959**, 3273.

205. Smith, D. C.; Pan, C.-Y.; Nielsen, J. R., *J. Chem. Phys.*, **1950**, *18*, 706.

206. a) Hébert, J.; Gravel, D., *Can. J. Chem.*, **1974**, *52*, 187. b) Gravel, D.; Hébert, J.; Thoraval, D., *Can. J. Chem.*, **1983**, *61*, 400. c) Gravel, D.; Murray, S.; Ladouceur, GT., *Chem. Commun.*, **1985**, 1828.

207. For excellent reviews see: a) Amit, B.; Zehavi, U.; Patchornik, A , *Isr. J. Chem.*, **1974**, *12*, 103. b) Pillai, W. N. R., *Synthesis*, **1980**, 1.

208. Reichmanis, E.; Gooden, R.; Wilkins, Jr., C. W.; Schonhorn, H., *J. Polym. Sci., Polym. Chem. Ed.*, **1983**, *21*, 1075.

209. Yip, R. W.; Sharma, D. K., *Rev. Chem. Intermed.*, **1989**, *11*, 109.

210. Yip, R. W.; Sharma, D. K.; Giasson, R.; Gravel, D., *J. Phys. Chem.*, **1984**, *88*, 5770.

211. Gravel, D.; Giasson, R.; Blanchet, D.; Yip, R. W.; Sharma, D. K., *Can. J. Chem.*, **1991**, *69*, 1192.

212. Pitha, J.; Jones, R. N., *NRRC Bull.*, **1968**, *No.12*.

213. a) Schupp, H.; Wong, W. K.; Schnabel, W. J., *J. Photochem.*, **1987**, *36*, 85. b) Wong, W. K.; Schupp, H.; Schnabel, W. J., *Macromolecules*, **1989**, *22*, 2176.

214. Frost, A. A.; Pearson, R. G., *Kinetics and Mechanism*, 2nd ed., Wiley: New York, **1961**.

215. a) Nelder, J. A.; Mead, R., *Comput. J.*, **1965**, *7*, 308. b) Cooper, J. W., *Introduction to Pascal for Scientists*, Wiley: New York, **1981**, p. 185.